Physicochemical characterization and anticancer activity evaluation of βcyclodextrin-gemini based nano-delivery systems

A Thesis Submitted to the College of

Graduate Studies and Research

in Partial Fulfillment of the Requirements

for the Degree of Doctor of Philosophy

in the College of Pharmacy & Nutrition

University of Saskatchewan

Saskatoon

By

Masoomeh Poorghorban

PERMISSION TO USE

In presenting this thesis/dissertation in partial fulfillment of the requirements for a Postgraduate degree from the University of Saskatchewan, I agree that the Libraries of this University may make it freely available for inspection. I further agree that permission for copying of this thesis/dissertation in any manner, in whole or in part, for scholarly purposes may be granted by the professors (Dr. Ildiko Badea and Dr. Pawel Grochulski) who supervised my thesis/dissertation work or, in their absence, by the Head of the Department or the Dean of the College in which my thesis work was done. It is understood that any copying or publication or use of this thesis/dissertation or parts thereof for financial gain shall not be allowed without my written permission. It is also understood that due recognition shall be given to me and to the University of Saskatchewan in any scholarly use which may be made of any material in my thesis/dissertation.

Requests for permission to copy or to make other uses of materials in this thesis/dissertation in whole or part should be addressed to:

Dean of the College of Pharmacy & Nutrition
University of Saskatchewan
Saskatoon, Saskatchewan S7N 2Z4
Canada

Abstract

Lipophilic anticancer agents such as curcumin analogs have low water solubility and low in vivo bioavailability. βCyclodextrin-gemini surfactant is a novel drug delivery agent synthesized by attachment of βcyclodextrin to cationic gemini surfactants. βCyclodextrin can accommodate lipophilic guest molecules in its cavity and form host/guest inclusion complexes. The amphiphilic nature of the gemini surfactants enable them to self-assemble into nano-structures. Herein, physicochemical properties of the delivery agent, free βcyclodextrin-gemini surfactant and the complexes composed of a curcumin analog (NC 2067) and βcyclodextrin or βcyclodextrin-gemini surfactant were evaluated to comprehend the geometry of the host/guest interactions and the nano-structural arrangements of the βcyclodextrin-gemini surfactant-based formulations. Anticancer activity and cell death mechanisms associated with NC 2067 in the presence of the delivery agent were evaluated.

The physicochemical characterization of the host/guest complexes was performed using various synchrotron and non-synchrotron based techniques such as powder X-ray diffraction, Fourier transform infrared spectroscopy and thermogravimetric analysis. 1D and 2D NMR techniques, namely rotating frame Overhauser effect spectroscopy, were employed to characterize the structural properties of the free βcyclodextrin gemini surfactant and NC 2067 complexes with βcyclodextrin or βcyclodextrin-gemini surfactant comprehensively. Size measurements and small and wide-angle X-ray scattering studies employed to study the nanoparticulate characteristics of the βcyclodextrin-gemini surfactant-based formulations. Cell viability analysis and flow cytometry assays were employed to appraise the cell death induction in A375 melanoma cells.

It was found that NC 2067 is able to form complexes with βcyclodextrin at 1:2 mole ratio through the interactions of the aromatic moieties with the βcyclodextrin cavity. Moreover, in βcyclodextrin-gemini surfactant, the hydrocarbon tail of the gemini moiety was inserted into βcyclodextrin through intra-molecular interactions. NC 2067 formed complexes with βcyclodextrin-gemini surfactant and retained its ability to kill selected cancer cells and showed proapoptotic activity. However, it was not able to alter the self-inclusion of the βcyclodextrin-gemini surfactant significantly.

The physicochemical assessment of the interaction of a novel gemini surfactant-based βcyclodextrin delivery agent with a model cytotoxic agent for the first time and evaluation of the

βcyclodextrin-gemini surfactant-based formulations will aid to design and develop more efficient anticancer drug delivery systems.

ACKNOWLEDGEMENTS

I would like to express my deepest appreciation and thanks to my supervisors Dr. Ildiko Badea and Dr. Pawel Grochulski for their support, guidance and encouragement. I am grateful for allowing me to grow as a researcher.

I also want to extend my gratitude to my advisory committee members Drs. Jonathan Dimmock, Michel Fodje and Peter Hull for their priceless advices and to committee chairs Drs. Ed Krol, Jane Alcorn and Fred Remillard for the time they spent on conducting the meetings.

I would especially like to thank Drs. Ronald Verrall, Lee Wilson and Abdalla Karoyo who offered valuable advices and contribution to the chemistry part of my research. I also want to appreciate Ms. Deborah Michel who trained me for the tissue culture experiments and helped me in working with flow cytometer. I would like to express many thanks to Drs. Jonathan Dimmock and Umshankar Das who synthesized NC 2067.

I would also like to thank Canadian Light source, the staff at CMCF-beamlines, Stanford Synchrotron Radiation Lightsource and Dr. Thomas Weiss for synchrotron-based data collection. I am so grateful for the help of Osama Alaidi and Dr. Joel Reid in synchrotron-based data analysis.

I would like to thank all G16 lab members, Drs. Anas El-Aneed, Jagbir Singh, Joshua Buse and McDonald, Waleed, Randeep, Hanan, Mays, Saniya and Mona.

Finally I would like to thank the Canadian Institutes of Health Research Training grant in Health Research Using Synchrotron Techniques (CIHR-THRUST) for financial support. I am so grateful to Dr. Ingrid Pickering for supporting me as a CIHR-THRUST fellow.

DEDICATION

This work is dedicated to my beloved and wonderful family:

My father “ Mohammadali Pourghorban” and my mother “Zahra Maleki”,

My sister and my brothers,

My nephew “Mahbod” with his bright lovely smile,

And all my friends,

Thank you for your love, patience, prayers, supports and friendship.

Table of contents

List of figures

List of Tables

List of Abbreviations

AIF	Apoptosis-inducing factor
Bak	Bcl-2-associated killer
Bax	Bcl-2-associated X protein
Bcl-2	B-cell lymphoma-2
Bid	BH3 interacting domain death agonist
Bim	Bcl-2-interacting mediator
βCD	βCyclodextrin
βCDgemini	βCyclodextrin-gemini
DISC	Death-inducing signal complex
DOPE	1,2-dioleoyl-*sn*-glycero-3-phosphoethanolamine
EPR	Enhanced permeability and retention
ER	Endoplasmic reticulum
FTIR	Fourier-transform infrared
HP-CD	Hydroxylpropyl cyclodextrin
IAP	Inhibitors of apoptosis protein
LLC	Lyotropic liquid crystalline
MAPK	Mitogen activated protein kinase
MMP	Mitochondrial membrane permeabilization
MPT	Mitochondrial permeability transition
NMR	Nuclear magnetic resonance
NOE	Nuclear Overhauser effect
PS	Phosphatidylserine
PTP	Permeability transition pores
RES	Reticuloendothelial system
ROESY	Rotating-frame nuclear Overhauser effect correlation spectroscopy
ROS	Reactive oxygen species
SAXS	Small angle X-ray scattering
SR	Synchrotron radiation
STAT3	Signal transducer and activator of transcription-3

TGA	Thermogravimetric analysis
TNF	Tumor necrosis factor
WAXS	Wide angle X-ray scattering
XIAP	X-linked inhibitor of apoptosis
z-VAD-fmk	Benzyloxycarbonyl-Val-Ala-DL-Asp(O-methyl)-fluoromethylketone

1. INTRODUCTION

1.1. Problem at hand, proposed solution and methodology

Many anticancer agents synthesized recently have poor water solubility, insufficient absorption through biomembranes and, subsequently, low bioavailability. Application of organic solvents such as dimethylsulfoxide (DMSO) and surfactants[1] for solubilization and delivery of these anticancer agents is limited due to the high risk of toxicity to biological systems. Various nanotechnology-based drug delivery systems have been developed to increase the solubility of hydrophobic anticancer compounds and enhance their efficacy. Hence, the design and development of a delivery agent which is capable of combining the advantageous properties such as solubilization enhancement, nano-assembly and low toxicity, are highly valued.

A curcumin analog, named NC 2067, was selected for this study as it showed strong *in vitro* cytotoxic activity towards a variety of cancer cell lines. Despite the fact that NC 2067 exerted toxicity towards a cancer cell line at a concentration in the order of μM, due to its high lipophilicity (log*P* value of 4.6)[2] the *in vivo* effect is limited. To overcome this deficiency, a novel cyclodextrin-substituted gemini surfactant-based drug delivery agent was designed[3], named βcyclodextrin-gemini surfactant (βCDgemini surfactant), to increase the solubility of a cytotoxic agent (curcumin analog) and enhance the delivery to cancer cells (A375 melanoma cell line). This novel carrier is composed of βcyclodextrin (βCD) attached by a linker to a cationic gemini surfactant, thus combining the properties of the two components into a single molecule. A ring-shaped molecule, βCD, is a solubilizing agent which has the capability to encapsulate insoluble drugs in its hydrophobic internal cavity and increase their aqueous solubility. The resulting host-guest complexes of βCD and hydrophobic compounds are well-defined in pharmaceutical research. Moreover, the amphiphilic nature of the gemini surfactants induce self-assembly which enhances the biomembrane diffusion and cellular penetration of the drug delivery system.

The physicochemical characterization of the possible inclusion of NC 2067 molecule into the ring-shaped inner cavity of the βCD is critical to understanding the interaction of the anticancer agent with the delivery agent in their complex form. Different methods such as powder X-ray diffraction, Fourier transform infrared spectroscopy (FTIR), thermogravimetric analysis (TGA)

and 1D/2D ^{1}H NMR were utilized to confirm the incorporation of NC 2067 into the βCD cavity. Specifically, the rotating frame Overhauser enhancement spectroscopy (ROESY) and docking played an important role in the simulation of the three dimensional structure of the inclusion complexes. Furthermore, to assess the nano-structured arrangements formed by NC 2067 complexed with the βCDgemini surfactant, synchrotron-based small- and wide angle X-ray scattering (SAXS/WAXS) was employed. By combining the results from these methods, we believed we would be able to resolve the molecular structure and physicochemical properties of the CD-based delivery systems to advance the development and optimization of the formulations.

In the second part of this work, the molecular mechanism associated with the anticancer activity of NC 2067 complexes with βCDgemini surfactants toward A375 melanoma was evaluated by flow cytometry-based assays. Different approaches, such as calculating the IC_{50} value, evaluation of the mechanisms of cell death, cell cycle arrest, mitochondrial related assays, reactive oxygen species (ROS) measurements and caspase inhibitor assays were used to explore the cell death pathways related to the toxicity of the curcumin analog delivery system.

2. BACKGROUND: NANOPARTICLES, CANCER AND CURCUMIN ANALOGS

2.1. Advancements of nanotechnology related to the delivery of anticancer drugs

Nanomedicine employs nanotechnology to design particles within a range of 5-200 nm as drug delivery agents. Different types of nanoparticles are utilized to enhance drug delivery into the site of therapy.[4] Novel nano-particulate delivery systems are promising carriers, especially for anticancer agents which encounter significant deficiency in terms of delivery and efficacy. Conventional chemotherapy agents comprised mostly of small molecules generally have poor solubility, leading to low efficacy and non-specific tissue distribution causing serious side effects. Nanomedicine approaches to cancer therapy have introduced an innovative tool to overcome these limitations.

Key physicochemical properties of nanoparticles such as size (average and distribution), surface charge, particle morphology and chemistry, drug loading and release capacity and the ability to enhance the solubility of poorly soluble anticancer agents render them as suitable options for anticancer drug delivery.

Permeation through biomembranes and internalization by the target cells of small molecule chemotherapeutics is highly dependent on their solubility in water. The "rule of 5" proposed by Lipinski *et al* explains four situations in which poor molecular solubility and permeation is expected, namely the molecular weight is greater than 500 Da and the calculated *log P* value of more than 5 are the major obstacles for penetration. Moreover, the number of hydrogen-bond donors (NHD, calculated as the sum of the OHs and NHs) of more than 5 and hydrogen-bond acceptors (NHA, associated with the sum of the Os and Ns) of greater than 10, limit the molecular permeation into biomembranes.[5] Even though, Lipinski's experimental rule primarily applied to the oral delivery, it can be applicable to other routes of administration. For absorption through skin, an investigation on 17 FDA-approved transdermal drugs suggested a more restrictive version of Lipinski's rule in which the thresholds of NHD, NHA and molecular weight are assigned to be less than 2, 5 and 335 Da, respectively.[6]

Incorporation of anticancer agents in nanoparticles can increase the solubility of hydrophobic compounds, protect them from unfavorable interactions with biological elements and improve

their pharmacokinetic properties to enhance the delivery into the target organ without significant exposure to non-target tissues.

Many new hydrophobic cytotoxic agents are synthesized every year in an effort to combat different cancers. The major challenge is typically their low water solubility which results in poor absorption through biomembranes and low bioavailability. Organic solvents such as dimethylsulfoxide (DMSO) and non-ionic surfactants such as Cremophor EL® (polyoxyethyleneglycerol triricinoleate 35)[7] and Tween 80® (polyoxyethylene (20) sorbitan monooleate) are used to enhance solubilization of these molecules. However, DMSO is not an appropriate solvent for *in vivo* application because of its own influence on the cells. Surfactants such as Cremophor EL® and Tween 80® used in conventional chemotherapy formulations are associated with fatal hypersensitivity reactions.[1,8] Nanoparticles having hydrophobic compartments are capable of the encapsulation of hydrophobic agents and increasing their solubility. For instance, it has been reported that a lipid-polymer based nanoparticle increased the solubility and stability of wortmannin along with its efficacy *in vivo*.[9]

Optimal nanoparticle size for cancer therapy is assumed to be in the range of 10-100 nm.[10] Even though the upper limit is still not well defined, the lower limit of 10 nm is related to the glomerular capillary wall measurement of the kidney glomeruli responsible for blood filtering and first-pass elimination.[11] On the upper end, particles larger than 200 nm in size can be removed from blood by the reticuloendothelial system (RES, previously known as the mononuclear phagocyte system) of the liver and spleen which is responsible for clearance of macromolecules from circulation.[12] There are strategies to create nanoparticles that evade the RES, thus improving their biodistribution and deposition in tumors.[13]

Nanoparticles benefit from enhanced permeability and retention (EPR) effect which leads to their accumulation in the tumor. Based on the permeable nature of tumor vasculature with a pore size range of 380-780 nm, nanoparticles can easily extravasate into the tumor, whereas in normal tissue, the pore size of the capillaries is small (1-2 nm) which only small molecules can traverse.[14] Furthermore, the lymphatic system with capability of macromolecular removal is damaged in tumors, further aiding the retention of nanoparticles within the tumors.[15] Another characteristic of nanoparticles affecting their uptake through RES is their surface chemistry. Surface modification of nanoparticles with polyethylene glycol (PEG) will prevent nanoparticle recognition by opsonin and subsequent phagocytosis.[16] Moreover, the presence of the

hydrophobic moieties on the nanoparticle surface will enhance the penetration into cell membranes.[17]

Generally, due to the negatively charged biomembranes, nanoparticles with a positive surface charge can enter cells more efficiently.[18] However, some studies confirmed that negatively charged nanoparticles are able to enter cells successfully as well.

In addition to the ability to overcome tumor environmental barriers such as microvasculature permeability and RES, the physicochemical properties of nanoparticles influence cellular internalization pathways and subcellular targeting in cancer. Cellular internalization known as endocytosis occurs in mammalian cells by different mechanisms such as macropinocytosis, caveolae-mediated endocytosis and clathrin-mediated endocytosis. Nanoparticles follow endocytotic internalization instead of diffusion or protein-channel mediated pathways, due to their larger size in comparison to small molecules. Even though intracellular trafficking of nanoparticles is a cell-type dependent phenomenon, the size and shape of nanoparticles can influence internalization rate and pathway in different cells. For example, it has been shown that increasing the size of the nanoparticles formed by latex beads from 200 nm to 500 nm changes their internalization mechanism from clathrin-mediated to caveolae-mediated pathway in melanoma B16 cells.[19] Another study showed that the rate of the internalization of PLGA nanoparticles with size of 100 nm is significantly higher than larger particles (more than 500 nm) in Caco-2 cells.[20] The shape or supramolecular arrangement is another property that can alter the internalization of the nanoparticles, though the findings in this area are diverse in various studies. Investigation of gold nanoparticles showed that spherical nanoparticles can be internalized more quickly and to a higher extent than rod-like structures[21], whereas other studies showed cylindrical shapes are able to be internalized more efficiently.[18] As well, engineering various nanoparticles decorated with surface functional groups plays an important role in the internalization (endocytosis) pathway.[22] For example, functionalization of dendrimers with cationic, anionic and neutral functional groups showed that dendrimers with cationic or neutral moieties were internalized by lung epithelial cells via non-clathrin and non-caveolae mediated mechanisms while anionic dendrimers entered cells through caveolae mediated pathway.[23]

Another area where nanoparticles might benefit cancer treatment is by interference with tumor resistance to chemotherapy. Tumor cells are able to develop drug resistance by various mechanisms. Overexpression of the efflux pumps such as P-glycoprotein is one of the most

common mechanisms in which the intracellular accumulation of the anticancer agents is decreased. Different strategies employed by nanoparticles to prevent multidrug resistance (MDR) such as combination delivery of pro-apoptotic agents, pump inhibitors or MDR-targeted siRNA with chemotherapeutics.[24] Moreover, some groups used pharmacologically active carriers such as polaxamers directly to inhibit drug efflux pumps.[25]

An issue requiring special attention in the study of nanoparticles encapsulating anticancer drugs is their intracellular fate. Following the internalization of nanoparticles, endosomes are formed and encapsulate the nanoparticles. The early endosomes transform into late endosomes and subsequently lysosomes, in which the internal pH decreases continously.[26] This endosomal/lysosomal degradation is an obstacle in the endocytotic internalization pathway. Modified nanoparticles such as pH-sensitive nanoparticles have been developed to bypass this barrier. A pH-induced fusion of particles with lysosomal membrane will result in drug release into cytoplasm; thus efflux pumps which are located in the cell membrane cannot excrete the drug out of the cell.[27]

The design and development of nanoparticles for subcellular targeting is a novel area of research dealing with the delivery of the drugs not only to target cells but also to subcellular organelles such as mitochondria[28], nucleus[29] and cytosol[30]. For example, in the case of targeting mitochondria, based on the negative mitochondrial membrane potential cationic liposomes such as ceramide[31] and sclareol[32] have been utilized to deliver anticancer agents.

In conclusion, there is a need for the design of delivery agents that can efficiently encapsulate chemotherapeutic agents to create pharmaceutically acceptable nanoparticulate delivery systems. Our research focuses on a new family of cyclodextrin-gemini surfactant delivery agents that can form nanostructures and incorporate poorly soluble anticancer drugs.

2.1.1 Lipid-based nanoparticles: focus on lyotropic liquid crystals

The introduction of liposomes, lipid-based vesicles as drug delivery agents, was a milestone in the design and development of an innovative class of drug carriers: lipid-based nanoparticles.[33] In general, the most important advantages associated with lipid-based formulations are biocompatibility and stability.[34] Amphiphilic lipids such as surfactants containing hydrophilic and hydrophobic moieties can self-assemble in aqueous media at certain concentrations (critical micelle concentration, CMC) and temperature, forming particles called micelles. In a micellar structure, the hydrophobic parts of the surfactant form a particle core while polar head groups

locate between the core and aqueous media. The hydrophilic part is made of cationic, anionic or nonionic head groups whereas the hydrophobic component is commonly formed by hydrocarbon aliphatic chains. Micelles subsequently can aggregate further and build ordered nanoparticulate structures known as lyotropic liquid crystals (LLC) based on the physicochemical properties of the amphiphilic lipid constituent. Liquid crystal mesophases illustrate characteristics between crystalline solid, and liquid.[35] Nanostructured LLCs can be distinguished from micelles or vesicular lipid aggregations by the presence of the internal molecular organization in the structure. Different types of lyotropic liquid crystals have been introduced as lamellar, hexagonal, cubic, nematic, gel and intermediate.[36] Examples of the LLC nanoparticles for drug delivery that have been reported to date are cubosomes, micellar cubosomes and hexosomes (Figure 2.1) which are formed by the dispersion of the bulk cubic and hexagonal LLC mesophases in excess water.[37] These nanoparticles have internal water channels with or without connections to the external aqueous environment.[38] Polar drugs can be loaded in water channels while lipophilic drugs can accommodate in the lipophilic part of the nanoparticles.[39] Nanoparticles built of LLC mesophases are able to incorporate small molecule anticancer agents to enhance their bioavailability via various routes of administration. Irinotecan, a hydrophilic anticancer drug, entrapped in glycerate-based amphiphiles in the form of hexosomes retained the active form of the drug at neutral pH which can be a substitute to the current low-pH formulation.[40] Paclitaxel, a hydrophobic drug loaded in LLC-based nanoparticles having reverse cubic and hexagonal phases, showed enhanced oral bioavailability.[41]

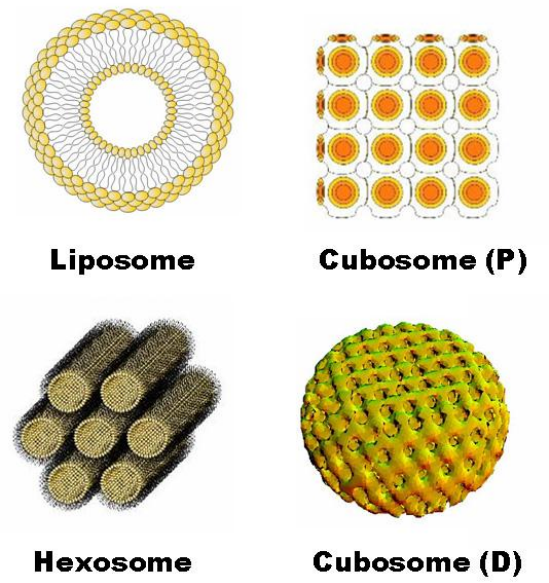

Figure 2.1- Schematic of different lyotropic liquid crystalline nanoparticles for drug delivery.[42]

[Open Access]

As described in this chapter, the assembly of nanoparticles is one of the key properties that influence the fate of the drug. Thus, in our studies we focus on understanding the interaction between a model cytotoxic agent and a delivery agent in addition to the structural elements contributing to the ability to form LLCs.

2.2. Melanoma: model cancer

Melanoma is the most fatal type of skin cancer and originates from gene mutations in melanocytes which are located deeply in the epidermis. Based on data from the World Health Organization, the incidence of malignant melanoma is increasing worldwide, converting this high-mortality cancer into a major public health issue. Malignant melanoma is one of the top 7 fastest growing cancers in Canada and it was estimated that 6800 new cases will be diagnosed in 2015(Canadian Cancer Society, www.cancer.ca).

Although the pathogenesis of melanoma is not fully understood, the role of oncogenes and impaired DNA is evident.[43] Various gene mutations and signaling molecules are responsible for proliferation of cutaneous melanoma such as cell survival pathways of mitogen activated protein kinase (MAPK) and AKt (protein kinase B). Moreover, oncogene BRAF mutations have been reported in 50% of cutaneous melanomas.[44] Nuclear factor-κB, which regulates DNA transcription, is another factor influencing metastasis and angiogenesis in melanoma.[45] A comprehensive review on the molecular pathology of melanoma was published recently.[46] Various melanoma cell lines derived from malignant melanoma express mitochondria-focused genes such as antioxidant, proapoptotic and antiapoptotic genes at different levels.[47]

2.2.1. Melanoma treatment

Despite significant efforts to treat melanoma, challenges such as chemoresistance[48,49] and fatal metastasis[50], problems addressing cancer management and survival, still remain. Treatment options vary depending on the severity and progress of the disease. According to the American Joint Committee on Cancer (AJCC), there are five stages of melanoma.[51]

Lentigo maligna (stage 0) arises on chronically sun-exposed skin and has a protracted *in situ*

phase. It is generally seen as pigmented asymmetric lesions on the head and neck in the elderly but other sun-exposed sites may be affected.[52] The surgical excision of such lesions is often difficult and may result in disfiguring scarring. The incidence of this melanoma subtype has increased in the past twenty years[53] and it has the potential to transform into invasive melanoma in 2-50% of the cases.[54,55] Non-surgical options for lentigo maligna are radiotherapy and topical therapies such as imiquimod. The effectiveness of imiquimod in the treatment of lentigo maligna is controversial. It has been reported that the use of topical imiquimod resulted in a low rate of cure in lentigo maligna.[56] On the other hand new findings showed that imiquimod cream was efficient as primary or adjuvant therapy in elderly patients with lentigo maligna.[57] Furthermore, the recurrence rate of lentigo maligna is the highest among other types of cutaneous melanoma because of the difficulty in the estimation of the lesion margins.[58] Therefore, the challenge for dermatologists is to balance the side effects of surgery and the low risk of possible progression to malignant melanoma.

The major management strategy for stage I and II which corresponds to localized melanoma is surgery. Isolated limb perfusion (ILP) with melphalan has been established for in-transit melanoma (stage III or regional metastatic melanoma) in patients whose lesions are not surgically excisable. The use of surgery and ILP is confined as they are invasive techniques and can be performed only by specialists.

Systemic chemotherapy and immunotherapy are the mainstay treatments for distant metastatic melanoma (stage IV). Conventional chemotherapeutics such as dacarbazine showed low response in metastatic melanoma.[59] Fotemustine, a nitrosurea, showed only 2% complete response and 24% overall response in a multicenter phase II study.[60] Carboplatin demonstrated 7% complete response in malignant melanoma in a phase II clinical trial.[61] Low response, chemoresistance and serious side effects restrict the use of chemotherapy agents. A meta-analysis demonstrated that immunotherapy agents such as interferon-α and interleukin-2 yielded the same results, but were associated with higher toxicity.[62]

Moreover, radiotherapy is not a suitable strategy for melanoma treatment as melanoma is more radioresistant in comparison to other cancers. In melanoma a fraction size of 4 Gy is needed for complete response while for the other types of cancer 1.8-2 Gy of fraction size is commonly used.[63] Clinical data showed that the average response rate for fractions less than 4 Gy is only 36%. Radiotherapy can be employed in selected patients with lentigo maligna as well.[64]

Recently a number of studies investigated the efficacy of a new family of antimelanoma agents, such as vemurafenib and imatinib that target the signaling molecules, BRAF and tyrosine kinase, respectively. BRAF belongs to the Raf kinase family that regulates the MAP kinase/ERKs signaling pathway and is mutated in approximately 50% of melanomas.[65] The selective BRAF inhibitor, vemurafenib, showed 80% response rate at the maximum daily dose in a phase I trial on 32 selected patients.[66] Early phase II clinical studies on tyrosine kinase inhibitors such as imatinib demonstrated a 16% overall response rate in metastatic melanoma.[67] Another anti-melanoma agent, ipilimumab, an anti-cytotoxic T lymphocyte antigen 4 antibody, increased the survival rate in patients suffering from metastatic melanoma at phase III clinical trials.[68] Moreover, recently two other therapies dabrafenib (BRAF inhibitor) and trametinib (MEK inhibitor) have been approved by the Food and Drug Administration. Although these novel anti-melanoma agents are promising, they still show high risks of relapse, low efficacy and severe side effects.[69] The use of these agents for malignant melanoma treatment needs further research.[70]

Since the systemic treatment and surgery for melanoma encounters some challenges, an urgent need exists to seek novel strategies. Nano-based drug delivery systems made of anti-melanoma agents are promising, particularly for the *in situ* or minimally invasive melanomas.

2.2.2. Nanoformulations for melanoma treatment

Nanotechnology-based pharmaceutical formulations have been widely studied in melanoma treatment. Liposomes[71], niosomes[72], carbon-based nanoparticles[73], dendrimers[74], and polymerosomes[75] are some examples that have been employed recently to increase the efficacy of anti-melanoma agents. For example 5-fluorouracil formulated in a bola-niosome showed 100 times lower IC_{50} *in vitro* and 8 times more percutaneous permeation compared to the free drug.[72] Furthermore, lipid-based nanoparticles have been investigated as promising nano-carriers for dermal delivery to overcome the stratum corneum barrier without irritating or sensitizing effects.[76,77] A number of studies evaluated the effects of liposomes as delivery agents for chemotherapeutics[78-81], immunotherapeutic agents[82] and nucleic acids[83,84] in melanoma *in vitro* and *in vivo*. A liposome composed of phosphatidylethanolamine was able to increase the tumor accumulation of cisplatin 3.6 times higher than the free drug.[78] Moreover, CD-based nano-vectors have been developed to increase the delivery of anti-melanoma agents.[85-87] Apart from ordinary chemotherapeutics on the market, novel chemical entities such as curcumin are also

incorporated into lipid- or cyclodextrin-based nano-carriers as well to enhance melanoma treatment.

2.3. Curcumin in cancer therapy

Curcumin, a non-steroidal diphenolic compound, is the major active ingredient of turmeric extracted from *Curcuma longa* rhizome (Figure 2.2).[88] The antiproliferative activity of curcumin and its analogs toward a variety of cancer cells lines such as breast [89], colon[90], pancreatic[91] cancers and leukemia[92] have been demonstrated.

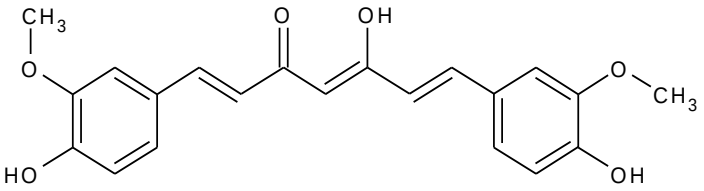

Figure 2.2- Chemical structure of curcumin

Current limitations in curcumin therapy are its high lipophilicity and low aqueous solubility and bioavailability.[93] For instance, it was reported that the oral bioavailability of curcumin in rat is only 1%.[94] Different nano-based drug delivery systems such as liposomes[95,96] , solid lipid nanoparticles[97,98], polymer-based nanoparticles[99] and CD complexes[100-104] have been developed to enhance curcumin delivery in various cancers. Curcumin encapsulated in liposome-PEG (polyethyleneglycol)–PEI (polyetherimide) showed 5 times lower IC_{50} towards different cancer cell lines *in vitro* and 60-90% decrease in tumor size induced by melanoma in mice in comparison to free curcumin.[95] In another nano-based formulation, curcumin integrated into bilayers of dodecanoic acid bound to magnetite nanoparticles, showed enhanced water solubility and toxicity towards melanoma *in vitro*.[105] Moreover, the solubility and stability of curcumin increased by its incorporation into poly(ethylene oxide)-b-poly(εcaprolactone) micelles while toxicity towards B16F10 mouse melanoma cell line was retained.[99]

Yallapu *et al* incorporated hydrophobic curcumin into a βCD cavity to increase its solubility towards prostate cancer cells.[103] Furthermore, they synthesized poly(βCD) which was capable of loading curcumin while forming self-assembling nanoparticles with a size of 250 nm.[104]

The relatively high IC_{50} and poor aqueous solubility of curcumin limited its application as an

anticancer drug *in vivo*. To further improve the performance of curcumin, derivatives and analogs were developed by medicinal chemists.

2.3.1. Curcumin analogs in melanoma treatment

Recently, several research groups dedicated their attention to synthesize new curcumin related compounds/analogs to improve its biological and anticancer activities.

Arezki *et al* grafted an organometallic moiety to curcumin and curcuminoids and synthesized new ferrocenyl derivatives which showed higher toxicity (lower IC_{50} values) in murine B16 melanoma cell line compared to curcumin.[106]

Based on computational modeling a novel curcumin analog (FLLL32) derived from curcumin and a diketone tautomer was synthesized to interact with transcription factor (STAT3) in melanoma cells. The results showed 10 times lower IC_{50} values towards A375, HT144 and Hs294T human melanoma cell lines via caspase-dependent apoptosis and STAT3 phosphorylation inhibition.[107] The *in vitro* analysis of a series of 1,5-diaryl-3-oxo-1,4-pentadienes (curcumin analogs) on various cancer cell lines such as G361 melanoma showed that some of the compounds had higher toxicity (at least 10 times) compared to curcumin.[108] Another biphenyl curcumin-related compound containing α,β-unsaturated ketone, named D_6, showed higher efficacy with 5-10 times lower IC_{50} value to a melanoma cell line and sub-cutaneous melanoma xenograft mouse model in comparison to curcumin.[109] Sodium 4-[5-(4-hydroxy-3-methoxyphenyl)-3-oxo-penta-1,4-dienyl]-2-methoxy-phenolate, another curcumin analog, was able to increase the survival by Mcl-1 and Bcl-xL downregulation and decrease tumor load in melanoma-bearing mice.[110]

A novel family of curcumin analogs/related compounds has been designed and synthesized by Dr. Dimmock and his colleagues (College of Pharmacy and Nutrition, University of Saskatchewan) and evaluated in several cancer cell lines.[111] The 1,5-diaryl-3-oxo-1,4-pentadienyl pharmacophore (Figure 2.3), a conjugated α,β-unsaturated ketone, has been attached to different moieties and formed large series of curcumin analogs.[112]

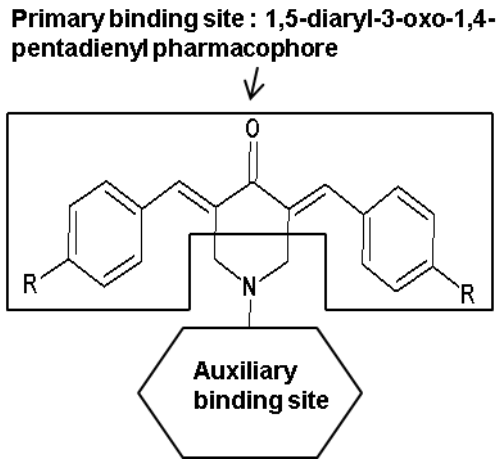

Figure 2.3- 3,5-bis-(Arylidene)-4-piperidone containing postulated pharmacophore binding sites.

The conjugated unsaturated styryl ketones in the pharmacophore have shown a high affinity toward thiol groups instead of amino or hydroxyl groups on the structure of nucleic acids.[113,114] Some of the existing anticancer therapeutic agents that target amino and hydroxyl groups on nucleic acids result in genotoxic outcomes.[115] In contrast, the curcumin analogs may avoid genotoxicity based on their thiol selectivity. Furthermore, the diaryldienone moiety of the pharmacophore has two thiol-alkylating groups which are able to target cellular thiol groups serially which can lead to higher toxicity toward tumor cells in comparison to the corresponding normal cells.[106] This phenomenon can be explained by the fact that when a primary alkylator attacks the cancer cells, chemosensitization may occur, resulting in greater vulnerability toward a subsequent alkylator in comparison to normal cells. Hence, curcumin analogs showed selective toxicity toward malignant cells through "sequential cytotoxicity".[116] Integrating a piperidine ring into 1,5-diaryl-3-oxo-1,4-pentadienyl pharmacophore formed the 3,5-bis-(arylidene)-4-piperidone compounds. The 4-piperidone group can act as a cyclic Mannich base which affects mitochondrial respiration.[117]

Moreover, inserting the N-acyl group to the latter compounds has yielded 48% higher potency in many cases attributed to the further attachment to a secondary binding site, strengthening the binding of the pharmacophore to the primary site. Due to their high cytotoxicity and specificity, curcumin analogs are ideal candidates for drug development for melanoma.

NC 2067, a 3,5-bis-(benzylidene)-4-piperidone compound (Figure 2.4) attached to the *N*-[4-(2-alkylaminoethoxy)phenylcarbonyl] group, was used as a model drug in our studies. Addition of the latter group resulted in three times higher cytotoxicity of NC 2067 toward human T-

lymphocytes (Molt4/C8 bioassay) compared to compounds lacking N-acyl group.[112] Moreover, NC 2067 induced mitochondrial respiration in rat liver at concentration of 10 μM and did not kill the mice at concentrations up to 300 mg/kg.[118]

In addition, different 3,5-bis-(benzylidene)-4-piperidone derivatives demonstrated high *in vitro* selective toxicity toward human leukemic cells and human squamous cell carcinomas[119], though they suffer from unfavorable pharmacokinetic properties and *in vivo* inefficacy.[120]

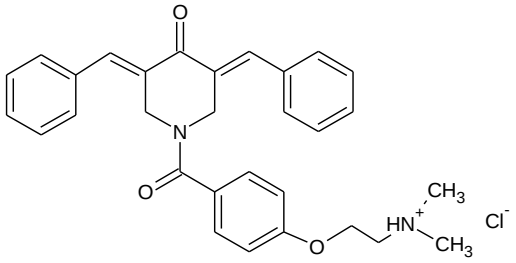

Figure 2.4- Chemical structure of NC 2067

Recent evaluation of NC 2067, dissolved in DMSO, has indicated the high *in vitro* toxicity towards the A375 human melanoma cell line with an IC_{50} value of 0.47±0.03 μM.[3] The highly lipophilic nature of curcumin analogs such as NC 2067 defined as high octanol-water partition coefficient value (log P of 4.6)[2], represents the major challenge for the utilization of these compounds as suitable drug candidates in cancer therapy. Although NC 2067 can penetrate easily into the stratum corneum via passive diffusion, it lacks the potential to enter viable cells such as melanocytes. The design and development of new drug delivery systems to counteract the unfavorable physicochemical characteristics of NC 2067 might improve the delivery into melanoma cells. In our research group, a novel nanocarrier consisting of CD attached to a gemini surfactant, was designed to improve NC 2067 solubility and deliver it into melanoma cells by crossing biomembranes. In a previous study, the IC_{50} of NC 2067 in complexed with βCDgemini surfactant towards A375 melanoma cells was calculated as 2 μM.[3] Moreover, NC 2067 /βCDgemini surfactant increased apoptotic markers, caspase-3 and -7, significantly in comparison to control cells whereas free βCDgemini surfactant did not induce apoptosis.[3] This study is a proof-of concept evidence for the suitability of the derivatized CDs for delivery of curcumin analogs.

2.4. Drug delivery agent: βCDgemini surfactant

This chapter depicts some of the pharmaceutical applications of the components of the βCDgemini surfactant, βCD and gemini surfactant.

2.4.1. Cyclodextrins

Cyclodextrins (CDs), discovered a century ago, are widely used in different fields such as food and cosmetic industries to stabilize flavoring agents and minimize unpleasant odors.[121] Nowadays, CDs are available as common pharmaceutical excipients, and accordingly, their novel and unique applications in pharmaceutical sciences have been studied comprehensively and continuously.[122]

CDs are macrocyclic oligosaccharides formed of six, seven or eight α-*D*-glucopyranose units called α, β and γ CD, respectively.

2.4.1.1. βcyclodextrin (βCD)

As mentioned above, βCD is composed of seven (α-1,4)-linked α-*D*-glucopyranose units (Figure 2.5.a) and based on the rigid construction of glucopyranose units, it forms a truncated cone shape with primary hydroxyl groups (OH-6 on the glucopyranose unit) extending from the narrow interface and secondary hydroxyl groups (OH-2 and OH-3 on the glucopyranose unit) from the wide interface (Figure 2.5.b)[123]. Moreover, the C-H bonds and nonbonding electrons of the etheric oxygen point toward the interior of the cavity. This configuration results in a hydrophilic outer surface and lipophilic inner cavity with high electron density which is the key property of βCD related to its ability to carry lipophilic agents.[124]

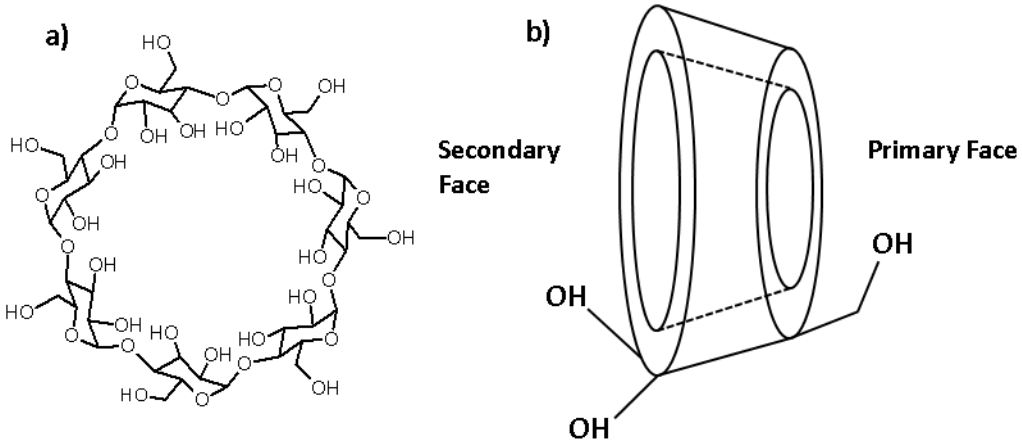

Figure 2.5- a) Chemical structure of βCD, **b)** hydroxyl groups of βCD.

The lipophilicity of the cavity has been approximated to be comparable to an aqueous ethanolic solution.[125] Moreover, secondary hydroxyl groups can interact with each other to form intermolecular hydrogen bonds which restricts the water solubility of βCD (18.5 mg/ml at room temperature).[125] To overcome the limitations associated with βCD, various βCD derivatives have been synthesized by substitution of methyl, hydroxypropyl, and sulfobutyl ether moieties on the secondary hydroxyl groups.[122]

Chemical characteristics of βCDs are listed in Table 2.1.[126,127]

Table 2.1- Characteristics of βCD and its derivatives.

	Molecular weight	Solubility* [g/100ml]	Cavity diameter [Å]	Cavity height [Å]	Cavity volume [Å^3]	Outer periphery diameter [Å]	LogP value	Crystal water content [wt%]
βCD	1135	1.85	6.0-6.5	7.9	262	15.4	-14	13.2-14.5
2-Hydroxylprpoyl-βCD (HP- βCD)	1400	>600	--	--	--	--	-11	--
Sulfobutylether-βCD (SB- βCD)	2163	>500	--	--	--	--	<-10	--
Randomly methylated- βCD (RM- βCD)	1312	>600	--	--	--	--	-6	--

*solubility in water at room temperature

The natural origin of βCD dictates its bioadaptability, low toxicity and biodegradability. However, the safety of βCDs in dermal administration is related to the possible interaction of βCD with lipid components of cell membranes. βCDs could cause hemolysis, related to their interaction with phospholipids of the erythrocyte cell membrane altering the morphology of the erythrocytes.[128] It has been reported that more hydrophobic βCDs such as methylated βCDs can extract cholesterol as well.[129] The ability of βCDs to solubilize and extract cholesterol from cell membranes can be used as a predictive criterion for cell toxicity.[130]

The traditional role of βCDs is to substitute organic solvents such as ethanol in drug delivery systems. For example, tretinoin complexes with βCD showed $3.4x10^5$ times higher solubility in

comparison to free tretinoin.[131]

2.4.1.2. Inclusion complexes of curcumin and its analogs with βCD

Application of βCD as a carrier for curcumin has drawn the attention of researchers lately. It was found that the inclusion of curcumin in βCD improved its cellular uptake and enhanced *in vitro* toxicity towards various prostate cancer cell lines.[103] In addition, the anti-proliferative and anti-inflammatory effects of curcumin and its half-life in cells increased via complexation with βCD in comparison to free curcumin.[101] Curcumin encapsulated in HP-βCD showed 3 times higher oral bioavailability in comparison to free curcumin at the same dose *in vivo.*[132] Moreover, a difluorinated curcumin complex with βCD showed a half IC_{50} value compared to the drug alone in different cancer cell lines.[133]

2.4.1.3. Cyclodextrin-based nanoparticles

As stated earlier, hydrophobic drugs can be encapsulated in the internal cavity of CDs by forming non-covalent bonds. The ability of CDs to encapsulate and solubilize hydrophobic drugs renders them suitable carriers in cancer therapy. For instance, βCD and its derivatives are used to increase the solubility of a number of anticancer drugs such as doxorubicin[134], paclitaxel[135] and cisplatin[136].

In addition to the traditional pharmaceutical role of CDs as solubilizer and stabilizer, CD-based nanoformulations have been used as drug delivery agents. Drug-in-CD-in-liposomes are nanoformulations in which the drug/CD complex is placed in the central aqueous core of the liposomes. In other words, the hydrophobic drugs will be carried by CDs instead of incorporation into the lipid bilayers. In this case, the drug does not change the structure of bilayers and the drug/CD complex is protected by liposome.[137] Furthermore, elastic liposomes can be utilized to encapsulate the drug/CD complex to enhance the penetration through skin similar to a system comprised of meloxicam-in-βCD-in-elastic liposome as a transdermal delivery system.[138] However, in this system there is a possibility that lipid components of liposome compete with the drug for the hydrophobic cavity and consequently obliterate the structure of the liposome. However, when the drug shows high affinity to CD, the liposome structure remains intact. For example, upon the inclusion of betamethasone in βCD derivatives in liposome made of cholesterol and other lipids, no liposomal deformation was observed.[139]

CD-grafted polymers are synthesized to provide multiple CD moieties to enhance drug inclusion

either by cross-linking of CDs or combining polymers with CDs.[140] Different compounds have been employed to cross-link CDs. To create a linear βCD-based polymer, the backbone was formed by cross-linking βCDs with polyethylene glycol (PEG).[141] Another study showed that βCDs can be covalently conjugated on the PEG backbone to build CD-flanking polymers, thus fabricating various types of self-assembling structures upon the inclusion of suitable guest molecules.[142]

Amphiphilic CDs are noteworthy CD derivatives synthesized by conjugation of various functional groups to enhance self-assembly and interaction of CDs with biomembranes.[143] They can be divided into three subcategories based on the nature of the conjugating components: neutral, cationic and anionic CDs. Neutral amphiphilic βCDs are synthesized by attaching aliphatic chains (five-carbon) with amide or ester linkers to the primary and secondary faces. These non-surfactant amphiphiles form nanospheres with a size of less than 300 nm. The CD moieties formed 1:1 mole ratio inclusion complexes with aromatic-bearing guest molecules.[144] Another group synthesized amphiphilic CDs by transesterification of CDs on the primary face with vinyl-acyl esters.[145] CD-grafted decanoic alkyl chain formed nanoparticles in the shape of nanospheres or nanoreservoirs with particles of sizes in a range of 70-220 nm which was used to load lipophilic artemisinin.[146] Cationic amphiphilic βCDs synthesized by substitution of alkyl groups on a primary face and ω-amino-oligo-(ethylene glycol) on a secondary face were able to form different nanoparticles and bilayer vesicles based on the chemical nature of the alkyl group.[147]

Cationic amphiphilic βCDs[148] and cationic polymer containing βCDs[149] have been used as promising nonviral gene delivery agents. Moreover, co-delivery of genes and drugs increased transfection efficiency[150,151], provided synergistic effects and decreased multidrug resistance[150] associated with P-glycoprotein efflux pumps. Sophisticated core-shell nanosystems were designed by grafting βCD on a cationic polymer with a hydrophobic polymer included in βCD as guest. This multifunctional nano-assembly system contains a hydrophobic core to load the hydrophobic drug and cationic surface to interact with DNA simultaneously.[152]

2.4.2. Cationic gemini surfactant as a delivery agent

Gemini surfactants, coded as m-s-m, are a family of surfactants composed of two tails of aliphatic chains (length of m) and two polar head groups attached to each other via a spacer

(length of s).[153] Quaternary ammonium ions can be used as the head groups in cationic gemini surfactants (Figure 2.6).

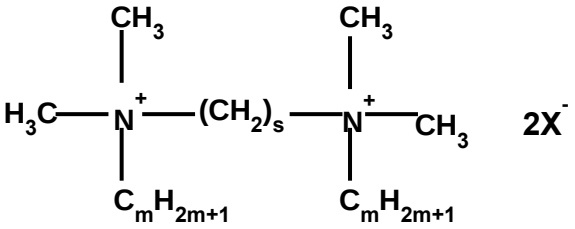

Figure 2.6- m-s-m structure of gemini surfactants.

Favorable characteristics of the gemini surfactants in comparison to mono cationic surfactants are their lower critical micelle concentrations (CMC)[153,154] and lower toxicity[155]. Cationic gemini surfactants are appropriate candidates for non-viral gene delivery, competing with the viral vectors. Their self-aggregation behavior is based on three types of interactions: intramolecular, intermolecular and interaction with solvent molecules.[156] The self-aggregation behavior of gemini surfactants results in the formation of various morphological structures which can be defined by the surfactant packing parameter, S,

$$S = \frac{\nu}{l a_0} \qquad \text{Equation (2.1)}$$

where ν and l are the volume and the length of hydrocarbon tail, respectively and a_0 is the surface area of the head group. Surfactant packing parameter is an indicator of the curvature of the structures. For example, spherical micelles with high curvatures have the packing parameter of 0.3.

Gemini surfactants have the potential to build LLC mesophases in excess of water similar to amphiphilic molecules. For example, the quaternary diammonium gemini surfactant (12-3(OH)-12) showed micellar aggregations altering to lamellar, hexagonal and monoclinic liquid crystalline mesophases at different concentrations and temperatures.[157] In another study, it was reported that ammonium and phosphonium based gemini surfactants demonstrate a bicontinous cubic phase. Quaternary ammonium gemini surfactants with higher lengths of tails displayed cubic, lamellar and hexagonal arrangements in their phase diagrams.[158]

The length, flexibility and nature (hydrophobic or hydrophilic) of the spacer are important parameters that affect the self-assembling behavior. Cationic gemini surfactants bearing

alkanediyl spacers, consisting of 5-6 carbon atoms[153] and bulky head groups[159] have the highest CMC values. Arginine-based gemini surfactants having a spacer length of 3 or 6 carbons showed lamellar and hexagonal phases whereas with the spacer of 9 carbon atoms only the lamellar phase was observed.[160] Comparison between 12-s-12 and 12-EOx-12 gemini surfactants showed that increased hydrophilicity of the spacer in 12-EOx-12 gemini surfactants will lead to the development of various LLC phases.[161] As well, the nature and length of the hydrocarbon tail and the type of the counter ion impact the phase behavior of gemini surfactants. Variable LLC phases such as a bicontinous cubic phase and intermediates were observed with a 16-s-16[162] gemini surfactant in comparison to 12-s-12 gemini surfactant[163]. The ion binding capability of aromatic counterions is higher than halide counterions (Cl^- and Br^-) leading to the formation of worm-like micelles instead of spherical micelles in monomeric cationic surfactants.[164]

Various generations of cationic gemini surfactants have been synthesized by different research groups to date and their efficacy in gene delivery[165-168] has been investigated extensively. Cationic nanoparticles of a 16-3-16 gemini surfactant have been used to enhance the skin penetration of interferon-γ-genes in mice models.[169,170] The gemini surfactants in our study are imino substituted gemini surfactants with different length of hydrocarbon tails as follows: 12-7NH-12 (Figure 2.7), 16-7NH-16 and 18-7NH-18:1.

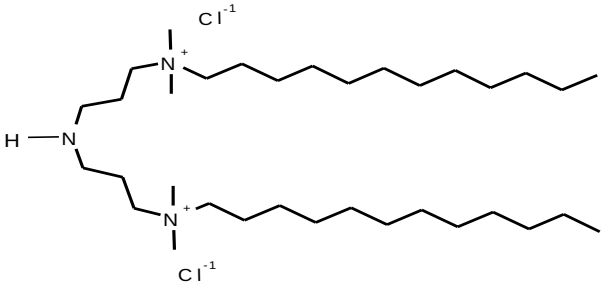

Figure 2.7- Molecular structure of 12-7NH-12 Gemini surfactant

Gene delivery efficacy of the 12-7NH-12 gemini surfactant was evaluated in COS7 cells using luciferase and the results showed higher protein expression even without helper lipids in comparison to other non-substituted or aza-substituted gemini surfactants. The spacing between each ammonium head group and the NH calculated as 5.1 Å which is the optimum distance to interact with DNA phosphate groups.[166]

2.4.3. βCDgemini surfactants

βCDgemini surfactants were synthesized[3] by mono-substitution of the gemini surfactants (12-7NH-12, 16-7NH-16 and 18-7NH-18:1) on O6 of the βCD via an ester or amide linkage (Figure 2.8) and are promising delivery agents *in vitro*. Theoretically, the lipophilic inner cavity of βCD in a βCDgemini surfactant can accommodate NC 2067 similar to the host-guest inclusion systems of βCD, while the hydrophilic outer membrane can increase the solubility of the poorly soluble drug. The tails of the gemini surfactant have the potential to self-assemble and form nanoparticles. Moreover, the cationic ammonium head groups will facilitate the attachment of the delivery system to a negatively charged cell surface. However, based on the average dimension of a linear hydrocarbon chain (4.85 Å), it is possible that the βCD cavity will accommodate hydrophobic tails. Studies showed that the hydrocarbon tails of gemini surfactants and other types of surfactants are able to be placed inside the cavity of various CDs.[171-180] Mutual interactions between a gemini surfactant and βCD can alter both the aggregation behavior of the gemini surfactant and the ability of βCD to accommodate another guest molecule. A major consequence of the inclusion of a gemini surfactant in βCD is that it can avoid or delay the self-assembly of the gemini surfactant. Accommodation of the hydrophobic tails of a gemini surfactant, bis (dodecyl dimethylammonium) diethyl ether dibromide (12-EO1-12), in βCD altered the micellization behavior of the gemini surfactant.[173] In another study on the complex system made of a cysteine-based anionic gemini surfactant inclusion in βCD, increasing the concentration of βCD resulted in an increase in the critical micelle concentration (CMC) as the gemini surfactant monomers became unavailable to self-assemble in the presence of the βCD cavity.[178] In the case of the βCDgemini surfactant, where the gemini surfactant is attached to the βCD, the possibility of the interaction of gemini surfactant tail(s) with βCD cavity (self-inclusion phenomenon) can play an important role in the physicochemical behavior of the inclusion complexes and supramolecular arrangements of the delivery system in solution. It was previously reported that in a modified βCD, the alkenyl part of the attached amphiphilic moiety can be encapsulated by the cavity.[181]

To comprehend the exact mechanism of the interaction between the guest molecule, NC 2067, and βCDgemini surfactant and also the self-inclusion behavior of βCDgemini surfactant, advanced techniques are required.

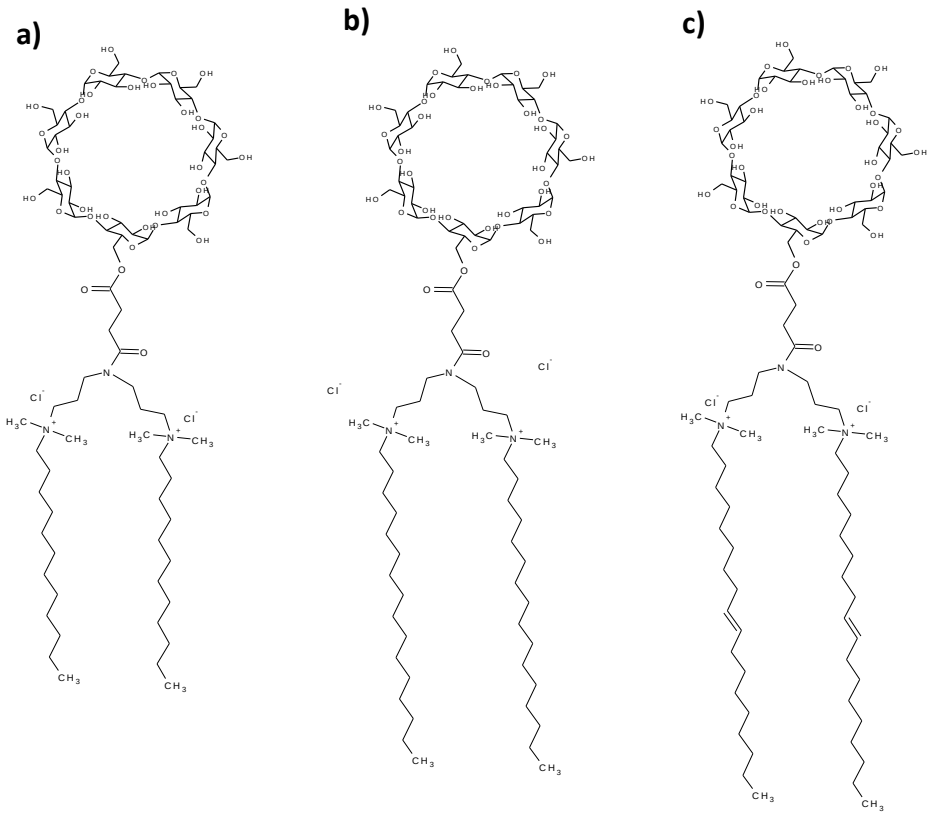

Figure 2.8- Molecular structures of βCDgemini surfactants made of different gemini surfactant moieties: **A)** 12-7N-12, **B)**16-7N-16 and **C)**18-7N-18 attached to βCD.

3. MOLECULAR MECHANISMS OF ANTICANCER AGENTS: FOCUS ON APOPTOSIS

In addition to the physicochemical characterization of the drug/delivery agent complexes, the evaluation of their biological activity is important in the process of drug discovery and development. Several cellular signaling pathways are involved in the procedures resulting in the development of cancer. Monitoring apoptosis, one of the desired pathways for cell death in cancer therapy, is frequently used for the assessment of drug efficacy.

3.1. Apoptosis

Apoptosis is a programmed cell death which is naturally occurring in a variety of cells to maintain homeostasis. The apoptotic stimulation initiates a volunteer suicidal process, resulting in the removal of the unhealthy cells. It is distinct from necrosis, an accidental cell death which develops based on the homicidal factors such as heat, toxic compounds and physical damages. During apoptosis, the cells experience different morphological and biochemical properties distinctive from the necrotic characteristics. Apoptotic morphological changes involve nuclear cell shrinkage[182], cytoskeleton disintegration[183], chromatin condensation[184], DNA fragmentation[185], membrane budding and formation of apoptotic bodies. Phagocytes recognize and engulf the apoptotic cells through the phosphatidylserine (PS) exposure signaling.[186,187] Studies showed that the presence of PS on lymphocytes and thymocytes experiencing apoptosis, will result in identification by phagocytes.[186] PS is an aminophospholipid located on the inner-leaflet of the cell membrane in normal cells. During apoptosis, PS will be externalized and localized on the surface of the cell membrane. This phenomenon, featuring the redistribution of the plasma membrane phospholipids, occurs before other hallmarks of apoptosis such as release of cytochrome *c* and decrease of the mitochondrial membrane potential happen.[188] The asymmetric presence of PS on the surface of the cell membrane, known as apoptotic flag, is used as a probe in flow cytometry assays to confirm apoptosis. In such assays, the fluorescent-labelled Annexin-V is used to bind to PS in the presence of calcium ions.[189] Conversely, cell death through necrosis pathway is initiated by cellular/organelle swelling and bursting, leading to inflammation and immunological responses.[190]

Apoptosis is a process of three steps: initiation, decision and degradation. At the initiation step, external or internal stimuli participate in the initiation of the signal transduction specific to the

type of the apoptotic pathway. In the external pathway, death receptors commence the apoptotic signals, whereas the internal pathway is initiated by the alterations in cell organelles such as mitochondria, endoplasmic reticulum, nucleus or lysosome. The decision phase involves the activation of caspases and mitochondrial effectors leading to the irreversible point of cell suicide. During the degradation phase, the cell death is completed by drastic alterations in the cell morphology and ultimately the clearance of the cell remnants.

3.1.1. Apoptotic signaling pathways: role of caspases

A hallmark biochemical change in apoptosis is the cleavage of a family of proteolytic enzymes known as caspases. Caspases are a group of cysteine aspartate-specific proteases[191] which are categorized by the size of their prodomain to two groups: initiators and executioners. Initiator caspases such as caspase-2, 8, 9 and 10 have a larger prodomain and are responsible for the caspase cascade initiation. Caspase-3 and 7 are executioners with a smaller prodomain. Caspases are able to be activated by two different pathways in apoptosis: extrinsic and intrinsic routes. The extrinsic pathway is triggered by cell death receptors and has a less significant role in chemotherapy-induced apoptosis.[192] Extracellular ligands, such as tumor necrosis factor (TNF) and Fas can form complexes with cell surface receptors to develop a death-inducing signal complex (DISC) which can activate the initiator caspases-8 and 10 (Figure 3.1).[193] Different internal stimuli such as cytotoxic agents, hypoxia and DNA damage activate the apoptosis via the intrinsic pathway. Chemotherapeutic agent-induced apoptosis is predominantly through the intrinsic pathway. Mitochondria, as the foremost players in this pathway, receive the signals from Bcl-2 protein family members which regulate the mitochondrial signal transduction.[194] Bcl-2 family comprises proapoptotic (Bid, Bad and Bim) and antiapoptotic (Bcl-2 and Bcl-xL) proteins.[195] Mitochondria release different proapoptotic proteins such as cytochrome *c* into the cytoplasm which can trigger caspase-9 via formation of apoptosome complex (cytochrome c/Apaf-1/caspase-9) and subsequently activate caspases-3 and -7 (Figure 3.1).[196] Caspases are synthesized in an inactive form and can be stimulated through proteolytic cleavage by upstream proteases in a cellular cascade.

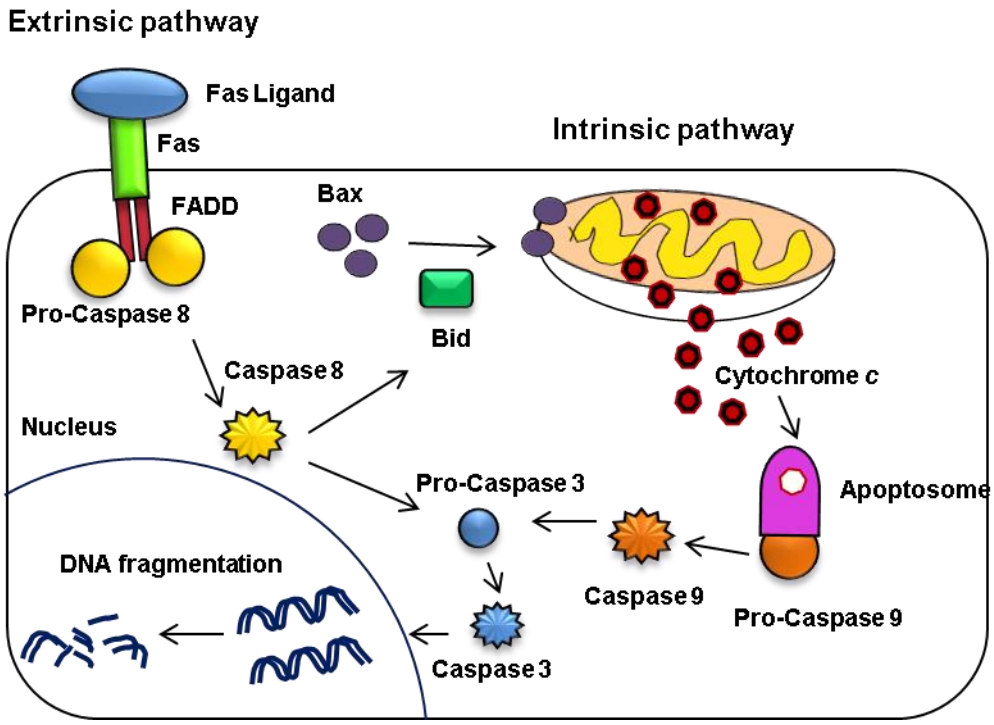

Figure 3.1- Simplified schematic of the intrinsic and extrinsic apoptotic pathways. Apoptosis pathway can be initiated through different sites, for instance, at the plasma membrane by ligation to cell death receptors such as Fas in extrinsic pathway or at mitochondria by activation of proapoptotic proteins such as Bax. In extrinsic pathway death receptor activation, activates caspase-8 and -3 and in the intrinsic pathway, cytochrome c release from mitochondria will form apoptosomes and consequently activates caspase-3.

3.1.2. Apoptosis in cancer cells: role of mitochondria

Oncogenic alterations in cancer influence the routine behavior of the cells. The most important changes occur in mitochondria and include the energy metabolism remodeling[197], increase in reactive oxygen species (ROS)[198] and resistance to apoptosis.[199] Chemotherapy, as one of the principal strategies to contend with cancer, performs its role by inducing apoptosis in cancerous cells. In addition, anticancer treatments seek strategies to target the cancer cells without affecting the normal cells.

Mitochondria (cell furnace) are key player organelles associated with different physiological activities in mammalian cells from energy production through metabolism to apoptotic cell death. Mitochondria are dynamic organelles made of two membranes (outer and inner) and the space between these two layers and within the inner membrane named as intermembrane space (IMS) and matrix, respectively.

Energy production in cancer shifts from the common metabolic oxidative phosphorylation to

lactic acid fermentation (Warburg theory).[200] Moreover, ROS, such as H_2O_2 produced by mitochondria, play an important role in regulating cell death.[201] Increased amount of ROS in cancer results in oxidative stress and finally death.[202] Cancer cells are able to evade apoptosis through various molecular mechanisms such as inactivation of transcription factor p53[203], downregulation of caspases[204], upregulation of antiapoptotic proteins such as inhibitors of apoptosis protein family (IAPs)[205] and even the death receptor (e.g. Fas) inhibition.

As it was mentioned earlier, mitochondria release proapoptotic proteins to activate caspases. The mitochondrial permeabilization can be triggered by two proposed mechanisms including mitochondrial membrane permeabilization (MMP) and mitochondrial permeability transition (MPT). MMP, known as a point of no return in cell death, is regulated by proapoptotic members of Bcl-2 family specifically Bcl-2-associated X protein (Bax) and Bcl-2-associated killer (Bak) proteins. The reconformation and oligomerization of these proteins build channel-like pores in the mitochondrial outer membrane which results in the release of cytochrome *c* from IMS into cytoplasm.[206] Release of cytochrome *c* from mitochondria triggers the activation of caspase -3 and -9.[207] Furthermore, MMP makes the transmembrane potential ($\Delta\Psi_m$) to decrease which can damage mitochondrial normal functions and increase ROS generation.[208]

Furthermore, oxidative stress can increase the Ca^{2+} release from endoplasmic reticulum (ER)[209] and subsequently enhance the Ca^{2+} uptake by mitochondria. This charge imbalance triggers the opening of the protein pores and induces MPT leading to mitochondrial swelling, membrane disruption and release of the proapoptotic agents.[210]

3.2. Molecular mechanism of apoptosis induced by curcumin and its analogs in cancer cells

Signal transduction pathways and morphological alterations, associated with curcumin-induced apoptosis, have been studied in different cancerous cell lines, revealing the cell-type dependent response to curcumin. Curcumin can induce apoptosis via both intrinsic and extrinsic pathways and apoptotic morphological hallmarks such as cell shrinkage and chromatin condensation are associated with the process.[211] Based on a microarray study, curcumin treatment can alter the expression of 104 apoptosis-associated genes out of the total 214 genes.[89] This study suggested that apoptosis induced by curcumin was controlled by various signal transduction pathways such

as mitochondrial pathway, caspase-mediated pathways, cell proliferation pathway (c-myc), cell survival pathway (Bcl-2 family and XIAP), tumor suppressor pathway (P53), cell death receptor pathway and protein kinase pathways (Table 3.1).

Curcumin demonstrated its proapoptotic activity in cervical cancer cells through the mitochondrial pathway by decreasing the expression of the antiapoptotic proteins such as Bcl-2 and Bcl-xL, increasing the expression of the proapoptotic proteins (e.g. Bax and AIF), releasing cytochrome *c* and activating of caspase-9 and 3.[212] In colorectal cancer cells, curcumin induced apoptosis by upregulating Bax and p53, downregulating Bcl-2 and survivin, decreasing mitochondrial membrane potential, releasing cytochrome *c* and activating caspase-3 and 9. [213] Curcumin was able to induce apoptosis in colon cancer by caspase-3 activation, mitochondrial membrane potential collapse, cytochrome *c* release, ROS generation, inhibition of Bcl-2 and increase of Bax, p53 and p21 and Ca^{2+} levels.[214]

Another study on gastrointestinal carcinoma cell lines confirmed that curcumin induced mitochondrial-dependent apoptosis via ER stress leading to alterations of Ca^{2+} levels in mitochondria, ER and cytoplasm. In addition, curcumin activated different caspases (3, 7, 8 and 9) associated with both intrinsic and extrinsic apoptotic pathways.[215] The impact of Ca^{2+} accumulation on mitochondrial apoptosis induced by curcumin at 25 μM concentration in hepatocellular carcinoma was described using a calcium chelating agent. The reduction in the intracellular Ca^{2+} resulted in decrease in ROS generation, caspase-3 and $\Delta\Psi m$ and increase in cell viability.[216]

In a lung cancer model, curcumin stimulated the ER stress, mitochondrial-mediated apoptosis and caspase-3 activation at 30 μM concentration.[217]

Another investigation demonstrated that curcumin promoted apoptosis via increasing the ROS and Ca^{2+} levels, decreasing the MMP, caspase-3 activation, antiapoptotic protein Bcl-2 inhibition and proapoptotic Bax protein increase.[218] In a human cutaneous squamous cell carcinoma cell line, curcumin acted as a pro-oxidant and increased ROS generation.[219] It was reported that curcumin inhibited the antiapoptotic protein expression (Bcl-2, Bcl-xL, survivin, XIAP) and enhanced the proapoptotic protein expression (Bax, Bak, PUMA, Bim, Noxa and cell death receptors) in prostate cancer cells.[220]

Furthermore, the molecular mechanisms of a number of curcumin analogs/derivatives were investigated. *Bis*-dehydroxy-curcumin induces ER stress, caspase activation and mitochondrial-

mediated apoptosis in colon cancer.[221] The anticancer activity of bis-demethoxy-curcumin towards breast cancer was associated with elevated ROS production, reduced mitochondrial membrane potential and p53 activation.[222] A tropinone-curcumin analog, named P1, inhibited the NF-κB pathway (DNA transcription factor known as for cell survival) and increased mitochondrial ROS generation at a lower concentration compared to curcumin in different cancer cell lines.[223] It was shown previously that two other mono ketone curcumin analogs, EF24[224] and GO-Y030[225], structurally similar to P1, induced apoptosis via NF-κB inhibition as well. The anti-proliferative effect of NC 2067 toward HCT-116 human colon cancer cell line has been evaluated recently.[226] The NC 2067 IC_{50} value towards HCT-116 cells was 0.65 μM while it was significantly less toxic toward normal colon cells, with a selectivity index of more than 39. Moreover, NC 2067 was able to decrease the mitochondrial membrane potential, increase ROS generation and produce mitochondrial swelling in isolated rat liver mitochondria. NC 2067 interacted with glutathione as a thiol alkylator which may circumvent genotoxicity that is a major deficiency of many anticancer drugs.[226]

Several studies showed that curcumin encapsulated by delivery agents enhanced its solubility and bioavailability and retained the ability of the drug to induce mitochondrial-dependent apoptosis. An inclusion complex of curcumin in hydroxylpropyl cyclodextrin (HP-CD) can stimulate apoptosis via ROS generation, mitochondrial membrane potential decrease and Ca^{2+} accumulation in lung cancer line.[227] Incorporated in solid lipid nanoparticles, curcumin retained its proapoptotic activity by releasing cytochrome *c*, reducing the mitochondrial membrane potential and causing caspase activation in various cancer cell lines.[228]

Similarly, curcumin and its analogs induced apoptosis through various alterations in signaling molecules and pathways in melanoma cells. It has been reported that curcumin was able to increase caspase-3 expression along with the decrease in c-myc oncogene expression in a concentration-dependent manner in A375 melanoma cell line at 30 μM concentration.[229] Another study on the same cell line showed that curcumin at concentrations more than 10 μM induced apoptosis by a decrease in cell proliferation proteins such as activators of transcription 3 (STAT3) and Bcl-2.[230] Curcumin caused apoptosis through the death receptor pathway by accumulation of Fas and activation of caspase 8 and 3 in various melanoma cell lines without any effect on p53.[231] Moreover, it was reported that curcumin at a low concentration of 5 μM did

not alter the mitochondrial membrane potential.[232] One of the mechanisms that cancer cells develop to evade apoptosis, is the activation of NF-κB.[233] Curcumin blocked NF-κB activity and induced apoptosis by caspase-3 activation in mouse melanoma cells.[234] Moreover, the inhibitory effect of curcumin on NF-κB was investigated in other melanoma cell lines revealing independence from BRAF/MEK/ERK and Akt pathways.[235] Another investigation demonstrated that in the A375 melanoma cell line, curcumin performed its anti-proliferative activity via downregulation of NF-κB and upregulation of p53 in a dose- and time-dependent manner.[236] As well, curcumin triggered apoptosis through ER stress enhancement, Ca^{2+}-ATPase pump inhibition and antiapoptotic protein inhibition in murine melanoma cells in a dose-dependent manner.[237]

Different curcumin analogs showed proapoptotic effects mostly through the mitochondrial mediated pathway showing caspase-3, 7, 9 activation and mitochondrial membrane potential decrease in melanoma cells. For example, a synthetic diphenyl curcumin-related compound was able to activate caspase-3 and 7, decrease mitochondrial membrane potential and increase cytochrome *c* release in a melanoma cell line and inhibit tumor growth in a melanoma mouse model.[109] Another curcumin analog, DM_1 induced apoptosis in the A375 melanoma cell line through downregulation of the antiapoptotic Bcl-2 proteins (e.g. Mcl-1 and Bcl-xL) and the inactive form of caspase-3 and upregulation of the active form of caspase-9.[238] FLLL32, a curcumin analog, synthesized based on the diketone tautomeric form of curcumin, blocked STAT3 phosphorylation, induced apoptosis in a caspase-dependent manner and lowered the mitochondrial membrane potential in the A375 melanoma cell line.[107] Diphenyl difluoroketone curcumin analog (EF24) inhibits NF-κB pathway and cyclin D1 (cell cycle regulator) in the B16 murine melanoma cell line.[239]

It was reported that curcumin induced the formation of the mitochondrial permeability transition pores (PTP) by oxidation of the thiol functional groups located on the membrane of the isolated mitochondria which resulted in mitochondrial swelling, mitochondrial membrane potential drop and finally apoptosis.[240] Curcumin analogs synthesized by the substitution of different functional groups on the aromatic rings or cyclohexanone with di-ketone moiety also had an effect on the PTP. It was shown that the presence of the hydroxyl groups on the aromatic ring and di-ketone moiety are crucial to trigger mitochondrial swelling.[241]

Overall, curcumin and its analogs have the potential to induce apoptosis in various melanoma cell lines via regulation of multiple molecules such as the death receptor mediated pathway, caspase-3 activation, decrease in antiapoptotic proteins, oncogenes and cell survival factors. We concluded that the proapoptotic performance of curcumin is related to cell type and experimental protocols.

3.3. Molecular mechanisms of cell cycle arrest induced by curcumin and its analogs in cancer cells

Curcumin can affect cell cycle phases. Morphologically, in G_1 phase, the cell increases in size and chromosomes arrange for replication, in the S phase, DNA replication occurs, in the G_2 phase the cell grows once again and in the M phase mitosis arises.

Most of the studies on the effect of curcumin treatment on cell cycle phases showed G_2/M cell cycle arrest. It has been shown that curcumin at low concentrations (5-10 μM) was able to arrest the cell cycle at the G_2/M phase in lung carcinoma.[217] Moreover, curcumin encapsulated in HP-CD retained its effect on G_2/M cell cycle arrest in lung cancer cells.[227] A similar behavior was reported in several studies on various cancer cell lines such as leukemia[218], cutaneous squamous cell carcinoma[219] and bladder cancer where curcumin induced a mitotic spindle defect[242]. The main metabolite of curcumin, tetrahydrocurcumin, inhibited cell growth in breast cancer cells by G_2/M arrest as well.[243] Conversely, curcumin arrested cells at the S phase and G_0/G_1 in colorectal cancer[213] and leukemia[244], respectively.

In addition, the influence of curcumin on the cell cycle was evaluated in melanoma cells. In A375 melanoma cells, curcumin arrested the cells at G_2/M.[236] Similar results were obtained by a curcumin analog, DM6, that inhibited cell growth by blocking the cell cycle at G_2/M.[245] G_0/G_1 cell cycle arrest was also reported by 5 μM concentration of curcumin in the SK-MEL-37 human melanoma cell line.[109]

Table 3.1- Molecular mechanism of curcumin and its analogs in various cancer cells.

Cytotoxic agent	Cancer cell line	Apoptosis							
		Caspase activation	**↑Proapoptotic proteins**	**↓Antiapoptotic proteins**	**↓MMP**	**Cytochrome c release**	**↑ROS generation**	**↑p53**	**↑ER stress**
Curcumin	Cervical[212]	Caspases 9 and 3	Bax, AIF	Bcl-2, Bcl-xL	-	√	-	-	-
	Colorectal[213]	Caspases 3 and 9	Bax	Bcl-2, Survivin	√	√	-	√	-
	Colon[214]	Caspase 3	Bax	Bcl-2	√	√	√	√	-
	Gastrointestinal[215]	Caspases 3,7,8 and 9	-	-	-	-	-	-	√
	Lung[217]	Caspase 3	-	-	-	-	-	-	√
	Leukemia[218]	Caspase 3	Bax	Bcl-2	√	-	√	-	√
	Prostate[220]	-	Bax, Bak, PUMA, Bim, Noxa	Bcl-2, Bcl-xL, Survivin, XIAP	-	-	-	-	-
	Melanoma cells[230-232,235,237]	Caspase 3 and 8	-	Bcl-2	-	-	-	√	√
Bis-dehydroxy-curcumin	Colon[221]	-	-	-	-	-	-	-	√
Bis-demethoxy-curcumin	Breast[222]	-	-	-	√	-	√	√	-
Curcumin Analogs	Melanoma[107, 238]	Caspase 3, 7 and 9	-	Bcl-2, Bcl-xL	√	√	-	-	-

		Cell Cycle Arrest		
		G_0/G_1	**S**	**G_2/M**
Curcumin/ Curcumin Analogs	Melanoma[234]	√	-	-
	Colorectal[214]	-	√	-
	Lung[217], Leukemia[218], Squamous carcinoma[219], Melanoma[236], Breast[243], Bladder[242]	-	-	√

4. PHYSICOCHEMICAL CHARACTERIZATION OF THE HOST-GUEST INCLUSION COMPLEXES USING NON-SYNCHROTRON TECHNIQUES

4.1. βCD-based host-guest complexes

The lipophilic inner cavity of βCD provides an opportunity to incorporate the lipophilic parts of the guest molecules whereas the hydrophilic compartments of the guest molecule interact with the solvent or βCD hydroxyl groups. Therefore, the formation of the βCD complexes depends on the polarity of the guest molecule which dictates the geometrical orientation inside the cavity. Based on the cavity diameter (6-6.5Å), aromatic moieties have the potential to be inserted into the βCD ring through van der Waal forces.[180] Other forces that play a role in host-guest inclusion complexes of CDs are hydrophobic interactions, dipole-dipole interactions and hydrogen bonding. The latter two forces are able to alter the conformational structure of the CD inclusion complexes.[246] No covalent bonds are formed during the inclusion process. Free βCD, free guest molecule and the inclusion complex in solution are at equilibrium. Association and dissociation of βCD/drug complexes occur continuously with rapid rates in the solution.[247] The dissociation of the drug from βCD/drug involves mechanisms such as dilution, competitive dislocation of the drug from the complex, and drug uptake by cells.[247]

The most common stoichiometry between CDs and their guests in binary systems is a 1:1 ratio. Overall, the binding constant (K_{ab}) of a complex containing a guest molecule and βCD can be calculated as:

$aG + bCD \rightarrow G_aCD_b$

$$K_{ab} = \frac{[G_aCD_b]}{[G]^a \times [CD]^b} \qquad (4.1)$$

Where, [G], [CD] and [GCD] are the molar concentrations of the guest, βCD and inclusion complex, respectively. In addition to stoichiometry and binding constant, the structural orientation of the guest molecule inside βCD, potential binding sites and the direction that the guest enters the cavity can give a better understanding of the host-guest inclusion conformation.

4.2. Infrared spectroscopy

Infrared spectroscopy is an efficient technique to evaluate molecular interactions. The infrared photons are not able to excite electrons, but may be large enough to vibrate covanently bonded atoms in the forms of stretching and bending. The comparison of the characteristic peaks in the spectra of a drug in an inclusion complex and a physical mixture can be employed to elucidate the placement of the drug in the βCD molecule. Any shift in the position or absence of the drug distinctive peaks such as carbonyl group in the inclusion complex denotes that the drug is shielded by βCD.[248]

A comparison between the IR spectrum of the inclusion complex of irbesartan and βCD expressed the shift in two absorption peaks of the drug corresponding to C═O and C-N groups at 1731 and 1622 cm^{-1}, respectively, as a result of the interaction with the βCD cavity.[249] When miconazole was included, the two peaks of the drug matching the aromatic ring at 1588 and 1546 cm^{-1} disappeared in the inclusion complex with βCD.[250]

The major challenge with this technique is the lack of the alteration in the drug characteristic peaks which makes the interpretation challenging or impractical. For example, the comparison of the physical mixture and inclusion of EO-9 (anticancer agent) with HP-βCD did not produce any significant changes in the fingerprint region of EO-9 spectrum. The only difference observed was the absence of some very weak peaks in the inclusion spectrum.[251]

There are several studies which compared the FTIR spectra of curcumin inclusion in βCDs with free curcumin to confirm the inclusion formation. For instance, the IR spectrum of curcumin in a complex with βCD showed alterations to the curcumin peaks at 1602 cm^{-1} corresponding to the C=C stretching vibrations of the aromatic rings.[252] Once again, monitoring the peaks associated with the aromatic moieties of the guest molecules can provide useful information on the host-guest interaction.

4.3. Thermal analysis: Differential scanning calorimetry and thermogravimetry

Thermal analyses are routinely used to qualitatively investigate the drug/βCD inclusion formation.[253] Any change in the thermal behavior of drug such as melting point, evaporation, degradation and polymorphic transition can be used. Differential scanning calorimetry (DSC),

recording the endothermic and exothermic events, and thermogravimetry analysis (TGA), evaluating mass changes in response to increase in temperature, can be useful tools in evaluating the nature of the host-guest interactions.

The difference in the thermograms of a physical mixture and inclusion sample in DSC, demonstrates the accommodation of the drug in the βCD cavity. Three regions are observable at βCD thermogram. At around 120 °C a broad peak corresponding to water loss is recognizable, following by the thermal degradation region beginning at 250 °C, and the ignition region occurs at 300 °C.[253] The absence or reduction of the drug melting peak in the inclusion complex represents the complete or partial inclusion formation, respectively.[253] For instance, the DSC thermogram of sulfamethoxazole in a complex with HP-βCD revealed the absence of the endothermic melting peak of the drug at 170.5 ºC in a freeze dried formulation in comparison to a physical mixture.[254] Moreover, the reduction of the characteristic melting peak of benzophenone at 68 ºC in the 1:1 ratio inclusion complex with HP-βCD confirmed that the free drug was still available and the inclusion was not complete.[255]

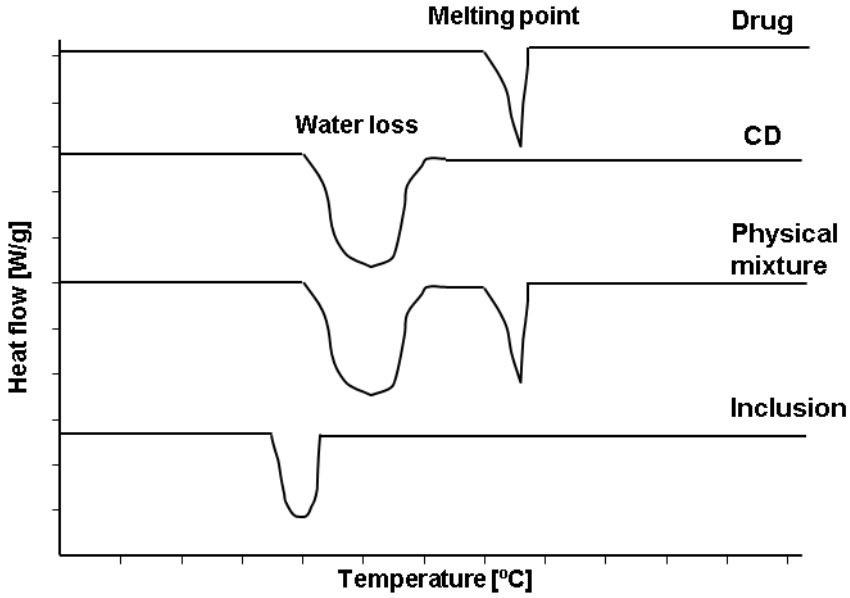

Figure 4.1- Schematic of DSC thermograms of drug, CD, physical mixture and inclusion.

In addition, the shift in the water loss peak of βCD demonstrated the substitution of drug molecules in the cavity (Figure 4.1).[256] In the inclusion of trimethoprim in βCD it was observed that the broad water loss peak of βCD shifted from 117.6 ºC to 118.7 ºC in the inclusion complex

suggesting the placement of the drug molecule into the cavity, changing the energy of the water molecules retained in the cavity.[257]

A TGA thermogram of βCD shows an initial weight loss (< 100 °C) according to the water evaporation succeeded by a major mass loss due to degradation which occurs at 250-400 °C.[258] The incorporation of a drug molecule in βCD, increases the degradation temperature.[256]

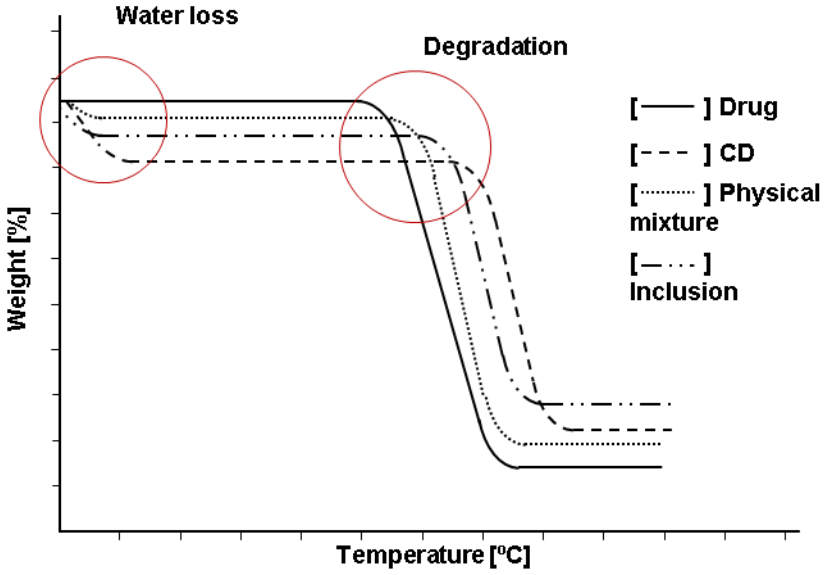

Figure 4.2- Schematic of TGA thermograms of drug, CD, physical mixture and inclusion.

For example, the inclusion of pyrimethamine in HP-βCD started to decompose at a higher temperature compared to the free drug (190 ^{0}C).[259] Since in the inclusion complex, the water molecules departed from the βCD ring already, the mass loss is less at the water loss region (Figure 4.2).[256] In another thermogravimetric study, the inclusion complexes of glimepiride with βCD, HP-βCD and sulfobutylether-βCD (SBE-βCD) also displayed lower water loss than the physical mixtures.[260] Thus, the degree of water loss can be used as an indication of formation of inclusion complexes.

4.4. UV/Visible spectroscopy

Monitoring the drug chromophore UV spectrum, an increase/decrease in the absorbance peak without changing the λ_{max} or a shift in λ_{max} was interpreted as inclusion confirmation. For instance, the UV spectrum of purine nucleosides in the presence of βCD showed a decrease in

absorption at 205 and 260 nm.[261] Furthermore, two major absorption peaks of ibuprofen at 258.5 and 266 nm showed a red shift in the presence of βCD.[262] Addition of βCD to diazepam caused a shift and decreased the intensity of the UV absorbance peak at 229 nm.[263]

Evaluation of the UV absorbance of NC 2067 in the presence of the βCD revealed an insignificant decrease, while in a βCDgemini surfactant, absorbance decreased significantly up to a βCDgemini surfactant: drug mole ratio of 2:1.[3]

4.5. Phase-solubility diagram

To evaluate the interaction between a drug and its carrier Higuchi and Conners suggested a model[264] to describe the βCD in complex with drug molecules (Figure 4.3).[265] A-type phase-solubility diagrams correspond to the profiles in which the solubility of the drug increases with the increase of the βCD concentration, resulting in a soluble complex. On the other hand, B-type phase solubility indicates the formation of insoluble complexes where the concentration of drug decreases at higher βCD concentrations.[264] The stoichiometry between drug and βCD can be estimated by subcategories of the A-type diagram (A_L, A_P and A_N). The linear correlation between drug solubility and βCD concentration in A_L profile indicates the 1:1 mole ratio for drug: βCD complex.

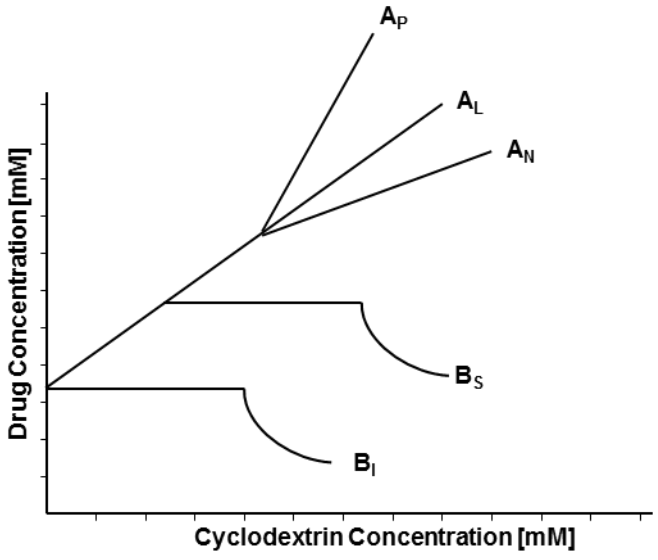

Figure 4.3- Different phase solubility diagrams of CD inclusion complexes.

In A_N profile, after a certain concentration of βCD, the positive gradient turns to negative which indicates that the drug: βCD ratio is smaller than 1. The A_P profile of the complex corresponds to the diagram in which, after a certain concentration of βCD, the positive gradient increases, suggesting formation of drug/βCD complex at a ratio larger than 1. Thus, based on the phase-solubility diagram, the stoichiometry of the drug/βCD inclusion complexes can be determined.[266-268]

When the phase-solubility profile is A_L type, the inclusion binding constant K_s (or $K_{1:1}$) can be calculated using the diagram slope and intrinsic solubility of the drug (S_0) as below:

$$K_{1:1} = \frac{slope}{S_0(1-slope)} \qquad (4.2)$$

$K_{1:1}$ value determines the strength of binding between the drug and βCD in the inclusion complex as shown in Table 4.1.[269]

Table 4.1- Inclusion bond strength according to $K_{1:1}$

$K_{1:1}$ value [M^{-1}]	**Bond strength**
<500	Very weak
500-1000	Weak
1000-5000	Moderate
5000-20000	Strong
>20000	Very strong

The inclusion complex of curcumin and its derivatives with βCD characterized by phase solubility diagram and proposed a drug: βCD ratio of 1:2.[102,133]

4.6. Nuclear Magnetic Resonance (NMR)

NMR is the most commonly used technique for structural characterization of the drug/βCD inclusion complexes by monitoring the chemical shift changes of proton (^{1}H-NMR) or carbon (^{13}C-NMR) atoms of the host (βCD) and/or the guest molecule (drug).

4.6.1. 1D proton NMR (^{1}H NMR)

4.6.1.1. Inclusion formation: chemical shift changes

^{1}H NMR shifts outline the different hydrogen environment based on the shielding or deshielding effect of the atoms located in the neighborhood. Protons of βCD are spatially located internal or external of the cavity (Figure 4.4). H_3 and H_5 are placed inside the cavity in a manner that H_3 is closer to the wider rim and H_5 to the narrower opening. Locations of the H_1, H_2 and H_4 are on the outside of the cavity whereas $H_{6,6'}$ are positioned closely on the smaller rim (Figure 4.4). Upon inclusion of an organic compound into βCD cavity, the internal protons (H_3 and H_5) and in some cases H_6 commonly show upfield chemical shifts compared to the empty βCD. For instance, upon an inclusion of a curcumin analog in βCD, chemical shift changes ($\Delta\delta=\delta_{complex}-\delta_{free}$) of 0.016 and 0.008 ppm observed for H_3 and H_5, respectively.[133]

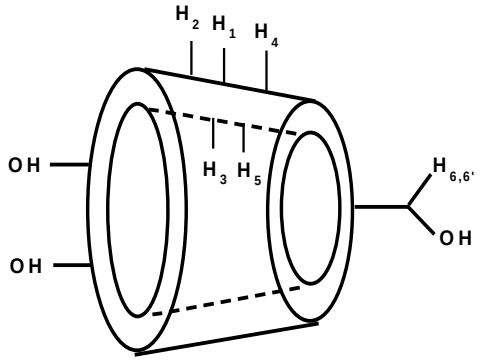

Figure 4.4- Location of the interior and exterior protons of βCD.

The presence of the π-electron rich groups such as aromatic rings is the main reason for the upfield shifts in the inclusion complexes of CDs which is known as an anisotropic effect. The upfield shift (shielding effect) in the inclusion complex of a few compounds containing aromatic rings with CDs has been demonstrated in the literature.[270-274]

It is challenging to elucidate conformational parameters of the inclusion complex solely based on 1D NMR data. However, there are several studies that compared the magnitude of the Δδ of the internal protons to speculate the depth and direction of the guest molecule entrance into βCD cavity. Equal values of $\Delta\delta_{H3}$ and $\Delta\delta_{H5}$ have been reported as an evidence of the deep placement of the guest molecules inside CD ring.[270,275,276] In others, the alteration in the chemical shift of only one of the internal protons (H_3 or H_5) was applied to describe the superficial interaction.[277]

Moreover, the comparison between the chemical shifts of the internal protons demonstrates the direction from which the guest molecules enter the CD cavity. It was shown that in the inclusion complex of naringenin with βCD, $\Delta\delta_{H3}$ (0.03ppm) was greater than $\Delta\delta_{H5}$ (0.01ppm).[278] Conversely, the inclusion of barbigerone in HP-βCD displayed Δδ values of 0.017 ppm and 0.042 ppm corresponding to H_3 and H_5 proposing that the insertion direction was from the narrow opening of the cavity.[279] Similar behavior was observed when omeprazole penetrated into the methylated derivative of βCD with chemical shift changes of 0.054 and 0.086 for H_3 and H_5, respectively.[280] Other evidence that may contribute to the concept of the insertion through the narrower rim is the upfield shift in the H_6 protons located at the edge of the smaller opening.[280] The interaction of celecoxib and βCD in freeze dried formulation revealed a significant chemical shift in the NMR spectrum for H_5 (0.06-0.07 ppm). Moreover, the shift in H_3 (0.01 ppm) and celecoxib protons (0.01-0.03 ppm) confirmed the deep inclusion of the drug in βCD.[271]

Furthermore, in the case of the guest molecules with sufficient aqueous solubility, NMR has the potential to discover which part of the guest molecule can interact with the βCD cavity.[281] A ^1H NMR study on digoxin encapsulated within βCD showed that digoxin was incorporated into the cavity from its A-ring according to the higher Δδ of the 19-methyl protons of digoxin in comparison to 18-methyl protons.[281]

4.6.1.2. Determination of the host-guest stoichiometry: Job's plot

One of the routine methods used to determine the stoichiometry of the guest inclusion in βCD is a continuous variation method known as Job's plot.[282] The modified Job's plot for NMR studies where the host-guest complexation rate is fast, can be calculated by the difference of the chemical shifts, $\Delta\delta = \delta_{Complex} - \delta_{Host \text{ or } Guest}$ which is proportional to the complex concentration. Thus, in the case of chemical shift alterations of βCD in inclusion, Δδ × [βCD] can be plotted as a function of mole fraction (r). The maximum point in a plotted graph corresponds to the stoichiometry of the inclusion complex.[283] Stoichiometry of 1:1 and 1:2 correspond to the maximum point of 0.5 and 0.66, respectively. While, Job's plot is able to show the 1:2 guest to host mole ratio theoretically, the simultaneous presence of GH and GH_2 complexes might result in erroneous determination of the actual stoichiometry by this method.[284]

The stoichiometry of several guest molecules such as tulfenamic acid and flufenamic acid, in complex with βCD have been calculated as 1:1 mole ratio based on Job's plot.[274,285] Few other

studies used Job's plot on NMR data to confirm the stoichiometry of 1:2 (guest to host mole ratio).[286]

4.6.1.3. Calculation of the binding constant: Scott's plot

To calculate the binding constant of the host-guest inclusion with 1:1 mole ratio, adopted form of the famous Benesi-Hildebrand equation[287], called Scott's equation[288] (Equation 4.3) can be employed as :

$$\frac{[G]}{\Delta\delta_{obs}} = \frac{[G]}{\Delta\delta_{max}} + \frac{\Delta\delta_{max}}{K_a} \qquad (4.3)$$

where [G] is the guest molar concentration, K_a is the binding constant, $\Delta\delta_{obs}$ and $\Delta\delta_{max}$ are the observed chemical shift in the complex and maximum chemical shift change at the saturation state, respectively. $[G]/\Delta\delta_{obs}$ can be plotted as a function of [G] resulting in the linear curve with a slope of $1/\Delta\delta_{max}$ and intercept of $\Delta\delta_{max}/K_a$. The mathematical models to calculate the binding constants of more complicated systems such as 1:2 are more challenging and need computer-based programs. Association constants of the inclusion of fluconazole[273] and loperamide[272] in βCD at 1:1 mole ratio, were calculated to be 68.7 M^{-1}.

4.6.2. 1D/2D Rotating frame nuclear Overhauser effect spectroscopy (ROESY)

In addition to monitoring the chemical shifts, nuclear Overhauser effect (NOE) provides valuable information regarding the conformational properties of the cyclodextrin-based inclusion complexes. NOE is a change in NMR intensity of a spin when the NMR resonance of the neighbor spin is saturated. This phenomenon results from a dipole-dipole cross-relaxation between nuclei and depends on the magnetic field and mobility of the molecule in solution. NOE-based methods are important techniques to estimate the inter-spin distances. The minimum spatial distance between two nuclei should be 4 Å to show NOE cross-linked peaks. In host-guest complex systems, intermolecular NOEs offer information regarding through space interactions of βCD and the organic guest. However, only small molecules with less than 1000 Da molecular weights show positive NOEs. Macromolecules (more than 5000 Da) provide negative but detectable NOE signals. Inclusion complexes of a small molecule in βCD with molecular weights in the range of 1000-2000 Da demonstrate unfavorable motional correlations which restrict the use of the conventional NOE-based techniques. Rotating frame nuclear Overhauser effect spectroscopy (ROESY) is a suitable technique to specifically detect NOE signals for βCD host guest inclusion complexes. ROESY provides spin lock in rotating frame

which results in the formation of permanent positive NOEs (the intensity of the affected resonances increasing).[289] The 2D ROESY spectrum presents NOE cross-peaks as positive phase and diagonal peaks (1D spectrum) as the negative phase. The selective 1D ROESY technique applies a discerning irradiation region to excite the peak of interest and trace the possible interactive peaks which appear inversely at the spectrum.[290]

Several studies employed 2D ROESY to evaluate the spatial proximity of guest molecules with βCD in form of complex. The ROESY spectrum of naringenin/βCD showed the interaction of the C ring protons of naringenin with H_3, H_5 and H_6 of βCD.[278] In another study, cross-peaks corresponding to internal cavity protons of βCD and C, D and E rings of nimbin, elaborated the structure of nimbin / βCD complex.[291] Inclusion of tryptophan in 6-O-a-D-glucosyl-β-cyclodextrin (G_1-βCD) displayed ROESY cross-peaks between H_3 and H_5 of the cavity and indole protons of tryptophan. Interestingly, another interaction observed between H_3 and H_5 of βCD and protons of β-carbon group in the tryptophan molecule. According to ROESY data, a model was built suggesting that one tryptophan molecule interacts with two G_1-βCDs as a result of deep insertion of the indole ring via the wider rim in one G_1-βCD whereas *gauche* and *trans* protons (β-carbon) penetrated through a wider opening of another G_1-βCD molecule.[292] Based on the ROESY spectra, different modes of econazole nitrate / βCD derivatives complexes have been explained. Econazole can enter the CD cavity mostly through three different orientations involving the interaction of the 4-chlorophenyl moiety, 2,4-dichlorophenyl moiety and imidazole ring.[293]

Moreover, a comparative study of the inclusion complexes of gemini surfactants containing different spacer lengths (alkyl-a,x-bis(dodecyldimethyl ammonium bromide)) with βCD showed that the cross-peak volumes between CD internal protons and H_λ (corresponding to the $7CH_2$ of each hydrocarbon tail) is consistent for gemini surfactants having spacer lengths of 2, 4, 6 and 8 atoms. However, in the case of the gemini surfactant with a 10 carbon spacer the interaction intensity decreased by 5% suggesting the possibility of the interaction of the spacer with the CD cavity.[177] In another study of the inclusion of the gemini surfactant, (dodecyl dimethylammonium) diethyl ether (12-EO1-12) dibromide in βCD, the effect of CD concentration on the inclusion conformation was assessed. It was observed that, at a lower concentration of CD, one hydrocarbon tail located inside the cavity whereas the second tail

interacted with the cavity surface. Increasing the concentration of CD resulted in the interaction of each tail with a different CD molecule.[173]

5. SYNCHROTRON TECHNIGUES FOR CHARACTERIZATION OF HOST-GUEST INCLUSION COMPLEXES AND NANOPARTICLES

As synchrotron-based techniques are significant analytical tools in the characterization of self-assembling LLPs, this chapter describes the theoretical aspects and applications of the synchrotron radiation relevant to nanotechnology.

5.1. Synchrotron radiation

Synchrotron radiation (SR) is a brilliant source of electromagnetic radiation ranging from far infrared to hard X-rays. SR is generated as a result of acceleration of charged particles, usually electrons, which are moving with a speed very close to the speed of light (relativistic velocity).[294]

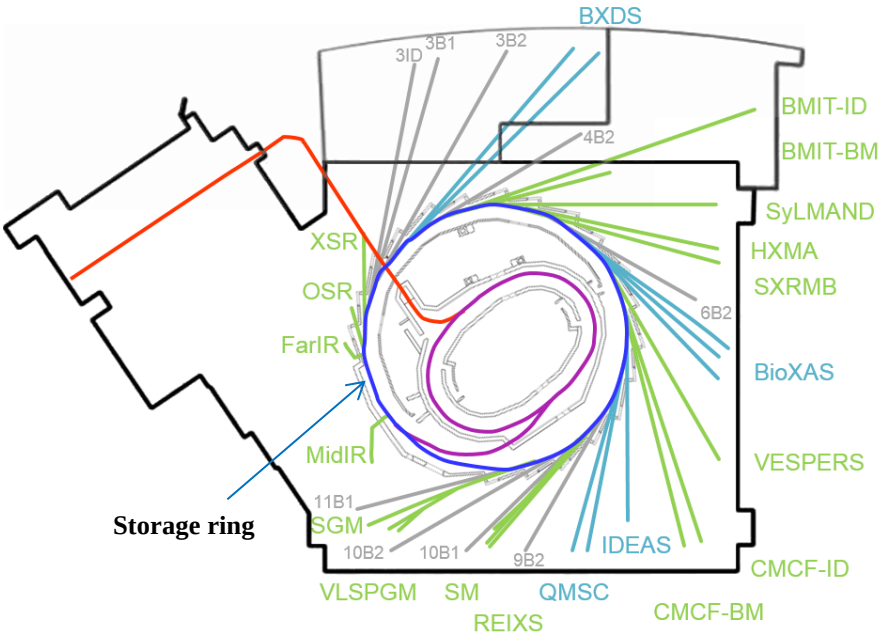

Figure 5.1- A simplified schematic of the Canadian Light Source beamlines

In practice, a specific magnetic field generated in the storage ring by either the bending magnets or insertion devices such as wigglers and undulators bends electron's trajectory which subsequently leads to X-ray radiation.[295] The decreased electron's energy due to creation of electromagnetic radiation is compensated by radio frequency (RF) cavities.[294]

The Canadian Light Source (CLS, Saskatoon, Canada) is a third generation SR facility with a 2.9

GeV storage ring (Figure 5.1). The Canadian Macromolecular Crystallography Facility (CMCF) located at CLS is composed of 08ID-1 and 08B1-1 beamlines providing X-rays in energy range of 5-18 keV, flux of $10^{11} – 10^{12}$ ph/s and variety of beam size.[296]

5.1.1. X-ray source: bench-top *vs* synchrotron

Synchrotron sources of X-ray in comparison to bench-top sources such as X-ray tubes demonstrate exclusive properties which make them versatile tools for research in different fields. Synchrotron sources of X-ray offer higher flux (10^{11}-10^{13} photon/s) in comparison to bench-top sources (10^{8} photons/s) resulting in lower data collection time[297,298] Moreover, SR is well collimated with low divergence and high polarity.[299] The tuneability of SR provides the opportunity to select the preferred wavelength and greater use of a multi-wavelength anomalous dispersion phasing technique.[297] The beam size of synchrotron-based X-ray beamlines is usually smaller than 100 μm but in some cases it is less than 1 μm.[294] Moreover, SR has pulsed nature including short pulses of beam continuing in a separated bunches in which X-ray beam lasts for picoseconds and is divided by nanoseconds breaks.[300] This property allows time resolved studies. From its introduction about 30 years ago SR revolutionized the physicochemical characterization of the biological materials such as pharmaceutically important molecules and improved the precision and specificity of numerous analysis methods.

5.1.2 X-ray scattering techniques

X-ray scattering is an expanding field which has a major role in molecular biology and introduction of synchrotrons facilitated detection of weak scattered X-rays from diluted samples. Macromolecular crystallography and non-crystalline scattering are major techniques employed in biological and medical sciences.

Synchrotron beamlines revolutionized macromolecular crystallography. As of today, more than 100,000 crystal structures of macromolecules have been deposited in the Protein Data Bank (PDB). The crystal structure determination of drug targets (proteins) provides precious knowledge for structure-based drug discovery (SBDD). Today with the development of sophisticated software and automation of the SR data collection, a huge amount of data can be obtained in a short time and employed in lead discovery and screening of new pharmacologically active molecules.[301] In addition, time-resolved crystallography improves the knowledge of molecular dynamics.

Non-crystalline scattering techniques such as small angle X-ray scattering (SAXS) advanced tremendously with the development of new beamlines at the SR facilities. Synchrotron-based SAXS benefits from the high intensity radiation and small sample volume that make it possible to characterize supra-atomic structures of nano-materials.

5.2. Host-guest inclusion characterization by synchrotron X-ray diffraction techniques

5.2.1. X-ray diffraction basics

When X-ray photons interact with matter, two important phenomena, absorption and scattering, occur. In scattering, the photon energy can be either preserved (elastic scattering) or partially conveyed to the material (inelastic scattering). Coherently scattered photons interfere with each other and create a diffraction pattern.[297] In 1913, Bragg (the son) described how the scattering waves with constructive interference from the atoms of a crystal are able to produce a diffraction pattern (Bragg's law).[302] Bragg's peaks in a diffraction pattern are versatile tools to obtain structural information about the scattering element (Figure 5.2).

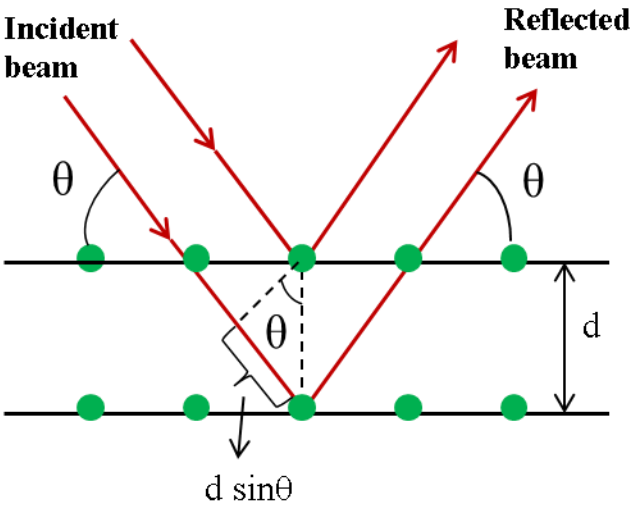

$n\lambda = 2dsin\theta$,
where n is an integer, λ is the wavelength of the incident beam, d is the distances between atomic planes and θ is the angle between incident beam and lattice plane (2θ is the scattering angle, which is the angle between incident beam and scattered beam).

Figure 5.2- Graphical illustration of the Bragg's law

Wide angle X-ray scattering (WAXS) is usually defined when scattering angle, 2θ, is larger than 5°. Depending if powder or a single crystal of a sample is used, it is defined as a powder X-ray diffraction or a single crystal X-ray crystallography. At very low resolution, when the scattering

angle is not much bigger than 5°, only the interatomic distances in the sample can be observed. When the sample diffracts to a higher angle closer to 90°, usually called higher crystallographic resolution, the crystal structure of the molecule can be determined. In pharmaceutical sciences, WAXS can be utilized to determine the atomic structure of drug molecules, drug targets and drug carriers.

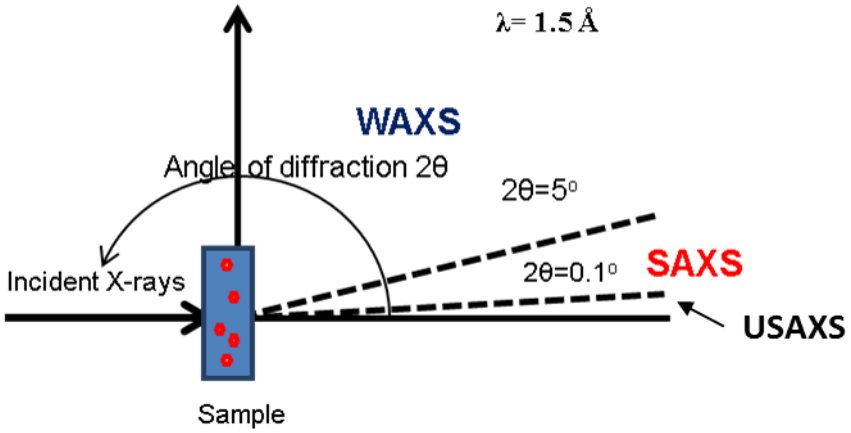

Figure 5.3- Definition of SAXS and WAXS with respect to scattering angle

On the other hand SAXS is an adaptable tool to characterize molecules in solution under the assumption that the molecules do not interact with each other. It is mainly used to study shapes of macromolecules and their complexes. In its "high resolution" range, close to 2θ = 5°, SAXS is used to study supramolecular arrangements of molecules such as liquid crystals and colloidal structures, which are of great pharmaceutical interest since information about the shape and size of nano-particulate drug delivery systems (1-100 nm) can be probed (Figure 5.3).[303]

An ultra-small angle X-ray scattering (USAXS) is covering scattering angles less than 0.1° and can be used to probe large colloidal structures and multi-layer polymer films (Figure 5.3).

Sometime in the literature a sample to detector distance is used to describe subareas of scattering (Table 5.1). According to this definition scattering experiments performed in this thesis would belong to middle-angle X-ray scattering (MAXS).

Table 5.1- Subareas of scattering as a function of the sample-detector distance (R), assuming an X-ray wavelength of λ~ 1.5 Å.

Adapted from Ezquerra et al, 2009.[304]

Subarea	R [m]	Focus	Application
WAXS	0.05-0.2	Arrangement of atoms	Crystallography
MAXS	0.2-1.0	Liquid-crystalline structure	Liquid-crystalline structure, drug delivery
SAXS	1-3	Nanostructure 2-50 nm	Macromolecules in solutions, semi-crystalline structure of polymers
USAXS	6-15	Nanostructure 15 nm- 2 μm	Multi-layer polymer films

5.2.2. Single crystal X-ray crystallography

A crystal is a three-dimensional periodic arrangements of the molecules packed together by intermolecular forces. The unit cell is the smallest part of the crystal which represents the properties of the whole crystal. Determination of the atomic content of unit cells will lead to solve the structure of the crystal.[305] The unit cell is defined by the crystal lattice made of **a**, **b** and **c** vectors, and **α**, **β**, and **γ** angles between vectors, respectively. The unit cell content is composed of identical parts called asymmetric units. Seven crystal systems have been defined by the unit cell dimensions, angles and symmetry.[306] There are 230 three-dimensional possible space groups that are used by crystallographers to describe crystal structures. However, in macromolecular crystallography due to the chiral nature of natural proteins only 65 space groups are possible. The most frequently reported space groups in macromolecular crystallography are $P2_1$, $P2_12_12_1$, C2 and $C222_1$.[306]

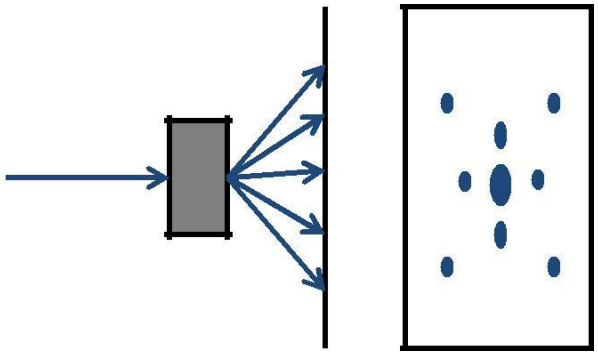

Figure 5.4- Schematic of single crystal diffraction pattern

Upon scattering of the X-ray from a crystal, scattered beams interfere with each other forming a diffraction pattern in the form of spots (reflections) on an X-ray detector (Figure 5.4). These spots are representative of the discrete beams reflected from atomic planes in the crystal. The position and intensity of each reflection provide valuable information about the direction and strength of each diffracted beam.[305] The diffraction pattern contains information about the spacing of the reflections called a reciprocal lattice which has inverse properties in comparison to the real spacing of the unit cells in the crystal lattice.[305] Therefore, it is possible to calculate the unit cell dimensions from the reciprocal lattice spacing whereas the intensities of reflections are used to calculate electron density.[305]

Each reflection can be assigned to three indices named Miller indices (*h*, *k* and *l*) determining the position of each reflection spot at the reciprocal space. Moreover, the intensities of the reflections (I(*hkl*)) are calculated as the square of the amplitude of the structure factors (F(*hkl*)).[305] The relation between electron density, ρ(*xyz*), and structure factors, F(*hkl*), is described as a Fourier transform (FT) in Equation 5.1 in which ϕ corresponds to the phase.

$$\rho(xyz) = \frac{1}{V}\sum_h \sum_k \sum_l |F(hkl)| \cos 2\pi\,(hx + ky + lz - \phi\,(hkl)) \qquad (5.1)$$

Single X-ray crystallography is capable of providing the most accurate structural information about host-guest inclusion complexes. However, crystallization is a rate-limiting step in crystallography and growing crystals out of amorphous samples is a tremendous challenge.

5.2.2.1 X-ray crystallography of the CD-based complexes

In CD-based host-guest complexes, the molecular weight and properties of the guest play an important role in forming complex crystals. In general, appropriate guests can form complexes with CDs in the overall shapes of cage or channel utilizing intermolecular hydrogen binding.[307] Crystallography was used to solve the crystal structures of inclusion complexes of small molecules with CDs. For example, the structures of the complexes of thymol, carvacrol and eugenol with βCD have been solved based on the synchrotron data. In all three complexes, βCD formed head-to-head dimers whereas the guest-host stoichiometry was observed as 1:2, 2:2 and 3:2 for carvacrol, thymol and eugenol, respectively.[308] In another study, X-ray crystallography provided information about the inclusion of menthol isomers in βCD suggesting the formation of the 2:2 mole ratio complexes in which βCD showed head to head and guest showed head to tail arrangements.[309]

5.2.3. Powder X-ray diffraction

In comparison to a single crystal, powder samples consist of randomly oriented polycrystalline with the grain size of less than 10 µm. Since the crystalline objects in the powder sample are randomly oriented, the scattered peaks will extend over the same scattering angle resulting in a diffraction pattern made of rings (Figure 5.5). It is almost unfeasible to measure the intensity of enough reflections in the powder diffraction pattern to solve large structures. However, some methods such as Rietveld method[310] has been successfully employed to refine the crystal structure from powder data.

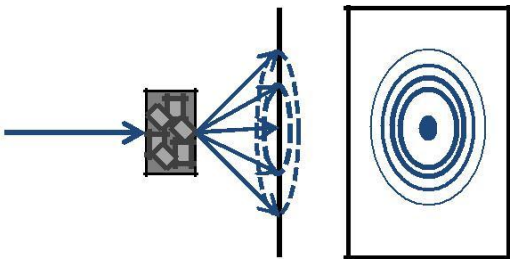

Figure 5.5- Schematic of powder diffraction pattern

5.2.3.1. Powder X-ray diffraction of the CD-based complexes

A crystalline powder of a guest molecule produces a diffraction pattern that is a "finger print" of the given compound. A diffraction pattern of the physical mixture of the guest molecule and a βCD molecule is mostly made of the superimposition of the peaks corresponding to the pure components while the diffraction pattern of the inclusion complex is mostly different from each component. In some cases the inclusion complex represents an amorphous structure lacking the crystallinity peaks of the components.[311,312] For example, the spray dried formulation of the complex of metformin with triacetyl-βCD showed none of the sharp characteristic peaks of the two molecules and instead an amorphous solid state was formed.[248] In other studies the absence of the characteristic peaks of the guest in the complex diffraction pattern is observed and a new diffraction pattern corresponding to the new solid phase is emerged. The inclusion of iprodione in βCD showed new sharp peaks in the inclusion diffractogram at 2θ angles of 11.3 º, 17.7 º and 26.0 º.[313] In addition, the complex made of ibuprofen and βCD employing superficial carbon dioxide, co-precipitation and freeze-drying methods resulted in new peaks at 2θ angle of 6.82º, 7.3º and 7.35º, respectively.[314]

Moreover, powder X-ray diffraction data can be employed directly to solve the crystalline structure of CD-based complexes. Rietveld refinement[315,316] is the most commonly used technique to determine the crystal structure based on the nonlinear least squares method. In this technique instead of obtaining the discrete integrated intensities or structure factors from diffraction pattern (direct method), a calculated profile is fitted to the experimental data.[317] In addition, the quality of the diffraction data plays an important role in the attainment of Rietveld refinement.[317] Although Rietveld refinement has been used for various CD-based structures, there are only a few examples that successfully employed powder diffraction data to solve the crystal structure of the complexes of organic molecules with CDs. The crystal structure of a lipoic acid complex with βCD having 98 non-hydrogen atoms has been solved and the guest molecule configuration in the cavity has been explained in detail.[318] Similarly, the guest conformation, mode of inclusion and crystal packing of atenolol[319] and mefenamic acid[320] complexes with βCD have been determined from the high resolution synchrotron powder diffraction data.

5.3. Characterization of nanoparticles using synchrotron SAXS/WAXS

Contrary to X-ray diffraction from crystalline material, non-crystalline materials such as partially ordered systems will not develop reflection spots but partial or full diffraction rings similar to powder diffraction pattern which can be used to characterize the partially ordered system.

In the case of monodisperse systems such as diluted solutions of nanoparticles where particles do not interact with each other, the scattering pattern is presented as a plot of scattering intensity *I(s)* [arbitrary units] versus the wave vector (s) in reciprocal space. The scattering vector (s) is the difference between incident and scattered beam and calculated as Equation 5.2.

$$s = 2sin\theta/\lambda \qquad (5.2)$$

where, 2θ and λ are the scattering angle and the beam wavelength, respectively.

Several studies in the literature have used momentum transfer, *q*, (calculated as 2π times the magnitude of *s* therefore,

$$q = 4\pi sin\theta/\lambda \qquad (5.3)$$

The SR brightness and associated equipment such as very long vacuum tubes and very sensitive X-ray detectors evoke SAXS as a versatile and robust technique to characterize nano-systems.[321] Currently, the submicron size of the synchrotron beam enables the use of samples as small as 10

μl which is critical for biological applications.[322] Furthermore, time-resolved SAXS studies can be performed applying the pulsed nature of the SR.[323] According to the storage ring magnets, the average time to do a SAXS experiment at synchrotron beamlines is between seconds and minutes.

5.3.1. Pharmaceutical applications of SAXS/WAXS

Among the wide range of samples that can be characterized by SAXS/WAXS, nanoparticles, colloidal systems and macromolecules in solutions are of great importance from a pharmaceutical point of view. Three different regions in the SAXS pattern can be applied to determine characteristics such as size, shape and surface of a dispersed system. A SAXS curve at lower angles (Guinier area), provides information to calculate an approximate molecule size (radius of gyration).[324] The radius of gyration is the root mean square distance of all scatterers from a common center of the mass. At higher angles in the SAXS pattern, the surface properties can be obtained based on Porod's rule[325] which describes the scattering from the interface in the two-phase systems. The region that extends towards higher resolution, determines the internal structure of the particles according to the Bragg's peak positions.

5.3.1.1. Characterization of the lipid-based nanoparticles by SAXS/WAXS

Lipid-based nanoparticles including nano-dispersed particles (matrix-based), liquid crystals and membrane-based lipid nano particulate systems such as liposomes have been characterized extensively using X-ray diffraction techniques particularly SAXS/WAXS as a golden technique. The peaks available in SAXS/WAXS curves are associated with the crystal lattice and the relative positions of the periodic peaks can describe the phase behavior of the lipid nanoparticles. Table 5.2 shows the most common lyotropic liquid crystalline mesophases based on the relative Bragg's peak positions corresponding to their space groups.[326]

Table 5.2- Ordinary crystalline mesophases featuring peak position ratios.[326]

Mesophase type	Peak position ratios
Lamellar	1:2:3:4, etc
Inverted Hexagonal	√3:√4:√7:√12, etc
Cubic (Bicontinuous)	√2:√4:√6:√8:√10, etc

A lamellar crystalline phase is commonly formed by the lipid bilayers stacking on top of each other with a water layer in between.[327] The inverted hexagonal phase is a 2D cylindrical structure composed of micelles packing parallel in a hexagonal lattice.[328] Various types of cubic phases reported so far in which bicontinuous cubic consists of lipid bilayers in 3D structure containing water channels.[329]

SAXS/WAXS patterns were used extensively to determine the LLC mesophases to improve the design and development of new drug delivery systems.[41,330,331] The inverted hexagonal mesophase of glyceryl monooleate LLC was studied in the presence of a skin penetration enhancer peptide for transdermal delivery of diclofenac.[332] It was found that the release rate of propranolol from cubic phases is more slowly compared to the other phases employing the SAXS/WAXS technique.[333] Moreover, an interesting study evaluated the effect of different drug molecules loaded in LLC phases on the structure by building computational models and subsequently confirming them by synchrotron SAXS/WAXS measurements.[334] Synchrotron time-resolved SAXS was able to discover the phase transformations occurring under different situations such as transformation from cubic to hexagonal[335] or lamellar to cubic phases[336].

Furthermore, SAXS/WAXS was employed to characterize the phase behavior of the solid lipid nanoparticles (SLN). For instance, the lamellar structure of cetyl palmitate was determined according to the Bragg's peak positions of 001, 002 and 003 in a manner that s-values for the first peak was half and one-third of the second and third peaks, respectively.[337]

In other studies the effect of the drug loaded into nanoparticles on phase transition has been investigated. Increasing the concentration of diclofenac, decreased the bilayer distance in phospholipid liposomal formulation and new micellar structures have been formed.[338]

A fast growing subcategory of lipid-based nanoparticles is the development of lipoplexes. Lipoplexes mostly consist of cationic liposomes in combination with nucleic acids as non-viral gene delivery vectors.[339] The study of structure-transfection relationship of different cationic liposomes/DNA formulations suggested that with the increase in the concentration of dendritic cationic lipids, the characteristic lamellar phase peaks changed to a novel self-assembly model called hexagonal tubular phase with higher transfection efficacy in comparison to lamellar and inverted hexagonal phases commonly observed in lipoplexes.[340] In another research, the gene silencing activity and phase transition of SiRNA/DOTAP/DOPE formulations were evaluated. It was found that increasing the DOPE concentration resulted in the phase transition from lamellar

to inverted hexagonal.[341]

5.3.1.2. Characterization of gemini-based nanoparticles by SAXS/WAXS

As mentioned before, cationic gemini surfactants can form complexes with nucleic acids and act as gene delivery vectors. The structure determination of various plasmid/amine substituted gemini surfactant/DOPE complexes were performed using SAXS/WAXS data. The results showed that the increased transfection efficacy in formulations containing gemini surfactants with pH-sensitive imine-based spacers can be correlated to the formation of less ordered phases other than the hexagonal phase. The main Bragg's peak observed for 12-7NH-12 gemini surfactant was at q of 0.105 $Å^{-1}$ corresponding to *d*-spacing of 59.6 Å. The presence of another strong peak at q of 0.117 $Å^{-1}$ along with several weak peaks confirmed the formation of other phases.[166] In another study, the phase behavior of lipoplexes consisting of glucose-based gemini surfactants showed three different morphologies called as lamellar, condensed lamellar and inverted hexagonal at pH range of 8.8 to 3 and the inverted hexagonal phase showed higher fusogenic activity.[342] The co-existence of condensed lamellar and lamellar phases was reported in alkane-α,ω-diyl-bis(alkyldimethylammonium bromide) gemini/DOPE/DNA complexes which is related to the ionic strength (NaCl solution), surface charge density and the sample preparation method.[343] Moreover, it was observed that SiRNA complexes with bis(quaternary ammonium)bromide gemini surfactants having a 12 hydrocarbon tail and different spacer lengths (s=3, 6, 12) formed a micellar sandwich model. Gemini surfactant self-assembly structures were globular with different radii of gyration dependent on spacer length.[344] The structural behavior of phytanyl substituted gemini surfactants complexes with DNA obtained by SAXS/WAXS data and correlated to their transfection efficiency and cytotoxicity in OVCAR-3 cells.[345]

In addition, phase diagrams of gemini surfactants can be determined through monitoring the changes in SAXS/WAXS pattern. The investigation of a ternary system of various gemini surfactant/octanol/water demonstrated the coexistence of four anisotropic phases as hexagonal, hexagonal/lamellar, lamellar and lamellar/micelle.[346] In another study, two zwitterionic bis(alkyltriazolium sulfobetaine) gemini surfactants showed an inverse discontinuous micellar cubic phase that was highly stable at a wide range of surfactant concentration and temperature.[347]

6. RESEARCH FOCUS

6.1. Rationale for the study

The majority of the anticancer agents synthesized every year, have poor water solubility leading to a low in vivo bioavailability. The use of organic solvents in anticancer formulations is limited due to their high cytotoxicity. However, nanotechnology revolutionized anticancer drug delivery by introducing various tunable nano-sized delivery agents. In brief, anticancer agents encapsulated by nano- drug delivery systems offer higher efficiency and lower resistance.

In our research group, novel lipid-based drug delivery agents, βcyclodextrin-gemini surfactants (βCDgemini surfactants), have been synthesized by attaching βcyclodextrin to various gemini surfactants.[3] βcyclodextrin (βCD), a ring-shaped oligosaccharide having seven α-D-glucopyranose units is able to incorporate hydrophobic molecules and form host-guest inclusion complexes.[277] The gemini surfactants employed to build these delivery agents, belong to imino substituted bisquaternary ammonium gemini surfactants extensively used as gene delivery vectors.[153] Previously, it was shown that the nano-structures formed by self-assembly of the gemini surfactant could insert foreign genes into mammalian cells.[166] The βCDgemini surfactants were designed to benefit simultaneously from βCD as a solubilizing agent and gemini surfactants as self-assembling agents.

Curcumin, the active ingredient of turmeric rhizome showed anticancer activity, but its potential to be used as a drug was hampered by a high IC_{50} value in cancer cell lines and low *in vivo* bioavailability.[94] To modify the characteristics of curcumin, various curcumin analogs have been synthesized. Dr. Dimmock and his colleagues synthesized a variety of curcumin analogs showing high *in vitro* cytotoxicity towards various cancer cell lines, including colon cancer and melanoma.[111] Despite formidable efforts in oncology research, treatment of melanoma, the deadliest type of skin cancer, remains largely ineffective. This is mostly due to the chemoresistance[48] to conventional chemotherapy agents and low penetration of drugs into the skin cells. Thus we proposed to utilize the knowledge on the curcumin analogs to develop new potential therapies for melanoma. We selected a curcumin analog, named NC 2067, which previously showed high *in vitro* cell toxicity towards A375 melanoma cell line and minimal toxicity to normal human keratinocytes. The high lipophilicity of NC 2067 (log *P* value of 4.6)[2] is an issue which can restrict its *in vivo* bioavailability. We previously reported that to overcome

this drawback, βCDgemini surfactant as a delivery agent for NC 2067 could be employed.[3] It was confirmed that NC 2067 in presence of βCDgemini surfactant was able to retain its anticancer activity *in vitro* and increased caspase 3 and 7 in A375 melanoma cells.[3]

In my research, I developed a series of formulations of NC 2067 and βCDgemini surfactants by varying the linker structure, βCDgemini surfactant moiety, the mole ratios between the anticancer agent to delivery agent and addition of helper lipid. The main purpose of my dissertation was the physicochemical characterization and evaluation of the anticancer activity of these formulations. The host-guest inclusion complexes of NC 2067 with βCD and βCDgemini surfactant were characterized using different synchrotron and non-synchrotron techniques. The nano-structural behavior of the formulations was evaluated to further understand the aggregation of the complexes formed by NC 2067 and various βCDgemini surfactants. Finally, the mechanism of cell death triggered by the formulations was assessed by flow cytometry in A375 melanoma cells.

6.2. Hypothesis

A curcumin analog, NC 2067 will interact with cyclodextrin-gemini surfactant-based delivery agents and its *in vitro* cytotoxic activity will increase in A375 melanoma cells.

6.3. Objectives

Overall objectives

- To characterize drug/βCDgemini surfactant conjugates using different techniques.
- To evaluate the anticancer activity mechanism of these formulations in melanoma cell line.

Specific objectives

1. Physicochemical characterization

1.1. To incorporate a selected drug (NC 2067) into βCDgemini surfactant complex

1.2. To develop formulations by varying the mole ratio between the drug and delivery agent, using βCDgemini surfactants with various gemini surfactant tails, having ester or amide bonds between the βCD and gemini surfactant moiety and addition of helper lipid

1.3. To characterize the βCDgemini surfactants

1.4. To confirm the formation of the inclusion of NC 2067 in βCD or βCDgemini surfactant qualitatively using different analytical techniques

1.5. To use advanced techniques such as synchrotron single crystal X-ray diffraction or 2D ROSEY NMR to understand the structural properties of the drug/βCD and drug/βCDgemini surfactant inclusion complexes

1.6. To use synchrotron small- and wide angle X-ray scattering (SAXS/WAXS) to evaluate the supramolecular arrangement of drug/βCDgemini surfactant delivery systems in solution

2. Molecular mechanism of the anticancer activity

2.1. To calculate the cell toxicity (IC_{50}) of different drug/βCDgemini surfactant formulations towards melanoma cell line

2.2. To elucidate the type of cell death mechanism and cell cycle arrest behavior of different drug/βCDgemini surfactant formulations using flow cytometry-based assays in melanoma cells

7. CHARACTERIZATION OF THE HOST-GUEST COMPLEX OF A CURCUMIN ANALOG WITH βCYCLODEXTRIN AND βCYCLODEXTRIN-GEMINI SURFACTANT AND EVALUATION OF ITS ANTICANCER ACTIVITY

Masoomeh Poorghorban[1], Umashankar Das[2], Osama Alaidi[1], Jackson M. Chitanda[2], Deborah Michel[1], Jonathan Dimmock[1], Ronald Verrall[3], Pawel Grochulski[1,4], Ildiko Badea[1]

[1] Drug Discovery and Development Research Group, College of Pharmacy and Nutrition, University of Saskatchewan, Saskatoon, Saskatchewan, Canada

[2] Department of Chemical and Biological Engineering, University of Saskatchewan, Saskatoon, Saskatchewan, Canada

[3] Department of Chemistry, University of Saskatchewan, Saskatoon, Saskatchewan, Canada

[4] Canadian Light Source, Saskatoon, Saskatchewan, Canada

Correspondence: Ildiko Badea
College of Pharmacy and Nutrition
University of Saskatchewan
Health Sciences Building, 3D01.5
107 Wiggins Road
Saskatoon, Saskatchewan, S7N 5E5, Canada
Phone: 306-966-6349
Fax: 306-966-6377
E-mail: ildiko.badea@usask.ca

The contents of this article were published in International Journal of Nanomedicine 2015, 10, 503-515.

This published manuscript describes the physicochemical characterization and *in vitro* cytotoxicity of NC 2067 complexes with βCD and βCDgemini surfactant. I used synchrotron-based powder X-ray diffraction, Fourier transform infrared spectroscopy and thermogravimetric analysis to confirm the inclusion formation in NC 2067 complexes with βCD and βCDgemini surfactant. Synchrotron-based small- and wide angle X-ray scattering and dynamic light scattering employed to characterize the nano-structures of NC 2067/βCDgemini surfactant complexes. Moreover, I determined the cellular toxicity of NC 2067/βCDgemini surfactant complexes towards A375 melanoma cells.

The co-authors of this paper synthesized the anticancer agent, NC 2067 and the delivery agent, βCDgemini surfactant.

This manuscript addresses the following specific objectives of my research

1.1. To incorporate a selected drug (NC 2067) into βCDgemini surfactant complex

1.2. To develop formulations by varying the mole ratio between the drug and delivery agent and having ester or amide bonds between the βCD and gemini surfactant moiety

1.4. To confirm the formation of the inclusion of NC 2067 in βCD or βCDgemini surfactant qualitatively using different analytical techniques

1.6. To use synchrotron small- and wide angle X-ray scattering (SAXS/WAXS) to evaluate the supramolecular arrangement of drug/βCDgemini surfactant delivery systems in solution

2.1. To calculate the cell toxicity (IC_{50}) of different drug/βCDgemini surfactant formulations towards melanoma cell line

7.1. Abstract

Purpose: Curcumin analogs, including novel compound NC 2067, are potent cytotoxic agents that suffer from poor solubility, and hence, low bioavailability. Cyclodextrin-based carriers can be used to encapsulate such agents. In order to understand the interaction between the two molecules, the physicochemical properties of the host-guest complexes of NC 2067 with βcyclodextrin (βCD) or βcyclodextrin-gemini surfactant (βCDgemini surfactant) were investigated for the first time. Moreover, possible supramolecular structures were examined in order to aid the development of new drug delivery systems. Furthermore, the *in vitro* anticancer activity of the complex of NC 2067 with βCDgemini surfactant nanoparticles was demonstrated in the A375 melanoma cell line.

Methods: Physicochemical properties of the complexes formed of NC 2067 with βCD or βCDgemini surfactant were investigated by synchrotron-based powder X-ray diffraction, Fourier-transform infrared spectroscopy and thermogravimetric analysis. Synchrotron-based small- and wide angle X-ray scattering and size measurements were employed to assess the supramolecular morphology of the complex formed by NC 2067 with βCDgemini surfactant. Lastly, the *in vitro* cell toxicity of the formulations toward A375 melanoma cells at various drug-to-carrier mole ratios were measured by cell viability assay.

Results: Physical mixtures of NC 2067 and βCD or βCDgemini surfactant showed characteristics of the individual components, whereas the complex of NC 2067 and βCD or βCDgemini surfactant presented new structural features, supporting the formation of the host-guest complexes. Complexes of NC 2067 with βCDgemini surfactants formed nanoparticles having sizes of 100-200 nm. NC 2067 retained its anticancer activity in the complex with βCDgemini surfactant for different drug-to-carrier mole ratios, with an IC_{50} (half-maximal inhibitory concentration) value comparable to that for NC 2067 without the carrier.

Conclusions: The formation of host-guest complexes of NC 2067 with βCD or βCDgemini surfactant has been confirmed and hence the βCDgemini surfactant shows good potential to be used as a delivery system for anticancer agents.

Keywords: host-guest complex, gemini surfactant, cyclodextrin, curcumin analog, small-angle X-ray scattering

7.2. Introduction

With the advances of combinatorial chemistry, many new anticancer agents are synthesized every year in an effort to combat different cancers. The major challenge with some compounds is their low water solubility, which results in poor absorption through biomembranes and leads to low bioavailability. Organic solvents (dimethylsulfoxide [DMSO]) and surfactants (Cremophor®) are used in laboratory experiments and formulations to enhance the solubilization of these molecules. However, DMSO is not safe for *in vivo* use because it has its own influence on the cells and the US Food and Drug Administration has not yet approved the use of DMSO as a delivery agent except for the treatment of interstitial cystitis.[348] In addition, Cremophor used in conventional chemotherapy formulations is associated with fatal hypersensitivity reactions.[1] Therefore, different nanotechnology-based drug delivery systems have been developed to increase the solubility of the hydrophobic anticancer compounds and enhance their efficiency.

Curcumin, the active ingredient of turmeric rhizome, and its analogs are some examples of poorly soluble drug candidates in aqueous medium. While they show strong *in vitro* anticancer activity towards different cancer cell lines[3,91,97,107,108,349,350] their lipophilicity (high log*P* value) is a limitation for *in vivo* applications. Various nanotechnology-based drug delivery systems, such as liposomes[95,96], solid lipid nanoparticles[97,98,351], polymer-based nanoparticles[99,349,352] and mesoporous nanoparticles[353], have been developed to encapsulate curcumin and its analogs so as to enhance solubilization and deliver them to cancerous cells. Beta-cyclodextrin (βCD) (Figure 7.1A) is a well-known carrier for insoluble drugs in the pharmaceutical industry. It is capable of encapsulating a lipophilic guest molecule in its hydrophobic internal cavity to form a complex and its hydrophilic outer surface leads to improved guest solubility in an aqueous environment.[123] Complexes of curcumin or curcumin analogs and βCD have been created previously to increase the water solubility of the drug.[103,133,354-357] Curcumin analogs with the 1,5-diaryl-3-oxo-1,4-pentadienyl pharmacophore structure have been synthesized and their cell toxicity toward various cancer cell lines has been demonstrated.[108,111] Among these structures, NC 2067 (Figure 7.1B) demonstrated high *in vitro* cell toxicity towards melanoma and colon cancer cell lines.[3,226] Its high log*P* value of 4.6[2] and the presence of aromatic ring moieties in its structure suggest that NC 2067 is a good candidate for encapsulation by βCD. Beta cyclodextrin-gemini surfactant (βCDgemini surfactant) is a novel carrier composed of βCD attached by an

ester or amide linker to a cationic gemini surfactant (Figure 7.1C and 7.1D, respectively). They were synthesized in order to create a suitable substitute for a solubilizing agent,[3] hypothesizing that the hydrophobic βCD cavity can accommodate NC 2067 while the gemini surfactant tail possibly could contribute to a supramolecular association that would enhance diffusion into biomembranes.

In a previous study[3], we have shown that NC 2067 in a complex with βCD or βCDgemini surfactant in a 1:2 mole ratio exhibited high *in vitro* cell toxicity toward A375 melanoma cell line. Moreover, based on UV spectroscopy findings, we have also suggested a hypothetical model of the interaction of the NC 2067 molecule with βCD and βCDgemini surfactant.[3] However, understanding the nature of the physicochemical interactions between NC 2067 and βCD or βCDgemini surfactant is necessary to confirm whether inclusion complexes are formed. Furthermore, examination of the structural behavior of the nanoparticles made of NC 2067 in a complex with the βCDgemini surfactant should help to optimize the use of these nanoparticles as delivery agents for poorly soluble anticancer agents such as NC 2067.

The objective of the current work is to determine to what degree inclusion of NC 2067 in βCD or βCDgemini surfactant can occur. Moreover, the nanoparticulate behavior of NC 2067 in a complex with βCDgemini will be assessed more comprehensively. Finally, the effect of variations in drug-to-carrier mole ratio and linker structure on the size and anticancer activity of the nanoparticulate systems are investigated.

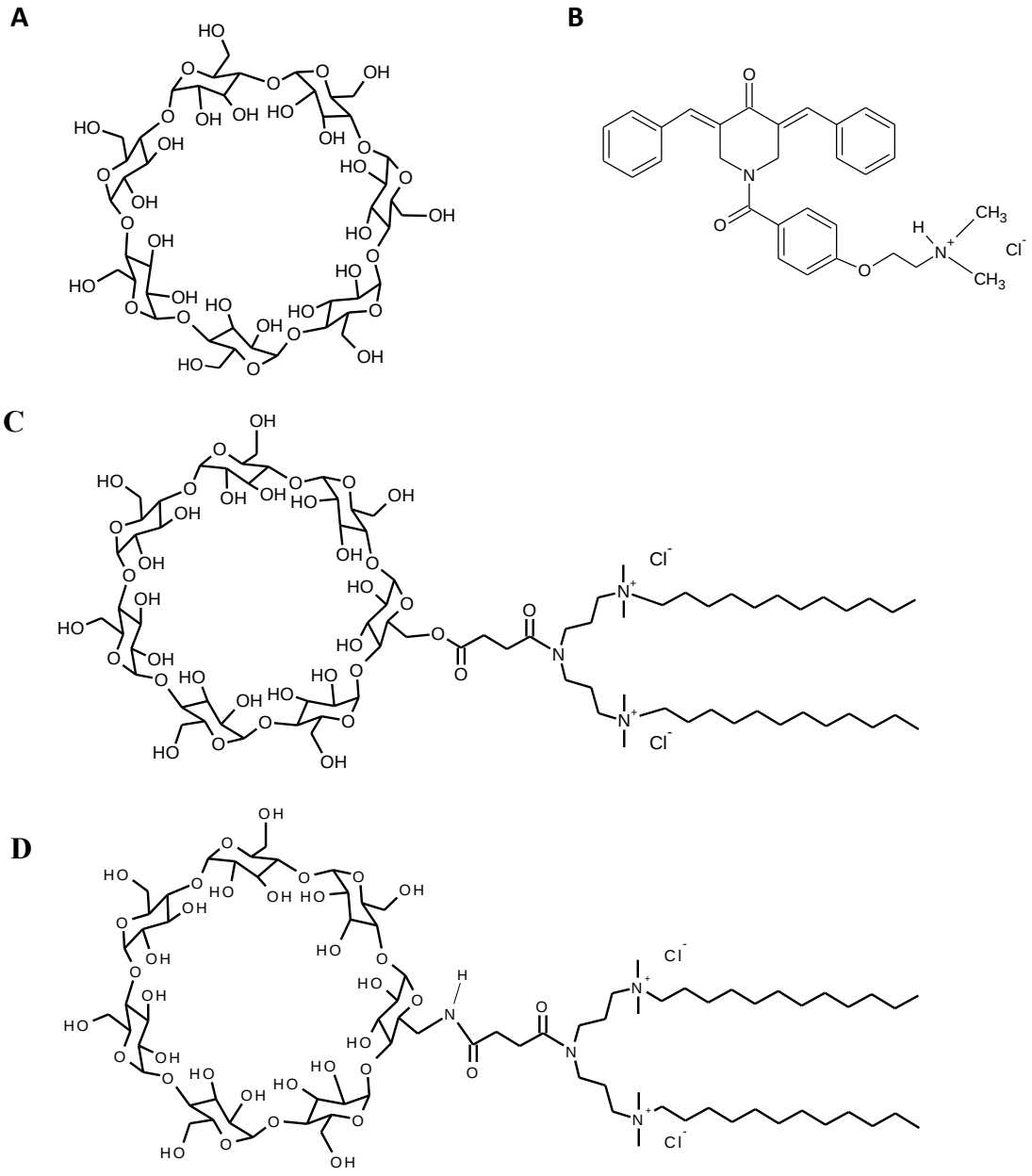

Figure 7.1- Chemical structures of **(A)** βCD, **(B)** NC 2067, **(C)** βCDgemini surfactant (ester linker) and **(D)** βCDgemini surfactant (amide linker).

Abbreviations: βCD, βcyclodextrin; βCDgemini surfactant, βcyclodextrin-gemini surfactant.

7.3. Materials and methods

7.3.1. Preparation of inclusion complexes

Curcumin analog NC 2067 was synthesized as described previously.[111] βCD was purchased from Alfa Aesar (Haverhill, MA, USA). βCDgemini surfactants with ester or amide linkages were synthesized previously.[3] All other chemicals were purchased from Sigma-Aldrich (Oakville, ON, Canada). Complexes of NC 2067 with βCD or βCDgemini surfactant were created as follows. Solutions of βCD and βCDgemini surfactant in water (10 mM) and NC 2067 in methanol (2 mM) were combined to obtain mole ratios of drug to delivery agent of 0.5, 1.0 and 2.0 and shaken overnight. The solvent mixture was removed by rotary evaporation under vacuum. These powders were used for the powder diffraction, thermogravimetric analysis (TGA), and Fourier-transform infrared (FTIR) spectroscopy experiments. For all other studies, the residue was reconstituted in water and shaken overnight. Physical mixtures were made by blending the appropriate amount of powders of NC 2067 and βCD or βCDgemini surfactant.

7.3.2. Characterization of the complex of NC 2067 with βCD or βCDgemini surfactant

7.3.2.1. Powder X-ray diffraction measurements

The powder samples of NC 2067 and its physical mixtures and complexes with βCD or βCDgemini surfactant were loaded into capillaries (MiTeGen, Ithaca, NY, USA). Powder X-ray diffraction patterns were obtained at beamline 08B1-1 (Canadian Macromolecular Crystallography Facility-bend magnet) at the Canadian Light Source Inc (CLS, Saskatoon, Canada) using X-ray energy of 12 keV at room temperature.[358] Data collection was performed at a sample-to-detector distance of 280 mm with 30-second exposure time. Data processing was carried out employing X-ray analysis software for partially ordered and disordered systems (Alaidi, personal communication), automating Fit2d.[359]

7.3.2.2. FTIR spectroscopy

Infrared spectra of the powder samples of NC 2067 and its physical mixtures and complexes with βCD or βCDgemini surfactant, embedded in a KBr matrix, were scanned over the 4,000–400 cm^{-1} region and recorded by using a Bruker IFS 66v/S Fourier-transform spectrometer (Bruker Optics, Billerica, MA, USA) at Mid-IR beamline at the CLS.

7.3.2.3. TGA study

The thermal behavior of NC 2067 and its physical mixtures and complexes with βCD or βCDgemini surfactant was evaluated using TGA. The scans were carried out employing a TGA Q500 instrument (TA instruments, New Castle, DE, USA) under nitrogen at a heating rate of 5^0C/min.

7.3.2.4. Small- and wide angle X-ray scattering measurements

Small- and wide angle X-ray scattering (SAXS/WAXS) measurements were performed at the BL4-2 beamline at Stanford Synchrotron Radiation Lightsource (SSRL, Stanford, CA, USA) at an energy of 11 keV and a sample-to-detector distance of 1.1 m at 20-second exposure time. Diffraction intensity versus *q (scattering vector)* plots were obtained by radial integration of the two-dimensional patterns using X-ray analysis software for partially ordered and disordered systems. The concentration of βCDgemini surfactant in all samples was fixed at 10 mM.

7.3.2.5. Size measurements

Particle sizes in solution were measured using a Zetasizer Nano ZS instrument (Malvern Instruments, Malvern, UK). Results are reported as the mean of three to five measurements ± standard deviation.

7.3.3. Cell viability assay

A375, human amelanotic melanoma cells (American Type Culture Collection, CRL-1619) were seeded at a density of 1 x 10^4 cells per well in 96-well tissue culture-treated plates. Cells were treated with the formulations at drug concentrations of 0.01–200 μM in quadruplicate wells for 48 hours to produce a balanced four-parameter curve. The experiments were conducted in triplicate. After treatment, 3-(4,5-dimethylthiazol-2-yl)-2,5-diphenyltetrazolium bromide (MTT; Invitrogen, Burlington, ON, Canada) at 450 μg/mL was added to each well and the plates were incubated for 2 hours at 37 ^{o}C. Absorbance at 550 nm was recorded using a Synergy BioTek plate reader. The values of the half-maximal inhibitory concentration (IC_{50}) for all samples were calculated using the four-parameter curves generated by the Gen5 software from BioTek.

7.3.4. Statistical analysis

Statistical analysis was performed using SPSS (version 19.0). One-way analysis of variance and Scheffe's comparison were used. The level of significance was considered at $p<0.05$ value.

7.4. Results

7.4.1. Physicochemical characterization of the host-guest inclusion complexes of NC 2067 in βCD and βCDgemini surfactant

7.4.1.1. Powder X-ray diffraction analysis

To confirm the formation of the complexes of NC 2067 and βCD or βCDgemini surfactant, analysis of powder diffraction patterns of the complexes were compared to the patterns of the physical mixtures of NC 2067 and βCD or βCDgemini surfactant. Because of the structure of the linker (amide or ester) in βCDgemini surfactant should have a minimal influence on the host-guest complexes, only βCDgemini surfactant with the ester linker was evaluated. Moreover, qualitative analysis of the host-guest complexes will not change with different drug-to-carrier mole ratios and hence, the 1:2 mole ratio was selected for these experiments. Diffractograms of βCD, NC 2067, their physical mixture, and the complex they formed are illustrated in Figure 7.2A. The βCD and NC 2067 diffractograms (Figure 7.2A-a and -b, respectively) display several peaks representative of a crystalline structure. The physical mixture of NC 2067 and βCD (Figure 7.2A-c) shows a pattern resembling the superposition of the NC 2067 and βCD peaks, with the most intense peaks of NC 2067, at 2θ angles of 3.9^0, 12.8^0, 13.2^0, 13.9^0 and 18.8^0, being most evident. Conversely, in the diffraction pattern of the complex of NC 2067 with βCD (Figure 2A-d), a new diffraction pattern emerges, with peaks in different positions such as 1.9º, 9.3º and 12.2º, which is not found in diffractograms of NC 2067 or βCD (All the peak positions are presented in Table S1).

Diffractograms of βCDgemini surfactant, NC 2067, their simple physical mixture and their complex are illustrated in Figure 7.2B. The diffused diffraction pattern of βCDgemini surfactant (Figure 7.2B-a) is representative of an amorphous structure. In the physical mixture of NC 2067 and βCDgemini surfactant (Figure 7.2B-c) and as seen in the NC 2067 and βCD physical mixture (Figure 2A-c), the strongest peaks of NC 2067 are visible (at 2θ angles of 3.9^0, 12.8^0, 13.2^0, 13.9^0 and 18.9^0). On the contrary, the diffractogram of the complex of NC 2067 with βCDgemini surfactant (Figure 7.2B-d) illustrates an expected amorphous structure similar to that of βCDgemini surfactant, confirming the formation of a complex between NC 2067 and the βCDgemini surfactant.

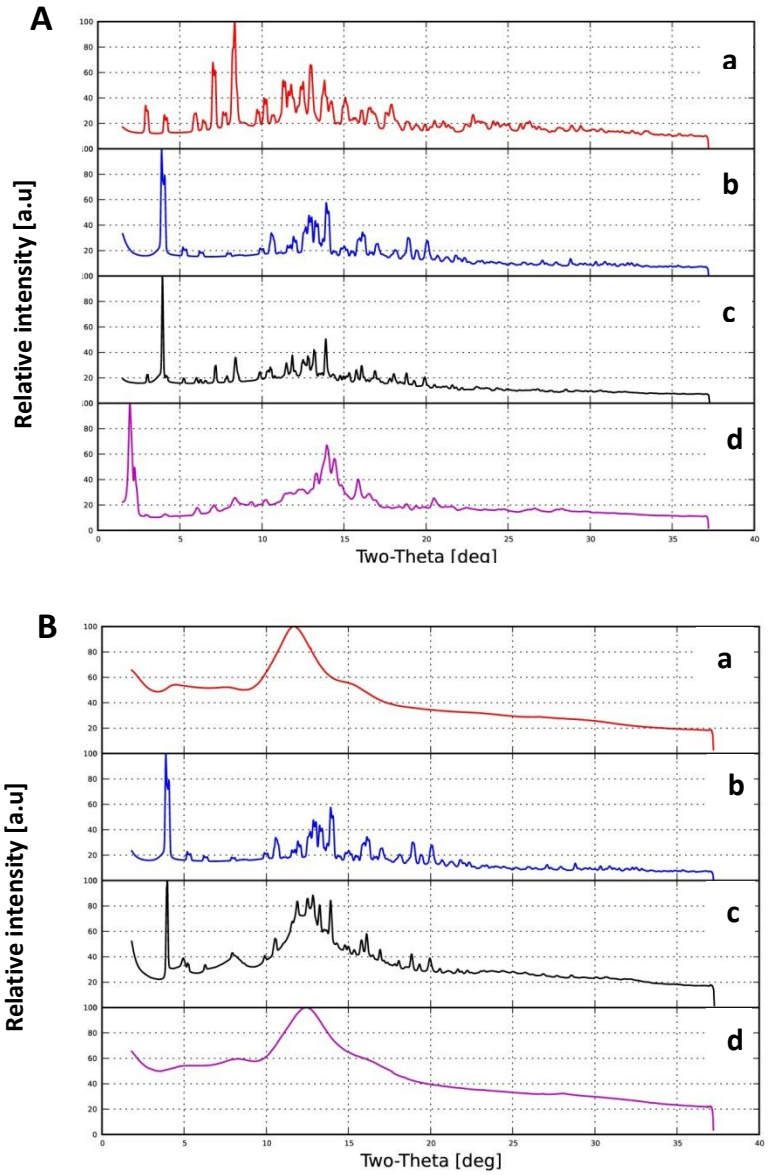

Figure 7.2- Diffractograms of **(A)** βCD (a), NC 2067 (b), Physical mixture (c) and inclusion complex of NC 2067 and βCD (d); and **(B)** βCDgemini surfactant (a), NC 2067 (b), Physical mixture (c) and inclusion complex of NC 2067 and βCDgemini surfactant (d).

Abbreviations: au, arbitrary unit; βCD, βcyclodextrin; βCDgemini surfactant, βcyclodextrin-gemini surfactant.

7.4.1.2. FTIR spectroscopy

Further evaluation of the complex between the drug and βCD or βCDgemini surfactant (using the ester linker as a model) was carried out by comparison of the FTIR spectra (Figure 7.3) of NC 2067, βCD, βCDgemini surfactant, their complexes, and physical mixtures. Generally, in the physical mixtures of NC 2067 and βCD or βCDgemini surfactant (Figure 7.3A-c and 7.3B-c), the infrared peaks of NC 2067 and βCD or βCDgemini surfactant are detectable, whereas in the complexes of NC 2067 with βCD or βCDgemini surfactant (Figure 7.3A-d and B-d), some peaks of the NC 2067 are missing or very weak. For example, the three bands corresponding to the aromatic ring conjugated with the alkene C=C bond of NC 2067 in the 1,450-1,600 cm^{-1} range are still detectable in the physical mixture at 1,468, 1,489 and 1,512 cm^{-1}, whereas in the complexes, they are very weak or undetectable. The peak of NC 2067 at 1,671 cm^{-1}, corresponding to the α,β-unsaturated ketone stretch, is still present in the physical mixture, whereas it is less intense in the complex. Moreover, there are several peaks of NC 2067 at 694 cm^{-1}, 1,278 cm^{-1}, 1,433 cm^{-1} and 3,022 cm^{-1}, which disappear after complexation of NC 2067 with βCD but are observable in the physical mixture. Similarly, the peaks of NC 2067 at 694 cm^{-1}, 1433 cm^{-1}, 1608 cm^{-1}, 1631 $cm^{-1}$and 3,022 cm^{-1} are lacking in the complex of NC 2067 with βCDgemini surfactant but observable in their physical mixture. The disappearance of the NC 2067 peaks at 694 cm^{-1}, corresponding to the monosubstituted aromatic ring, and at 3,022 cm^{-1}, corresponding to the C-H stretch of the aromatic ring, from the complexes supports the theory that one or both aromatic rings conjugated with the alkene bond in the NC 2067 structure are involved in the inclusion. On the other hand, a peak at 1,248 cm^{-1}, corresponding to the aryl alkyl ether group (side chain in NC 2067 structure), can be detected in all physical mixtures and complexes with βCD and βCDgemini surfactant, thus suggesting that this side chain is not involved with the βCD moiety in the complex (Figure 7.3).

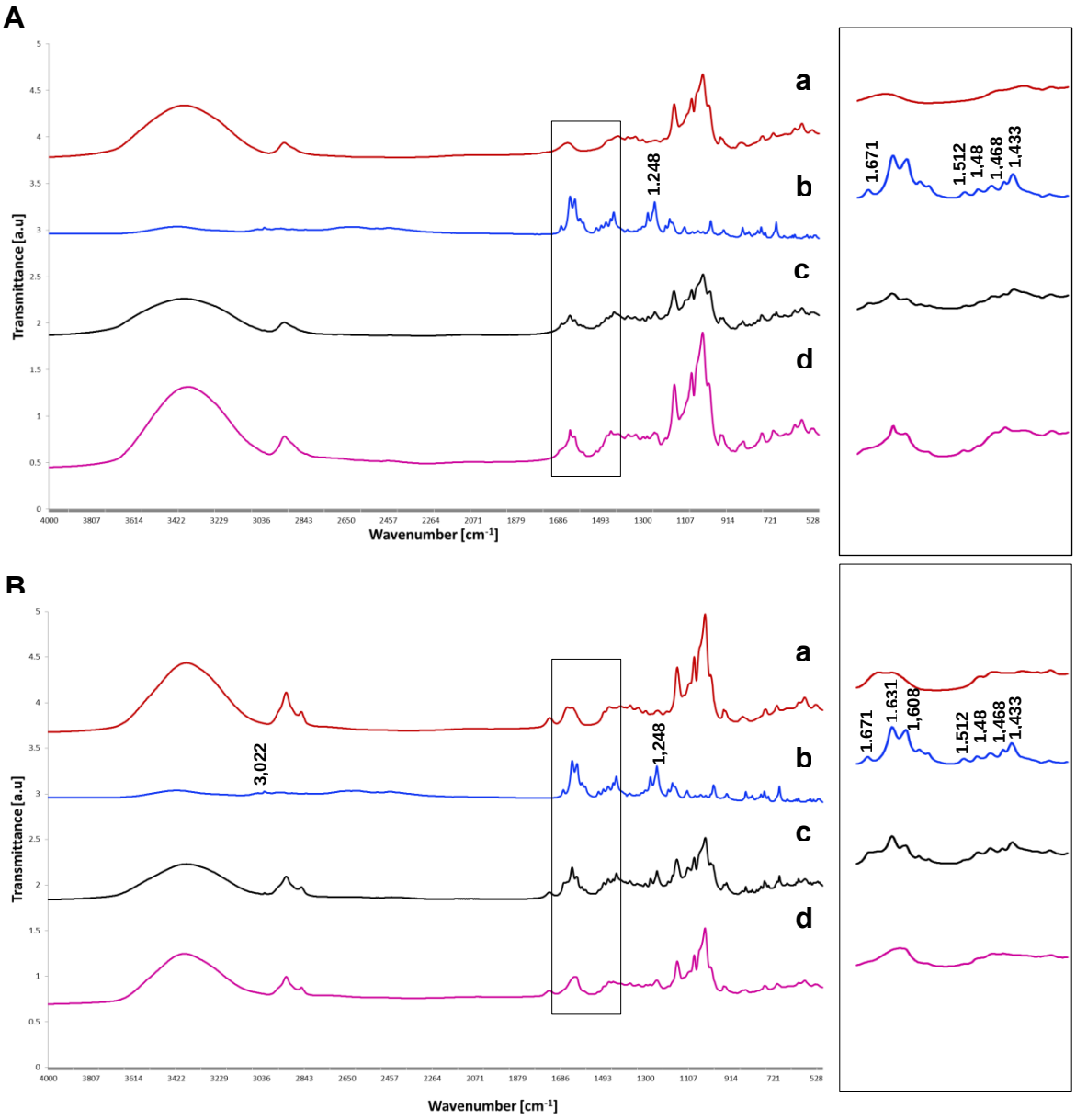

Figure 7.3- FTIR spectra of **(A)** βCD (a), NC 2067 (b), physical mixture (c) and inclusion complex of NC 2067 and βCD (d); **(B)** βCDgemini surfactant (a), NC 2067 (b), physical mixture (c) and inclusion complex of NC 2067 and βCDgemini surfactant (d).

Note: Expansions for the 1,720-1,380 cm^{-1} region are illustrated in the insets.

Abbreviations: au, arbitrary unit; βCD, βcyclodextrin; βCDgemini surfactant, βcyclodextrin-gemini surfactant; FTIR, Fourier-transform infrared.

7.4.1.3. TGA study

Thermal behavior of the complexes and physical mixtures of NC 2067 and βCD or βCDgemini surfactant (using ester linker) was investigated to further corroborate the results obtained from powder X-ray diffraction and FTIR studies. The thermal profile of βCD (Figure 7.4A) showed a water loss of 10% from 30^{0}C to 70 ^{0}C and degradation occurring in the range of 275^{0}C to 315 ^{0}C, with a concomitant 65% weight loss, which is in agreement with a previous report.[258] The physical mixture displayed 8% water loss in the same temperature range as βCD whereas no water loss was recorded in the complex in this range (Figure 7.4A). Thermal decomposition of NC 2067 began at 218 ^{0}C, while the complex of NC 2067 with βCD showed delayed onset of the degradation, shifting to a higher temperature of 240 ^{0}C (Figure 7.4A). The thermogram corresponding to βCDgemini surfactant (Figure 7.4B) did not show the initial water loss at or below 70 ^{0}C. The complex of NC 2067 with βCDgemini surfactant showed marginally less water loss in comparison to βCDgemini surfactant alone. Moreover, the degradation temperature of NC 2067 in the complex increased to 232 ^{0}C (Figure 7.4B).

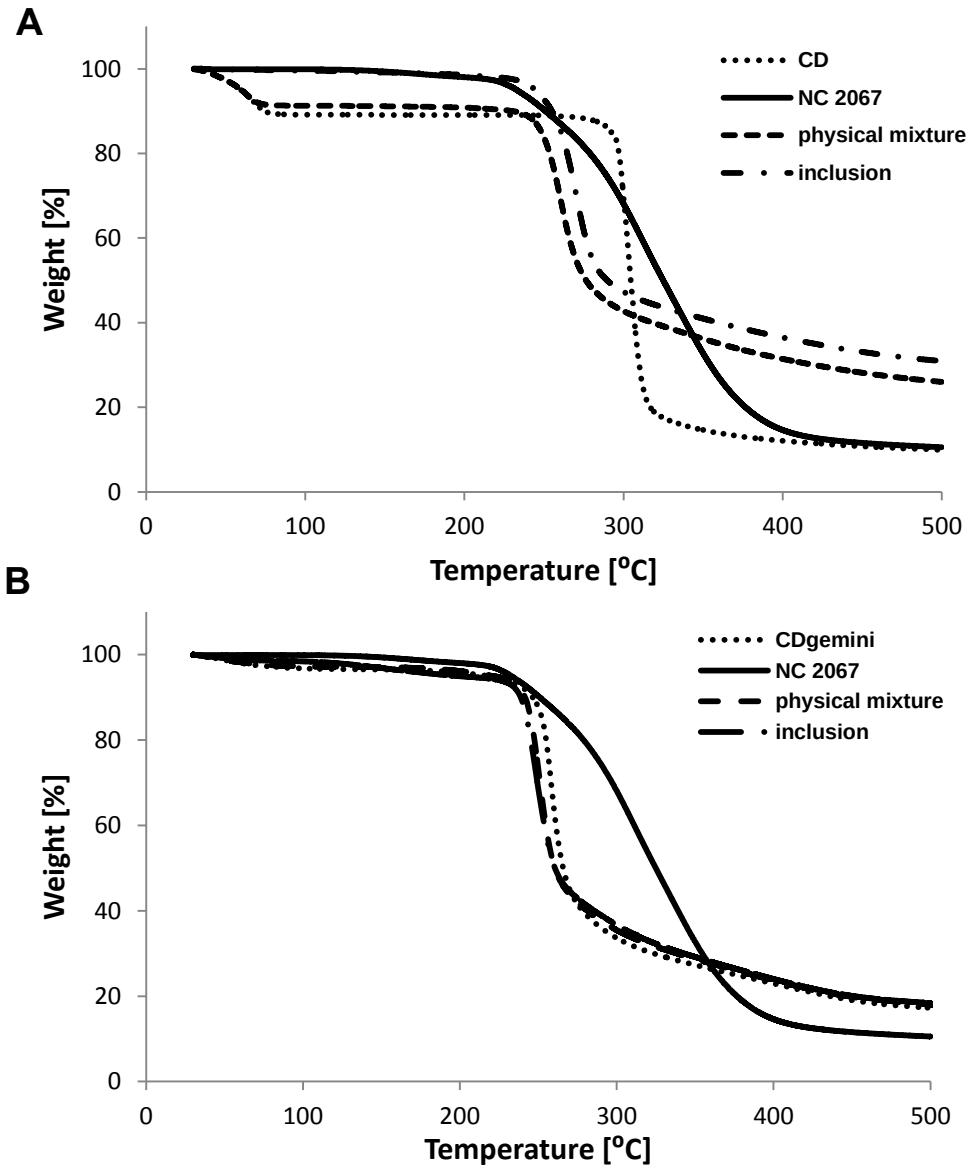

Figure 7.4- TGA thermograms of **(A)** βCD, NC 2067, physical mixture and inclusion complex of NC 2067 and βCD; and **(B)**

βCDgemini surfactant, NC 2067, physical mixture and inclusion complex of NC 2067 and βCDgemini surfactant.

Abbreviations: **β**CD, βcyclodextrin; βCDgemini surfactant, βcyclodextrin-gemini surfactant; TGA, thermogravimetric analysis.

7.4.2. Nanoparticulate behavior of NC 2067 in complex with βCDgemini surfactant

7.4.2.1. Size measurements of nanoparticles

Because a complex of NC 2067 with βCD will not form nanoparticles, only the size of nanoparticulate systems of NC 2067 in a complex with the βCDgemini surfactant (ester and amide linkers) in water at three different drug-to-carrier mole ratios (1:0.5, 1:1 and 1:2) was measured. All the nanoparticles had sizes in the range of 101-199 nm, with a polydispersity index ≤ 0.3 (Table 7.1). The average size of the nanoparticles formed by NC 2067/βCDgemini surfactant (ester linker at 1:2 mole ratio) was significantly different ($p<0.05$) from the size of particles in other formulations. The size of the nanoparticles at 1:0.5 mole ratio was significantly higher than that at the other two mole ratios for both ester and amide linker groups. βCDgemini surfactant size measurements provided variable values with high polydispersity index, suggesting the inhomogeneous nature of the aggregations of free βCDgemini surfactant in solution.

Table 7.1- Size of different nanoparticulate formulations and corresponding PDI.

NC2067/βCDgemini surfactant nanoparticles	NC 2067-to-βCDgemini surfactant mole ratio	size (nm) ± SD	PDI
Ester linker	1:0.5	160 ± 3	0.1
	1:1	140 ± 1	0.2
	1:2	101 ± 2	0.3
Amide linker	1:0.5	199 ± 6	0.3
	1:1	131 ± 3	0.2
	1:2	131 ± 1	0.2

Note: Sizes are the average of three to five measurements ± SD.

Abbreviations: βCD, βcyclodextrin; βCDgemini surfactant, βcyclodextrin-gemini surfactant; PDI, polydispersity index; SD, standard deviation.

7.4.2.2. SAXS/WAXS measurements

To evaluate the lipid phase behavior of the nanoparticles, we assessed the SAXS/WAXS pattern of the complexes of NC 2067 with βCDgemini surfactant (ester linker) at three different drug-to-

carrier mole ratios (1:0.5, 1:1 and 1:2) (Figure 7.5). Surprisingly, the βCDgemini surfactant, alone, showed a broad peak pattern in the SAXS region (q < 0.1 $Å^{-1}$), corresponding to the formation of aggregates, without showing any peak in the WAXS region (Figure 7.5A). Moreover, the scattering pattern of different concentrations of βCDgemini surfactant (1-30 mM) in the q range of 0.02-0.2 $Å^{-1}$ did not alter in position (data not shown). Once again, because the nature of the linker has minimal effect on the self-assembling behavior of the gemini surfactants, we focused on the ester linker. Interestingly, adding NC 2067 to the βCDgemini surfactant at different mole ratios (1:0.5, 1:1 and 1:2) resulted in a flattening of the peak corresponding to the free βCDgemini surfactant phase and, simultaneously, appearance of a peak at q of 0.27 $Å^{-1}$ in the scattering pattern (Figures 7.5B-D). Furthermore, at higher q or 2θ angles, some peaks at q of 0.42 $Å^{-1}$, 0.56 $Å^{-1}$, 0.66 $Å^{-1}$ and 0.8 $Å^{-1}$ (corresponding to 2θ angles of 4.3^0, 5.7^0, 6.8^0 and 8.3^0, respectively) are observed for the complexes of NC 2067 and βCDgemini surfactant with higher drug-to-carrier mole ratio. These peaks correspond to the most intense peaks observed in the powder X-ray diffraction pattern of the free NC 2067.

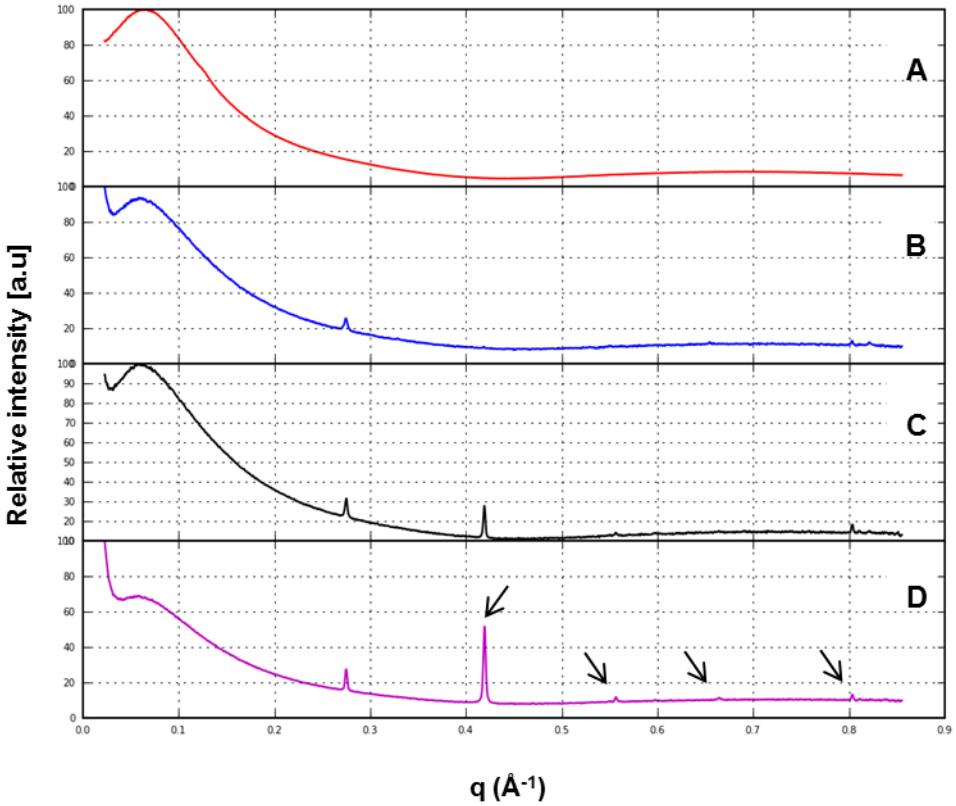

Figure 7.5- SAXS/WAXS patterns of **(A)** βCDgemini surfactant; and complexes of NC 2067 with βCDgemini surfactant at three different mole ratios of **(B)** 1:2, **(C)** 1:1 and **(D)** 1:0.5. Arrows show the peaks corresponding to precipitated NC 2067.

Abbreviations: βCD, βcyclodextrin; βCDgemini surfactant, βcyclodextrin-gemini surfactant; SAXS/WAXS, small- and wide-angle X-ray scattering.

7.4.3. Cell activity of NC 2067 /βCDgemini surfactant formulations

Our aim was to evaluate the effect of various NC 2067/βCDgemini surfactant nanoparticulate formulations, made at different drug-to-carrier mole ratios and with different linkers, on the cell viability of the A375 cell line to complete our previous study.[3]

7.4.3.1. In vitro activity of NC 2067 in complexes with βCDgemini surfactants having different linkers

To evaluate the efficiency of the anticancer agent encapsulated in the carrier, we assessed the ability of NC 2067, in the form of a complex with βCDgemini surfactant, to kill A375 melanoma cells (Table 7.2). NC 2067 in the complex with βCDgemini surfactant (having both amide and ester linkers), at 1:2 mole ratio, showed strong cytotoxic effects, with IC_{50} values of 2.1 ± 0.3 μM and 2.0 ± 0.25 μM, respectively, comparable to the values reported in previous work.[3] The IC_{50} values of NC 2067 in βCDgemini surfactants having different linkers were similar ($P>0.05$).

In order to gain some estimate of the contribution of the delivery agent (βCDgemini surfactant) to the overall toxicity shown by the inclusion complexes (Table 2), the toxicity of the βCDgemini surfactants (both ester and amide linker) was evaluated at a 200 μM carrier concentration. This concentration is approximately 50-fold higher compared to the carrier concentration at the IC_{50} values shown in Table 2 for the complexes. The toxicity of βCDgemini surfactant with amide linker (95% ± 0.5%) was significantly ($P<0.05$) greater than that of βCDgemini surfactant with an ester linker (18% ± 6%) (Table 7.2).

7.4.3.2. In vitro activity of NC 2067 in complex with βCDgemini surfactant in different drug-to-delivery agent mole ratios

We next determined whether the ratio of the drug to delivery agent had any influence on the overall efficiency of the nanoparticles. In a previous study, a 1:2 mole ratio of NC 2067/βCDgemini surfactant was evaluated.[3] Here, we assessed whether lower amounts of the delivery agent could be used for intracellular delivery of the NC 2067. Because the intrinsic toxicity of amide linker was high, we eliminated it from further study. Comparison of the NC

2067 in βCDgemini surfactant (ester linker) at three different drug-to-carrier mole ratios (1:0.5, 1:1 and 1:2) showed comparable efficiency, with IC_{50} values in the range of 2.0-2.4 μM (Table 7.2). Although the three different drug-to-carrier mole ratio formulations showed significantly higher IC_{50} in comparison to NC 2067 dissolved in DMSO, they showed high enough toxicity toward A375 melanoma cell line and were significantly more efficient than mephalan ($P<0.05$).

Table 7.2- IC_{50} values of melphalan in acidified ethanol and NC 2067 in DMSO and various βCDgemini surfactant formulations and percentage intrinsic toxicity of the βCDgemini surfactants.

Anticancer agent	**Delivery agent/Solvent**	**Mole ratio of drug to delivery agent**	**IC_{50} [μM] ± SD**	**% toxicity of βCDgemini surfactant [200 μM] ± SD**
Melphalan	Acidified ethanol	NA	40 ± 9	NA
NC 2067	DMSO	NA	0.5 ± 0.1	NA
	βCDgemini surfactant (amide linker)	1:2	2.1 ± 0.3	94.6 ± 0.5
	βCDgemini surfactant (ester linker)	1:0.5	2.2 ± 0.2	18 ± 6
		1:1	2.4 ± 0.4	
		1:2	2.0 ± 0.25	

Abbreviations: βCD, βcyclodextrin; βCDgemini surfactant, βcyclodextrin-gemini surfactant; DMSO, dimethyl sulfoxide; IC_{50}, half-maximal inhibitory concentration; SD, standard deviation; NA, not applicable.

7.5. Discussion

The comparative analysis of the powder X-ray diffraction patterns of complexes formed between NC 2067 and βCD or βCDgemini surfactant, their physical mixtures and the individual components leads to the conclusion that the complex is a new structure with altered diffraction pattern in comparison to its components, whereas the physical mixture pattern is the overlay of the guest, NC 2067, and the hosts, βCD or βCDgemini surfactant. Similar to these results, it has

been shown that the inclusion of iprodione in βCD displayed new sharp peaks in the diffractogram of the inclusion complex.[313] Furthermore, a complex formed by ibuprofen and βCD, using supercritical carbon dioxide, coprecipitation, and freeze-drying methods, resulted in new peaks, confirming the formation of complexes.[314]

Based on the comparison of the FTIR spectra of the complexes of NC 2067 in βCD or βCDgemini surfactant and their physical mixtures, it has been observed that the peaks corresponding to the aromatic ring conjugated with the alkene C=C bond of NC 2067 are available in physical mixtures, whereas in the complexes, they are weakened or disappear. We hypothesize that the NC 2067 complex with βCD or βCDgemini surfactant arises from the complexation of the 1,5-diaryl-3-oxo-1,4-pentadienyl pharmacophore moiety and not from the side chain moiety substituted on the 4-piperidineone nitrogen atom.

TGA study on NC 2067 complexed with βCD showed no water loss at 30 ºC -70 ºC in comparison to βCD, which lost 10% of its weight in the same temperature region. This phenomenon could be attributed to the fact that NC 2067, accommodated in the βCD cavity, displaced the water from the cavity, similar to a number of inclusion systems in βCD.[260,360] Furthermore, it was observed that βCDgemini surfactant weight did not decrease due to water loss, supporting the argument that inclusion of the hydrocarbon tail of the gemini surfactant in the βCD cavity could have displaced the water molecules commonly located in the βCD ring. This finding is consistent with other studies that show the βCD cavity has the affinity to accommodate the tail of the gemini surfactants and other double-chain surfactants.[173,176-178,361,362]

Moreover, the thermal degradation of NC 2067 complexes formed with βCD or βCDgemini surfactant started at higher temperatures in comparison to that of free NC 2067, suggesting the formation of a more stable complex. Similar thermal behavior was observed in the case of complexation of sulfamethoxazole with hydroxypropyl-βCD, wherein the degradation temperature of the pure compound shifted from 200 ^{0}C to 243 ^{0}C in the complex, confirming that the inclusion complex is more stable than the drug.[254] It is hypothesized that NC 2067 was shielded by the βCD ring and required a higher temperature to degrade due to greater stabilization of the drug in the complexes in comparison to NC 2067 alone.

Overall, it seems that the potential for the gemini surfactant tail to locate whitin the βCD cavity of the βCDgemini surfactant competes with inclusion of NC 2067 and creates a more complicated system in comparison to the binary system consisting of NC 2067 and βCD. Further

studies of the possible inter- and intramolecular self-inclusion behavior of βCDgemini surfactant will be carried out by using proton nuclear magnetic resonance spectroscopy to elucidate the intimate interaction between the guest and host.

Among the formulations, NC 2067/βCDgemini surfactant (ester linker) at a 1:2 mole ratio showed average size of 101 nm, which is optimal for cellular uptake, because particles in the nanometer range can evade the reticulo-endothelial system[13] and enter the cells by endocytosis.[22] An additional benefit of the nano-carriers for anticancer agents is that the presence of nanoparticles in the endosomes prevents the expulsion of the drug through efflux pumps, overcoming the dominant mechanism of resistance toward anticancer agents.[363]

The SAXS/WAXS data of free βCDgemini surfactant showed a diffused pattern that did not change by increasing the concentration. Based on the affinity of the βCD cavity to accommodate the gemini tail(s) of the βCDgemini surfactant, the gemini moiety will be unavailable to form supramolecular assembly in the traditional manner of the gemini surfactants.[153] Moreover, contrary to the case of studies with free gemini surfactants, the constant mole ratio of gemini surfactant to βCD moiety in βCDgemini surfactant compounds leads to the result that increasing the concentration of βCDgemini surfactant does not enhance self-assembly to form micellar structures. This can explain the fact that specific conductivity *vs* concentration profiles of the βCDgemini surfactant (results not shown) do not have a sharp break point, the critical micelle concentration, consistent with that of gemini surfactant, alone. A similar type of aggregate of a long-tailed gemini surfactant with βCD molecules was investigated by small-angle neutron scattering.[364] In the SAXS/WAXS pattern of NC 2067/βCDgemini surfactant complexes (different mole ratios) a new peak emerged. This change in the scattering pattern may be related to the partial displacement of the gemini hydrophobic tail by the NC 2067 from the βCD cavity, providing the gemini surfactant moiety freedom to self-assemble as traditional surfactants. This conclusion is consistent with other observations demonstrating that the gemini monomers, in the presence of βCD, are initially involved in complexation with βCD until the point that the βCD cavity is saturated by gemini surfactant. This phenomenon delays the routine self-assembly of gemini surfactant, resulting in a higher CMC.[174] Similarly, in our system, addition of NC 2067 competes for inclusion in the βCD cavity, possibly replacing the gemini tail(s) from the βCD cavity to some extent, and drives the self-assembly behavior of the gemini surfactant moiety. We speculate that the presence of NC 2067 in the cavity of the βCDgemini acts as a ‘promoter’ to

release the gemini tail from the βCD cavity and to form a more organized and repetitive supramolecular structure with interplanar distances of 22.9 Å (corresponding to q of 0.27 $Å^{-1}$). At this point, the peaks observed in complexes of NC 2067 and βCDgemini surfactant are too few for assignment of a specific supramolecular arrangement, resulting in the hypothesis that the new supramolecular arrangement is formed, partially and that it coexists with the previous self-inclusion arrangements. Moreover, at 0.5:1 and 1:1 mole ratios of NC 2067/βCDgemini surfactant, some peaks related to free NC 2067 became visible. The presence of these peaks is possibly related to the precipitation of NC 2067 in the formulations having lower βCDgemini surfactant-to-NC 2067 mole ratio. On balance, characterization of the βCDgemini surfactant-based nanoparticles suggests that self-inclusion could occur.

The low IC_{50} values of the NC 2067 in complexes with βCDgemini surfactants having amide or ester linkages indicate a high potency toward cancer cell lines. The intrinsic toxicity of the βCDgemini with amide linker was significantly higher than that with the ester linker and could be related to the ability of the amide linker to form hydrogen bonds with the hydroxyl groups of proteins,[365,366] interfering with cellular homeostasis and resulting in an increase in cellular death. Because the long-term goal is to design nanoparticulate formulations for targeted cancer therapy, the intrinsic toxicity of a carrier is a major concern. Therefore, the βCDgemini surfactant with amide linker was excluded from several of the studies in this work. NC 2067/βCDgemini surfactant (ester linker) at different mole ratios showed similar IC_{50} values, which indicates that mole ratio alteration does not change the formulation's efficiency.

Although βCD is considered as a safe excipient and is used in the pharmaceutical industry, some reports suggest that it can remove cholesterol from the cellular membranes of Caco-2 cells, leading to membrane perturbation.[130] Moreover, the presence of a guest molecule in the βCD cavity could decrease its affinity to attach to cell membrane components.[129,130] Gemini surfactants, due to their concentration, spacer length, charge density of the head group, and geometrical packing parameters, have shown different cytotoxicity toward normal skin cell lines such as human keratinocytes and human dermal fibroblasts.[367] Even though both components of the βCDgemini surfactant compound have the capability to be cytotoxic, our study showed that the conjugated βCDgemini surfactant is not toxic for A375 melanoma cell line and shows potential as an inert delivery agent.

7.6. Conclusion

Different analytical techniques such as powder X-ray diffraction, FTIR spectroscopy and TGA support the complexation of NC 2067 with βCD or βCDgemini surfactant. Evidence of the interaction of the aromatic ring(s) of NC 2067 with the interior of the βCD cavity was provided from FTIR studies. Although SAXS/WAXS results suggested that βCDgemini surfactant alone did not show common micellar self-assembly, the presence of NC 2067 initiated the formation of a new supramolecular arrangement. Attention-grabbing self-inclusion behavior of βCDgemini surfactant has been suggested from analysis of TGA thermograms. NC 2067/βCDgemini surfactant nanoparticulate formulations containing different linker types and drug-to-delivery agent mole ratios did not affect the anticancer activity towards A375 melanoma cell line. In the future, more in-depth evaluation of the NC 2067/βCDgemini surfactant aggregation will be performed; techniques such as two-dimensional nuclear magnetic resonance spectroscopy, rotating frame Overhauser effect spectroscopy, and single-crystal X-ray crystallography will be utilized to provide more geometrical details regarding the host-guest complex structures.

7.7. Acknowledgment

Masoomeh Poorghorban is a fellow of the Canadian Institutes of Health Research Training grant in Health Research Using Synchrotron Techniques (CIHR-THRUST) and thanks the program for financial support. We thank Dr. Ferenc Borondics, Canadian Light Source for the IR data collection. Research described in this paper was partly performed using beamline 08B1-1 at the Canadian Light Source, which is supported by the Natural Sciences and Engineering Research Council of Canada, the National Research Council Canada, the Canadian Institutes of Health Research, the Province of Saskatchewan, Western Economic Diversification Canada, and the University of Saskatchewan. Portions of this research were carried out at the Stanford Synchrotron Radiation Lightsource (SSRL), a Directorate of SLAC National Accelerator Laboratory and an Office of Science User Facility operated for the U.S. Department of Energy Office of Science by Stanford University. The SSRL Structural Molecular Biology Program is supported by the DOE Office of Biological and Environmental Research, and by the National Institutes of Health, National Institute of General Medical Sciences (including P41GM103393). The contents of this publication are solely the responsibility of the authors and do not necessarily

represent the official views of NIGMS or NIH. We acknowledge the assistance of Dr. Thomas Weiss, SSRL with instrument setting and data collection.

7.8. Disclosure

The authors report no conflict of interest in this work.

7.9. Supplementary material

S1- Most intense peaks in diffractograms of CD, NC 2067, physical mixture and their inclusion complex powder samples (20 peaks have been shown).

	βCD		**NC 2067**		**Physical mixture**		**Inclusion complex**	
	2θ[^{0}]	d [Å]	2θ[^{0}]	d [Å]	2θ[^{0}]	d [Å]	2θ[^{0}]	d [Å]
1	8.35	7.10	3.89	15.22	3.93	15.07	1.95	30.36
2	7.01	8.45	4.07	14.55	13.89	4.27	13.95	4.25
3	12.95	4.58	13.91	4.27	13.17	4.50	14.41	4.12
4	11.29	5.25	12.87	4.61	11.85	5.00	13.33	4.45
5	13.81	4.30	13.03	4.55	12.79	4.64	15.87	3.74
6	12.51	4.74	13.25	4.48	8.39	7.06	14.83	4.00
7	11.77	5.04	13.41	4.42	12.51	4.74	12.47	4.76
8	11.61	5.11	12.67	4.68	11.49	5.16	12.27	4.83
9	15.07	3.94	16.13	3.68	7.19	8.24	11.75	5.05
10	10.15	5.84	10.57	5.61	16.07	3.70	11.45	5.18
11	14.23	4.17	1.51	39.21	10.51	5.64	16.53	3.59
12	17.89	3.32	11.91	4.98	15.75	3.77	8.35	7.10
13	2.91	20.34	18.91	3.14	16.89	3.52	20.47	2.91
14	16.61	3.58	15.95	3.72	9.89	5.99	10.25	5.78
15	9.71	6.10	20.09	2.96	15.31	3.88	9.33	6.35
16	16.11	3.69	17.03	3.49	13.65	4.35	18.81	3.16
17	7.63	7.76	11.55	5.13	18.81	3.16	7.07	8.38
18	7.81	7.59	15.01	3.96	13.47	4.40	19.39	3.07
19	17.53	3.39	5.19	11.41	18.03	3.30	21.59	2.76
20	5.97	9.92	9.89	5.99	14.33	4.14	18.37	3.24

8. A ^{1}H NMR STUDY OF HOST /GUEST SUPRAMOLECULAR COMPLEXES OF A CURCUMIN ANALOG WITH βCYCLODEXTRIN AND A βCD-CONJUGATED GEMINI SURFACTANT

Masoomeh Poorghorban[a], Abdalla H. Karoyo[b], Pawel Grochulski[ac], Ronald E. Verrall[b], Lee D. Wilson[b*], Ildiko Badea[a*]

[a]Drug Discovery and Development Research Group, College of Pharmacy and Nutrition, University of Saskatchewan, Saskatoon, SK S7N 5E5, Canada

[b]Department of Chemistry, University of Saskatchewan, Saskatoon, SK S7N 5C9, Canada

[c]Canadian Light source, Saskatoon, SK S7N 2V3, Canada

Corresponding authors:

*Ildiko Badea
College of Pharmacy and Nutrition
University of Saskatchewan
Health Sciences Building, 3D01.5
107 Wiggins Road
Saskatoon, Saskatchewan, S7N 5E5, Canada
Phone: 306-966-6349
Fax: 306-966-6377
E-mail: ildiko.badea@usask.ca

*Lee D. Wilson
Department of Chemistry
University of Saskatchewan
Thorvaldson 156
Saskatoon, Saskatchewan, S7N 5C9, Canada
Phone: 306-966-2961
Email: lee.wilson@usask.ca

The contents of this manuscript were submitted to Molecular Pharmaceutics.

In this manuscript we used NMR techniques to elucidate the self-inclusion behavior of the βCDgemini surfactant. One- and two-dimensional rotating frame Overhauser spectroscopy (ROESY) was employed to further comprehend the geometrical interaction of NC 2067 with βCD and βCDgemini surfactant. I prepared all samples and performed experiments except for ROESY samples which Dr. Karoyo helped me in running the samples.

This manuscript addresses the following specific objectives of my research

1.3. To characterize the βCDgemini surfactants

1.5. To use advanced techniques such as 2D ROSEY NMR to understand the structural properties of the drug/βCD and drug/βCDgemini surfactant inclusion complexes

8.1. Table of Contents

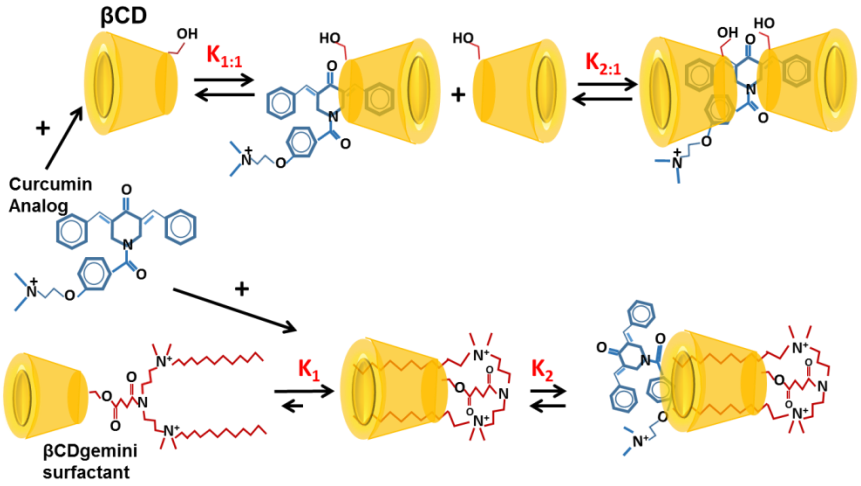

A scheme of various equilibrium processes of the interaction of a curcumin analog (NC 2067) with βCD and βCDgemini surfactant based on 1D/2D ^{1}H NMR studies.

8.2. Abstract

Host systems based on βcyclodextrin (βCD) were employed as pharmaceutical carriers to encapsulate a poorly soluble drug, curcumin analog (NC 2067), in order to increase its water solubility. βCD was chemically conjugated with an amphiphilic gemini surfactant with the ability to self-assemble and to form nanoscale supramolecular structures. The conjugated molecule, βCDgemini surfactant, was shown to be a promising drug delivery agent. In this report, its physicochemical properties were assessed in aqueous solution using 1D and 2D ^{1}H NMR spectroscopy. The results showed that the apolar hydrocarbon domain of the gemini surfactant was self-included within the βCD internal cavity. The host/guest complexes composed of native βCD or βCDgemini surfactant with NC 2067 were examined using 1D/2D ROESY NMR methods. The stoichiometry of βCD/NC 2067 complex was estimated using Job's method via ^{1}H NMR spectroscopy. The binding geometry of NC 2067 within βCD was proposed using molecular docking and further supported by 1D and 2D ROESY NMR results. Addition of NC 2067 to βCDgemini surfactant revealed minimal changes to the overall structure of the βCDgemini surfactant system.

8.3. Introduction

βcyclodextrin (βCD; Figure 8.1a) is a toroidal-shaped macrocyclic oligosaccharide comprised of seven α-*D*-glucopyranose units with a hydrophilic outer surface and hydrophobic internal cavity. βCD and its derivatives have been used widely in pharmaceutical formulations as solubilizing and stabilizing agents. The non-covalent interactions between the βCD host and a hydrophobic drug molecule can result in the formation of stable host/guest inclusion complexes.[246,277,368,369] Moreover, CD-based nanoparticles were recently designed by grafting CDs onto polymers[140,142], incorporating CDs into liposomes[370] and through synthesis of amphiphilic βCDs[143].

Curcumin is an active ingredient of turmeric rhizome and has variable pharmacological activity such as anti-cancer and anti-inflammatory properties; however, curcumin suffers from poor solubility, instability, and low bioavailability. βCD and its derivatives have been utilized in various studies as carriers for curcumin delivery.[100,252,371-373] Recently Jahed *et al.* evaluated the structure of βCD/curcumin inclusion complex by NMR spectroscopy and molecular modeling.[372] They reported that the aromatic rings of curcumin interact with the internal cavity protons of βCD through hydrophobic forces. In another study, the inclusion complex of a curcumin analog in βCD at the 2:1 host/guest mole ratio showed an increased *in vivo* anti-cancer activity.[133] Molecular docking of this complex revealed that the most stable configuration occurred when the curcumin analog was included through its aromatic rings containing the difluoro and methoxy/hydroxyl groups, where several hydrogen bonds were formed with βCD.[133]

In this study, we selected a curcumin analog NC 2067 (Figure 8.1b), as a model guest compound with low water solubility (log*P* = 4.6) that was previously reported to have high cell toxicity toward the A375 melanoma cell line.[3] A novel modified βCD-based carrier named βCDgemini surfactant (*cf.* Figure 8.1c) was designed to enhance the solubility and bioavailability of NC 2067.[3] This bifunctional surfactant was formed by covalently linking βCD to a gemini surfactant (12-7NH-12) through a succinyl group at the primary hydroxyl group of βCD. In a previous study[374], the physicochemical characterization of the inclusion complexes of NC 2067 with βCD and βCDgemini surfactant, respectively, was carried out in the solid state using powder X-ray diffraction (PXRD), thermogravimetric analysis (TGA) and Fourier transform infrared spectroscopy (FTIR).

Herein, we report an NMR study in aqueous solution to examine the geometry of the CD-based host/guest systems. The molecular level interactions in solution were elucidated using complexation-induced shifts (CIS) data of the ^{1}H nuclei located within the βCD cavity, in the presence and absence of NC 2067. In particular, nuclear Overhauser enhancement (NOE) spectroscopy in the rotating frame (i.e. ROESY) proved to be useful in probing *through-space* interactions between the host and guest, especially when the proximity of the nuclei are within 4-5 Å.[289] ROESY is exclusively employed for NOE enhancements in molecules with intermediate (~1000-2000 Da) molecular weight range for host/guest complexes of βCD and small molecules or in molecule systems where the tumbling rates (correlation time) make the measurable NOEs zero or close to zero using conventional NMR methods.[375] ROESY has previously been used to probe the spatial molecular arrangement of the guest in the bound state with CD hosts.[291-293,372,376] For example, three modes of inclusion of econazole nitrate with βCD derivatives were demonstrated based on the correlation of the βCD interior ^{1}H nuclei with 4-chlorophenyl, 2,4-dichlorophenyl and imidazole rings, respectively, using NMR results derived from ROESY experiments.[293]

The structure of βCD and βCDgemini surfactant, respectively, with NC 2067 in the bound state was investigated using ^{1}H NMR and 1D selective/2D ROESY NMR spectroscopy. Furthermore, NMR ROESY results were used to monitor changes in the conformation of the self-included gemini surfactant within the βCD cavity upon addition of NC 2067. 1D/2D NMR results were used to provide evidence for the formation of a ternary complex between βCDgemini surfactant and the NC 2067 drug system.

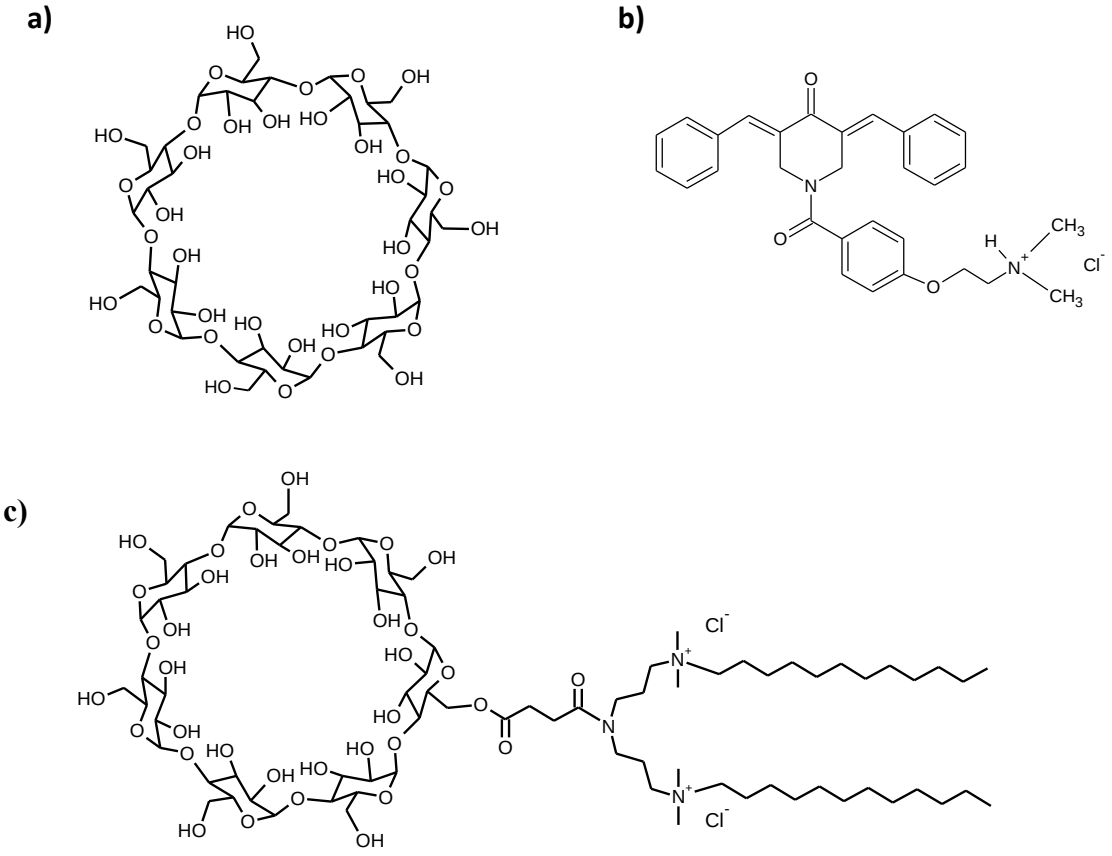

Figure 8.1- Molecular structures of **a)** βCD, **b)** NC 2067 and **c)** βCDgemini surfactant.

8.4. Experimental

8.4.1. Materials

βCDgemini surfactant and NC 2067 were synthesized as described elsewhere.[3,111] βCD was purchased from Alfa Aesar (Haverhill, MA, USA). All other chemicals were purchased from Sigma-Aldrich (Oakville, ON, Canada). Complexes of NC 2067 with βCD or βCDgemini surfactant were prepared as described previously.[374] Samples of βCD or βCDgemini surfactant (host) with NC 2067 (guest) were prepared in 2:1 (host/guest) mole ratios by employing variable concentration ratios (2.5:1.25, 5:2.5 and 10:5 mM). The samples were then reconstituted in D_2O, shaken overnight and analyzed using NMR spectroscopy. The NMR spectrum of Gemini surfactant (12-7NH-12) was obtained at 15 mM.

8.4.2. NMR Spectroscopy

1D/2D ^{1}H ROESY NMR spectra in solution were recorded on a 500 MHz 3-channel Bruker Avance spectrometer in D_2O at 298 K. Chemical shifts (δ) are reported in ppm with respect to trimethylsilane (TMS; δ 0.0 ppm) as external standard and residual water (HOD; δ 4.79) as an internal standard. Complexation-induced chemical shift (CIS) values were calculated as $\Delta\delta = \delta_{\text{free}} - \delta_{\text{complex}}$.

1D selective and 2D ROESY spectra were obtained at variable parameters which were optimized as follows; spin-lock time of 350 ms, recycle delay of 3 s with 8 scans and 1k data points.

8.4.3. Determination of the Stoichiometry

A series of ten βCD/NC 2067 sample mixtures were prepared in D_2O. The concentration of βCD in the samples was varied from 1 to 10 mM with 1 mM increments, where the sum of the mole concentrations of the βCD/NC 2067 mixtures in each sample was kept constant at 10 mM. The mole fraction r ($0 < r < 1$) was determined from the respective mole quantities and volume as shown by the equation below;

$$r = \frac{n_{\beta CD}}{n_{\beta CD} + n_{NC\ 2067}} \qquad (8.1)$$

where, *n* is the moles of the various components. Chemical shift changes (Δδ) of the internal protons (H_3 and H_5) of βCD were evaluated in each sample and a graph of $\Delta\delta \times n_{\beta CD}$ versus mole fraction (r) was used to create the Job plot.[377]

8.4.4. Molecular Modeling

8.4.4.1 3D Structure Optimization

The molecular structure of βCD was downloaded from the Worldwide Protein Data Bank (PDB: DB03995). The molecular structure of NC 2067 was based on an unpublished single X-ray crystallographic study [Appendix 13.1]. Structures were loaded in the Molecular Operating Environment (MOE)[378] software and hydrogen atoms were subsequently added. The structures were minimized geometrically using the force field function of Merck Molecular Force Field (MMFF94X) and applied in the MOE at a RMS (root-mean-square) gradient of 0.001 Å.

8.4.4.2. Docking

Docking with MOE consists of five stages: conformational analysis, placement, rescoring (1), refinement and rescoring (2). In the conformational analysis, a series of torsion angles were applied to the rotatable bonds of the guest (ligand). The alpha triangle was used as a placement method in which the ligand atom triplets and triplets of receptor alpha sphere centers are superimposed. For two stages of scoring, the affinity dG scoring function was used to estimate the impact of enthalpy on the free energy of binding. At the refinement stage the conventional molecular mechanics force field (MMFF94X) was applied for energy minimization. For the first docking run NC 2067 and βCD were set as ligand and receptor, respectively. To estimate the best pose from this run, another βCD was added for the second docking step. Both runs were set to produce 100 poses which were listed and ranked in a database by their relative scoring level in a fashion that the lowest score was the criteria for the optimized complex. At the end of the cycle, the energy of the docked poses was minimized once again.

8.5. Results & Discussion

8.5.1. ^{1}H NMR and 1D/2D ROESY Characterization of βCDgemini Surfactant

To characterize the structure of the bound and unbound host systems, ^{1}H NMR CIS values and NOE effects were used to characterize the βCDgemini surfactant system in the solution, as described below.

8.5.1.1. ^{1}H NMR Spectrum of βCDgemini Surfactant

As a prelude to obtaining ^{1}H NMR spectrum of the βCDgemini surfactant, ^{1}H NMR spectra of βCD and gemini surfactant (12-7NH-12) were acquired in D_2O for comparison. The structures of βCD and βCD-conjugated gemini surfactant are shown in Figure 8.1a and 8.1c and that of 12-7NH-12 is shown in Figure 8.2c. The ^{1}H NMR spectra are presented in Figure 8.3. The chemical shifts (δ) of the βCD protons (both interior and exterior; *cf.* Figure 8.2b) in D_2O are shown in Table 1 and are in good agreement with literature values.[379,380] Positive Δδ values indicate upfield shifts and negative Δδ values downfield shifts.

In the ^{1}H NMR spectrum of the βCDgemini surfactant (Figure 8.3c), the βCD cavity internal protons (H_3 and H_5) showed considerable upfield shift (cf. Table 8.1). The Δδ values for H_3 (0.094 ppm) and H_5 (0.172 ppm) indicate a partial or complete inclusion of the gemini surfactant moiety within the βCD cavity creating considerable shielding effects. This is in agreement with results for well-defined inclusion complexes formed between βCD and alkyl carboxylate anions.[381] Moreover, the ^{1}H NMR spectrum of the external surface protons (H_4) of the βCD moiety for the βCDgemini conjugate displayed downfield shifts (Δδ = -0.03 ppm) indicating a deshielding effect for these protons. This might be related to the proximity of a quaternary ammonium head group near the exterior surface of βCD or a combination of conformational effects of the macrocycle. A similar phenomenon was observed in complexes of βCD with gemini surfactants such as 12-OE_1-12[173] and 12-s-12[177]. Furthermore, the H_6 protons at the narrower rim of the βCD cavity showed an upfield shift of 0.019 ppm (cf. Table 8.1). This may suggest that the inclusion of the gemini surfactant occurs through the narrower rim of the CD host and is consistent with the grafting of the gemini surfactant at the primary end of the βCD, at the O_6 position, as was confirmed previously.[3]

The ^{1}H NMR δ values (ppm) of the gemini surfactant (12-7NH-12; *cf.* Figure 8.2c) are assigned as listed in Table 8.2. These results are in good agreement with previous proton assignments of similar gemini surfactant species.[177] As shown in the spectra of Fig. 3, most of the proton nuclei of the gemini surfactant tail (e.g. H_γ, H_λ, and H_ω) are significantly broadened in the βCDgemini surfactant conjugate relative to the free gemini surfactant (Figure 8.3, shown by asterisks). These observations are consistent with changes in the motional dynamics and hydration states between the bulk solvent and the βCD cavity, and provide further evidence for the interaction of the gemini surfactant with the βCD cavity. The results are similar to a previous

study of a mono-substituted βCD with an amphiphilic moiety containing an alkenyl chain, where self-inclusion of the amphiphilic moiety was reported.[181]

Self-inclusion for this system is supported by previous thermogravimetric results of βCDgemini surfactant system.[374] It was observed that the TGA thermogram of the βCDgemini surfactant did not show any significant water loss at lower temperature (~70 °C) when compared to βCD. This difference in hydration suggested that the βCD cavity in βCD-conjugated gemini surfactant was devoid of hydrate water due to self-inclusion of the gemini surfactant moiety. As well, it was found that increasing the concentration of βCDgemini surfactant did not show any overt break point in a plot of specific conductivity *vs* concentration that is often typical of regular surfactants that undergo self-assembly to form supramolecular structures (e.g., micelles, vesicles or rods). It was herein hypothesized that the βCD cavity was likely fully or partially occupied by whole or a segment of the alkyl chain of the gemini surfactant moiety, precluding the anticipated self-assembly phenomenon. Moreover, results from small- and wide angle X-ray scattering did not provide evidence that the gemini surfactant moiety of βCDgemini surfactant underwent formation of self-assembled structures.[374] The latter is in contrast to the formation of self-assembled structures for non-conjugated (conventional) gemini surfactants.[382] A 1D/2D ROESY NMR study was undertaken to further characterize the structure of the βCD-conjugated gemini surfactant.

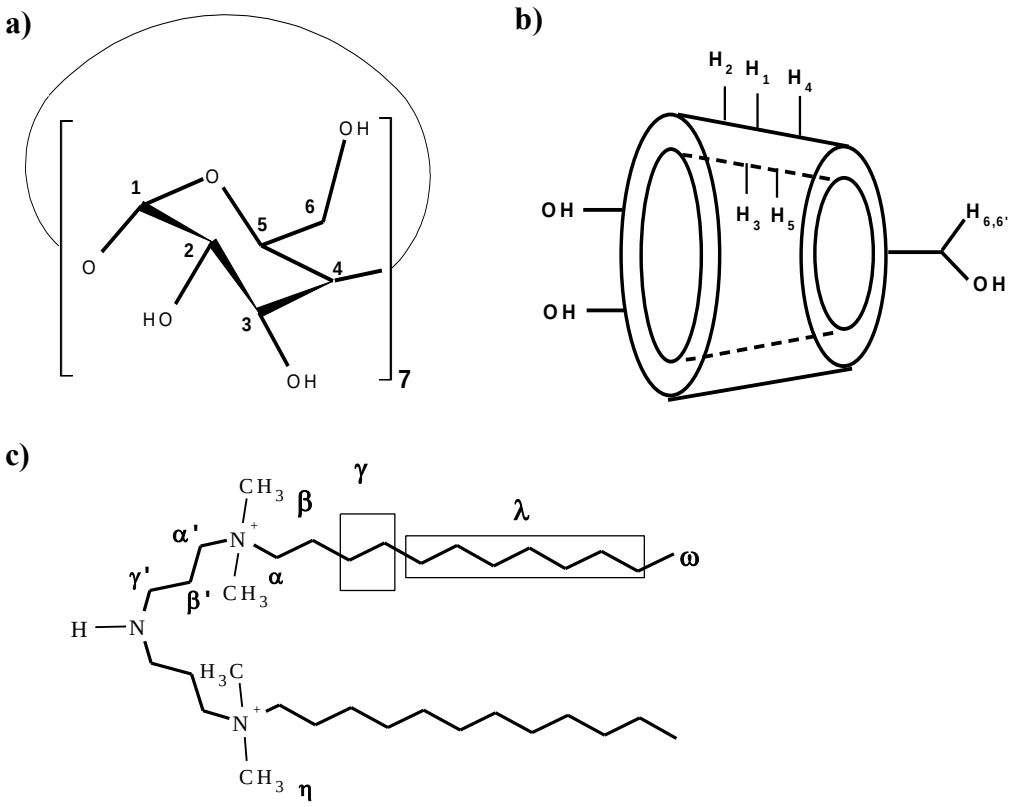

Figure 8.2- a) Numbering of the carbon atoms for the α-*D*-glucopyranosyl unit of βCD, **b)** the relative location of interior and exterior protons of βCD and **c)** proton assignment of gemini surfactant (12-7NH-12).

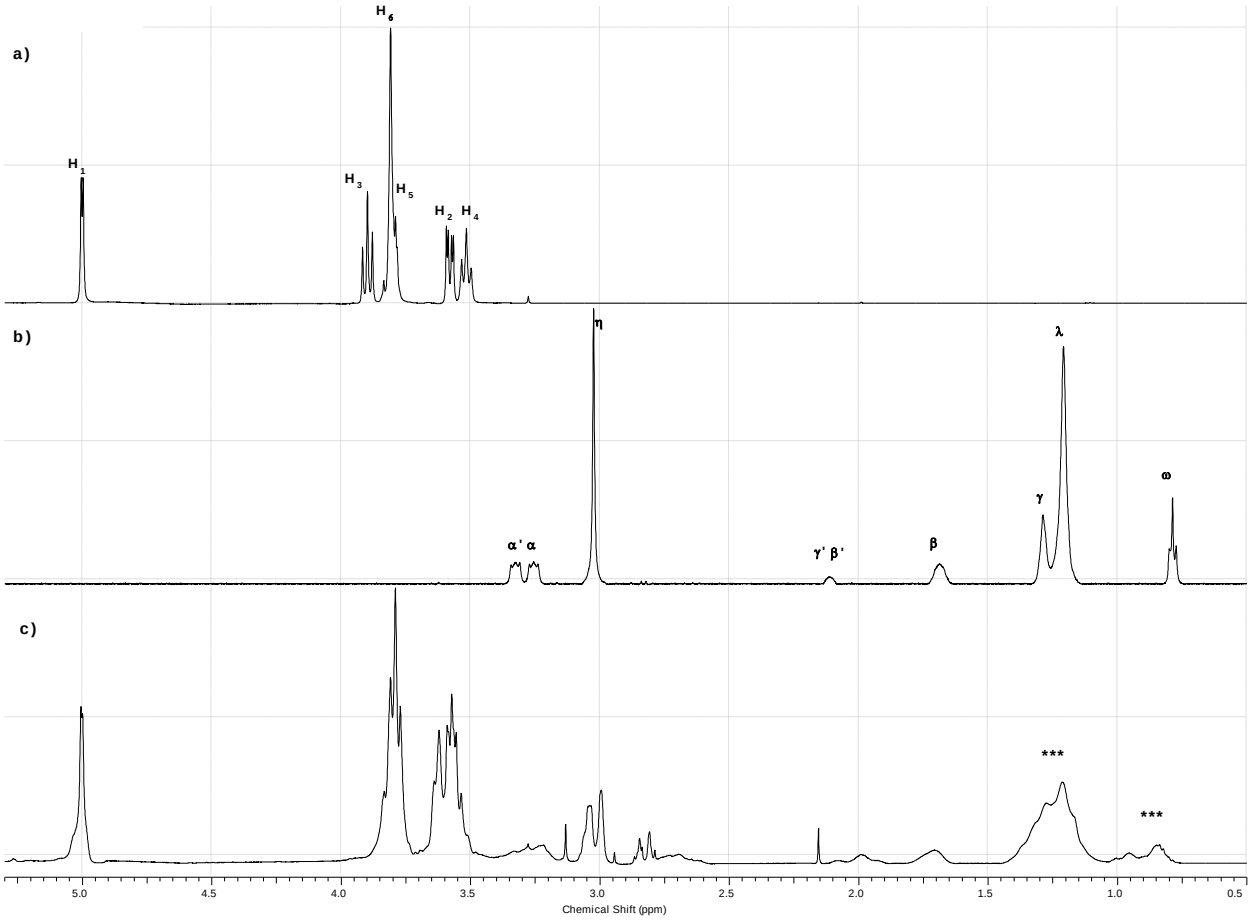

Figure 8.3- ^{1}H NMR spectra of **a)** βCD, **b)** gemini surfactant (12-7NH-12) and **c)** βCDgemini surfactant obtained in D_2O at 298 K. Broadened resonance lines of the hydrocarbon tail (H_ω, H_λ and H_γ) of the gemini moiety are shown by asterisks.

Table 8.1 - Chemical shifts (ppm) for the protons of βCD in free form and in βCDgemini surfactant in D_2O at 298 K.

		βCD	**βCDgemini surfactant**	
		δ (ppm)	δ (ppm)	Δδ (ppm)
H_1	*d*	5.001	5.003	-0.002
H_2	*dd*	3.580	3.582	-0.003
H_3	*t*	3.898	3.804	**0.094**
H_4	*t*	3.516	3.546	-0.030
H_5	*m*	3.803	3.631	**0.172**
H_6	*m*	3.809	3.790	0.019

$\Delta\delta = \delta_{\beta CD} - \delta_{\beta CDgemini\ surfactant}$

d = doublet; *dd* = doublet of doublets; *t* = triplet; *m= multiplet.*

Multiplicity of the protons corresponds to the spectral signatures of βCD hydrate.

Table 8.2- Chemical shifts (ppm) for the ^1H nuclei of gemini surfactant (12-7NH-12) in D_2O at 298 K.

Chemical shifts of gemini surfactant (12-7NH-12) [ppm]		
H_ω	6H $(CH_3)_2$	0.826
H_λ	28H $(CH_2)_{14}$	1.248
H_γ	8H $(CH_2)_4$	1.327
H_β	4H $(CH_2)_2$	1.727
$H_{\beta'+\gamma'}$	4H $(CH_2)_2$ + 4H $(CH_2)_2$	2.151
H_η	12H $(CH_3)_4$	3.064
H_α	4H $(CH_2)_2$	3.292
$H_{\alpha'}$	4H $(CH_2)_2$	3.366

8.5.1.2. 1D/2D ROESY Spectrum of βCDgemini Surfactant

A 2D ROESY spectrum for the βCDgemini surfactant system was obtained to further investigate the self-inclusion phenomenon and the results are shown in Figure 8.4. Well-defined cross-peaks were observed between the internal protons of βCD (H_3 and H_5) and the protons of the gemini hydrocarbon tails (H_ω, H_λ and H_γ) (*cf.* Figure 8.4). Such results suggest that the gemini apolar alkyl chain interacts with the βCD cavity and are consistent with the 1D ^{1}H CIS effects described previously (*cf.* Section 8.4.1.1). Similarly, it was previously shown using 2D ROESY that the alkyl tail or spacer of a gemini surfactant is included in the cavity of native βCD.[173,177]

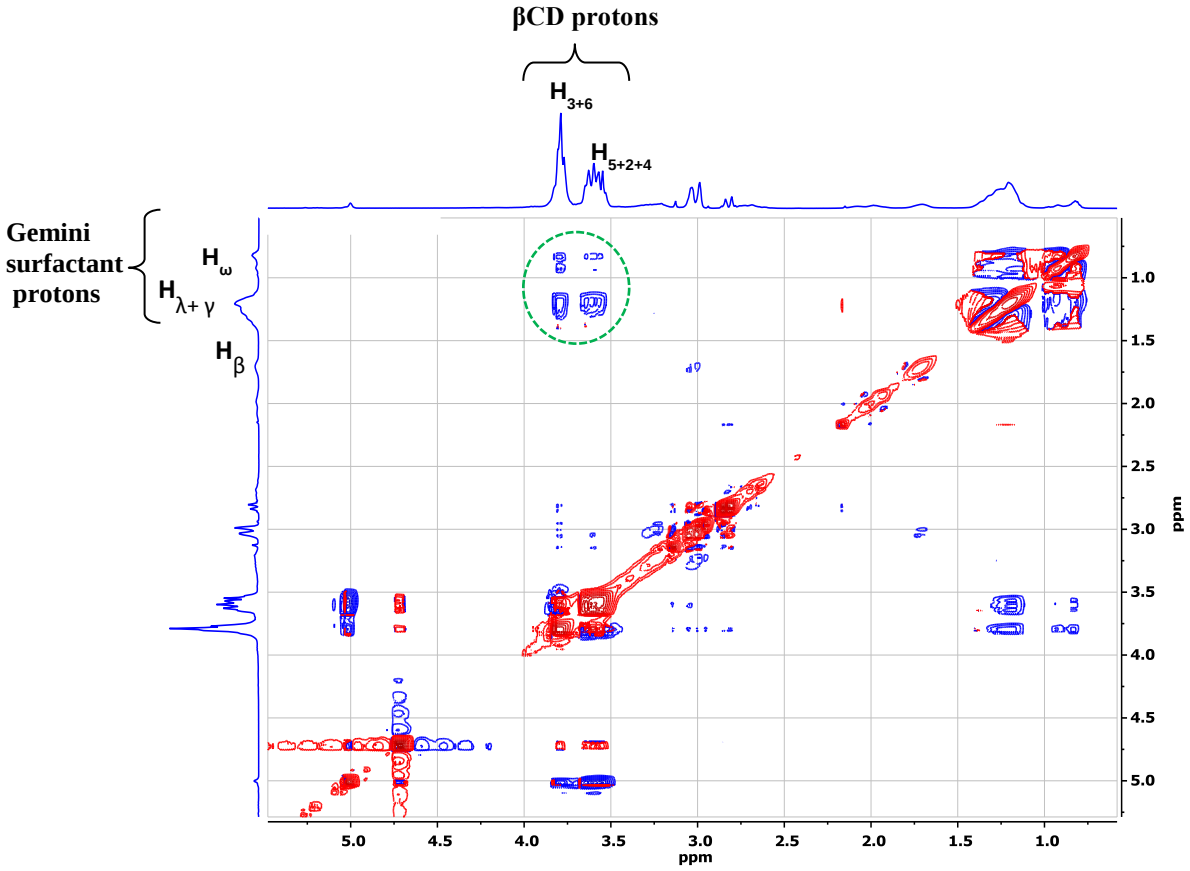

Figure 8.4- Expansion of the 2D ROESY spectrum of βCDgemini surfactant showing the dipolar cross-peaks between βCD cavity nuclei (H_3, H_5) and the gemini alkyl tail (H_ω, H_λ and H_γ).

The greater sensitivity of the 1D ROESY technique offers an option to further confirm the self-inclusion of the gemini tail within the βCD cavity by selectively irradiating the nuclei of interest. The 1D ROESY results for the βCDgemini surfactant in aqueous solution at 298 K are

shown in Figure 8.5. The inversion of the βCD nuclei between 4.0-3.5 ppm was observed due to irradiation of the regions that correspond to H_{ω} (1.0-0.5 ppm) and $H_{\lambda+\gamma}$ (1.5-1.0 ppm) in Figure 8. 5a and b, respectively. Similarly, the excitation of the region corresponding to H_{β} (1.8-1.5 ppm) showed observable interactions with the βCD cavity nuclei (*cf.* Figure 8.5c). This interaction was not evident in the 2D ROESY spectrum and may be attributed to the relatively weak *through space* interactions and the conditions under which the ROESY results were obtained for H_{ω} and $H_{\lambda+\gamma}$. H_{β} ($2CH_2$) is located closer to the gemini polar head group (*cf.* Figure 8.2c) and has weaker interactions with the βCD internal cavity as evidenced by *through space* interactions with the methyl groups (H_{η}) on the quaternary ammonium head groups at δ ~ 3ppm (*cf.* Figure 8.2c, interaction denoted by an asterisk in Figure 8.5).

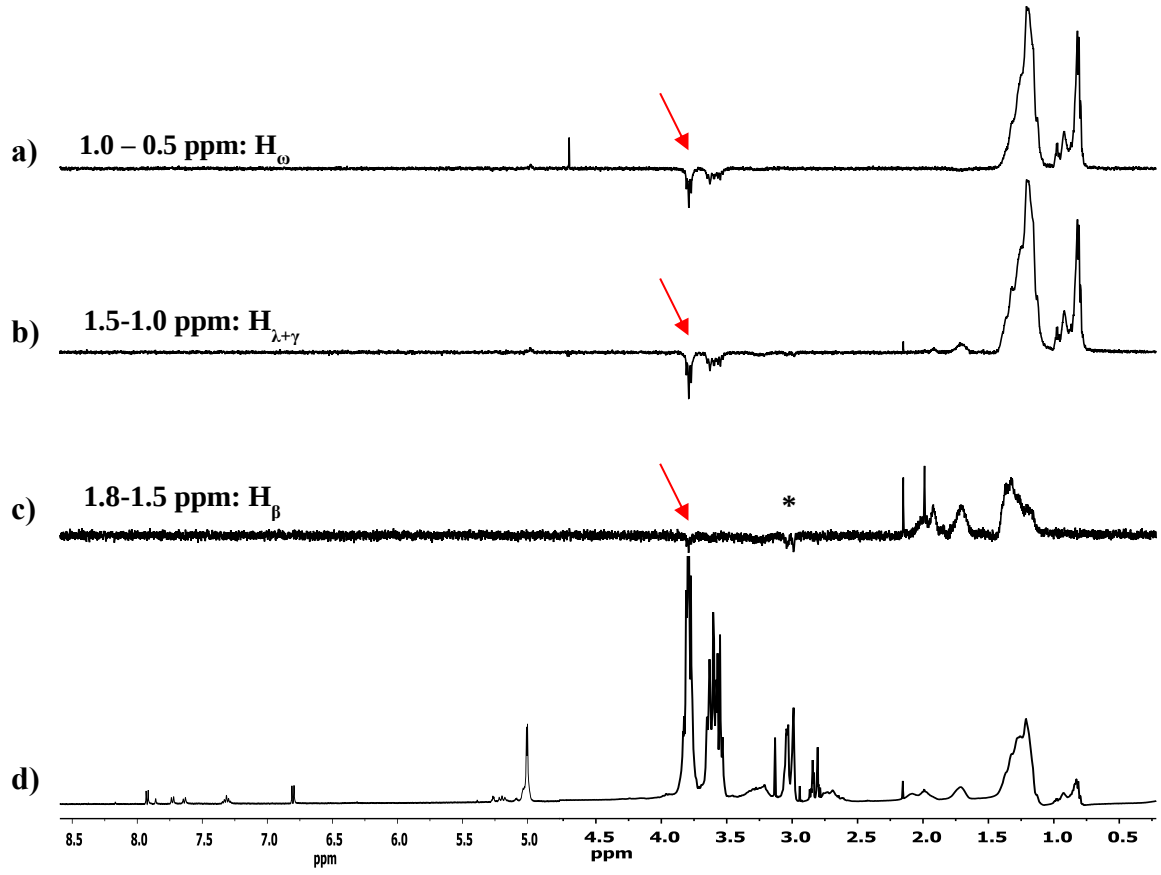

Figure 8.5- 1D ROESY spectra of βCDgemini surfactant (10 mM) with irradiation of various nuclei **a)** 1.0-0.5 ppm (H_{ω}), **b)** 1.5-1.0 ppm (H_{λ} and H_{γ}), **c)** 1.8-1.5 ppm (H_{β}) and **d)** 1D ^{1}H NMR spectrum of βCDgemini surfactant. Arrows show inverted peaks due to interaction with βCD cavity.

8.5.1.3. Self-inclusion of the βCDgemini Surfactant

The inclusion of the gemini alkyl tail(s) may occur due to self-inclusion (intra-molecularly) or by associative interaction between two βCDgemini (inter-molecularly). To understand the nature of the interactions, the chemical shifts of the βCD internal protons (H_3 and H_5) were monitored as a function of concentration of the βCDgemini surfactant. The correlations between concentration and chemical shift changes are shown in Figure 8.6, where Δδ (ppm) were computed by subtracting the chemical shift values of unbound βCD from those of βCD-conjugated gemini surfactant. The chemical shift data are presented as supplementary information (S1). The following observations were noted from Figure 8.6;

(a) No correlations were observed between the chemical shifts changes of H_3 and H_5 and the concentration of βCDgemini surfactant (*cf.* Figure 8.6). The foregoing observation suggests that the self-inclusion process of βCDgemini surfactant occurs intramolecularly such that increasing the concentration of βCDgemini surfactant does not lead to proportionately higher chemical shifts of the internal cavity nuclei, as compared with intermolecular association phenomena.

(b) Even though no correlation was observed between the chemical shifts changes of H_3 with incremental amount of βCDgemini surfactant, increasing the concentration from 1.8 mM to 15 mM yielded a subtle change of $\Delta\delta = 0.013$ ppm for H_5 (*cf.* Figure 8.6). The weak concentration dependence in Fig. 6 could also be interpreted as evidence that intramolecular association (self-inclusion) occurs between the gemini surfactant and βCD cavity.

We concluded from the above scenarios and the results of Fig. 6 that increasing the concentration of βCDgemini surfactant did not affect the magnitude of the chemical shifts of H_3 and H_5 significantly. This result indicates that intramolecular interactions occur between βCD and parts of the gemini surfactant. The subtle chemical shift changes observed for H_5 between the highest and lowest concentration of βCDgemini surfactant cannot be used to unequivocally characterize intermolecular interactions.

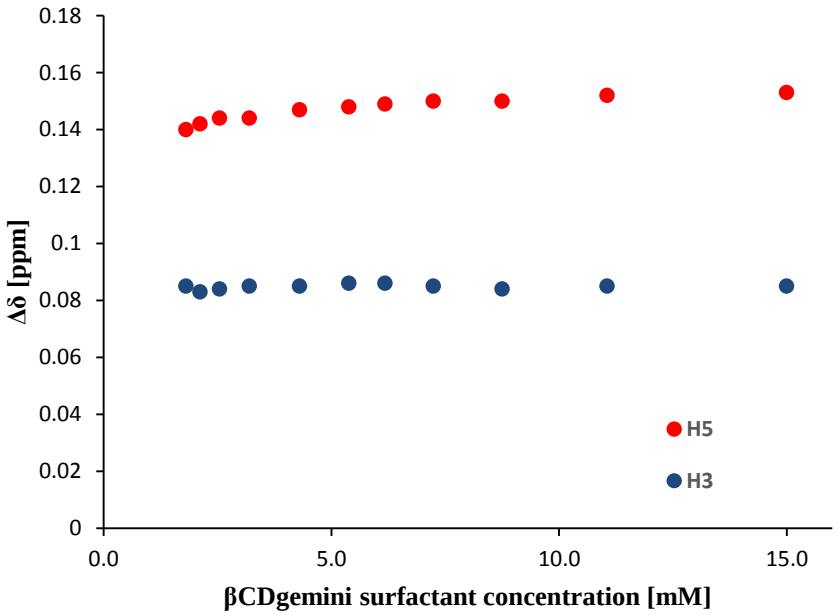

Figure 8.6- Chemical shift changes of H_3 and H_5 observed at incremental concentrations of βCDgemini surfactant (1 to 15 mM).

8.5.2. ^{1}H NMR and 1D/2D ROESY Characterization of βCD/NC 2067 Complexes

8.5.2.1. ^{1}H NMR Spectrum of βCD/NC 2067 Complexes

The ^{1}H NMR spectra of the complexes of βCD and NC 2067 at a host/guest mole ratio of 2:1 at different concentrations were obtained and compared to free βCD (Figure 8.7). The ^{1}H NMR spectrum of NC 2067 in D_2O could not be acquired due to its poor solubility in water. The upfield shifts of the cavity protons of βCD (i.e., H_3 and H_5) in Figure 8.7 indicate a shielding effect due to the inclusion of NC 2067 within the host cavity.

A comparison of the βCD/NC 2067 complex at the highest concentration (10/5 mM) (*cf.* Figure 8.7d) showed significant upfield shifts of ~0.040 and 0.072 ppm for the H_3 and H_5 cavity protons, respectively (*cf.* Table 8.3). This is due to the shielding effects of the apolar phenyl moieties of NC 2067, the anisotropic effect of the π-electrons of the aromatic rings and displacement of cavity bound water.[270-272,274] Increasing the concentration of βCD/NC 2067 from 2.5:1.25 to 10:5 mM resulted in an increase in the magnitude of Δδ for both H_3 and H_5 suggesting a concentration dependent insertion of NC 2067 in the βCD cavity. Although the

inclusion process showed negligible effect on the exterior protons (H_1, H_2 and H_4) of βCD, as expected, the H_6 protons at the narrow face of the cavity also showed an upfield shift of $\Delta\delta \sim$ 0.02-0.03 ppm (Table 8.1). This could be accounted for due to changes in rotamer populations of the CH_2 (C_6) due to approach of the NC 2067 aromatic moiety near the annular hydroxyl groups.[383] The results herein indicate that NC 2067 interacts with the βCD cavity without affecting the CIS values of the external cavity protons.

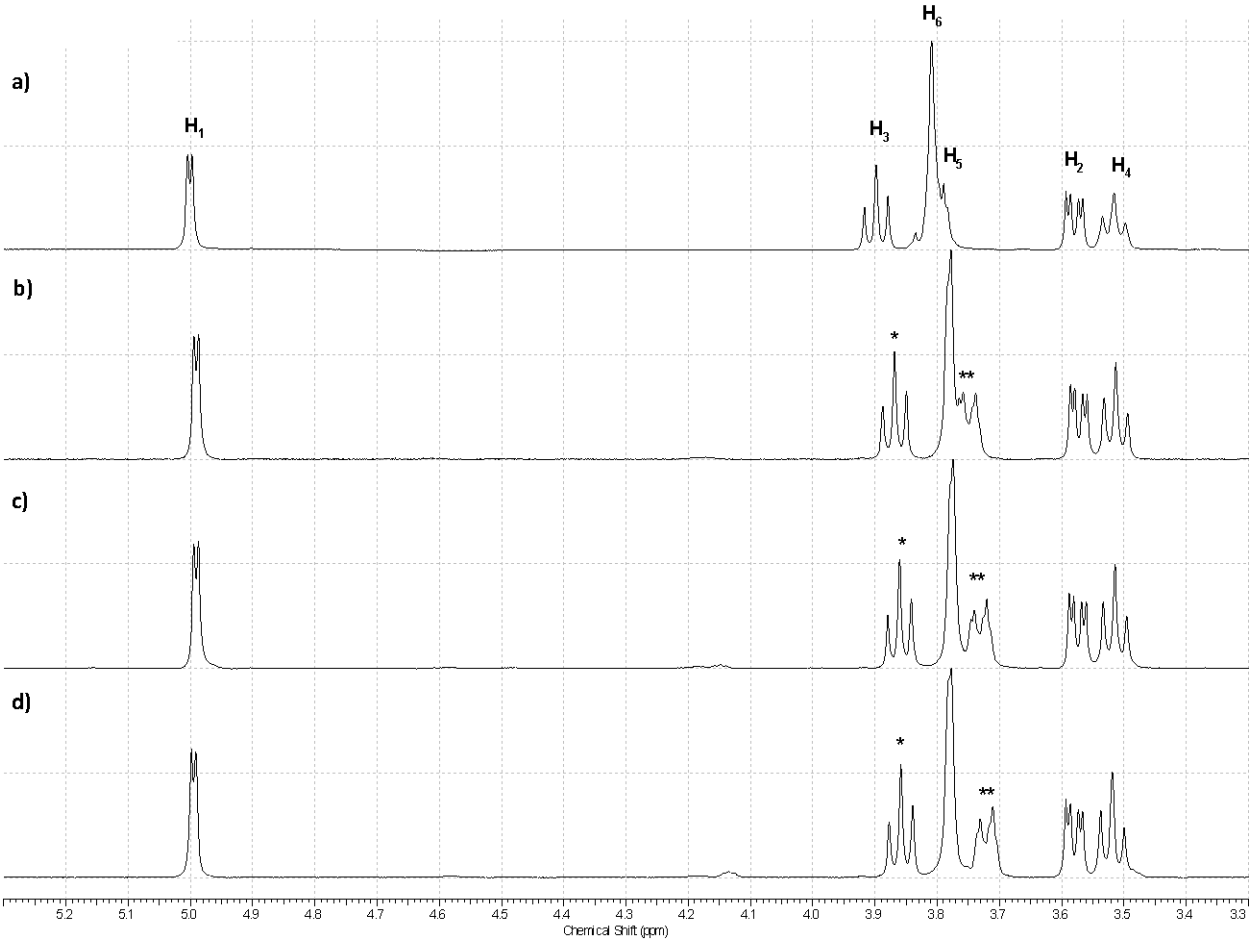

Figure 8.7. Expansion of ^{1}H NMR spectra of **a)** free βCD, and βCD/NC 2067 host/guest complexes at various concentrations of **b)** 2.5/1.25 mM, **c)** 5/2.5 mM and **d)** 10/5 mM collected in D_2O at 298 K. Asterisks correspond to the chemical shifts of H_3 and H_5 for various concentrations of βCD/NC 2067.

Table 8.3 - Chemical shifts (ppm) for the ^{1}H nuclei of unbound βCD and in the bound state with NC 2067 at various concentrations.

	βCD (15 mM)	**βCD/ NC 2067**					
		2.5/1.25 mM		**5/2.5 mM**		**10/5 mM**	
		δ	Δδ	δ	Δδ	δ	Δδ
H_1	5.001	4.991	0.010	4.992	0.009	4.995	0.006
H_2	3.580	3.573	0.007	3.574	0.006	3.580	0.000
H_3	3.898	3.868	**0.030**	3.860	**0.038**	3.858	**0.040**
H_4	3.516	3.513	0.003	3.514	0.002	3.519	-0.003
H_5	3.803	3.753	**0.050**	3.735	**0.068**	3.731	**0.072**
H_6	3.809	3.778	0.031	3.774	0.035	3.778	0.031

$\Delta\delta = \delta_{\beta CD} - \delta_{\beta CD/NC\ 2067}$

8.5.2.2. Stoichiometry of βCD/NC 2067 Complexes

The stoichiometry of the host/guest complex of βCD with NC 2067 was determined using the continuous variation (Job's plot) method.[282] A series of βCD/NC 2067 samples was prepared with different host to guest mole fractions (0 <r <1) and the total concentration was maintained constant. A plot of $\Delta\delta \cdot n_{\beta CD}$ *vs* mole fraction (r) is shown in Figure 8.8. The plots showed a maximum value for H_3 and H_5 protons of βCD when r ~ 0.67, which corresponds to host/guest mole ratio of 2:1 βCD/NC 2067.[283] The 2:1 host/guest stoichiometry is reasonable since there are two styryl ring systems (*cf*. Figure 8.1b) which can be potentially included by two βCD hosts. 1D/2D ROESY results were studied to further understand the structure of the complexes formed between βCD and the drug (NC 2067).

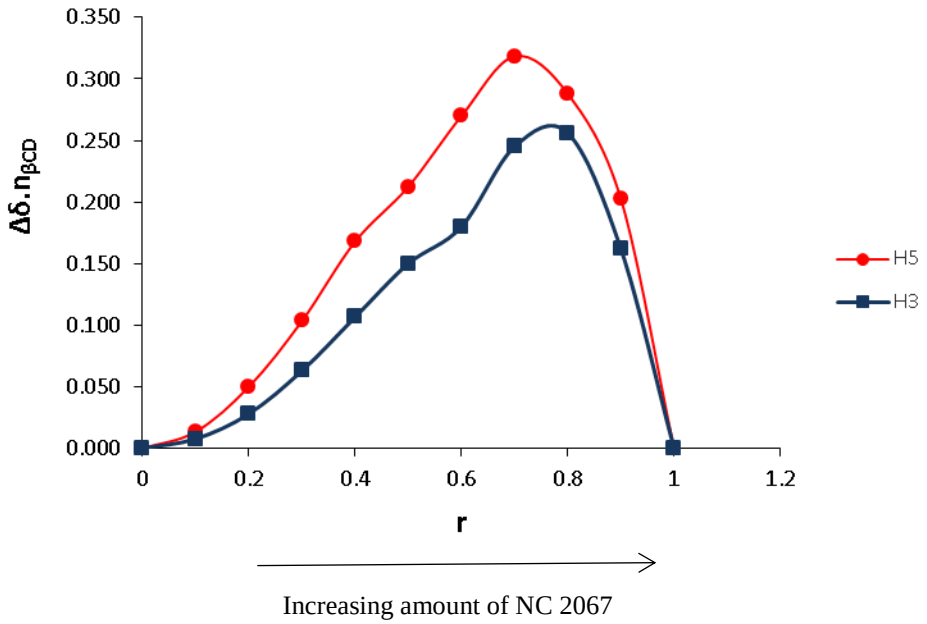

Figure 8.8- Job's plot of βCD/NC 2067 inclusion complex showing an approximate 2:1 host/guest mole ratio in the complex. Lines on the graph serve as a guide and have no other physical meaning.

8.5.2.3. 1D/2D ROESY Spectra of βCD/NC 2067 Complexes

The 2D ROESY spectrum of βCD/NC 2067 was obtained at 2:1 host/guest ratio (*cf.* Figure 8.9). As mentioned above, a detailed assignment of the protons of the aromatic rings of free NC 2067 was precluded due to the poor solubility of the drug in D_2O. However, in the presence of βCD the solubility was enhanced such that the ^1H NMR signatures were observed in the range of 8.0-6.5 ppm, downfield from the βCD protons (~5.3-3.0 ppm; *cf.* Figure 8.9). Moreover, the well resolved 1D spectrum in Figure 8.9 allowed for the assignment of the NC 2067 peaks to its respective aromatic and alkenic protons. The 2D ROESY spectrum of the βCD/NC 2067 complex showed cross-peaks between H_3 and H_5 protons of the βCD cavity and the styryl protons of NC 2067 ($H_{2'}$ and $H_{1'}$; Figure 8.9). All aryl protons (*ortho*-, *meta*- and *para*-) of the styryl group interacted strongly with H_3 protons of the βCD host. The presence of strong cross-peaks for the H_3 protons of βCD was reported elsewhere for the inclusion of fluconazole within βCD through its difluorophenyl moiety.[273] Moreover, it was recently shown from a 2D ROESY study of polymer/dye systems that the phenyl moiety of *p*-nitrophenol was bound by the βCD cavity for a CD-based copolymer.[384]

In general, the NC 2067 guest reported herein displays interaction with the cavity protons of βCD at the position of the styryl, alkene and benzoyl groups (*cf.* Figure 8.9). It is not straightforward in this case to unequivocally characterize a well-defined geometry of the bound drug based on the intensity of the cross-peaks for the different nuclei due to the broadening of the guest signatures. Therefore, the use of molecular modeling may provide an insight regarding the topology of the drug in the bound state with βCD.

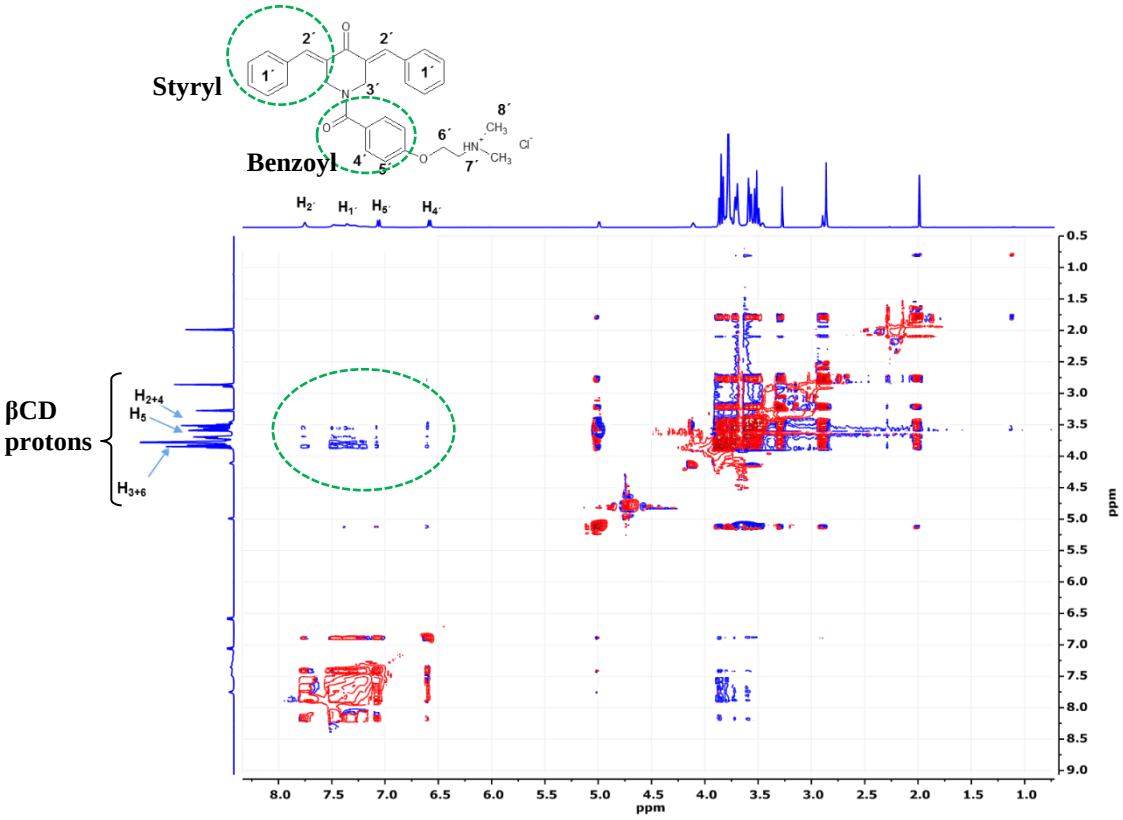

Figure 8.9- 2D ROESY spectrum of βCD/NC 2067 at a 2:1 host/guest mole ratio (10:5 mM), showing cross-peaks between βCD internal cavity protons and NC 2067 protons.

The 2D ROESY technique is prone to sensitivity issues when the solubility of the host/guest system is limited or the fraction of bound species is low. Therefore, the host/guest interactions of βCD/NC 2067 system were further examined using 1D selective ROESY. Various spectral regions of the host or guest were irradiated and the *through space* interactions between NC 2067 and βCD were monitored as inverted signals, as shown in Figure 8.10. Excitation of the

region corresponding to the aromatic and alkenic nuclei of NC 2067 (~8.0-6.5 ppm) showed interactions with the βCD cavity (~4.0-3.5 ppm) region (*cf.* Figure 8.10a) confirming that the aromatic and alkenic nuclei are bound by the βCD cavity. These results were further confirmed by irradiation of the NC 2067 alkenic guest region (~8.0-7.6 ppm), styryl nuclei (~7.6-7.2 ppm) and the benzoyl moiety (~7.2-6.5 ppm), as shown in Figure 10b, c, and d, respectively (denoted by arrows).

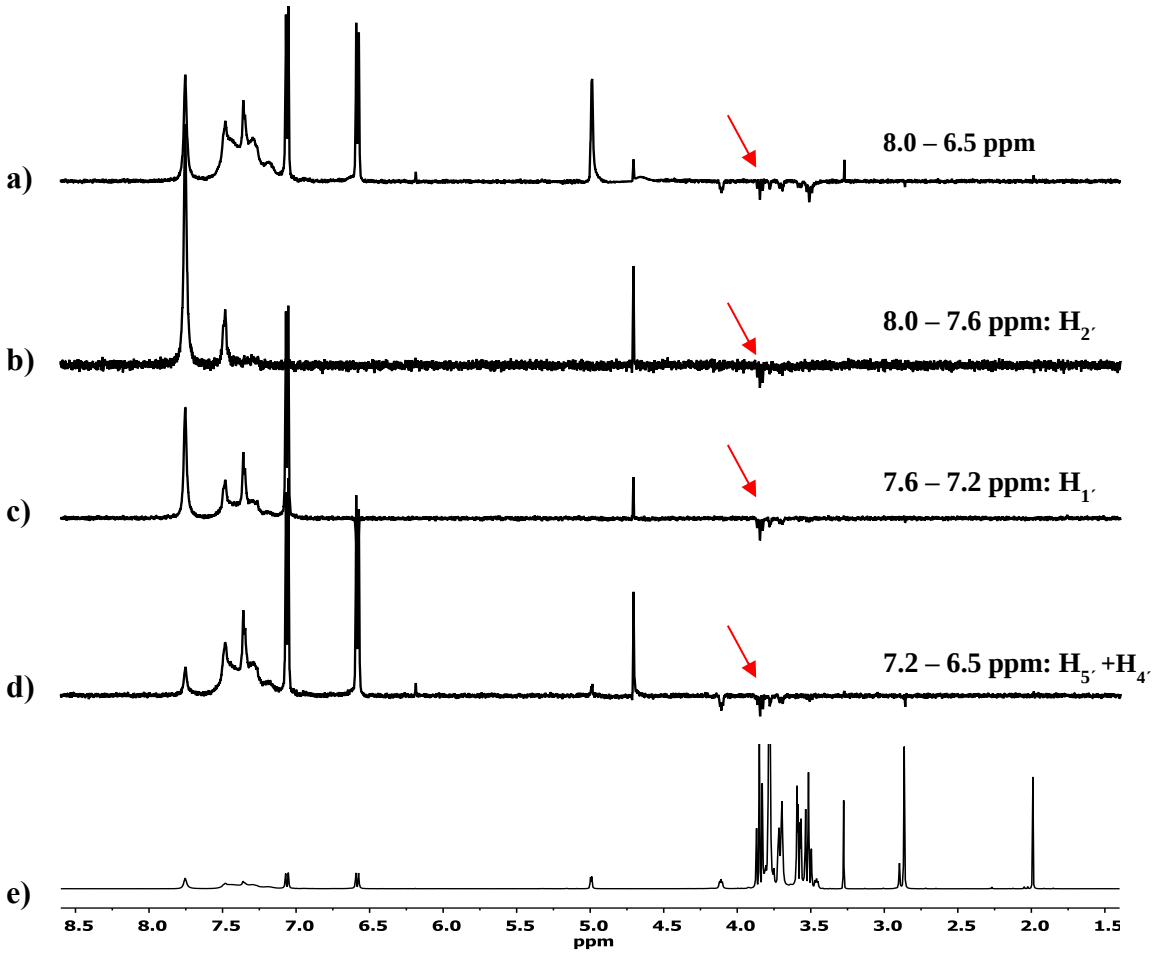

Figure 8.10- 1D ROESY spectrum of βCD/NC 2067 at the 2:1 host/guest mole ratio (10:5 mM) with irradiation at resonance regions between **a)** 8.0-6.5 ppm ($H_{2'}$, $H_{1'}$, $H_{5'}$ and $H_{4'}$), **b)** 8.0-7.6 ppm ($H_{2'}$), **c)** 7.6-7.2 ppm ($H_{1'}$), **d)** 7.2-6.5 ppm ($H_{5'}$ and $H_{4'}$); and **e)** 1D ^{1}H NMR spectrum of βCD/NC 2067. Arrows show the inverted peaks due to interactions with βCD cavity.

8.5.2.4. Molecular Modeling and Mode of Binding of βCD/NC 2067 complexes

Molecular docking results were performed by MOE to illustrate feasible structures of the complexes for the βCD-drug system. The results were used to complement the experimental findings from the 1D/2D ROESY findings and to establish a better understanding of the complex. The initial docking (NC 2067 and βCD set as ligand and receptor, respectively) of the 1:1 host/guest mole ratio showed the most stable binding mode in which the NC 2067 molecule is included within the cavity of βCD with one of the styryl groups (*cf.* Figure 8.11a). This styryl ring is distally remote to the side chain containing the quaternary ammonium group. The non-covalent interactions that occur between the styryl ring of the drug and the βCD cavity (H_3 nuclei) are reasonable based on favorable van der Waals interactions and hydrophobic association. Moreover, the inclusion complexes in which the NC 2067 was inserted in the βCD cavity through the narrower rim were more stable (lower energy of 1.5 kcal/mol) relative to other "poses" where the penetration was performed from the wider side of the cavity and this may be understood on the basis of the dipole moment of the βCD macrocycle. It should be noted that hydration contributions may negate such small energy differences.

The second docking was achieved using the best pose of the first docking attempt in conjunction with a second molecule of βCD which resulted in a series of poses. The lowest energy (best) pose indicated that the second βCD may encapsulate the unbound styryl ring and the benzoyl ring of the drug at the 2:1 host/guest mole ratio (*cf.* Figure 8.11b). βCD may encapsulate a second styryl ring and benzoyl ring, whilst minimizing steric hindrance between each binding site due to the spatial proximity (~4 Å) between the two rings. In addition, the internal diameter of the βCD cavity (6.5 Å) affords inclusion of these two aromatic rings of NC 2067. The modeling results are in good agreement with the 1D/2D ROESY data (*cf.* Section 8.2.2.3) and the *size-fit* requirements of the βCD cavity (6.5 Å) and guest. The interaction of the benzoyl ring ($H_{4'}$ and $H_{5'}$; 7.2-6.5 ppm) occurs with the cavity protons of the second βCD, according to NMR results in Figures 8.9 and 8.10.

In Figure 8.11b, the terminal quaternary ammonium of the side chain of NC 2067 is located outside of the βCD cavity to enable hydration in the solvent phase. However, the carbonyl groups of NC 2067 are positioned between the two βCD rings and form hydrogen bonds with the C_6-OH of βCD. Hydrogen bonds between C_3-OH and C_2-OH at the wider rim and C_6-OH at the narrow rim were observable. It is important to note that the orientation of βCD in

the βCD/NC 2067 complex is tail to tail which may also be stabilized by host-host and water mediated H-bonding interactions.

Finally, the MOE calculations provide a basis for rationalizing the *size-fit* relationship for this host/guest system, however, the global minimum energy for this system may require a fuller account of hydration phenomena. For example, hydrophobic effects are anticipated to be an important driving force in complex formation judging by the relatively low water solubility of the guest (NC 2067).[385]

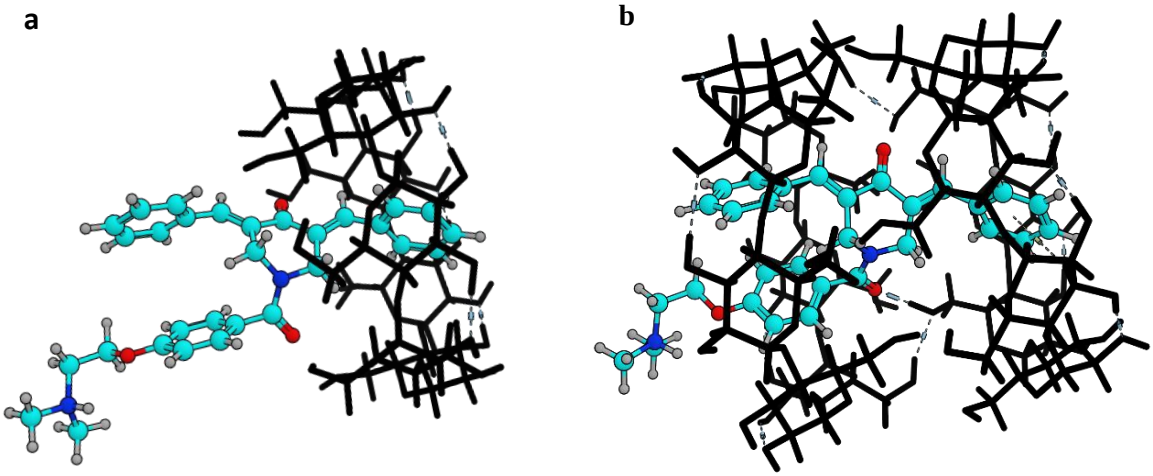

Figure 8.11. The most stable conformation of βCD/NC 2067 complex at **a)** 1:1 and **b)** 2:1 host/guest mole ratios. The βCD host is presented as the wire frame model and NC 2067 guest is presented as the ball and stick model.

8.5.3. ^{1}H NMR and 1D/2D ROESY Characterization of NC 2067/ βCDgemini surfactant Complexes

8.5.3.1. ^{1}H NMR spectrum of NC 2067 / βCDgemini surfactant Complexes

In order to elucidate the molecular interactions between the βCDgemini surfactant with NC 2067, the ^{1}H NMR spectra of different concentrations of βCDgemini surfactant/NC 2067 at the 2:1 host/guest mole ratio were measured and compared with the free βCD and βCDgemini surfactant. The chemical shifts data are shown in Table 8.4 and the ^{1}H NMR spectra are provided as supplementary information (S2). A detailed assignment of the ^{1}H nuclei of the gemini surfactant moiety of the βCDgemini surfactant was difficult to fully resolve due to the spectral broadening and overlap of the nuclei. The addition of NC 2067 to βCDgemini surfactant did not significantly alter the chemical shifts of the βCDgemini surfactant nuclei at various host/guest concentrations. This is in contrast to the βCDgemini surfactant (Section 8.2.1) and βCD/NC 2067 (Section 8.2.2) systems which display significant CIS values for H_3 and H_5 nuclei. The variation in the H_3 and H_5 CIS values for the βCDgemini surfactant/NC 2067 system are less apparent. The formation of a ternary complex (βCDgemini surfactant/ NC 2067) may result in less pronounced chemical shift changes due to the disordered nature of the complex and the likelihood that the drug is bound in an outer-sphere arrangement. Based on the known binding affinity of βCD/surfactant systems,[28] the binding affinity of the self-included alkyl chain of the βCDgemini system is likely 10^3 L/mol or greater. By contrast, the binding affinity of the 1:1 complex for the βCD/NC 2067 guest system must be less than or equal to this value since the drug binding by the βCDgemini surfactant does not displace the self-included alkyl tail upon formation of the ternary complex (i.e. βCDgemini surfactant/NC 2067). 1D/2D ROESY measurements were carried out to study the possibility of competing interactions between the gemini surfactant alkyl chain and NC 2067 within the βCD cavity of the βCDgemini surfactant/NC 2067complex.

Table 8.4 - Chemical shifts (ppm) for the ^{1}H nuclei of βCD in βCDgemini surfactant, alone without drug and at various concentrations of βCDgemini surfactant/NC 2067.

	βCDgemini surfactant	**βCDgemini surfactant/NC 2067**					
		2.5 /1.25 mM		**5/2.5 mM**		**10/5 mM**	
	δ [ppm]	δ [ppm]	Δδ [ppm]	δ [ppm]	Δδ [ppm]	δ [ppm]	Δδ [ppm]
H_1	5.003	4.999	0.003	5.002	0.001	5.005	-0.002
H_2	3.582	3.593	-0.010	3.593	-0.011	3.589	-0.007
H_3	3.804	3.790	**0.014**	3.784	**0.020**	3.802	**0.002**
H_4	3.546	3.542	0.004	3.547	-0.001	3.544	0.003
H_5	3.631	3.649	**-0.019**	3.639	**-0.009**	3.635	**-0.004**
H_6	3.790	3.780	0.010	3.794	-0.004	3.793	-0.003

$\Delta\delta = \delta_{\text{βCDgemini surfactant}} - \delta_{\text{βCDgemini surfactant/ NC 2067}}$

8.5.3.2. 1D/2D ROESY Results of βCDgemini surfactant/NC 2067 Complexes

The 2D ROESY spectrum of βCDgemini surfactant/NC 2067 (Figure 8.12) shows cross-peaks between ^{1}H nuclei of the alkyl chain of the βCDgemini surfactant (H_λ, H_γ and H_ω) and the βCD cavity, similar to the free βCDgemini surfactant in the absence of the drug. However, in contrast to the 2D ROESY results of βCD/NC 2067 system, no interactions of the aromatic protons of the guest drug (8.0-6.5 ppm) with βCD host protons were observed. This reinforces the possibility that the gemini alkyl chain has greater affinity for βCD as described above. By contrast, aromatic ring-containing compounds ordinarily show binding constants of an order of lower magnitude.[372,386] The most notable feature of the 2D ROESY results of βCDgemini surfactant/NC 2067 system in Figure 8.12 are compared with the results of the single component βCDgemini surfactant in Figure 8.5. The absent (or very weak) interaction of H_ω (gemini tail) with H_5 (βCD cavity) is evidenced by the absence of relevant cross-peaks, and provides indirect evidence that the drug may interact with βCDgemini surfactant, further indicating the biological benefit of the complexation.[3,374] The apparent lack of observable interactions between the drug and βCDgemini surfactant host indicates that a non-inclusion ternary complex is formed. It is well established that ternary complexes comprised of a βCD host and two different guest molecules are known in the case of the co-inclusion complexes of pyrene and alcohols with βCD.[387] Therefore, the absence of well-defined cross-peaks between the βCD interior and drug

protons are consistent with the possible formation of a ternary complex, as described above. In a previous study by Udachin *et al*., it was shown that aromatic guests such as pyrene can form non-inclusion complexes within the peripheral hydroxyl region of βCD, whereas 1-octanol can be encapsulated within the CD cavity interior according to single crystal X-ray studies.[388] Based on the structure of such ternary complexes, the absence of *through space* interactions may be expected due to their disordered nature, in agreement with the broadened lines of NC 2067 in the presence of βCDgemini surfactant (*cf*. Figure 8.12).

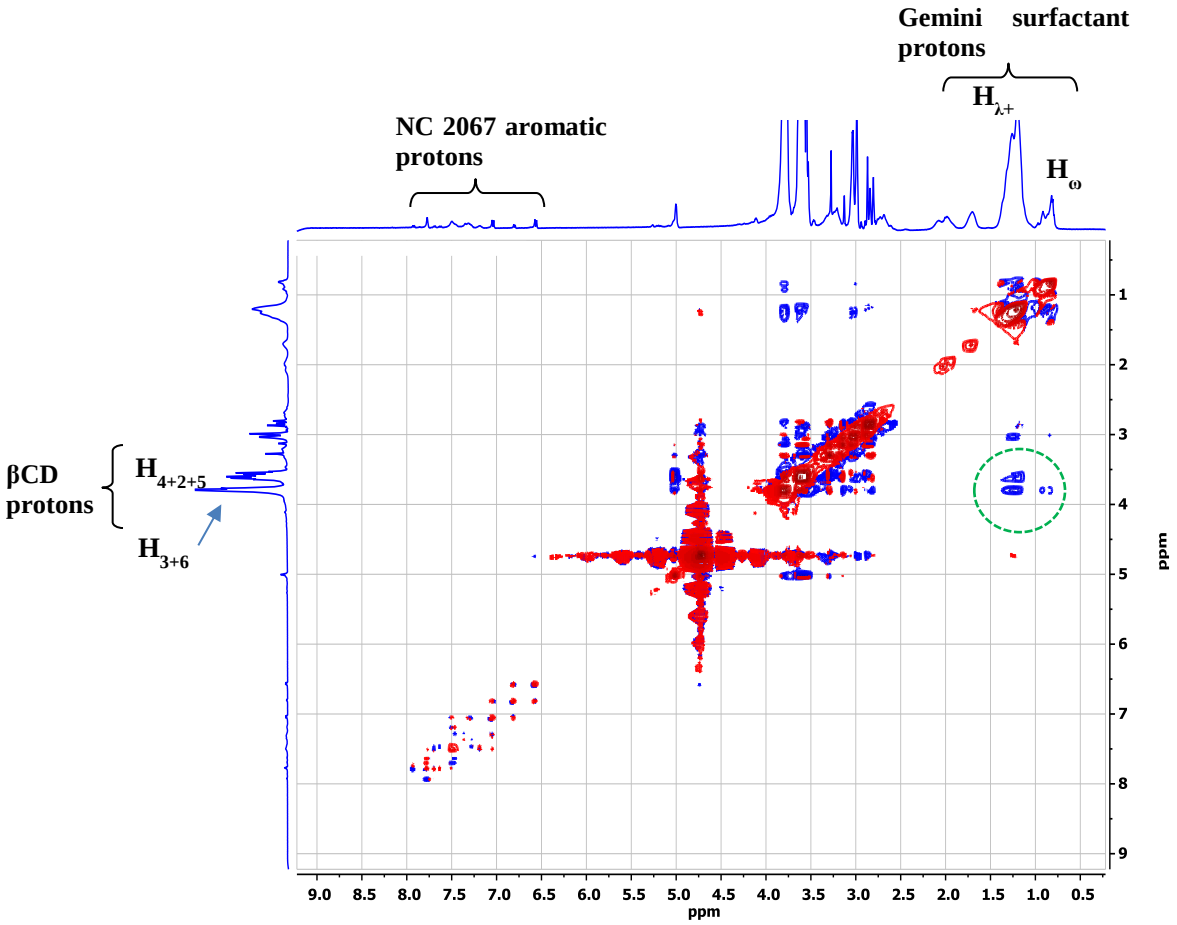

Figure 8.12- 2D ROESY spectrum of βCDgemini surfactant/NC 2067 at the 2:1 host/guest mole ratio (20:10 mM), showing cross peaks between the βCD cavity nuclei and the gemini surfactant alkyl tail.

Once again, due to the higher sensitivity of the 1D- *versus* 2D-ROESY technique, an evaluation of the molecular interactions was estimated from the 1D ROESY spectra for the βCDgemini surfactant/NC 2067 system (Figure 8.13). Irradiation of the aromatic region (8.0-6.5 ppm) did not result in any spectral inversion (Figure 8.13a). Similarly, irradiation of the individual areas corresponding to styryl protons of NC 2067 at 8.0-7.6 ppm ($H_{2'}$) and 7.6-7.2

ppm ($H_{1'}$), did not significantly perturb the resonance lines in the 1D spectrum (Fig. 13b,c). However, irradiation of the benzoyl group at 7.2-6.5 ppm ($H_{4'}$ and $H_{5'}$) resulted in the inversion of the spectral region corresponding to H_5, H_2 and H_4 (Figure 8.13d). Irradiation of the gemini tail nuclei (H_ω, $H_{\lambda+\gamma}$ and H_β) between 1.0-0.5 ppm, 1.5-1.0 ppm and 1.8-1.5 ppm, respectively, resulted in an inversion of the βCD nuclei (*cf.* Figure 8.13e, f, and g). These results are consistent with those for the βCDgemini surfactant in the absence of drug (Figure 8.5). It appears that the addition of the NC 2067 to βCDgemini surfactant did not reveal any notable spectral changes; however, there is a strong possibility of a weak interaction with the cavity due to formation of a ternary complex as revealed by the interaction of the benzoyl moiety. The gemini surfactant alkyl chain shows stronger affinity for βCD cavity as described above.

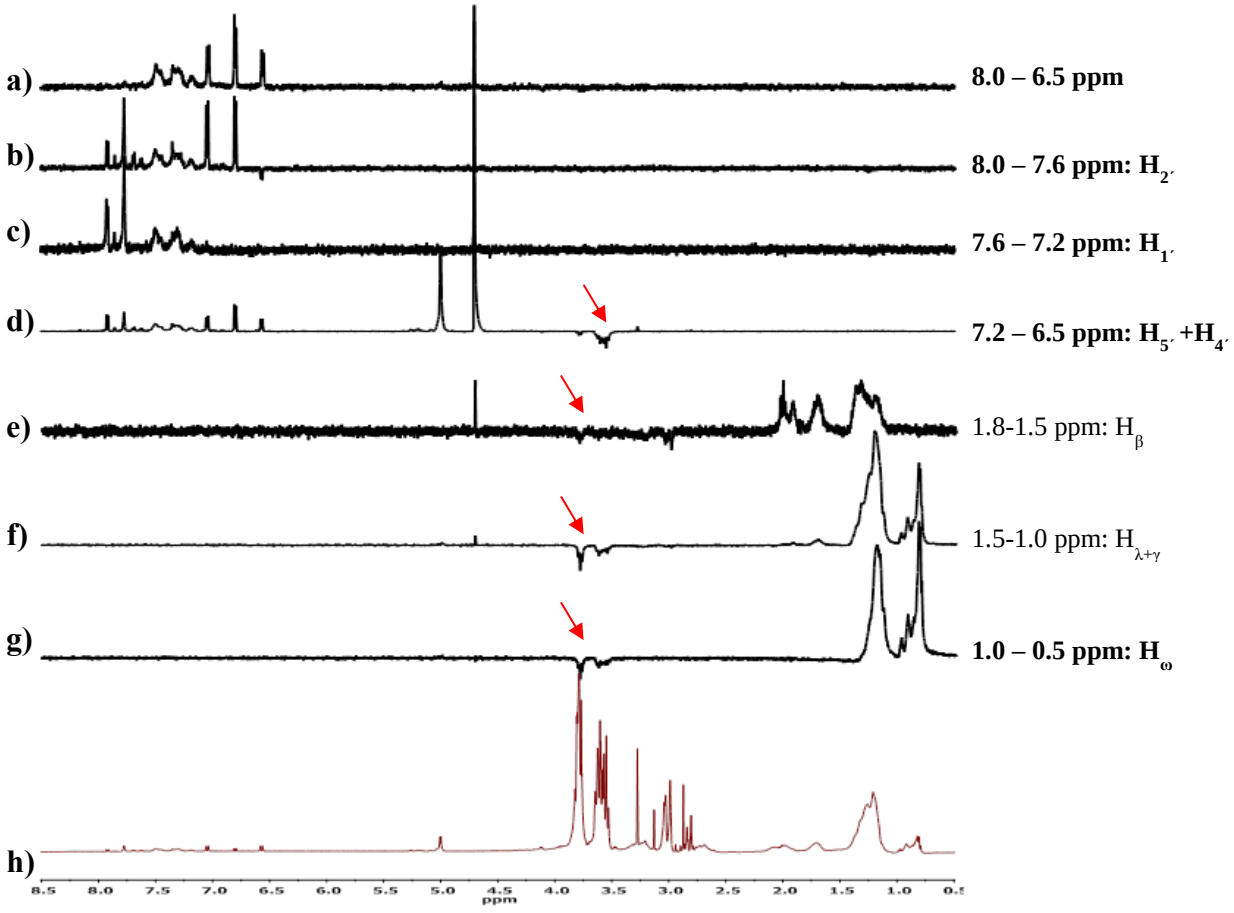

Figure 8.13- 1D ^{1}H ROESY spectra of βCDgemini surfactant/NC 2067 with irradiation of variable spectral regions between **a)** 8.0-6.5 ppm (aromatic protons), **b)** 8.0-7.6 ppm ($H_{2'}$), **c)** 7.6-7.2 ppm ($H_{1'}$), **d)** 7.2-6.5 ppm ($H_{5'}$ and $H_{4'}$), **e)** 1.8-1.5 ppm (H_{β}), **f)** 1.5-1.0 ppm (H_{λ} and H_{γ}), **g)** 1.0-0.5 ppm (H_{ω}) and **h)** 1D ^{1}H NMR spectrum of βCDgemini surfactant/NC 2067 (no irradiation). Arrows show the inverted peaks due to dipolar *through space* interactions within the complex.

The high *in vitro* activity of the NC 2067 manifested in formulations containing βCDgemini surfactant[3,374] is related to the formation of a weakly bound inclusion complex, in agreement with the idea of a ternary complex for the drug and βCDgemini surfactant. The formation of a ternary complex accounts for the weak interactions, structural disorder of the complex, solubilization phenomena and bioavailability of NC 2067 with A375 melanoma cells, as depicted in Scheme 8.1. In addition, the promising results of the *in vitro* studies such as low toxicity of βCDgemini surfactant[374] and the ability to solubilize the drug and increase the bioavailability with the A375 melanoma cell line illustrate the utility of the βCD-conjugated gemini surfactant to act as a unique drug delivery agent.

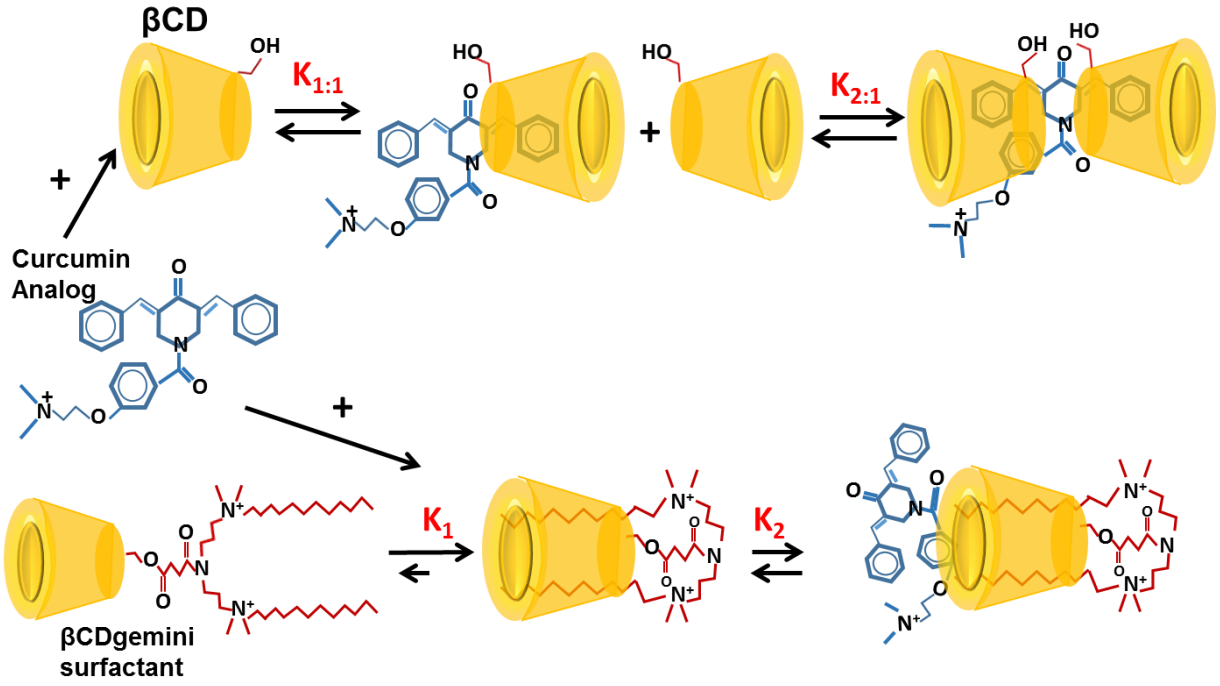

Scheme 8.1- Illustration of various equilibrium processes for βCD and βCDgemini surfactant systems; 1:1 and 2:1 host/guest complex formation for βCD and NC 2067 (Drug), self-inclusion

of the alkyl chains of the gemini moiety according to K_1 and the formation of a ternary complex between the self-included form of βCDgemini surfactant and NC 2067 (Drug) according to K_2. Solvent is not shown for the sake of clarity. K_2 is assumed to be less than K_1 on the basis of the greater extent of inclusion complex formation for K_1.

8.6. Conclusions

In conclusion, three systems were characterized (βCDgemini surfactant, βCD/NC 2067, and βCDgemini surfactant/NC 2067) in order to study the structure of NC 2067 (drug) in βCD-conjugated gemini surfactant complexes. The alkyl tail of the gemini surfactant moiety undergoes intramolecular self-inclusion within the internal cavity of βCD of the βCDgemini surfactant system. The structure of the NC 2067 guest in its complexed form with βCD was evaluated using 1D/2D NMR techniques. The stoichiometry of βCD/NC 2067 system was estimated to be a 2:1 host/guest complex according to the Job continuous variation method. Moreover, 1D/2D ROESY spectra and molecular modeling indicated that NC 2067 was included by two βCD molecules through its styryl and/or benzoyl groups. By contrast, the addition of NC 2067 to the βCDgemini surfactant resulted in only subtle measurable changes to the system[374], and that favorable βCDgemini surfactant self-inclusion still persists. The drug (NC 2067) is weakly bound to the βCDgemini surfactant system and likely forms a ternary complex (*cf.* Scheme 1, in agreement with other related systems[387,388], including the known stability of loosely bound facial complexes for βCD/guest systems.[389]

The results of this study reveal the behavior of a poorly soluble drug molecule in the presence of complexing/solubilizing agents and represent a major step forward in the design of delivery agents that are safe for the formulation of hydrophobic cytotoxic agents. Future steps will be taken to modify the structure of the βCDgemini surfactant conjugate to control self-inclusion phenomena whilst promoting drug encapsulation by βCD to afford effective delivery to the target cells. Moreover, grafting of pH-sensitive moieties that facilitate the intracellular release of the drug from the βCDgemini carrier will also be considered.

8.7. Acknowledgements

Masoomeh Poorghorban is a fellow of the Canadian Institutes of Health Research Training grant in Health Research Using Synchrotron Techniques (CIHR-THRUST) and thanks the program for financial support. We also thank Dr. Jonathan Dimmock and Dr. Umashankar Das who synthesized NC 2067. We are grateful for financial support from NSERC and CIHR to carry out this study.

8.8. Supplementary Data

Table S1. Chemical shift changes of H_3 and H_5 of various concentrations of βCDgemini surfactant relative to βCD.

	Δδ relative to βCD [ppm]	
βCDgemini surfactant concentration [mM]	**H_3**	**H_5**
15.0	0.085	0.153
11.1	0.085	0.152
8.8	0.084	0.150
7.2	0.085	0.150
6.2	0.086	0.149
5.4	0.086	0.148
4.3	0.085	0.147
3.2	0.085	0.144
2.5	0.084	0.144
2.1	0.083	0.142
1.8	0.085	0.140

$\Delta\delta = \delta_{\beta CD} - \delta_{\beta CDgemini\ surfactant}$

Figure S2- Expansion of ^{1}H NMR spectra of **a)** free βCD, **b)** free βCDgemini surfactant, βCDgemini surfactant/NC 2067 complexes at various concentrations of **c)** 2.5/1.25 mM, **d)** 5/2.5 mM and **e)** 10/5 mM in D_2O collected at 298 K.

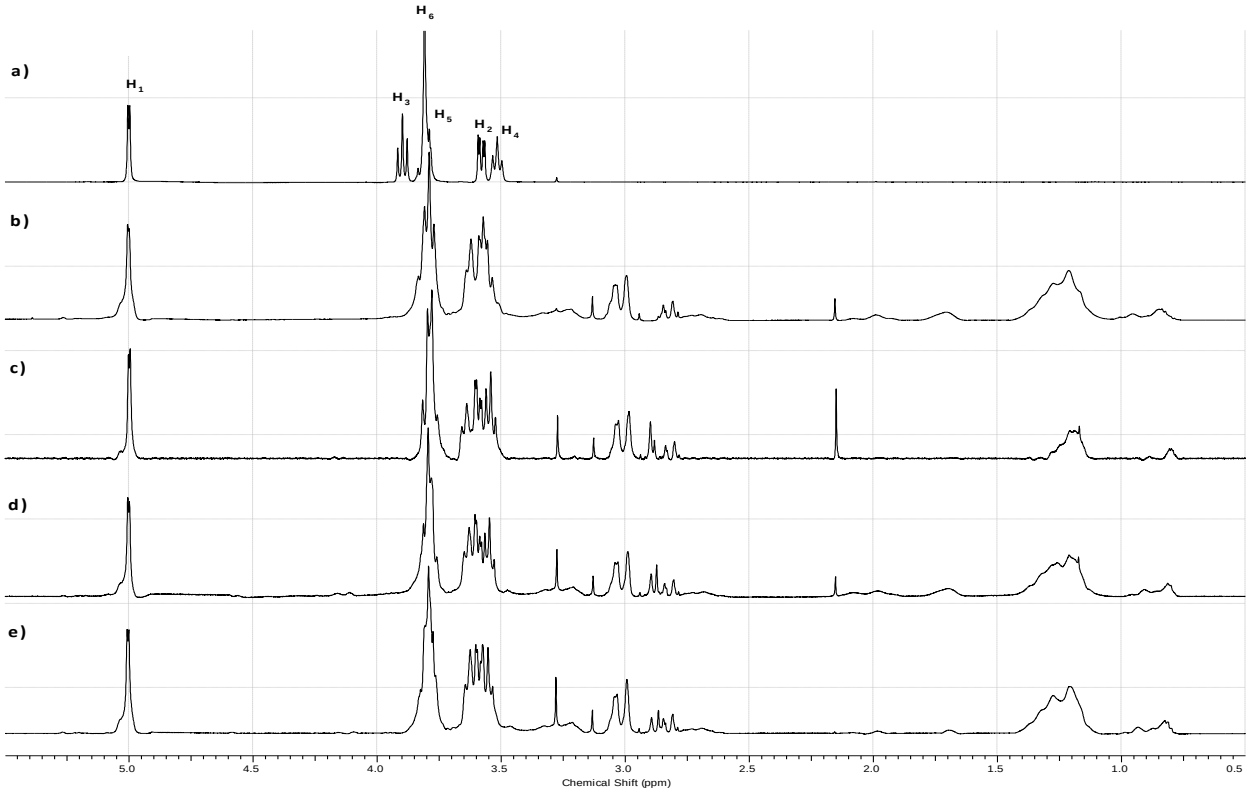

9. βCDGEMINI SURFACTANT-BASED FORMULATIONS OF A CURCUMIN ANALOG: NANOPARTICULATE BEHAVIOR AND MECHANISM OF CELL DEATH IN MELANOMA MODEL

Masoomeh Poorghorban[1], Deborah Michel[1], Umashankar Das[2], Peter R. Hull[3], Jonathan Dimmock[1], Pawel Grochulski[1,4], Ildiko Badea[1*]

[1] Drug Discovery and Development Research Group, College of Pharmacy and Nutrition, University of Saskatchewan, Saskatoon, Saskatchewan, Canada

[2] Department of Chemical and Biological Engineering, University of Saskatchewan, Saskatoon, Saskatchewan, Canada

[3] Division of Clinical Dermatology & Cutaneous Science, Department of Medicine, Dalhousie University, Halifax, Nova Scotia, Canada

[4] Canadian Light Source, Saskatoon, Saskatchewan, Canada

Corresponding author:
*Ildiko Badea
College of Pharmacy and Nutrition
University of Saskatchewan
Health Sciences Building, 3D01.5
107 Wiggins Road
Saskatoon, Saskatchewan, S7N 5E5, Canada
Phone: 306-966-6349
Fax: 306-966-6377
E-mail: ildiko.badea@usask.ca

In this manuscript βCDgemini surfactants having various chain length and degree of unsaturation of the tail of the gemini surfactant moiety were used in NC 2067/βCDgemini surfactant formulations and their nanostructural behavior in solution was evaluated. Moreover, the cell death mechanism associated with the formulations toward A375 melanoma cells was assessed.
The co-authors of this manuscript contributed in the synthesis of NC 2067 and running the flow cytometer.

This manuscript addresses the following specific objectives of my research,

1.2. To develop formulations by varying the mole ratio between the drug and delivery agent, using βCDgemini surfactants with various gemini surfactant tails

1.3. To characterize the βCDgemini surfactants

1.6. To use synchrotron small- and wide angle X-ray scattering (SAXS/WAXS) to evaluate the supramolecular arrangement of drug/βCDgemini surfactant delivery systems in solution

2.1. To calculate the cell toxicity (IC_{50}) of different drug/βCDgemini surfactant formulations towards melanoma cell line

2.2. To elucidate the type of cell death mechanism and cell cycle arrest behavior of different drug/βCDgemini surfactant formulations using flow cytometry-based assays in melanoma cells

9.1. Abstract

Lipid-based nanoparticles are widely used to encapsulate lipophilic anticancer agents to enhance their bioavailability and efficacy. We evaluated the nano-structural behavior of a curcumin analog encapsulated by gemini surfactant-based carriers. Furthermore, the cell death mechanism of the curcumin analog in presence of the delivery agents was evaluated.

The aggregation behavior of the curcumin analog with various βCDgemini surfactants were investigated using synchrotron-based small- and wide angle X-ray scattering and size measurements. Finally, the *in vitro* cytotoxicity and cell death mechanism of the formulations were measured by cell viability assay and flow cytometry, respectively.

We showed that the addition of a curcumin analog to βCDgemini surfactants having various chain length and degree of unsaturation formed nano-sized structures. Moreover, these formulations induced apoptosis without any influence on cell cycle in A375 melanoma cells.

9.2. Introduction

To increase the accumulation of a chemotherapeutic agent at cancer site, and minimize non-specific distribution in the body, a novel approach is to encapsulate the active agent into nanoparticles.[390] Drugs encapsulated into nanoparticles preferentially accumulate in tumors due to the enhanced permeability and retention effect that permits extravasation of the nanoparticles into the tumor through the leaky vasculature.[391] In addition, barriers such as the epithelial tight junctions might be overcome by the utilization of nanoparticles.[392]

Amphiphilic lipids such as surfactants containing hydrophilic and hydrophobic parts are frequently employed for the delivery of anticancer drugs.[36] They can self-assemble in aqueous media and subsequently build ordered nanoparticulate structures known as lyotropic liquid crystals (LLC). Nanostructured LLCs can be distinguished from micelles or vesicular lipid aggregations by the presence of the internal molecular organization in LLC structure. Nanoparticles built of LLC mesophases are able to incorporate different small molecule anticancer agents[40,41] to enhance their bioavailability via various routes of administration. Gemini surfactants as amphiphilic lipids have the potential to form lyotropic liquid crystalline mesophases in excess of water.[157,158] Nature and length of the hydrocarbon tail impact the phase behavior of gemini surfactants.[162,163] A new class of cationic gemini surfactants named as βCDgemini surfactant has been synthesized by addition of βcyclodextrin (βCD) to different cationic gemini surfactants (12-7NH-12, 16-7NH-16 and 1:18-7NH-18:1)[3] (Figure 9.1) in our laboratory. The presence of the βCD that can encapsulate hydrophobic molecules renders βCDgemini surfactant a promising carrier for insoluble anticancer agents such as curcumin analogs.[3,133-136]

A variety of curcumin analogs were synthesized with anticancer activity towards melanoma cell lines.[107,239] Molecular mechanism associated with the anti-melanoma activity of curcumin and its analogs toward different cell lines has been reported in the literature, as some form of apoptosis.[107,231,237,238]

Apoptosis is the targeted cell death mechanism induced by the chemotherapeutic agents in cancer treatment. This programmed type of cell death, is naturally occurring in a variety of cells to maintain homeostasis. Apoptotic morphological changes involve nuclear cell shrinkage[182], cytoskeleton disintegration[183], chromatin condensation[184], DNA fragmentation[185], membrane budding and formation of the apoptotic bodies. Moreover, during apoptosis, phosphatidylserine

(PS), an aminophospholipid located on the inner-leaflet of the cell membrane, is externalized and localized on the surface of the cell membrane.[186] Curcumin analogs showed to induce apoptosis in melanoma cells mainly through mitochondrial mediated pathway activating caspase-3, -7 and -9.[3,107,109] For example, the proapoptotic effect of a curcumin analog, named DM_1, was reported to be implemented in A375 melanoma cell line by downregulation of the antiapoptotic Bcl-2 proteins (e.g. Mcl-1 and Bcl-xL) and the inactive form of caspase-3 and upregulation of the active form of caspase-9.[238]

In this paper, our aim is to assess the proapoptotic effect of NC 2067 (Figure 9.1D), a model curcumin analog, that showed high *in vitro* cell toxicity towards A375 melanoma cell line.[3] In addition, we previously introduced a formulation made of NC 2067 complex with βCDgemini surfactant surfactant-12 (Figure 9.1A) so as to overcome the poor solubility associated with the anticancer agent.[3] We reported that NC 2067 in βCDgemini surfactant- based nanoparticulate formulation retained its high *in vitro* activity toward A375 cell line and increased the executioner caspases (-3 and -7).[3] Furthermore, we evaluated the physicochemical properties and nanoparticulate behavior of the formulation of NC 2067/βCDgemini surfactant-12 extensively.[374] Herein, cell death mechanism of the formulation comprised of the βCDgemini surfactants (Figure 9.1) are assessed using flow cytometry. Moreover, we evaluated the correlation between chain length and degree of unsaturation of the tail of the gemini surfactant moiety and the behavior of the lipid-based nanoparticulate formulations.

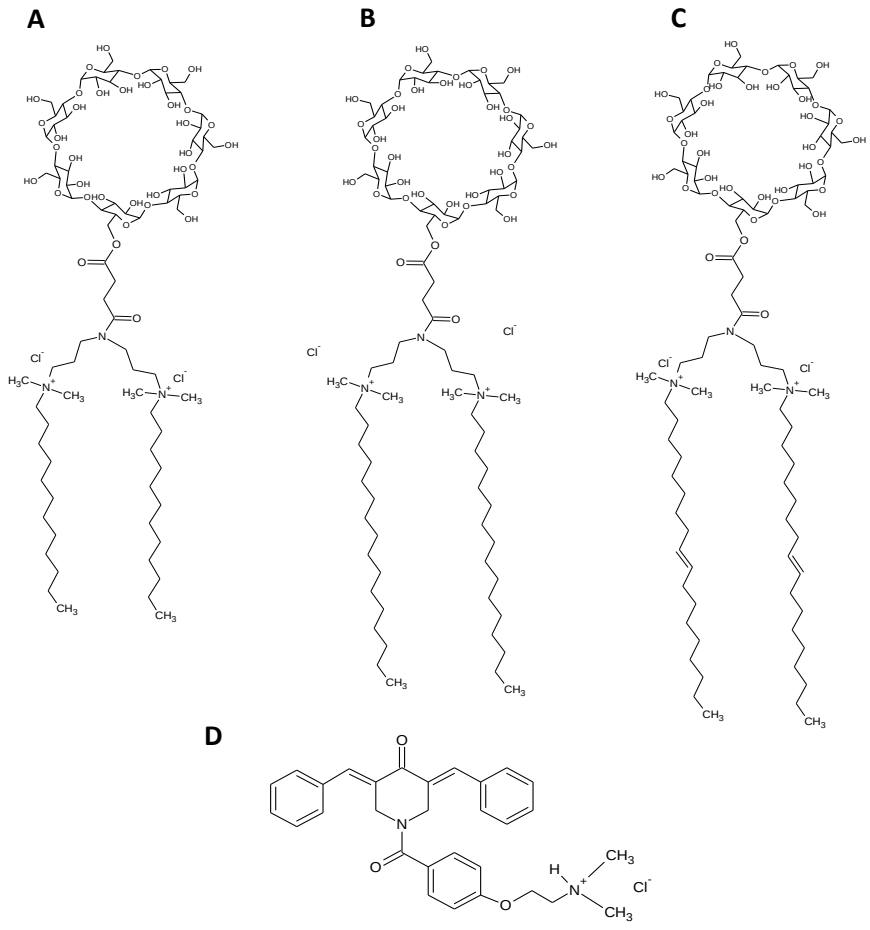

Figure 9.1- Chemical structures of βCDgemini surfactants **A)** -12, **B)** -16, **C)** -18:1; synthesized by the attachment of βCD to different gemini surfactant moieties and **D)** NC 2067.

9.3. Materials and Methods

9.3.1. Preparation of inclusion complexes

NC 2067 and βCDgemini surfactants were synthesized as described previously.[111,3] All other chemicals were purchased from Sigma-Aldrich (Oakville, ON, Canada). Complexes of NC 2067 with βCDgemini surfactants (-12, -16 and -18:1) were formulated as described previously.[374]

9.3.2. Size measurements

Particle sizes in solution were measured by using a Zetasizer Nano ZS instrument (Malvern Instruments, UK). Results are reported as the mean of 3-5 measurements ± standard deviation.

9.3.3. Small- and wide-angle X-ray scattering (SAXS/WAXS) measurements

SAXS/WAXS measurements were performed at the BL4-2 beamline at Stanford Synchrotron Radiation Lightsource (SSRL, Stanford, CA, USA). The samples containing NC 2067/βCDgemini surfactant complexes with constant concentration of surfactant (10 mM) were studied at energy of 11 keV, a sample to detector distance of 1.1 m and exposure time of 20 second. Diffraction intensity *versus* q (scattering vector) plots were obtained by radial integration of the 2D patterns using GSAS-II software.[393]

9.3.4. Cell viability assay

A375, human amelanotic melanoma cells (American Type Culture Collection, CRL-1619) were seeded at a density of 1 x 10^4 cells per well in 96-well tissue culture-treated plates. Cells were treated with the formulations at cytotoxic agent concentrations of 0.01–200 μM in quadruplicate wells for 48 h to produce a balanced 4-parameter curve. The experiments were conducted in triplicate. After treatment, 3-(4,5-dimethylthiazol-2-yl)-2,5-diphenyltetrazolium bromide (MTT, Invitrogen, Burlington, ON, Canada) at 450 μg/mL was added to each well and the plates were incubated for 2 h at 37 °C. Absorbance at 550 nm was recorded using a Synergy BioTek plate reader. The IC_{50} values for all samples were calculated using the 4-parameter curves generated by the GEN5 software from BioTek.

9.3.5. Apoptosis analysis using flow cytometry

Cells were seeded in 6-well plates at a density of 25 x 10^4 cells /well and incubated for 24 hours at 37 °C in a humidified incubator with 5% CO_2 before treatment. Treatments of NC 2067 formulations and melphalan as a control at the IC_{50} concentrations were applied and the cells

were incubated for 24 hours. After treatment, the cells in triplicate were detached from the plates with trypsin, combined and resuspended in 500 µL Dulbecco's phosphate-buffer saline (DPBS, Sigma, Oakville, ON, Canada) containing calcium and magnesium. Early stage of apoptosis was measured by the externalization of the phosphatidylserine (PS) to the outer leaflet of the cell membrane using Annexin V-FITC Apoptosis Detection Kit (BioVision, AB, Canada). Late stages of apoptosis were detected by the loss of cell membrane integrity, permitting the permeation of propidium iodide (PI) (Sigma, Oakville, ON, Canada) into the cell. Cells were incubated with 5µL FITC-conjugated annexin V for 15 minutes in the dark followed by the addition of 5 µL PI. Cells were analyzed with a FACScalibur flow cytometer (Becton Dickinson, San Jose, CA, USA) with excitation from the 488 nm laser and simultaneous monitoring of green fluorescence from the annexin V in the 530/30 nm filter and propidium iodide red fluorescence in the 585/42 filter.

9.3.6. Evaluation of mitochondrial membrane potential ($\Delta\Psi_m$)

We used two different mitochondrial fluorescent dyes named JC-1[394] ((5,5′,6,6′-tetrachloro-1,1′,3,3′- tetraethylbenzimidazolylcarbocyanine iodide) and TMRM[395] (tetramethylrhodamine methyl ester) to probe mitochondrial membrane potential loss.

Cells seeded in 6-well plates (25 x 10^4 cells/well) and after 24 h of incubation at 37°C in a humidified incubator with 5% CO_2, they were treated with formulations at IC_{50} concentration. After 12 and 24 hours of incubation, JC-1 (2.5 µg/ml) or TMRM (0.5 µM) added to each well and incubated at 37°C for 20 min. CCCP (80 µM) was added at the same time as JC-1. Immediately, media removed from wells and cells were washed twice by DPBS to remove the dyes remaining outside of the cells. Then cells were trypsinized and harvested. Cell pellets resuspended in 500 µl DPBS, filtered and analyzed with a FACScalibur flow cytometer with excitation from the 488 nm argon laser and emission in the 585/42 and 530/30 nm filters. The percentage of the green fluorescence of JC-1 monomers and intensity of the red fluorescence of TMRM were employed to identify the cells with mitochondrial membrane potential drop.

9.3.7. Fluorescence microscopy

Cells were seeded in 96-well plate (1 x 10^4 cells/well) and kept under cell culture conditions (37 °C in a humidified incubator with 5% CO_2). Cells were treated with formulations at concentration of IC_{50} for 24 hours. Then cells were stained by 4,6-diamidino-2-phenylindole (DAPI, Life

technologies Inc., Burlington, Canada) at concentration of 30 μM and further incubated for 2 hours . Cells were washed with PBS twice and imaged by fluorescence microscopy.

9.3.8. Cell cycle analysis using flow cytometry

Cell cycle analysis was performed by seeding 25 x 10^4 cells / well in 6-well plates and incubated for 24 hours at 37 $^{\circ}$C in a humidified incubator with 5% CO_2 before treatment. The cells were treated with NC 2067 formulations and melphalan at the IC_{50} concentration for 24 h. Sodium butyrate (2 mM), a compound arresting the cell cycle in G1 phase and resveratrol (30 μM) arresting the cells in S phase were used as positive control. Both adherent and floating cells were collected using trypsin and versene. Approximately 1x10^6 cells were suspended in 300 μL PBS. Cold 100% ethanol was added drop by drop until final concentration of 70% was obtained. Cells were incubated for 24 hours at -20 $^{\circ}$C. The ethanol was removed by centrifugation at 1500 rpm for 10 minutes at 4 $^{\circ}$C. The pellet was resuspended in 1000 μL PBS containing 0.3 mg/mL RNase. PI was added to a final concentration of 20μg/ml. Cells were analyzed with a FACScalibur flow cytometer (Becton Dickinson, San Jose, CA, USA) with excitation from the 488 nm laser and emission in the 585/42 filter. Cell cycle analysis was performed on ModFit LT (Verity Software House, Topsham, ME, USA).

9.3.9. Statistical analysis

Statistical analysis was performed using SPSS (version 19.0). One-way analysis of variance, Scheffe comparison was used. The level of significance was considered at $p<0.05$ value.

9.4. Results and Discussion

9.4.1. Size measurements of βCDgemini surfactant-based nanoparticles

We previously measured the size of the NC 2067/βCDgemini surfactant-12 systems at different drug to delivery agent ratios.[374] In the current work, we investigated the effect of the tail length and degree of unsaturation on the size of the nanoparticles by using different βCDgemini surfactants. Surprisingly, we observed that free βCDgemini surfactant-18:1 was able to form nanoparticles with average size of 117±5 nm at 2 mM concentration. βCDgemini surfactant-16 showed inconsistent values in size measurements with high polydispersity index (PDI) value. This finding is similar to the size measurement of free βCDgemini surfactant-12[374] suggesting a

heterogeneity of the aggregations made of free βCDgemini surfactants having 12 and 16 carbon containing saturated tails. Formulations comprised of NC 2067 complexes with various βCDgemini surfactants (-16 and -18:1) at 1:2 drug to delivery agent mole ratio formed nanoparticles in a size range of 90-131 nm (Table 9.1) comparable to the size of NC 2067/βCDgemini surfactant-12 systems.[374]

The use of nanoparticles in cancer drug delivery systems, is highly advantageous since nano-sized particles facilitate drug delivery of the chemotherapeutics at cellular level by enhanced cellular uptake mechanisms such as endocytosis.[23] Nanoparticles similar to macromolecules bypass the transport systems that are used by small molecules such as diffusion or protein-channel mediated pathways, due to their greater size.[396] Moreover, nanoparticles showed to have the potential to contribute to reverse the multidrug resistance (MDR).[24] The pH-sensitive nanoparticles have been developed to fuse with lysosomal membrane and consequently release the drug into cytoplasm. Therefore, efflux pumps which are located in the cell membrane cannot excrete it out of the cell.[27]

Table 9.1-Size of different βCDgemini-based nanoparticles (average of 3-5 measurements ± standard deviation, SD) and corresponding polydispersity index (PDI).

βCDgemini surfactant-based nanoparticles	**Size [nm] ± SD**	**PDI**
βCDgemini surfactant-18:1	117 ± 5	0.2
NC 2067/βCDgemini surfactant-12*	101 ± 2	0.3
NC 2067/βCDgemini surfactant-16	90 ± 7	0.3
NC 2067/βCDgemini surfactant-18:1	131 ± 3	0.4

*Data is adopted from our previous study.[374]

9.4.2. SAXS/WAXS measurements of βCDgemini surfactant based formulations

In our former work, we found that in βCDgemini surfactant-12, the hydrocarbon tail interacts with βCD cavity resulting in self-inclusion behavior. Moreover, the supramolecular behavior of the free βCDgemini surfactant -12 at 10 mM concentration showed a diffused scattering pattern which is in good agreement with the self-inclusion behavior.[374] Herein, we monitored SAXS/WAXS patterns of free βCDgemini surfactants at various concentrations (1-30 mM) to

better understand their aggregation behavior. As previously reported, βCDgemini surfactant-12 showed a broad peak (at q less than 0.1 $Å^{-1}$) corresponding to the diffused scattering and increasing the concentration of the surfactant did not change the aggregation behavior in this system. Similar results were observed for βCDgemini surfactant-16 and -18:1 (data is not shown). This is further evidence that, self-inclusion of the alkyl tail of the gemini surfactant in the βCD cavity in the βCDgemini surfactants will prevent supramolecular assembly in aqueous media and formation of lyotropic liquid crystals.

The scattering behavior of formulations containing complexes of NC 2067 and βCDgemini surfactants (16 and 18 hydrocarbon tails) at various drug to carrier mole ratios (1:0.5, 1:1 and 1:2) (Figure 9.2B,C) examined and compared to the similar systems comprising of βCDgemini surfactant-12 (Figure 9.2A)[374]. We formerly demonstrated that the SAXS/WAXS pattern of NC 2067/βCDgemini surfactant-12 at various drug to delivery agent mole ratios (1:0.5, 1:1 and 1:2) showed a new peak at q of 0.27 $Å^{-1}$ (velvet arrows) corresponding to a *d*-spacing of 23 Å formed in the system upon the addition of NC 2067 (Figure 9.2A)[374]. The appearance of the other peaks at higher q are associated with the precipitated form of NC 2067 in the systems (black arrows-Figure 9.2A) expressly observable in systems with lower amount of βCDgemini surfactant-12, 1:0.5 and 1:1 mole ratios, respectively (Figure 9.2A).[374]

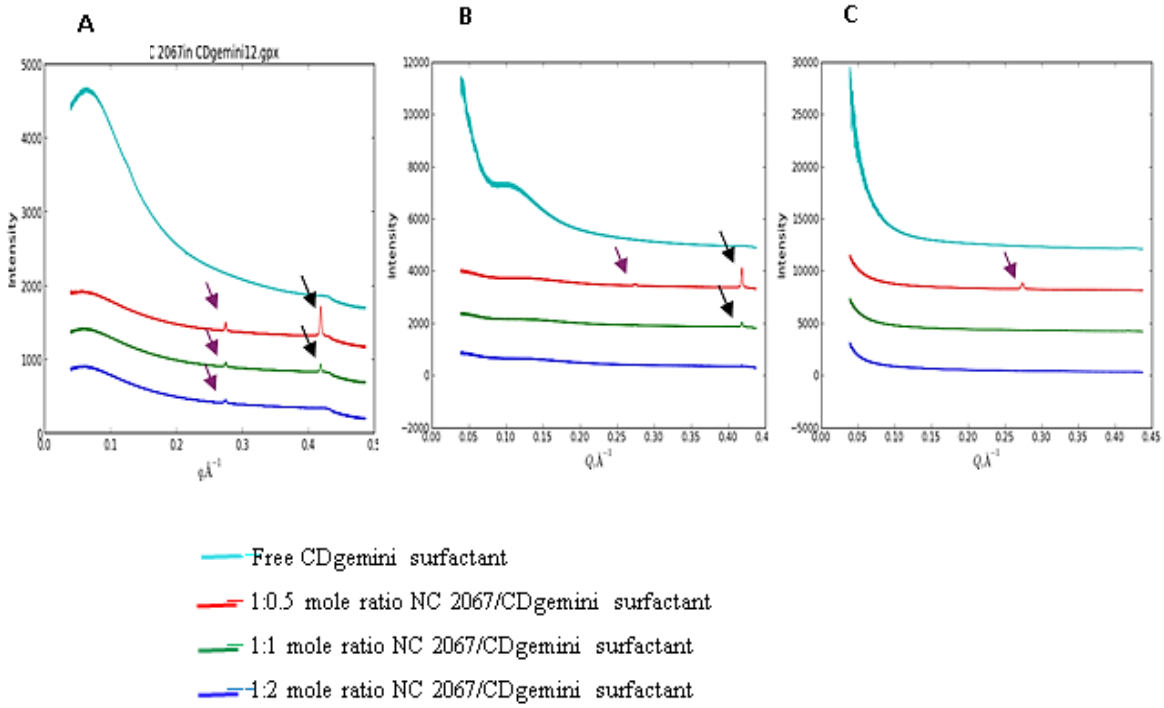

Figure 9.2- SAXS/WAXS patterns of the formulations containing **A)** βCDgemini surfactant-12 [reproduced from Poorghorban et al, 2015], **B)** βCDgemini surfactant-16 and **C)** βCDgemini surfactant-18:1.

SAXS/WAXS study of free βCDgemini surfactants (-16 and -18:1) displayed diffused scattering patterns which were different in shape in comparison to βCDgemini surfactant-12 (Figure 9.2B, C). The addition of NC 2067 to βCDgemini surfactant-16 resulted in flattening of the broad peak corresponding to the free βCDgemini surfactant-16 and appearance of the new peaks at higher q range corresponding to NC 2067 precipitated in the samples (black arrows, Figure 9.2B). Conversely, no peaks detected at higher q values in the scattering patterns of the formulations composed of NC 2067/βCDgemini surfactant-18:1 at various mole ratios. We speculate that the interaction of NC 2067 with βCDgemini surfactant-18:1 is different from the other two βCDgemini surfactants even at lowest amount of the delivery agent (mole ratio of 1:0.5) leading to a better solubilization of the cytotoxic agent. This could be related to the monounsaturated nature of the hydrocarbon tail of βCDgemini surfactant-18:1 which alters its geometry. It is well documented the monosaturation of the acyl chain can disturb the lipid bilayers by providing a kink in the structure.[397] We hypothesized that the self-inclusion behavior possibly is less robust in the case of the free βCDgemini surfactant-18:1 due to the "bend" in the structure and geometrical hindrance. A weaker interaction of the gemini-18:1 tail with βCD cavity could be favorable for more efficient insertion of the NC 2067 into βCD cavity. Furthermore, the direct interaction of NC 2067 with the unsaturated bonds of βCDgemini surfactant-18:1 might also increase the solubility of NC 2067. According to the better interaction of NC 2067 with βCDgemini surfactant-18:1, either CD cavity or gemini surfactant moiety, NC 2067 was solubilized more even at 1:0.5 mole ratio.

Monitoring the NC 2067/βCDgemini surfactant-16 and NC 2067/βCDgemini surfactant-18:1 systems at various mole ratios, we detected the peak at q of 0.27 $Å^{-1}$ (velvet arrow, Figure 9.2B and C). Unlike the βCDgemini surfactant-12 containing systems, this peak was observed only for the systems with the lowest amount of the delivery agent at mole ratio of 1:0.5. The presence of this peak indicates the formation of a new phase in the βCDgemini surfactant containing systems upon addition of NC 2067 which is not governed by the length and nature of the gemini surfactant hydrocarbon tail.

9.4.3. Molecular mechanism of the anticancer activity of NC 2067 complexes with different βCDgemini surfactants

9.4.3.1. In vitro activity of NC 2067 complexes with βCDgemini surfactants having different hydrocarbon tails (-12, -16 and -18:1)

We previously showed the anticancer activity of NC 2067/βCDgemini surfactant-12 in which βCDgemini surfactant-12 synthesized by structurally different linkers (ester and amide) and drug to carrier mole ratios were various as well. Herein, we extended our study by the *in vitro* assessment of the other two βCDgemini surfactant (-16 and -18:1) containing systems to understand the effect of the acyl chain length and unsaturation of the hydrocarbon tail on cellular toxicity.

The *in vitro* activity of NC 2067 complexes with three different βCDgemini surfactants (16 and 18:1 hydrocarbon tail) (Table 9.2) at 1:2 drug to carrier mole ratio, toward A375 melanoma cell line was determined and compared to the previous results of βCDgemini surfactant-12[374]. IC_{50} values (half-maximal inhibitory concentration) used as an indicator of the ability of NC 2067 to kill cancerous cells. The IC_{50} values of all NC 2067/βCDgemini surfactant formulations were calculated as less than 3 μM suggesting the high toxicity toward A375 melanoma cells (Table 9.2). No significant difference was observed by comparing the IC_{50} values for the various βCDgemini surfactant containing systems ($P>0.05$).

To evaluate the safety of the delivery agents, the βCDgemini surfactants (-16 and -18:1), the intrinsic toxicity was evaluated at 200 μM concentration. We observed that the intrinsic toxicity of free βCDgemini surfactant-16 was significantly ($P<0.05$) higher than the βCDgemini surfactants -12 and -18:1 (Table 9.2). This observation possibly related to the fact that βCDgemini surfactant-16 was less soluble and precipitated easily in cell culture media (visual examination by light microscopy not shown).

The IC_{50} value for NC 2067/βCDgemini surfactants (-16 and 18:1) were comparable to our previous study on βCDgemini surfactant-12 based systems.[374]

Low IC_{50} values of NC 2067/βCDgemini surfactant (-12, -16 and -18:1) formulations showed that an anticancer activity of NC 2067 can be retained in these systems and the chain length and unsaturation of the gemini surfactant tail did not alter their *in vitro* efficiency toward A375 cell line. However, the comparison of the intrinsic toxicity of the free βCDgemini surfactants (-12, -16 and -18:1) (Table 9.2) revealed that βCDgemini surfactant-16 is the least appropriate carrier

due to its significantly higher cellular toxicity and βCDgemini surfactant-12[374] and -18:1 showed low intrinsic toxicity. The cytotoxicity of the gemini surfactant moiety of βCDgemini surfactant-12 (12-7NH-12) reported to be high in rabbit epithelial cells.[165] Moreover, other gemini surfactant derivatives comprised of the substitution of various amino-acids on gemini surfactant-12 (12-7NH-12) revealed low cell viability as well.[165] However, as we reported previously βCDgemini surfactant-12 showed low intrinsic toxicity whereas βCD grafted gemini surfactants with exception of -16 tail showed favorable low cytotoxicity as drug delivery agents.

Table 9.2- IC_{50} values of NC 2067 complexes with three different βCDgemini surfactants (12, 16, 18:1 hydrocarbon tail) at 1:2 drug to delivery agent mole ratio and % intrinsic toxicity of the free βCDgemini surfactants.

NC 2067/βCDgemini surfactant drug delivery systems	**IC_{50} [µM] ± SD**	**% toxicity of βCDgemini surfactant [200 µM] ± SD**
-12*	2.0 ± 0.25	18 ± 6
-16	2.63 ± 0.17	80 ± 0.8
-18:1	2.65 ± 0.14	22.6 ± 2.1

*Data is adapted from our previous study.[374]

9.4.3.2. Proapoptotic activity of NC 2067 complexes with βCDgemini surfactants having different hydrocarbon tails (-12, -16 and -18:1)

Cytotoxic drugs can destroy cancer cells by apoptosis, necrosis or autophagy. We formerly reported an increase in the caspase -3 and -7 in A375 cells upon treatment with NC 2067 formulations.[3] Here in, we examined the mode of cell death in melanoma cells treated with the NC 2067 in presence of the βCDgemini surfactant-based carrier to differentiate apoptosis from necrosis. Early signs of apoptosis can be tracked by the translocation of PS on the outer cell leaflet. We evaluated the effect of NC 2067 complexes with different βCDgemini surfactants (12, 16 and 18:1) toward A375 melanoma cell line by measuring the PS exposed on the cell surface using flow cytometry. An anti-melanoma agent, melphalan was used as a positive control.

We observed that the untreated cell population was healthy (96.6% of cells); both early and late apoptotic cells combined represented 3% of the total population and only 0.4% was in a necrotic state (Table 9.3). The NC 2067 complexes with different βCDgemini surfactants (-12, -16 and -18:1) at 1:2 drug to carrier mole ratio or dissolved in 1% DMSO at IC_{50} values showed an

increased population of apoptotic cells (late and early) and decreased healthy populations (Table 9.3). The percentage of the necrotic population did not alter significantly compared to the untreated cells suggesting that NC 2067 did not induce necrosis in A375 melanoma cells.

Melphalan, an antimelanoma drug on market, showed similar proapoptotic behavior at its IC_{50} concentration with 31.3% of cells undergoing apoptosis. The early apoptotic population of cells treated with NC 2067/βCDgemini surfactant-12 (8.7%) was comparable to melphalan (9.8%) (Table 9.3). The majority of the cells treated with free βCDgemini surfactants (-12 and -18:1) or 1% DMSO were healthy (93.3-95.3%) whereas treatment with free βCDgemini surfactant-16 resulted in the increase in necrotic/apoptotic population (Table 9.3). This observation is in good agreement with the high intrinsic toxicity of free βCDgemini surfactant-16 obtained with MTT assay (Table 9.2).

Moreover, cells stained with DAPI showed chromatin condensation (Figure 9.3A, yellow arrows) after 24 hour of treatment with NC 2067/βCDgemini surfactant-12 formulation while cells treated with free βCDgemini surfactant-12 did not show signs of apoptosis in fluorescent micrographs (Figure 9.3B).

These results suggested that NC 2067 complexed with different βCDgemini surfactants (-12, -16 and -18:1) at 1:2 mole ratio was able to preserve its ability to trigger cell death via apoptosis, at a comparable level to NC 2067 dissolved in 1% DMSO. Our finding is in good agreement with other studies showing the proapoptotic activity of curcumin and its analogs in melanoma cells through regulation of the mediators of intrinsic or extrinsic apoptosis pathways.[107,109,231,238]

Autophagy is a cellular degradation process in which cellular organelles will be eaten by autolysosomes in response to various stimuli such as chemotherapeutics.[398] Even though autophagic mechanism of cell death is not defined entirely, there are several studies confirmed the cross talks between apoptosis and autophagy. [399,400] There are reports in the literature showing that curcumin is able to induce autophagy in various cancer cells.[401-403] Moreover, it was shown that autophagy and apoptosis can occur simultaneously by curcumin and its analogs.[400,404-406] However, caspases are not related to autophagic cell death mechanism whereas in apoptotic modes of cell death, they have crucial role.[398] The caspase-dependent cell death mechanism of NC 2067/βCDgemini surfactant-12 in A375 melanoma cells[3] supports our finding regarding apoptosis involvement in cell death mechanism. There is an essential need to perform more experiments to confirm whether autophagy occurred simultaneously with apoptosis.

Furthermore, we evaluated the mitochondrial membrane potential loss of A375 melanoma cells treated with NC 2067 formulations as an indicator to discriminate the intrinsic (mitochondrial mediated) apoptosis from extrinsic pathway. NC 2067 in presence of βCDgemini surfactants or 0.1% DMSO did not alter the mitochondrial membrane potential.

Albeit curcumin and its analogs mainly induce apoptosis in cancer cells in a mitochondrial-dependent manner[109,212,214,215,238] and NC 2067 decreased mitochondrial membrane potential in HCT-116 colon cancer cell line[226], our findings did not confirm the loss of the mitochondrial membrane potential in A375 melanoma cells. This result is consistent with few studies verifying the non-mitochondrial dependent apoptosis induced by curcumin in melanoma cells.[231,232] Finally, free βCDgemini surfactants (-12 and -18:1) showed minimal proapoptotic activity in A375 melanoma cell line.

Table 9.3 - Apoptotic cell death induced by NC 2067 complexes with different βCDgemini surfactants (12, 16 and 18:1) after 24 hours of treatment at IC_{50} concentrations toward A375 melanoma cell line (samples were pooled from triplicates).

	Populations percentage									
	Untreated	**Melphalan**	**NC 2067 in 1% DMSO**	**NC 2067 /βCDgemini surfactant**			**βCDgemini surfactant**			**1% DMSO**
				-12	**-16**	**-18:1**	**-12**	**-16**	**-18:1**	
Healthy	96.6	68	88.6	76	86	91.7	93.3	88.8	94.2	95.3
Early Apoptotic	0.6	9.8	1.8	9.85	2.5	2.8	1	1.6	0.5	0.5
Late Apoptotic	2.4	21.5	9.2	13.4	10.7	4.9	5	8.1	5	3.8
Necrotic	0.4	0.7	0.4	0.69	0.8	0.6	0.7	1.5	0.3	0.4

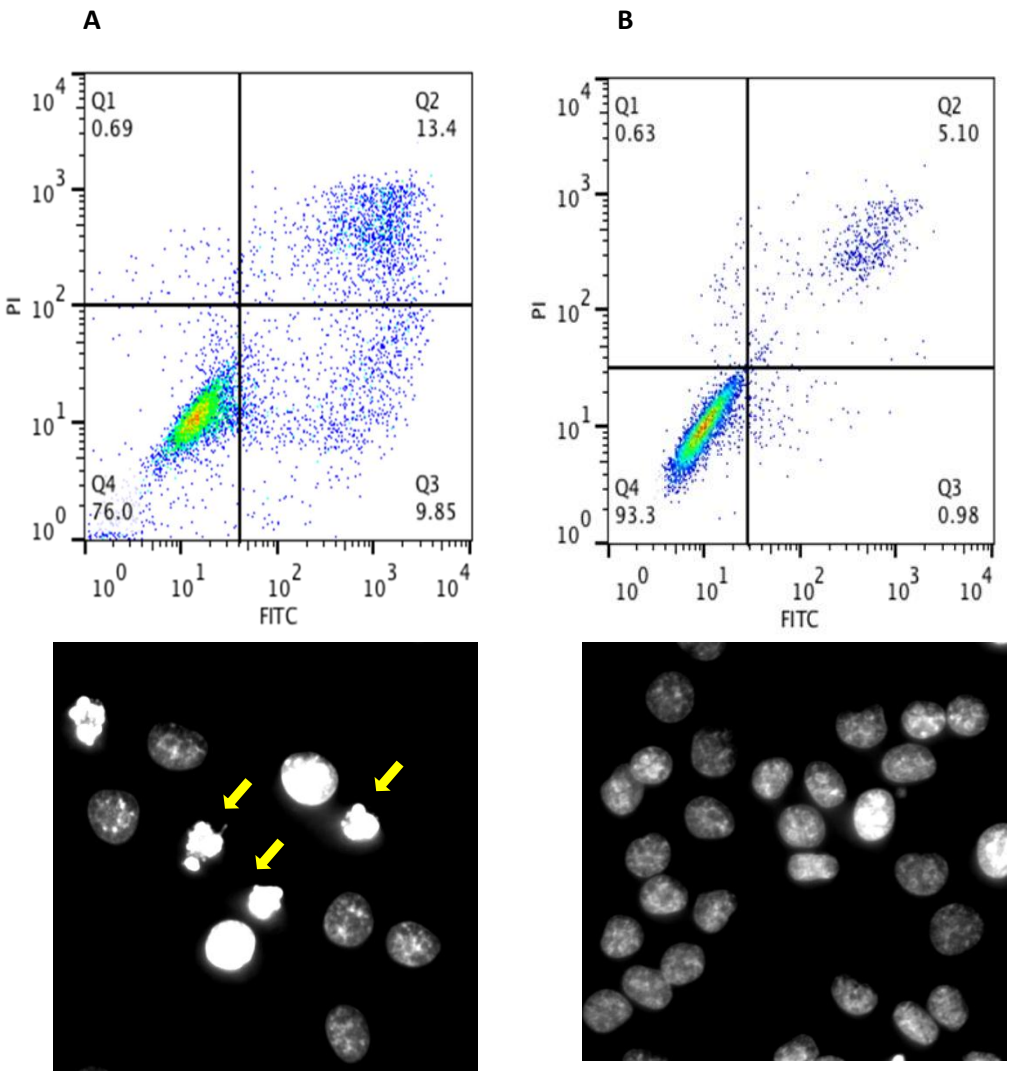

Figure 9.3- Biexponential apoptotic rate of (annexin V-FITC/PI dual staining) and fluorescence micrographs (DAPI staining) in A375 melanoma cells treated with **A)** NC 2067/βCDgemini surfactant-12 and **B)** free βCDgemini surfactant-12 for 24 hours. Yellow arrows show chromatin condensation.

9.4.3.3. Cell cycle analysis of NC 2067 complexes with βCDgemini surfactants having different tails (12, 16 and 18:1)

We used flow cytometry based analysis to evaluate the effect of NC 2067 complexes with various βCDgemini surfactants on the cell cycle distribution. The fluorescence intensity of cells stained by PI indicates DNA concentration in different cell cycle phases. Sodium butyrate[407] and resveratrol[408], specific cell cycle arresters at G_0/G_1 and S phases, respectively, were used as positive controls (data not shown). Cells treated by NC 2067 complexes with different βCDgemini surfactants (12, 16 and 18:1) or NC 2067 dissolved in 1% DMSO showed minimal effect on the cell cycle phases comparable to untreated cells (Table 9.4). NC 2067/βCDgemini surfactant-16 increased the cell population in G_2/M and *S*-phases moderately (P=0.05) while decreasing the cells at G_0/G_1 phase. Conversely, NC 2067/ 1% DMSO and 1% DMSO showed slight increase of the population in G_0/G_1 phase in comparison to healthy cells (Table 9.4). Since rise in the cell population at G_0/G_1 phase by these two samples are similar, the effect is undoubtedly caused by 1% DMSO. The ability of 2% DMSO to arrest cell cycle at G_0/G_1 phase by inhibiting the gene expression in fibroblast cells, is well documented.[409] Melphalan arrested cells predominately at *S*-phase of the cell cycle at 76.3%, a 52.3% increase over the untreated population. This finding is consistent with literature proposing the anticancer mechanism of the melphalan in melanoma cell lines.[410] There are reports showing that curcumin treatment is able to arrest cancer cells at G_0/G_1[232,244], S[213] and G_2/M[219,227,236] phases at various cancer cell lines such as melanoma cell lines. However, NC 2067 most likely exerted its effect by thiol alkylation without interfering with DNA.[113,114] Some of the existing anticancer therapeutic agents that target amino and hydroxyl groups on nucleic acids result in genotoxic outcomes.[115] Free βCDgemini surfactants (12, 16 and 18:1) did not influence cell cycling (Table 9.4).

Table 9.4- Cell cycle analysis of A375 cells treated with NC 2067/βCDgemini surfactant (-12, 16 and 18:1) formulations after 24 hours at IC_{50} concentrations in comparison to NC 2067 dissolved in 1% DMSO and model drug melphalan (samples were pooled from triplicates).

Cell Cycle	Untreated	Melphalan	NC 2067 in 1% DMSO	NC 2067 /βCDgemini surfactant			βCDgemini surfactant			1% DMSO
				-12	-16	-18:1	-12	-16	-18:1	
G_0/G_1	68	16.3	73.9	65.1	48.4	62.6	64.5	62	65	74.5
G_2/M	8	7.3	8	0.3	14.9	8	8	8	8	8
S	24	76.3	18.1	34.6	36.7	29.4	27.5	30	27	17.5

9.5. Conclusion

Overall, NC 2067 complexes with βCDgemini surfactants (12, 16 and 18:1) formed nano-sized aggregations that were able to trigger non-mitochondrial apoptosis without affecting cell cycle distribution in A375 melanoma cells. Despite the fact that the self-inclusion behavior of βCDgemini surfactants (12, 16 and 18:1) hinder the formation of LLC phases, SAXS/WAXS patterns of the NC 2067/βCDgemini surfactant nanoformulations showed that upon addition of NC 2067 to the system new phase was formed. To understand the molecular mechanism of cell death induced by these formulations further investigations will be required.

9.6. Acknowledgements

Masoomeh Poorghorban is a fellow of the Canadian Institutes of Health Research Training grant in Health Research Using Synchrotron Techniques (CIHR-THRUST) and thanks the program for financial support. We thank Dr. Joel Ried, Canadian Light Source who guided in working with GSAS II. Portions of this research were carried out at the Stanford Synchrotron Radiation Lightsource (SSRL), a Directorate of SLAC National Accelerator Laboratory and an Office of Science User Facility operated for the U.S. Department of Energy Office of Science by Stanford University. The SSRL Structural Molecular Biology Program is supported by the DOE Office of Biological and Environmental Research, and by the National Institutes of Health, National Institute of General Medical Sciences (including P41GM103393). The contents of this

publication are solely the responsibility of the authors and do not necessarily represent the official views of NIGMS or NIH. We acknowledge the assistance of Dr. Thomas Weiss, SSRL with instrument setting and data collection.

10. EVALUATION OF THE ANTICANCER ACTIVITY AND NANO-STRUCTURAL BEHAVIOR OF NC 2067/βCDGEMINI SURFACTANT FORMULATIONS IN THE PRESENCE OF HELPER LIPID

Masoomeh Poorghorban[a], Deborah Michel[a], Pawel Grochulski[ab], Ildiko Badea[a*]

[a]Drug Discovery and Development Research Group, College of Pharmacy and Nutrition, University of Saskatchewan, Saskatoon, SK S7N 5E5, Canada
[b]Canadian Light source, Saskatoon, SK S7N 2V3, Canada

Corresponding author:
*Ildiko Badea
College of Pharmacy and Nutrition
University of Saskatchewan
Health Sciences Building, 3D01.5
107 Wiggins Road
Saskatoon, Saskatchewan, S7N 5E5, Canada
Phone: 306-966-6349
Fax: 306-966-6377
E-mail: ildiko.badea@usask.ca

In this manuscript, the influence of the addition of 1,2-dioleoyl-s*n*-glycero-3-phosphoethanolamine (DOPE) on assembling of the nanostructures formed of NC 2067 with various βCDgemini surfactants was evaluated using SAXS/WAXS. In addition, the *in vitro* anticancer activity of the formulations was assessed in A375 melanoma cells. I made all the formulations, performed experiments and analyzed data.

This manuscript addresses the following specific objectives of my research

1.2. To develop formulations by addition of helper lipid

1.6. To use synchrotron small- and wide angle X-ray scattering (SAXS/WAXS) to evaluate the supramolecular arrangement of drug/βCDgemini surfactant delivery systems in solution

2.1. To calculate the cell toxicity (IC_{50}) of different drug/βCDgemini surfactant formulations towards melanoma cell line

10.1. Abstract

Helper lipids such as 1,2-dioleoyl-*sn*-glycero-3-phosphoethanolamine (DOPE) are commonly used in the gene delivery formulations composed of cationic surfactants in order to increase the transfection efficiency and lower the cytotoxicity associated with gemini surfactants. βCyclodextrin-gemini surfactant-based formulations were designed to increase the solubility of the model lipophilic anticancer agent, NC 2067, and enhance its delivery to A375 melanoma cells. The influence of the addition of DOPE was evaluated on the anticancer activity and nano-structural arrangements of the NC 2067/βCyclodextrin-gemini surfactant complexes.

Size measurements and SAXS/WAXS were used to compare the nanoparticulate behavior of the formulations upon addition of DOPE. Cell viability assay was employed to track the alterations in the efficiency of NC 2067 formulated with βCyclodextrin-gemini surfactants and DOPE towards A375 melanoma cells.

It was found that the addition of DOPE did not significantly alter the IC_{50} of the NC 2067 in the formulations whereas it increased the intrinsic toxicity of the βCyclodextrin-gemini surfactant. Moreover, formulations containing DOPE formed nano-sized particles and their scattering pattern was not drastically different from their DOPE-free counterparts.

10.2. Introduction

Cationic lipid-based nano-formulations are widely used for the delivery of the drug small molecules[411] and nucleic acids[412,413]. It was shown that the self-assembling behavior of these nanoparticles play an important role in the enhancement of the efficiency of the chemotherapy and gene therapy. The fusion of the lipid moieties of such formulations with biomembranes increases the delivery of the drugs and genes into the target cells, but not all cationic lipids possess fusogenic properties.

Helper lipids are neutral lipids which commonly added to cationic liposomes to increase the transfection efficiency. Among the helper lipids, DOPE (1,2-dioleoyl-*sn*-glycero-3-phosphoethanolamine) (Figure 10.1), a neutral phospholipid extensively studied to improve the transfection efficiency of the cationic lipid formulations in gene therapy.[414,415] It was shown that in comparison to other helper lipids, DOPE enhanced the transfection to higher extend.[416]

DOPE can destabilize lipid bilayers and disturb endosomes resulting in the release of nucleic acids into cytosol.[415,417] From the structural point of view, the cone-shaped DOPE forms the inverse hexagonal phase (H_{II}^{C}) in lipoplexes.[328,418] Studies showed that DOPE was able to contribute to the formation of various lipid-based supramolecular arrangements that enhanced the fusogenic activity of the nanoparticles and improved the cellular uptake.[341]

Previously, DOPE was added to lipoplexes containing gemini surfactants in order to improve the transfection compared to the formulations lacking DOPE.[419] βCDgemini surfactants are new class of dicationic gemini surfactants built by attachment of gemini surfactants (m-7NH-m) to βcyclodextrin.[3] We previously demonstrated that βCDgemini surfactants can be employed as delivery agents for hydrophobic anticancer agents such as a curcumin analog (NC 2067).[374] Moreover, the nanoparticulate behavior, anticancer activity and cell death mechanism of formulations comprised of NC 2067 and βCDgemini surfactants with various chain length and degree of unsaturation of the alkyl tail were examined. In the current study, our aim is to evaluate the effect of the addition of DOPE to NC 2067/βCDgemini surfactant formulations on the structural properties and cytotoxicity activity.

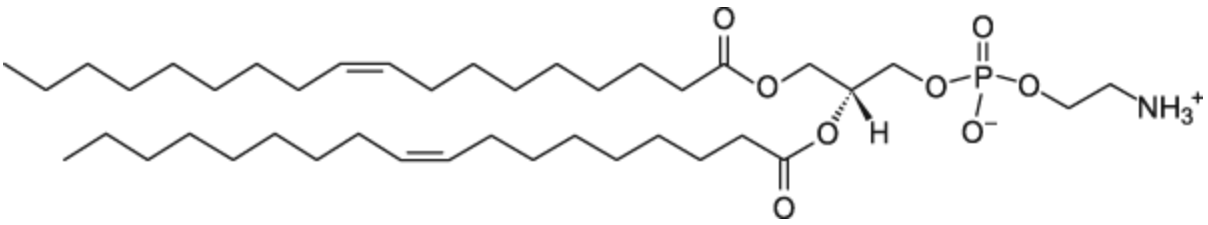

Figure 10.1- Molecular structure of DOPE.

10.3. Materials and Methods

10.3.1. DOPE preparation

DOPE (Avanti Polar Lipids, Alabaster, AL, USA) and α-tocopherol (Spectrum, Gardena, CA, USA) in 1:0.2 weight ratios were dissolved in 100% ethanol (Commercial Alcohols Inc., Brampton, ON, Canada) and deposited as a thin film on a round-bottomed flask. The lipid was lyophilized overnight, to remove traces of solvent, and resuspended at 1 μmol/ml concentration in 9.25% w/v isotonic sucrose (Spectrum) solution (pH 9) by sonication, then filtered through 0.45 μm Acrodisc® filters.[413]

10.3.2. Preparation of inclusion complexes

NC 2067 and βCDgemini surfactants were synthesized as described previously.[111],[3] All other chemicals were purchased from Sigma-Aldrich (Oakville, ON, Canada). Complexes of NC 2067 with βCDgemini surfactants (-12, -16 and -18:1) were formulated as described previously[374] and reconstituted in DOPE (1 mM).

10.3.3. Size measurements

Particle sizes in solution were measured by using a Zetasizer Nano ZS instrument (Malvern Instruments, UK). Results are reported as the mean of 3-5 measurements ± standard deviation.

10.3.4. Small- and wide-angle X-ray scattering (SAXS/WAXS) measurements

SAXS/WAXS measurements were performed at the BL4-2 beamline at Stanford Synchrotron Radiation Lightsource (SSRL, Stanford, CA, USA) at 20 s exposure time. The samples containing NC 2067/βCDgemini surfactant complexes dispersed in DOPE with constant concentration of gemini surfactant (10 mM) studied at energy of 11 keV and a sample to

detector distance of 1.1 m. Diffraction intensity *versus q* (scattering vector) plots were obtained by radial integration of the 2D patterns using GSAS-II software.[393]

10.3.5. Cell viability assay

A375, human amelanotic melanoma cells (American Type Culture Collection, CRL-1619) were seeded at a density of 1 x 10^4 cells per well in 96-well tissue culture-treated plates. Cells were treated with the formulations at cytotoxic agent concentrations of 0.01–200 μM in quadruplicate wells for 48 h to produce a balanced 4-parameter curve. The experiments were conducted in triplicate. After treatment, 3-(4,5-dimethylthiazol-2-yl)-2,5-diphenyltetrazolium bromide (MTT, Invitrogen, Burlington, ON, Canada) at 450 μg/mL was added to each well and the plates were incubated for 2 h at 37 °C. Absorbance at 550 nm was recorded using a Synergy BioTek plate reader. The IC_{50} values for all samples were calculated using the 4-parameter curves generated by the GEN5 software from BioTek.

10.3.6. Statistical analysis

Statistical analysis was performed using SPSS (version 19.0). One-way analysis of variance, Scheffe comparison was used. The level of significance was considered at $p<0.05$ value.

10.4. Results and Discussion

10.4.1. Size measurements of NC 2067/βCDgemini surfactant-12 dispersed in DOPE at different mole ratios

The size of nano-particulate systems of NC 2067/βCDgemini surfactant-12 at three different drug to carrier mole ratios (1:1, 1:2 and 1:0.5) in the presence of DOPE (1 mM) was measured and compared to previous results in which the nano-formulations were dispersed in water[374] (Table 10.1). At 1:2 mole ratio, the average size of the nanoparticles dispersed in DOPE of 109±6 nm was comparable to the same formulation without DOPE ($P>0.05$). However, at the ratios of 0.5:1 and 1:1 the nanoparticles dispersed in DOPE showed sizes of 93±1.3 and 87±0.6 nm, respectively, which were significantly smaller in comparison to formulations dispersed in water ($P<0.05$). All formulations containing DOPE exhibited the average size under 110 nm with a polydispersity index (PDI) of ≤ 0.3. DOPE at 1 mM concentration formed nanoparticles with the size of 97 ± 0.3 nm (Table 10.1).

Table 10.1- Size of different nanoparticulate formulations (average of 3-5 measurements ± standard deviation, SD) and corresponding polydispersity index (PDI).

	Dispersion media	Mole ratio of drug to delivery agent	size [nm] ± SD	PDI
NC2067/βCDgemini surfactant-12 nanoparticles	Water*	1:0.5	160 ± 3	0.1
		1:1	140 ± 1	0.2
		1:2	101 ± 2	0.3
	DOPE	1:0.5	93 ± 1	0.2
		1:1	87 ± 1	0.2
		1:2	109 ± 6	0.3
DOPE (1 mM)	Water	NA	97 ± 0.3	0.2

* Data is adapted from our previous study.[374]

10.4.2. SAXS/WAXS measurements of NC 2067 complexes with different βCDgemini surfactants (12, 16 and 18:1) dispersed in DOPE at different mole ratios

We evaluated the SAXS/WAXS pattern of the complexes of NC 2067 with βCDgemini surfactants (12, 16 and 18:1) at three different drug to carrier mole ratios (1:0.5, 1:1 and 1:2) dispersed in DOPE (Figure 10.2). Free βCDgemini surfactant-12 and -16 dispersed in DOPE showed diffused scattering pattern (Figure 10.2A and B) comparable to the similar βCDgemini surfactants dispersed in water discussed in section 9.4.2, Figure 9.4. Interestingly, the free βCDgemini surfactant-18:1 dispersed in DOPE showed a different scattering pattern with peaks at q_{10}, q_{11} and q_{20} of 0.095, 0.166 and 0.192 $Å^{-1}$, respectively, corresponding to inverted hexagonal phase ($1:\sqrt{3}:\sqrt{4}$) (velvet arrows in Figure 10.2C). The two-dimensional inverted hexagonal phase is well-defined for DOPE in solution.[420] Moreover, the peak at q of 0.095 $Å^{-1}$ retained in the scattering pattern of NC 2067/βCDgemini surfactant-18:1 at 1:2 mole ratio in the presence of DOPE (Figure 10.2C). As well, a peak at q of 0.27 $Å^{-1}$ appeared in the scattering pattern of NC 2067/βCDgemini surfactant-18:1 at 1:0.5 mole ratio dispersed in DOPE (Figure 10.2C; orange arrow) which is related to the new phase forming by addition of NC 2067 to the lipid system.

Furthermore, another peak detected at higher *q* of 0.43 $Å^{-1}$, corresponding to NC 2067 powder diffraction pattern (d=15 Å) which arises from drug precipitation in formulations comprised of NC 2067 complexed with βCDgemini surfactants (-16 and 18:1) containing lower amount of delivery agent (1:0.5 and 1:1 mole ratios) (Figure 10.2-A and B; black arrows). The same observation was reported previously for NC 2067/βCDgemini surfactant-12 surfactant in water.[374]

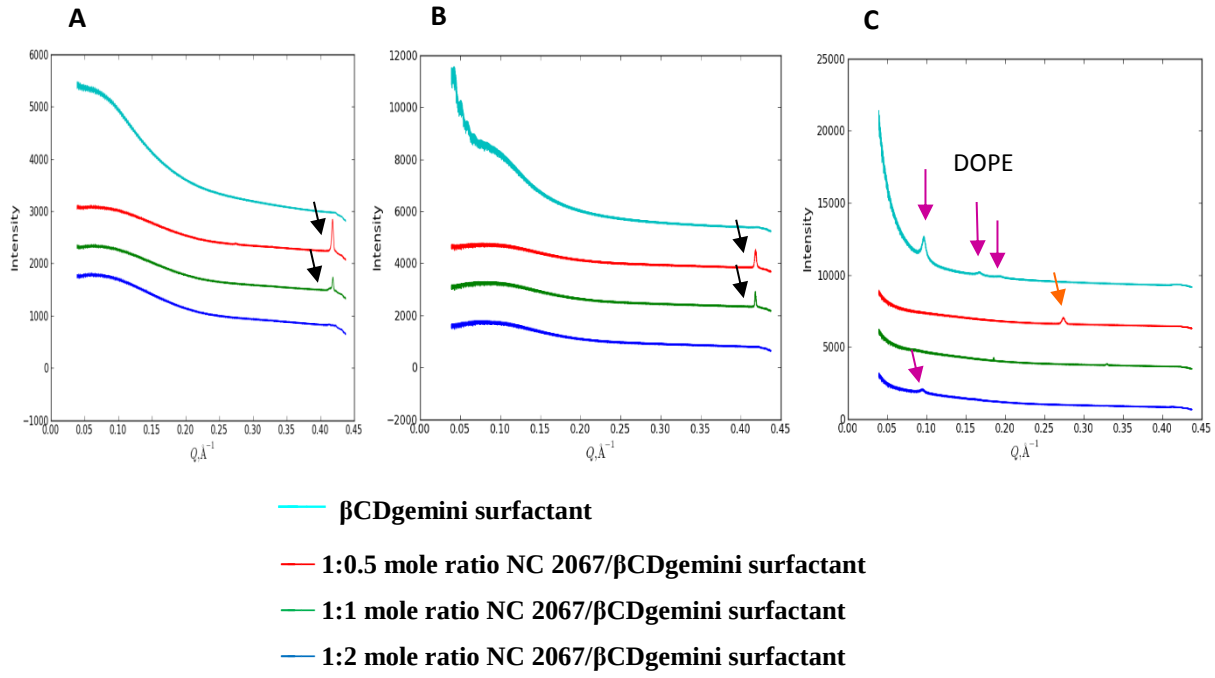

Figure 10.2- SAXS/WAXS patterns of formulations dispersed in DOPE containing **A**) βCDgemini surfactant-12, **B)** βCDgemini surfactant-16 **C)** βCDgemini surfactant-18:1.

Overall, the scattering pattern of free βCDgemini surfactants (-12 and -16) dispersed in DOPE (Figure 10.2-A and B) were similar to the delivery agents dispersed in water. In contrast to the formulations dispersed in water, addition of NC 2067 did not result in the formation of new phase. In case of the βCDgemini surfactant-18:1 dispersed in DOPE, the dominant inverted hexagonal phase, characteristic to DOPE, was detected. The formulation prepared of NC 2067/βCDgemini surfactant-18:1 dispersed in DOPE at the highest βCDgemini surfactant mole ratio (1:2) still showed the DOPE hexagonal phase (first peak) while at the lowest amount of the delivery agent to drug (mole ratio of 1:0.5) a new phase related to the NC 2067 was detectable.

Based on our knowledge regarding the self-inclusion behavior of βCDgemini surfactants, the addition of DOPE to these formulations did not change the lipid phase behavior of the system drastically. Moreover, this can be related to the low concentration of DOPE used (1 mM).

We previously discussed in section 9.4.2 that the complex of NC 2067/βCDgemini surfactant-18:1 dispersed in water showed different scattering pattern compared to the other complexes. We speculate that the mono-unsaturated oleyl chains of βCDgemini surfactant-18:1 behave differently from the saturated tail resulting in a weaker self-inclusion behavior, thus forming LLC more readily. Addition of DOPE to this surfactant in the absence of NC 2067 resulted in the formation of the inverted hexagonal phase corresponding to DOPE. This observation supports the previous finding regarding the higher possibility that the gemini surfactant hydrocarbon tails are available to interact with DOPE in βCDgemini surfactant-18:1.

10.4.3. *In vitro* activity of NC 2067/βCDgemini surfactant-12 dispersed in DOPE at different mole ratios

The delivery efficacy of various formulations of NC 2067/βCDgemini surfactant-12 dispersed in DOPE (1mM) at three different drug to carrier mole ratios (1:0.5, 1:1, 1:2) was assessed and IC_{50} values were calculated. The *in vitro* activity of formulations dispersed in DOPE at each mole ratio was not significantly different from the similar formulations dispersed in water[374] ($P>0.05$) (Table 10.2).

The intrinsic toxicity of βCDgemini surfactant-12 dispersed in DOPE was significantly higher than the free βCDgemini surfactant-12 ($P<0.05$) (Table 10.2). However, the overall cell viability in the βCD-substituted gemini surfactants is significantly higher than in their amino acid-substituted counterparts.[165]

Table 10. 2- IC_{50} values of NC 2067 in various βCDgemini surfactant-12 formulations and % intrinsic toxicity of the βCDgemini surfactants.

	Dispersion media	Mole ratio of drug to delivery agent	IC_{50} [μM] ± SD	% toxicity of βCDgemini surfactant [200 μM] ± SD
NC2067/βCDgemini surfactant-12 nanoparticles	Water*	1:0.5	2.2 ± 0.2	18 ± 6
		1:1	2.4 ± 0.4	
		1:2	2.0 ± 0.25	
	DOPE	1:0.5	1.8 ± 0.3	32 ± 4
		1:1	2.0 ± 0.35	
		1:2	2.0 ± 0.2	

* Data is adapted from our previous study.[374]

10.5. Conclusion

In conclusion addition of DOPE to NC 2067/βCDgemini surfactant-12 complexes did not change their nano-size or nano-structural behavior at 1:2 mole ratio. Moreover, DOPE was able to change the scattering pattern of βCDgemini surfactant-18:1 surfactant to inverted hexagonal phase though it did not alter the other two βCDgemini surfactants behavior in solution. Further studies needed to elucidate the effect of DOPE on βCDgemini surfactant-based formulations.

11. GENERAL DISCUSSION AND FINAL CONCLUSIONS

Numerous novel anticancer agents are designed and synthesized yearly in order to treat variety of cancers, the major public issue worldwide. Advancements of nano-based drug delivery systems revolutionized cancer therapy. One innovative approach is the utilization of nano-formulations to increase the solubility of poorly soluble anticancer agents and, consequently, enhance their bioavailability.

Curcumin, the active ingredient of turmeric rhizome, is a natural polyphenol with various pharmacological activities. The anticancer activity of curcumin has been confirmed in different cancer cells. Several curcumin analogs were designed and synthesized to improve the anticancer activity of curcumin. Dr. Dimmock and his colleagues synthesized series of curcumin analogs, named NC compounds with high *in vitro* cytotoxicity towards various cancer cells.[111,226] Among them NC 2067 was shown to have high *in vitro* cell toxicity towards A375 melanoma cells with low IC_{50} value (less than 1 μM).[3] The main challenge of this anticancer agent was the low water solubility (log P = 4.6)[2] which is not favorable for *in vivo* efficacy.

To address the solubility and bioavailability issue of NC 2067, a delivery agent was designed in our group. This novel carrier, called βCDgemini surfactant, was synthesized by chemical attachment of a βCD to a gemini surfactant. βCD, an oligosaccharide macrocycle, is a well-known pharmaceutical carrier which can encapsulate lipophilic molecules and increase their solubility. Gemini surfactants are amphiphilic molecules with the ability to self-assemble and form nano-structures which enhance the delivery of small molecules and biotechnology drugs such as DNA into the mammalian cells. Gemini surfactants used to build βCDgemini surfactants are classified as imino substituted quaternary ammonium gemini surfactants (m-7NH-m) with various tail length and degree of unsaturation. Physicochemical characteristics and *in vitro* activity of the complexes of NC 2067 with βCDgemini surfactants were examined to expand our knowledge about this delivery agent. The previous work in our research group showed that NC 2067 in complexed with βCD and βCDgemini surfactant (with twelve carbon tail, 12C) at 1:2 drug-to-carrier mole ratio, was able to selectively kill A375 melanoma cells without affecting the human epidermal keratinocytes. Moreover, NC 2067/ βCDgemini surfactant increased caspase 3 /7, apoptotic executioners in A375 melanoma cells and formed nanoparticles with positive charge. This study showed that encapsulation of NC compounds by βCD cavity can act as a delivery agent to replace cytotoxic organic solvents such as DMSO.[3]

The first step in my research was to further discover and explain the structural mode of the interaction of NC 2067 with βCD and βCDgemini surfactant. βCDgemini surfactant having gemini surfactant with twelve hydrocarbon tail, (12-7N[CD]-12) was selected for proof-of-principle studies. It was previously found that having three interposing methylene moieties between nitrogen atoms of the spacer of the gemini surfactants, enhanced the formation of various lipid structures and transfection efficacy in lipoplex formulations.[166] The presence of the non-carbon atoms (nitrogen) in the structure of the gemini surfactant spacer is crucial for addition of various functional groups. Moreover, hydrocarbon tails with more than 12 carbon atoms have limited solubility which made 12-7NH-12 gemini surfactant a suitable candidate to be attached to the βCD. Even though βCDgemini surfactant is the delivery agent that was reported to form nanoparticles and enhance the penetration through biomembranes in the previous study[3], the physicochemical characteristics of the NC 2067/βCD complexes were not fully evaluated and the nanoparticle model was built on limited experimental data. Thus the need to comprehend the interaction of NC 2067 and βCDgemini surfactant to a greater extent and build evidence-based models was obvious.

We proposed to examine the complexation of the βCD and its hydrophobic guest molecules by variety of techniques based on the alterations in spectroscopic properties, thermal behavior, ability to diffract X-ray and solubility in aqueous media. The original plan was to crystallize the complexes of NC 2067 with βCD or βCDgemini surfactant and employ single crystal X-ray crystallography to solve the structure. Unfortunately, the crystallization process was not successful and crystals obtained were single crystals of unbound NC 2067 or βCD (Appendix 13.1). In this research the formation of the inclusion complexes of NC 2067 with βCD or βCDgemini surfactant (12 carbon atoms in alkyl chain) was confirmed qualitatively with synchrotron-based powder X-ray diffraction, FTIR and TGA. The comparison of the inclusion complex pattern with the individual components and physical mixture was used to corroborate inclusion formation. In general, the behavior of the physical mixture was a representative of the properties of the two components whereas the inclusion complex was a new compound with new structural properties. Our studies confirmed (section 7.6) that the Bragg's peaks of the individual components were identifiable in diffraction pattern of the physical mixture of NC 2067 with βCD or βCDgemini surfactant. On the other hand, new Bragg's peaks were detected in diffractogram of the inclusion of NC 2067 with βCD. Powder X-ray diffraction of the complexes composed of

βCD and other small molecules, confirmed inclusion formation by revealing new peaks, which were not related to any of the components.[313,314] The NC 2067/βCDgemini surfactant diffractogram showed an amorphous structure similar to native βCDgemini surfactant without any crystalline peaks corresponding to NC 2067. This data supported the inability to crystalize the βCDgemini surfactant-based systems. Moreover, in the FTIR spectra of the inclusion of NC 2067 with βCD or βCDgemini surfactant, the signature peaks of NC 2067 corresponding to styryl moiety was absent or weakened, while they were observable in the physical mixtures' spectra. TGA was another technique used to confirm the inclusion formation in these host/guest systems. In the thermogram of NC 2067/βCD complex, the water loss region corresponding to CD, disappeared. The similar results were reported in the other studies on the βCD complexes confirmed that the water located in the cavity of βCD was replaced by the guest molecule.[260,360] In contrast to βCD, βCDgemini surfactant did not lose any water at 30 ºC -70 ºC. This finding showed for the first time that the βCD cavity of βCDgemini surfactant was most likely occupied by another hydrophobic part of the molecule. It was hypothesized that the hydrocarbon tails of the gemini moiety might be encapsulated by βCD cavity, consistent with other studies showing the interaction of the tail of surfactants with CD cavity.[173,176-178,361,362] Because we did not detect similar water loss trend for βCDgemini surfactant compared to βCD, the water loss mechanism could not be used to confirm the inclusion formation for NC 2067/βCDgemini surfactant complex. Nevertheless, the degradation temperature of NC 2067 complexed with βCD and βCDgemini surfactant was elevated and proved that a complex was formed with a higher stability compared to the free NC 2067. A similar thermal degradation was found for the inclusion complex of sulfamethoxazole with CD that started at higher thermal degradation in comparison to free drug.[254] This behavior was assumed to occur because the drug molecule was protected by CD and formed a complex with greater stability. Further evidence of self-inclusion was provided by attempts to determine the critical micelle concentration (CMC) of the βCDgemini surfactants. In contrast to the expected behavior of gemini surfactants in aqueous media, increasing the concentration of free βCDgemini surfactant did not result in the formation of the self-assembling structures. This finding was supported by the conductivity *versus* concentration plot in which no CMC break point was detected (Appendix 13.2). Based on these findings, it seemed that βCDgemini surfactant had unexpected and complicated properties.

NMR techniques were used to further understand the self-inclusion behavior of the βCDgemini surfactant. These techniques are the most accurate spectroscopy methods employed to assess the geometry of the host/guest inclusion complexes composed of CDs.

The ^{1}H NMR spectrum of the βCDgemini surfactant showed that the internal protons of the βCD cavity were shifted significantly upfield and the protons of the hydrocarbon tail of the gemini surfactant moiety were considerably broad. Further examination of this system, by 1D- and 2D ROESY techniques confirmed the spatial proximity of the βCD internal cavity (H_3 and H_5) to the gemini surfactant tail (H_γ, H_λ, and H_ω) of the βCDgemini surfactant. This finding was in agreement with other studies showing the interaction of the βCD cavity with alkyl components of the regular surfactants[381] and gemini surfactants[173,177]. A similar self-inclusion behavior was reported with a βCD derivative which was mono-substituted by an enyl containing amphiphilic moiety.[181] To understand the mode of the inclusion of gemini tail into βCD cavity (intra- *vs* inter-molecular interactions), the correlation between chemical shift as a function of surfactant concentration was monitored. It was concluded that the likelihood of the intramolecular interaction is significantly greater because no constant correspondence between the concentration of the βCDgemini surfactant and the chemical shifts of the cavity protons was detected. Overall, the physicochemical characterization of βCDgemini surfactant confirmed that the gemini surfactant moiety interacting with βCD and such interaction complicated the behavior of βCDgemini surfactant either as a self-assembling agent or a βCD derivative.

The ^{1}H NMR spectra of the NC 2067/βCD complexes displayed upfield shifts of the internal protons of the βCD cavity in a concentration dependent manner. It was hypothesized that this was due to the anisotropic shielding effect of the aromatic moieties of NC 2067. Similar findings were observed with guest molecules with π-electron containing moieties that interacted with CDs and replaced the water molecules inside the cavity.[270,271,273,274] Moreover, the stoichiometry of NC 2067/βCD complexes estimated to be 1:2 mole ratio based on the continuous variation method. According to the molecular structure of NC 2067 having two styryl moieties, the encapsulation of NC 2067 by two βCD molecules was logical. Furthermore, 1D- and 2D ROESY spectra of NC 2067/βCD complex showed the interaction of the protons of not only styryl but also benzoyl moiety of the NC 2067 with βCD internal protons. Even though we formerly hypothesized that NC 2067 can interact with βCD exclusively through the pharmacophore moiety (1,5-diaryl-3-oxo-1,4-pentadienyl)[374], NMR results showed that the benzoyl aromatic

ring substituted on the 4-piperidineone nitrogen atom was involved in the interaction with cavity as well. Because the benzoyl moiety in NC 2067 structure located in the vicinity of the quaternary ammonium group, molecular docking was used to further examine the feasibility of the NMR findings and illustrate the topological mode of the NC 2067/βCD complex. Molecular docking results confirmed the 1D- and 2D ROESY observations and proposed a final model in which two βCD molecules encapsulated one drug molecule. First βCD cavity accommodated by one styryl ring and the other styryl moiety and benzoyl ring were co-included within the second βCD. Moreover, the polar carbonyl moieties were located between two βCD molecules. This model seems reasonable because of the hydrophobic effect and van der Waals interaction between aromatic rings of NC 2067 and βCD cavity. Moreover, the co-encapsulation of the second styryl moiety and benzoyl group, which are located at proximate spatial distance, reduced the steric hindrance. The quaternary ammonium was positioned outside of the cavity to form hydrated state and the carbonyl groups interacted with βCD protons by hydrogen bindings.

The ^{1}H NMR spectrum of NC 2067/βCDgemini surfactant did not show any alterations in chemical shifts of the internal protons of βCD compared to free βCDgemini surfactant. As well, in 2D ROESY spectrum of NC 2067/βCDgemini surfactant no correlation was found between βCD and NC 2067 while the interaction of the gemini surfactant moiety with βCD was evident.

It was suggested that NC 2067 was not able to modify the self-inclusion behavior of βCDgemini surfactant. This can be explained by the fact that based on the previous studies of surfactant/βCD complexes[381] the binding constant of the gemini surfactant alkyl chain moiety is most likely in order of 10^3 L/mol or greater. However, the molecules bearing aromatic rings[372,386] similar to NC 2067 have lower binding affinity. Hence, in the NC 2067/βCDgemini surfactant system, the drug presumably was not able to displace the alkyl tail from βCD cavity. Based on the biological activity of NC 2067 complexed with βCDgemini surfactant[3,374], the other possibility could be the formation of a ternary complex in which NC 2067 interacted weakly with the carrier. It was previously shown that a ternary complex of pyrene/n-octanol/βCD could be formed in which the alcohol was encapsulated by βCD and the aromatic ring of pyrene interacted with the hydroxyl groups on the rim of the βCD in a non-inclusion mode.[388] A similar behavior can be anticipated with NC 2067/βCDgemini surfactant. Moreover, 1D ROESY spectrum showed a weak interaction of the benzoyl moiety of the NC 2067 with βCD of βCDgemini surfactant.

The other aspect of the physicochemical characterization of the NC 2067 complexes with βCDgemini surfactant was to evaluate their nanoparticulate behavior in the solution. The size of the free βCDgemini surfactants having various alkyl chain length and degree of unsaturation was measured. Among them, βCDgemini surfactant (18 carbon alkenyl chain) formed nano-sized particles. Even though it was previously reported that βCDgemini surfactant (12 carbon alkyl chain) produced nanoparticles with low PDI value[3], the size measurement of the βCDgemini surfactants having 12 and 16 carbon alkyl tail resulted in inconsistent values corresponding to the heterogeneous aggregations. However, addition of NC 2067 to βCDgemini surfactants formed formulations with sizes ranging from 87 to 199 nm. It was demonstrated that changing a variety of parameters such as the structure of βCDgemini surfactant (various alkyl chain length, degree of unsaturation and linker nature), drug to delivery agent mole ratio and addition of helper lipid (DOPE) did not alter the nanoparticle size drastically. Formation of nanoparticles is advantageous for drug delivery as they can improve cellular uptake by endocytosis[23] and elude the reticulo-endothelial system[13]. The other favorable mechanism of the nanoparticles is to overcome the multidrug resistance.[24,363] Nanoparticles interact with the biomembrane of lysosomes and release the loaded drug into cytoplasm where the efflux pumps are not able to expel it outside the cell.[421]

Thus, to assess our system, the nano-structural arrangements of the βCDgemini surfactant-based formulations were evaluated by the synchrotron-based SAXS/WAXS. Lipid-based self-assembling molecules such as gemini surfactants are able to build different lyotropic liquid crystalline nanostructures in solution.[157] Structural parameters of gemini surfactants such as nature and length of the hydrocarbon tail dictated the nano-arrangement of the amphiphiles.[162] The X-ray scattering pattern of various βCDgemini surfactants (different alkyl chain length and degree of unsaturation) showed a diffused peak independent from the surfactant concentration.[374] In a study about a system composed of a gemini surfactant and CDs, similar aggregations were detected using small-angle neutron scattering.[364] This observation is consistent with the self-inclusion behavior of βCDgemini surfactants resulting in the occupancy of the hydrocarbon tails of the gemini moiety due to the interaction with βCD.

Addition of DOPE as a helper lipid to free βCDgemini surfactants (12 and 16 carbon alkyl chain) did not change the scattering pattern whereas the βCDgemini surfactant having 18 carbon alkenyl chain, dispersed in DOPE showed inverted hexagonal phase, characteristic to DOPE.[420]

Once again, the self-inclusion of βCDgemini surfactants hindered the interaction of gemini surfactant with the helper lipid. However, the presence of the inverted hexagonal phase of DOPE in βCDgemini surfactant (18 carbon alkenyl chain) /DOPE system could be attributed to the weaker propensity of the unsaturated tail for self-inclusion. It was shown that the mono-unsaturation of the hydrocarbon tail of the lipids changed their geometry by producing a bend in the structure.[397] Similar geometrical property of the gemini surfactant moiety of βCDgemini surfactant (18 carbon) resulted in less interaction with βCD.

Addition of NC 2067 to βCDgemini surfactants at various drug-to-carrier mole ratios resulted in the appearance of a new Bragg's peak (*d*-spacing of 23 Å). Prior to NMR results, we speculated that NC 2067 was able to compete with gemini surfactant and partially release the gemini tail from βCD cavity.[374] Based on NMR spectra and the binding affinity estimations, NC 2067 showed minimal effect on βCDgemini surfactant system. We hypothesized that this new peak is related to the weak interaction of NC 2067 with βCDgemini surfactant in a ternary complex system. This finding was confirmed with the fact that this new peak was observable in all NC 2067/βCDgemini surfactant systems. Moreover, at lower concentrations of the delivery agent (βCDgemini surfactants having 12 and 16 carbon alkyl chain), other peaks corresponding to precipitated NC 2067 were detected. In contrast, the scattering pattern of NC 2067/βCDgemini surfactant (18 carbon alkenyl chain) did not show the NC 2067 peaks indicating the higher capacity of this βCDgemini surfactant to solubilize the drug. This finding further supports our hypothesis regarding the weaker self-inclusion of βCDgemini surfactant (18 carbon alkenyl chain) compared to saturated derivatives, which might result in the greater interaction of NC 2067 with βCD.

The anticancer activity of NC 2067 complexes with various βCDgemini surfactants was evaluated towards A375 melanoma cells. Based on the previous study in our group, NC 2067 dissolved in DMSO showed high cytotoxicity towards A375 melanoma cell line with a low IC_{50} value (half-maximal inhibitory concentration) without affecting healthy human epidermal keratinocytes. Moreover, the IC_{50} value for NC 2067/βCDgemini surfactant (12 carbon alkyl chain) reported to remain as low as 2 μM. To conduct a systematic evaluation and build data towards assessment of structure-activity relationships, the anticancer efficacy of NC 2067 was evaluated in various βCDgemini surfactant-based formulations by varying parameters such as the type of the βCDgemini surfactant, linker structure, drug-to-delivery agent mole ratio and addition

of helper lipid. It was found that NC 2067 complexed with a variety of βCDgemini surfactants retained its high toxicity towards A375 melanoma cells. The IC_{50} values were in the range of 1.8 to 2.6 μM which were significantly more efficient compared to melphalan, an approved therapeutic agent for melanoma. Alterations of the structure of the βCDgemini surfactants (different acyl chain length and the degree of unsaturation of the hydrocarbon tail), the nature of the linker[374] and the drug-to-carrier mole ratio[374], in addition to the presence of DOPE in the formulations, did not influence the potency of NC 2067 to kill A375 melanoma cells. Moreover, intrinsic toxicity of various free βCDgemini surfactants was assessed towards A375 melanoma cells to corroborate the potential involvement of the delivery agent in the total toxicity of the formulations and estimate the safety of the βCDgemini surfactants. The intrinsic toxicity of the βCDgemini surfactants having 12 and 18 carbon chain was low whereas the compound with 16 carbon alkyl chain showed higher cytotoxicity. The latter observation is possibly due the lower water solubility of the βCDgemini surfactant with 16 carbon tail that led to precipitation in cell culture. Even though βCD assumed to be an inert carrier, there are some studies showed that it could interact with biomembrane components such as cholesterol and distress cells. Conversely, the encapsulation of small molecules by the βCD cavity hindered the interaction with cellular membranes.[130] In addition, the gemini surfactant component of the delivery system could have the potential to show cytotoxicity towards various cell lines according to their structural properties and concentration.[367] Overall, the βCDgemini surfactants showed lower cytotoxicity in comparison to the amino acid-grafted gemini surfactants having similar gemini moiety.[165] It was speculated that the low cytotoxicity of the βCDgemini surfactants might be related to the self-inclusion behavior that impeded the negative interaction of either the βCD or gemini surfactant moiety with biological compounds. Altering the nature of the linker from ester to amide and addition of DOPE significantly increased the intrinsic toxicity of the βCDgemini surfactant. This observation can be explained with the fact that amide moieties are able to interact through hydrogen bindings with proteins consequently lead to cell death mechanisms.[365]

In my research, the cell death mechanism of NC 2067 in presence of the βCDgemini surfactants was examined using flow-cytometry assays. The NC 2067 complexes with various βCDgemini surfactant induced apoptosis in A375 melanoma cells without triggering necrosis in the cell populations. This result confirmed the results of an earlier study showing that NC 2067 complexed with βCDgemini surfactant (12 carbon alkyl chain) increased caspases 3 and 7

(apoptotic probes) in A375 melanoma cells.[3] Among the formulations, NC 2067/βCDgemini surfactant (12 carbon alkyl chain) showed proapoptotic effect comparable to melphalan and caused chromatin condensation. Free βCDgemini surfactants did not induce apoptosis in A375 melanoma cells excluding the 16 carbon alkyl chain which increased the population of necrotic/apoptotic cells, consistent with other cell viability assays. Based on the literature, curcumin and its analogs are able to induce cell death through both intrinsic and extrinsic apoptotic pathways. Mitochondrial membrane potential loss is a well-defined consequence of the stimulation of the intrinsic apoptotic cascade. Unfortunately, the NC 2067/βCDgemini surfactant formulations did not change the mitochondrial membrane potential in A375 melanoma cells. Similar results were obtained with various melanoma cells treated with curcumin revealing no mitochondrial membrane potential loss was detected.[231,232] Moreover, NC 2067 based formulations were not able to induce ROS production. Lastly, the influence of the formulations on the cell cycle arrest was evaluated. Even though curcumin and its analogs arrested cancer cells at different phases of the cell cycle, NC 2067/βCDgemini surfactant formulations did not show any alterations in the cell cycle, confirming that the curcumin analogs bearing conjugated unsaturated styryl ketones, are possibly thiol alkylators and do not act through interference with genetic materials.

In conclusion the inclusion formation of NC 2067 with βCD and βCDgemini surfactant was confirmed qualitatively by various analytical techniques such as powder X-ray diffraction, FTIR spectroscopy and TGA. Moreover, 1D- and 2D ROESY results showed the details of the geometrical interactions of the host/guest complexes of the βCDgemini surfactant, NC 2067/βCD and NC 2067/βCDgemini surfactant. It was noted that βCDgemini surfactant showed intramolecular self-inclusion in which the hydrocarbon tails of the gemini moiety encapsulated by the βCD cavity. NC 2067 interacted with βCD cavity through its styryl and benzoyl moieties in a 1:2 drug-to-βCD mole ratio. It was confirmed that the addition of NC 2067 had minimal influence on the self-inclusion behavior of βCDgemini surfactant. As such the SAXS/WAXS study of NC 2067/βCDgemini surfactant complexes in solution did not show regular lyotropic liquid crystalline patterns corresponding to the self-assembling potential of the surfactants. However, various NC 2067/βCDgemini surfactant formulations formed nano-sized structures with high *in vitro* cytotoxicity towards A375 melanoma cells. The cell death mechanism of NC 2067 in the presence of βCDgemini surfactant was reported to be a non-mitochondrial mediated

apoptosis without affecting cell cycle phases. Identification of the physicochemical properties and anticancer activity of NC 2067/βCDgemini surfactant drug delivery system, extend our knowledge to further develop more proficient anticancer therapies.

12. FUTURE DIRECTIONS

βCDgemini surfactant as a novel delivery agent was able to solubilize a model anticancer agent, NC 2067. *In vitro* evaluation of NC 2067 in presence of the βCDgemini surfactant showed high cytotoxicity and proapoptotic activity. Moreover, it was reported that the βCDgemini surfactant was a safe delivery agent not affecting cancer cells on its own. These favorable properties made βCDgemini surfactant a promising carrier for lipophilic anticancer agents. However, the self-inclusion behavior of βCDgemini surfactant complicated the interaction of the guest molecule and altered the self-assembling of the gemini surfactant moiety. Future work will focus on the modification of the βCDgemini surfactant to minimize the self-inclusion behavior. It seems that any structural alteration that can inhibit the gemini surfactant tail to be incorporated into βCD cavity is favorable to this system. For example, addition of bulky chemical moieties to the hydrocarbon tails of the gemini surfactant could produce steric hindrance. βCDgemini surfactant is synthesized by mono-substitution of gemini surfactant on βCD. Amphiphilic poly-substituted βCD derivatives could be designed to potentially lower the self-inclusion. Any changes in the structure of the βCDgemini surfactant can be probed by NMR techniques.

In addition, other strategies can be employed to design modified substitutes for βCDgemini surfactant. One approach could be the use of the polymer-based βCDs in which the βCD cavities are available for hydrophobic small molecules and the polymer moiety form nanostructures. The use of the βCD in liposomes and dendrimers are other examples that can modify the delivery agent.

This work was the first step in elucidating cell death mechanisms. However, further studies are needed to understand which apoptotic pathway was triggered in A375 melanoma cells treated with NC 2067/βCDgemini surfactant systems. The activity and concentration of the protein molecules involved in the intrinsic and extrinsic apoptotic pathways such as cytochrome c, caspases and Bcl-2 family proteins can be evaluated. Moreover, the role of autophagy in the cell death can be examined.

13. Appendices

Appendix 13.1- Single crystal X-ray Crystallography of βCD and NC 2067

Crystallization procedure

Different techniques and organic solvents were used as solvent and anti-solvent to obtain crystals from the inclusion complex of NC 2067/βCD and NC 2067/βCDgemini surfactant-12. The liquid-liquid diffusion (layering) technique was employed to crystalize NC 2067/βCD in which a mixture of water/DMSO (%60/40 v/v) and acetone were used as solvent and anti-solvent, respectively. The crystallization of the NC 2067/βCDgemini surfactant-12 was performed using EchoTherm^{TM} IN35 chilling incubator (Torrey Pines Scientific, USA). The temperature was cooled down from 40^{o}C to 10^{o}C with cooling rate of 0.1^{o}C per an hour. Unfortunately after data collection and analysis we found that the crystals obtained from NC 2067/βCD and NC 2067/βCDgemini surfactant-12 samples were free βCD and free NC 2067, respectively.

Data collection

Synchrotron X-ray diffraction measurements were performed at Canadian light source (CLS, Saskatoon) on the beamline 08B1-1 (CMCF-BM, CLS) which is equipped with a versatile MD2 micro-diffractometer and a Rayonix MX300HE CCD detector. A goniometer base with 18 mm copper pin length with GB-B3S-R-10 design (MiTeGen, USA) was employed as sample holder to mount sample on the beamline. A suitable single crystal, of 0.05-0.2 mm size in each dimension, was removed from the solution, quickly coated with oil (Paratone 8277, Exxon), collected inside a mounted CryoLoop^{TM} (Hampton Research, USA) with 10 μm nylon fiber diameter and 0.1-0.2 mm loop diameter attached to the goniometer base and immediately transferred into liquid nitrogen. Then, the sample holder was mounted on the beamline where a cold stream of cryojet (Oxford, UK) maintained the 100 K temperature to avoid crystal degradation.

Data was collected at 18 KeV (corresponding to λ=0.68878 Å) at a 150 mm crystal to detector distance with exposure time of 1-2 seconds. A series of data frames at 1^{o} increments of ω were collected. Data collection was completed by changing the detector angle to 2θ=10^{o} and curving the cooper wire resulting in at least 4 data series for each crystal.

Data collection was performed using Macromolecular Crystallography Data Collector (MXDC) graphical interface.[422]

Data processing

The in-house script called Autoprocess[358] was applied to index, integrate, merge and scale the diffraction data. Cell dimension refinement and data reduction were also performed using SAINT (Bruker,USA) or XPREP (Sheldrick)[423]. The programs used to solve structure were Shelxd or Shelxs (Sheldrick)[424,425]. For structure refinement Shelxl-97 was occupied (Sheldrick)[424]. The refined structure was visualized by XP (ShelxTL, Bruker, USA)[426] or RasMol[427].

The flow chart of data processing has been shown in (Figure 13.1).

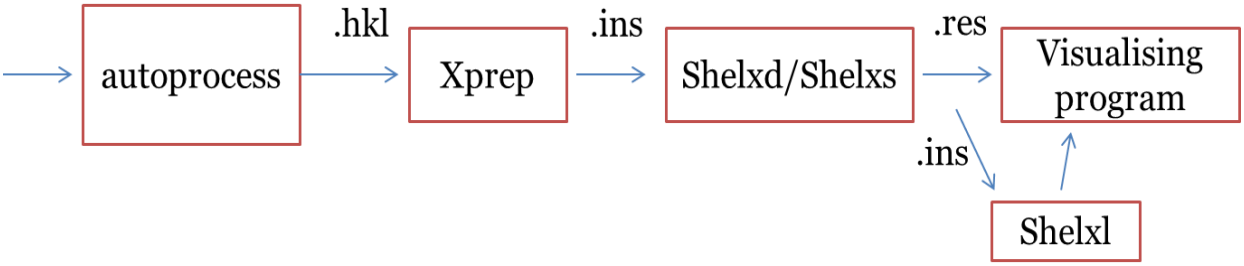

Figure 13.1- Crystallography data processing chart

Structure determination of βCD

Crystal data, data collection and refinement statistics were shown in Table 13.1. The most probable crystal system and symmetric space group for βCD was suggested as triclinic and P_1, respectively. Molecular structure of apo-βCD was solved, refined and visualized (Figure 13.2).

Table 13.1- βCD crystal data and data collection and refinement

Crystal data	Data collection and refinement
$C_{42}H_{70}O_{35}$	Energy: 18 KeV
MW: 1135 g/mol	λ: 0.6888 Å
Space group: triclinic, P_1	T: 100 K
Z=2	d: 150 mm (crystal to detector distance)
Unit cell dimensions:	$4.45° < 2\theta < 53.96°$
a= 15.33 Å	
b= 15.35 Å	
c= 15.61 Å	
Unit cell angles:	
α= 81.4°	
β= 86.9°	
γ=77.6°	
V: 3548 $Å^3$	

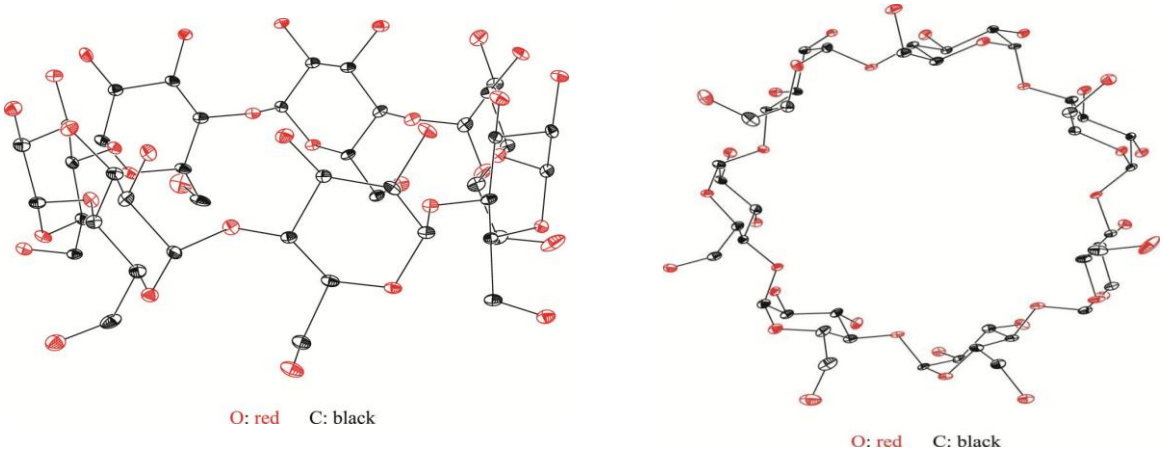

Figure 13.2- Molecular structure of the apo-beta-cyclodextrin is illustrated by XP (SHELXTL). Hydrogen atoms have been omitted for clarity. The non-hydrogen atoms are represented by displacement ellipsoids at the 20% probability level.

Structure determination of NC 2067

NC2067 needle shape crystals obtained from NC 2067/βCDgemini surfactant-12 sample by slow cooling down.

Crystal data, data collection and refinement statistics were shown in Table 13.2. Molecular structure of NC 2067 was solved, refined and visualized (Figure 13.3).

Table 13. 2- NC 2067 crystal data and data collection and refinement

Crystal data	Data collection and refinement
$C_{30}H_{30}N_2O_3$	Energy: 18KeV
MW: 503.05 g/mol	λ: 0.6888Å
Space group: monoclinic, $P2_1$	T: 100K
Z=4	d: 150 mm (crystal to detector distance)
Unit cell dimensions:	$4.45° < 2\theta < 53.96°$
a= 11.41Å	
b= 11.67Å	
c= 22.89Å	
Unit cell angles:	
$\alpha = 90^o$	
$\beta = 91.53^o$	
$\gamma = 90^o$	

O:red
C:grey
N:blue

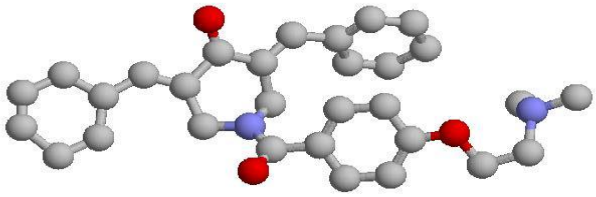

Figure 13.3- Molecular structure of NC2067 by RasMol. Hydrogen atoms have been omitted for clarity. The non-hydrogen atoms are represented by displacement balls.

Appendix 13.2- Critical micelle concentration (CMC) measurement of βCDgemini surfactant-12 using conductivity method

Conductivity method was used to determine the CMC of βCDgemini surfactant-12 in water. In general, increasing the concentration of a regular surfactant will result in the formation of micellar self-assemblies. Increasing the concentration above CMC will lower the rate of the water conductivity increase. The gemini surfactant compartment of βCDgemini surfactant-12, showed as 12-7NH-12, showed CMC of 2.4 mM measured by conductivity method.[167] However, increasing the concentration of βCDgemini surfactant-12 to 6 mM did not result in any change in the conductivity rate suggesting that βCDgemini surfactant-12 most likely did not form self-assemblies (Figure 13.4).

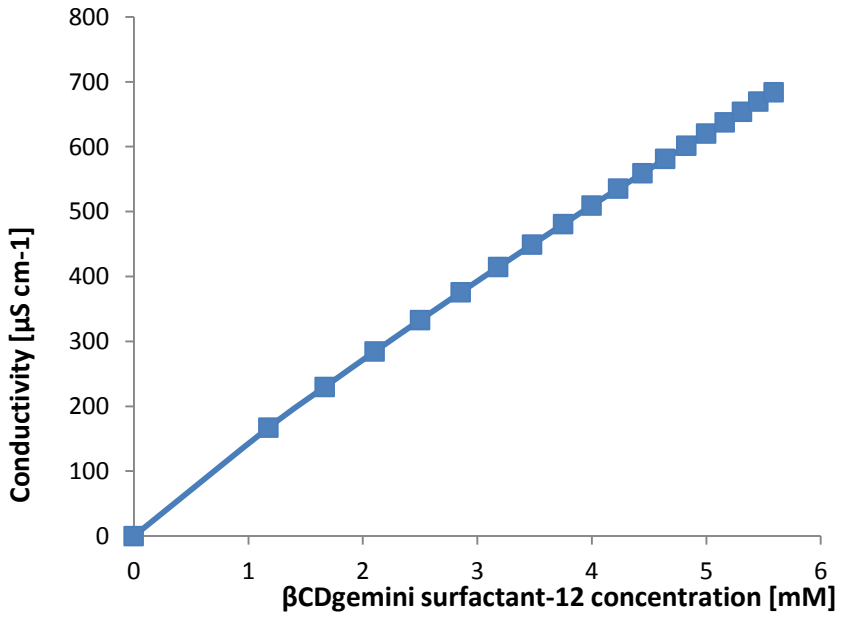

Figure 13.4- CMC measurement of βCDgemini surfactant-12 using conductivity method

Appendix 13.3- Circular dichroism spectra of NC 2067/βCD and NC 2067/βCDgemini surfactant-12

Circular dichroism spectra of NC 2067, βCD, βCDgemini surfactant-12 and NC 2067/βCD and NC 2067/βCDgemini surfactant-12 were obtained (Figure 13.5A and B). The results did not show any meaningful alteration in circular dichroism spectra of the complexes, NC 2067/βCD and NC 2067/βCDgemini surfactant-12 compared to free βCD or βCDgemini surfactant-12.

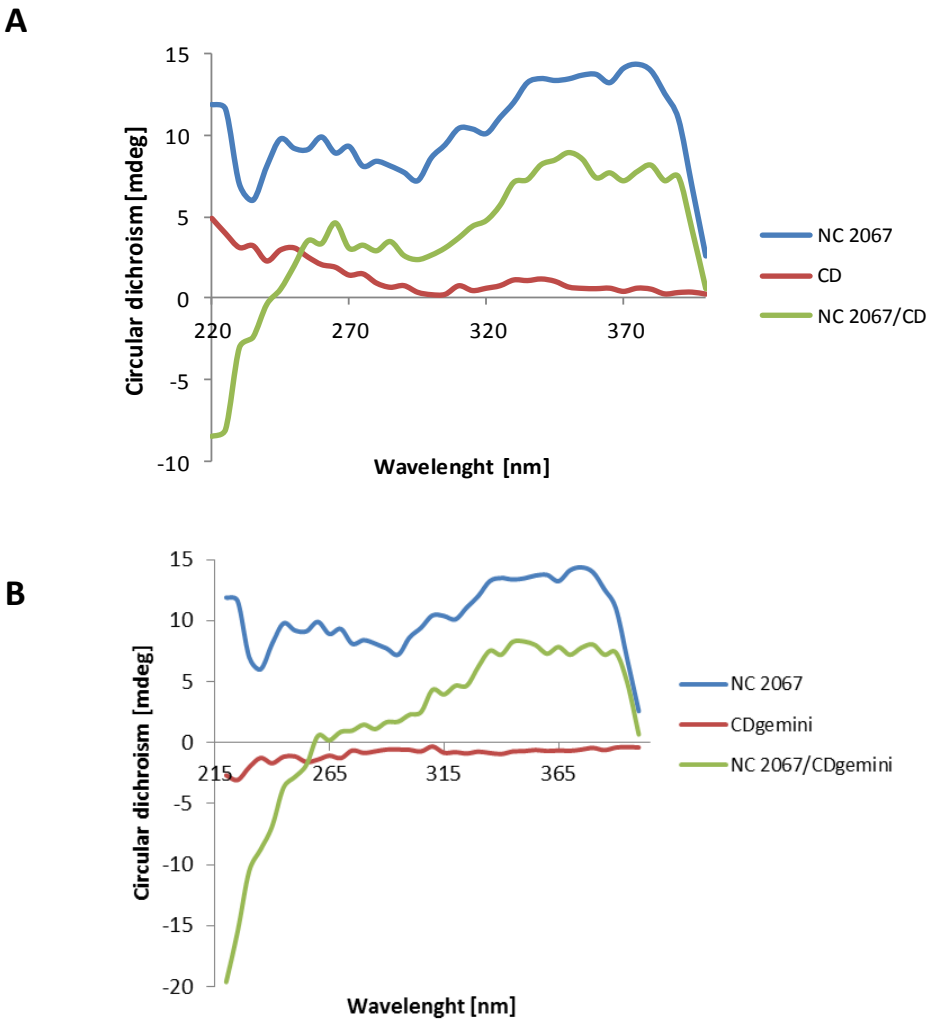

Figure 13.5- Circular dichroism spectra of **A)** NC 2067, βCD and NC 2067/βCD and **B)** NC 2067, βCDgemini surfactant-12 and NC 2067/βCDgemini surfactant-12.

Appendix 13.4- Phase solubility diagram of NC 2067/βCDgemini surfactant-12 using UV spectroscopy

To evaluate the ability of βCDgemini surfactant-12 to solubilize NC 2067, extra amount of NC 2067 was added to different concentrations of βCDgemini surfactant-12 and UV absorbance of NC 2067 at 330 nm measured (Figure 13.6). Although, increasing the βCDgemini surfactant-12 concentration to 0.8 mM, enhanced the solubilization of NC 2067, the solubility of NC 2067 (UV absorbance) decreased at higher concentrations of βCDgemini surfactant-12. These results suggested a more complicated system in comparison to a binary system of CDs and guest molecules.

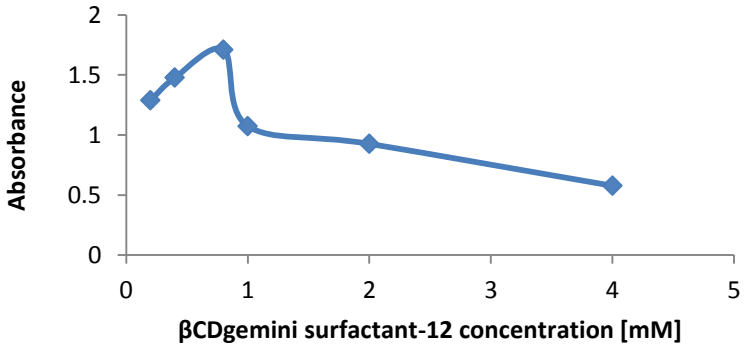

Figure 13.6- Phase solubility diagram of NC 2067 in presence of βCDgemini surfactant-12 using UV absorbance.

Appendix 13.5- ^{1}H NMR study of βCDgemini surfactant-16 and βCDgemini-surfactant-18:1

We obtained the ^{1}H NMR spectra of βCDgemini surfactant-16 and βCDgemini surfactant-18:1 in D_2O to evaluate their potential self-inclusion behavior. NMR spectra showed that the internal protons of βCD (H_3 and H_5) shifted upfield, with Δδ values of 0.052 ppm (H_3) and 0.096 ppm (H_5) for βCDgemini surfactant-16 and 0.077 ppm (H_3) and 0.095 ppm (H_5) for βCDgemini surfactant-18:1. The Δδ value of H_3 for βCDgemini surfactant-18:1 is higher whereas the Δδ value of H_5 is similar in both βCDgemini surfactants. Moreover, in both spectra the chemical shift change of H_5 is greater than H_3 (Table 13.3).

Table 13.3- Chemical shifts (ppm) of the βCD protons in βCDgemini surfactant-16 and βCDgemini surfactants-18:1 compared to free βCD.

	βCD	**βCDgemini surfactant-16**		**βCDgemini surfactant-18:1**	
	δ	δ	Δδ	δ	Δδ
H_1	5.001	4.988	0.013	4.992	0.009
H_2	3.580	3.568	0.011	3.597	-0.018
H_3	3.898	3.846	0.052	3.821	0.077
H_4	3.516	3.520	-0.004	3.551	-0.036
H_5	3.803	3.707	0.096	3.708	0.095
H_6	3.809	3.806	0.003	3.788	0.021

Appendix 13.6- *In vitro* cell toxicity of NC 2081 compared to NC 2067

NC 2081 (Figure 13.7) is another curcumin analog with comparable structure to NC 2067 (Figure 2.4). We evaluated the *in vitro* cytotoxicity of NC 2081 towards A375 melanoma cell line and compared with NC 2067 (Table 13.4). NC 2081 dissolved in DMSO showed high toxicity toward A375 cells comparable to NC 2067 with IC_{50} value of 0.8±0.2 μM. NC 2081 in presence of βCDgemini surfactant-12 (ester linker) at 1:2 drug to delivery agent mole ratio (IC_{50} = 4 ± 1.9 μM) was not significantly different compared to NC 2067 formulation with an IC_{50} value of 2 ± 0.25 μM (P>0.05). However, the IC_{50} value of NC 2081/βCDgemini surfactant-12 having amide linker was significantly greater than the similar formulation with NC 2067.

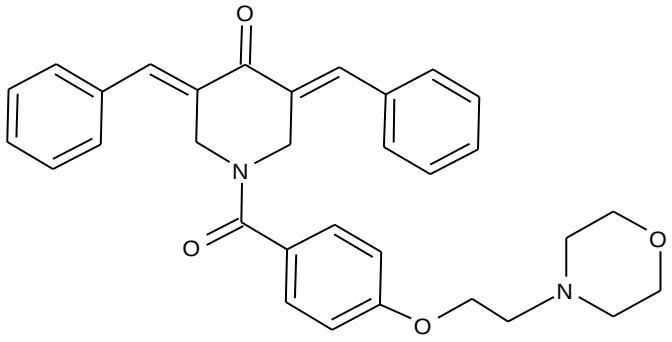

Figure 13.7- Chemical structure of NC 2081.

Table 13.4- IC_{50} values of NC 2081 compared to NC 2067 dissolved in DMSO or in complexes with CDgemini surfactant-12 having ester or amide linker

Curcumin analog	Solvent /Delivery agent	linker	IC_{50} [μM] ± SD
NC 2081	DMSO	NA	0.8 ± 0.2
	CDgemini-12	Ester	4 ± 1.9
		Amide	32 ± 7
NC 2067	DMSO	NA	0.5 ± 0.1
	CDgemini-12	Ester	2.0 ± 0.25
		Amide	2.1 ± 0.3

Appendix 13.7- Evaluation of the mitochondrial membrane potential ($\Delta\Psi_m$) in A375 cells treated with NC 2067/βCDgemini surfactant complex by flow cytometry

Mitochondrial membrane potential disruption is one of the key events in mitochondrial-dependent apoptosis. The fluorescent dyes to probe $\Delta\Psi_m$ are lipophilic cationic compounds that can accumulate in mitochondrial intermembrane matrix inversely proportional to $\Delta\Psi_m$ (more negative $\Delta\Psi_m$, more accumulation of dye). We used two different mitochondrial fluorescent dyes named JC-1 ((5,5′,6,6′-tetrachloro-1,1′,3,3′- tetraethylbenzimidazolylcarbocyanine iodide) and TMRM (tetramethylrhodamine methyl ester).

1. Evaluation of $\Delta\Psi_m$ using JC-1

We employed JC-1 dye to calculate the percentage of the cells having mitochondrial membrane potential loss. In healthy cells, JC-1 (cationic dye) accumulates in mitochondria with high membrane potential. Higher rate of the accumulation of JC-1 results in the formation of the J-aggregates. Monomers of JC-1 emit fluorescence at green region (527 nm) whereas the aggregates are able to exhibit green and red fluorescence at 527 and 590 nm, respectively. The shift from red to green indicates the presence of higher amounts of monomers in comparison to aggregates subsequently showing the mitochondrial membrane potential loss (depolarization) and apoptosis.[394]

Material and Methods- Cells seeded in 6-well plates (25 x 10^4 cells/well) and after 24 h of incubation at 37°C in a humidified incubator with 5% CO_2, they were treated with Melphalan (10 μM), NC 2067 dissolved in DMSO (0.5 and 1 μM) and in ethanol (1 μM), NC 2067/βCDgemini surfactant-12 (2.5 μM) and βCDgemini surfactant-12 (5 μM). After 24 hours of incubation, JC-1 (2.5 μg/ml) added to each well and incubated at 37°C for 20 min. CCCP (80 μM) was added at the same time as JC-1. Immediately, media removed from wells and cells were washed twice by DPBS to remove JC-1 remaining outside of the cells. Then cells were trypsinized and harvested. Cells pellets resuspended in 500 μl DPBS, filtered and analyzed with a FACScalibur flow cytometer with excitation from the 488 nm argon laser and emission in the 585/42 and 530/30 nm filters. The percentage of the green fluorescence of JC-1 monomers was employed to identify the cells with mitochondrial membrane potential drop.

Results- The percentage of the cells showing red and green fluorescence after treatment with different compounds is illustrated in Table 13.5. Cells treated with CCCP (80 μM) and apigenin (50 μg/ml) as positive controls, showed a shift from red to green in comparison to healthy cells confirming the decrease in mitochondrial membrane potential. This shift is significantly higher for cells treated with CCCP (%94.1 of cell population at Q_3) (Figure 13.8-B) compared to untreated cells (Figure 13.8-A). NC 2067 dissolved in DMSO at 0.5 and 1 μM did not show any significant change in the cell population with green fluorescence compared to untreated cells (Table 13.5) (Figure 13.8-C). Surprisingly, 1% DMSO showed significantly higher green fluorescent population comparable to apigenin suggesting the effect of DMSO on mitochondrial membrane potential (data is not shown). To remove the possible effect of 1% DMSO we dissolved NC 2067 in lower amount of DMSO (0.1%) or ethanol. However, the results did not alter (data is not shown). Cells treated with NC 2067/βCDgemini surfactant-12 formulation and free βCDgemini surfactant-12 presented red and green fluorescent populations similar to untreated cells (Table 13.5) (Figure 13.8-D). These results showed that NC 2067 did not decrease mitochondrial membrane potential in A375 melanoma cells.

Table 13.5- A375 melanoma cell populations stained with JC-1 showing red and green fluorescence after 24 hours of treatment with NC 2067- based formulations.

% cells	**Untreated**	**CCCP [80 μM]**	**Apigenin [50 μg/ml]**	**Melphalan [10 μM]**	**NC 2067/ DMSO [0.5 μM]**	**NC 2067/ DMSO [1 μM]**	**NC 2067/ βCDgemini surfactant [2.5 μM]**	**βCDgemini surfactant [5 μM]**	**NC 2067/ Ethanol [1 μM]**
Green+, Red+	87.8	5.89	61.2	97.1	82.5	81.3	94.2	87.5	96.8
Green+, Red-	12.2	94.1	38.8	2.9	17.5	18.7	5.83	12.5	3.19

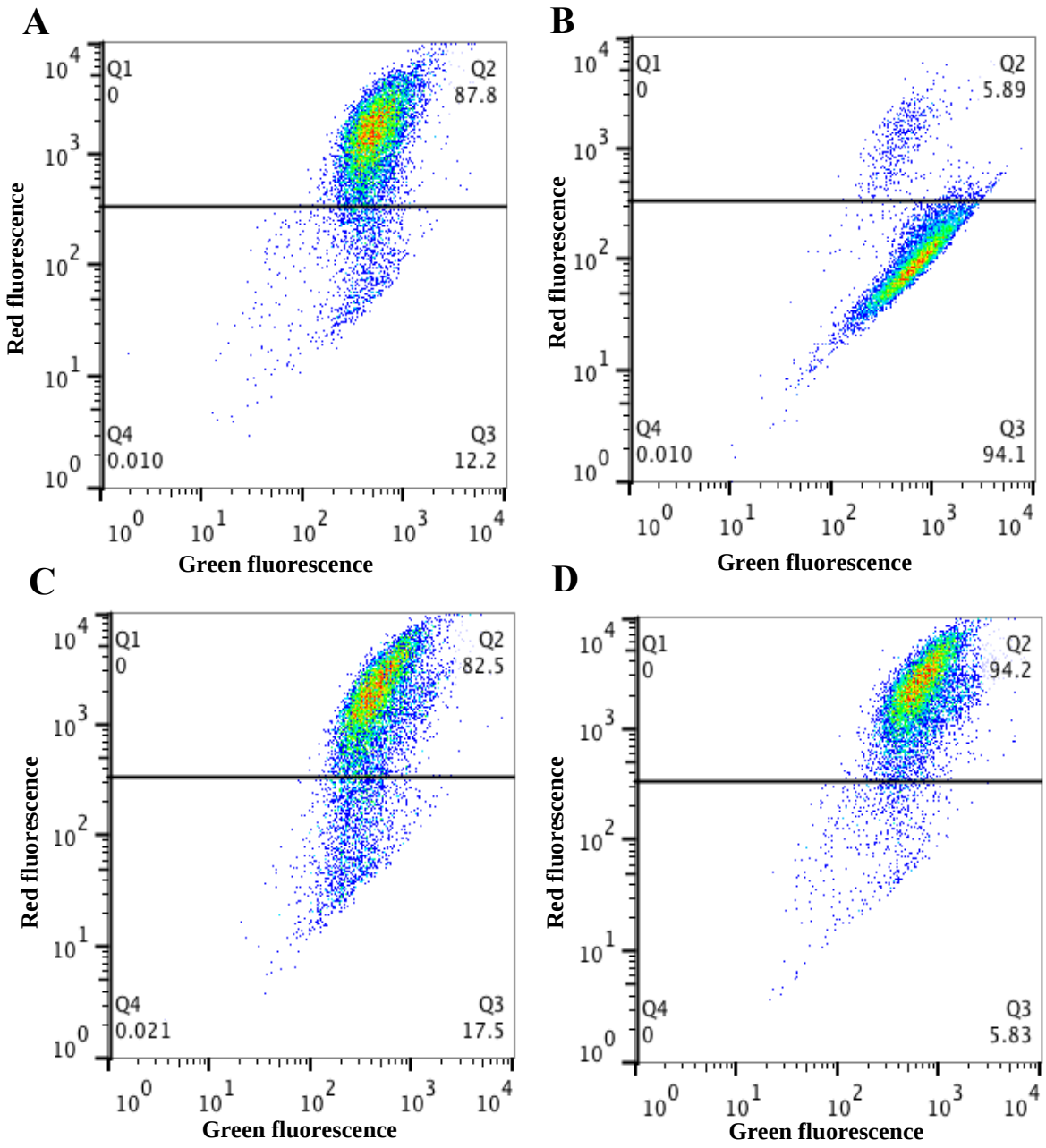

Figure 13.8- Biexponential mitochondrial membrane potential loss of A375 melanoma cells stained with JC-1 in **A)** untreated and treated with **B)** CCCP, **C)** NC 2067 dissolved in DMSO and **D)** NC 2067/βCDgemini surfactant-12 formulation for 24 hours by flow cytometry.

2. Evaluation of $\Delta\Psi_m$ using TMRM

TMRM is a fluorescent rhodamine derivative which its fluorescence intensity will be quenched upon accumulation in mitochondria.[395] Therefore, the decrease in red fluorescence is the indicator of the mitochondrial membrane potential disruption.

Material and Methods- Cells seeded in 6-well plates (25 x 10^4 cells/well) and after 24 h of incubation at 37°C in a humidified incubator with 5% CO_2, they were treated with Melphalan (10 μM), NC 2067 dissolved in DMSO (0.5 and 1 μM), NC 2067/βCDgemini surfactant-12 (2.5 μM) and βCDgemini surfactant-12 (5 μM). After 12 and 24 hours of incubation, cells were trypsinized and harvested. Then TMRM (0.5 μM) added to each sample and incubated at 37°C for 30 min. CCCP (80 μM) was added at the same time as TMRM. Immediately, media removed by centrifugation and cells were washed twice by DPBS to remove TMRM remaining outside of the cells. Cells pellets resuspended in 500 μl DPBS, filtered and analyzed with a FACScalibur flow cytometer with excitation from the 488 nm argon laser and emission in the 585/42 nm filter. The intensity of the red fluorescence of TMRM was employed to identify the cells with mitochondrial membrane potential drop.

Results- The red fluorescence intensity of the cells treated with different compounds is illustrated in Table 13.6. Cells treated with CCCP (80 μM) as a positive control, showed a significant decrease in red fluorescence intensity (27.6) compared to untreated cells (243.3) (Table 13.6) confirming the mitochondrial membrane potential loss. Cells treated with NC 2067 dissolved in DMSO (0.5 and 1 μM) or in complexed with βCDgemini surfactant-12 (2.5 μM) for 12 or 24 hours exhibited red fluorescence intensity similar to the untreated A375 melanoma cells (Table 13.6). Moreover, cells treated with free βCDgemini surfactant-12 (5 μM) surfactant and 0.1% DMSO did not alter the red intensity compared to untreated (data is not shown). The decrease in red fluorescence intensity was observed at the concentration of 10 μM of NC 2067 dissolved in DMSO which is approximately 20 times more than IC_{50} value after 4-6 hours of incubation (data is not shown). This result is probably due to the high toxicity at this concentration which is not necessarily related to the mitochondrial-dependent apoptosis. Once again our findings suggested that NC 2067 did not decrease mitochondrial membrane potential in A375 melanoma cells at IC_{50}.

Table 13.6- Red fluorescence intensity of A375 melanoma cells stained with TMRM after treatment with NC 2067 based formulations.

	untreated	**CCCP [80 µM]**	**NC 2067/ DMSO [0.5 µM]**		**NC 2067/ DMSO [1 µM]**		**NC 2067/ βCDgemini surfactant-12 [2.5 µM]**	
			12 h	**24 h**	**12 h**	**24 h**	**12 h**	**24 h**
Relative fluorescence intensity	243.3	27.6	271.3	242.3	276.2	263.4	269.7	242.8

Appendix 13.8- Evaluation of ROS generation in A375 cells treated with NC 2067

ROS generation is the stimulus for mitochondrial membrane potential disruption. To evaluate the ROS generation in A375 cells following the treatment with NC 2067 formulations, we used a cell permeable probe called 2′-7′-Dichlorodihydrofluorescein diacetate (DCFH-DA). This non-fluorescent compound will be cleaved by intracellular esterases to form H2DCF, a cell impermeable molecule. Subsequently, the oxidation of H2DCF by intracellular ROS will result in the formation of the final product (DCF) which is highly fluorescent. An increase in the fluorescence intensity of cells stained with DCF at 530 nm when excited at 485 nm is the indicator of ROS generation. We probed ROS generation in A375 cells using DCF by both flow cytometry and plate reader.[428]

Material and Methods- The cell culture media used for the following experiments did not contain phenol red.

Flow cytometry

Cells seeded in 6-well plates (25 x 10^4 cells/well) and after 24 h of incubation at 37℃ in a humidified incubator with 5% CO_2, they were treated with 5FU (10 μM) and NC 2067 dissolved in DMSO (0.5 and 1 μM). After 24 hours of incubation, cells were trypsinized and harvested. Then DCFH-DA (5 μM) added to each sample and incubated at 37℃ for 15 min. Immediately, media removed by centrifugation and cells were washed twice by DPBS to remove DCF leaked outside of the cells. Cell pellets resuspended in 500 μl DPBS (without magnesium and calcium ions), filtered and analyzed with a FACScalibur flow cytometer with excitation from the 488 nm argon laser and emission in the 530/30 nm filter. The intensity of the green fluorescence of DCF was employed to identify the cells produced ROS.

Plate reader

Cells seeded in 96-well plates (1 x 10^4 cells per well) and after 24 h of incubation at 37℃ in a humidified incubator with 5% CO_2, they were treated with NC 2067 dissolved in DMSO (0.5, 1 and 5 μM). After 24 hours of incubation, cells were stained with DCFH-DA (5 μM) and incubated at 37℃ for 15 min. As a control H_2O_2 (100 μM) was added and incubated for 30 min before staining with DCFH-DA. Immediately, media removed and 100 μl of DPBS (without magnesium and calcium ions) added. The excitation and emission filters of 485/20 and 528/20 nm, respectively used and fluorescence intensity recorded on a Synergy BioTek plate reader.

Results- A375 cells treated with 5FU (10μM) and NC 2067 (0.5 and 1 μM) and evaluated by flow cytometry showed no alteration in fluorescence intensity compared to the untreated cells (Table 13.7). The intensity slightly increased with higher concentration of NC 2067 (5 μM) which is ten times greater than IC_{50} value.

Moreover, we observed that treatment with H_2O_2 (100 μM) significantly increased the intensity recorded by plate reader in comparison to the untreated cells (approximately four times greater intensity). Once more, NC 2067 at various concentrations (0.5, 1 and 5 μM) did not change the green fluorescence intensity.

Based on our observations, we concluded that NC 2067 was not able to induce ROS generation at A375 melanoma cell line. Because the results for NC 2067 dissolved in DMSO was not desirable we did not evaluate NC 2067/βCDgemini surfactants.

Table 13.7- Green fluorescence intensity detected in A375 melanoma cells stained with DCFH-DA after treatment with NC 2067 based formulations.

Relative fluorescence intensity	**untreated**	**5FU [10 μM]**	**H_2O_2 [100 μM]**	**NC 2067/ DMSO [0.5 μM]**	**NC 2067/ DMSO [1 μM]**	**NC 2067/ DMSO [5 μM]**
Flow cytometry	97.1	92.8	NA	137	86.7	132.1
Plate reader	354.9	NA	1525.4	375.8	317.8	305.2

Appendix 13.9- Evaluation of the caspase-dependent apoptosis in A375 cells treated with NC 2067 /βCDgemini surfactant-12 complex

We previously showed that NC 2067 dissolved in DMSO and in complexed with βCDgemini surfactant-12 were able to increase caspases -3 and -7 in A375 melanoma cells.[3] Here, our aim was to evaluate the effect of a general caspase inhibitor such as z-VAD-fmk on cell toxicity of NC 2067/βCDgemini surfactant complexes.

Material and Methods- Cells seeded in 96-well plates (1 x 10^4 cells/well) and after 24 h of incubation at 37°C in a humidified incubator with 5% CO_2, they were treated with NC 2067 dissolved in DMSO (1 μM) and melphalan (36 μM). After 24 hours of incubation, cells were treated with z-VAD-fmk (50 μM) and incubated at 37°C for 1 hour. This stage was performed by either spiking the media with higher concentration of z-VAD-fmk or removing the media and providing fresh media containing z-VAD-fmk (50 μM). Afterwards, fresh supplemented media containing a final concentration of 450 μg/mL 3-(4,5-dimethylthiazol-2-yl)-2,5-diphenyltetrazolium bromide (MTT, Invitrogen, Burlington, Canada) solution was added to each well and the plates were incubated for 2 h at 37 °C. Excess MTT solution was removed and the plates were dried. DMSO was added to each well and the plates were incubated for 10 min at 37 °C to dissolve the trapped formazan. Absorbance at 550 nm was recorded using a Synergy BioTek plate reader.

Results- The intrinsic toxicity of z-VAD-fmk at concentrations of 20-50 μM was evaluated. It was found that the %toxicity induced in A375 cells was less than 6% (data is not shown). Unfortunately, NC 2067 (1 μM) showed low toxicity at A375 cells in contrast to our previous findings and addition of z-VAD-fmk increased the toxicity. Moreover, the toxicity associated with melphalan did not change upon addition of z-VAD-fmk (Figure 13.9).

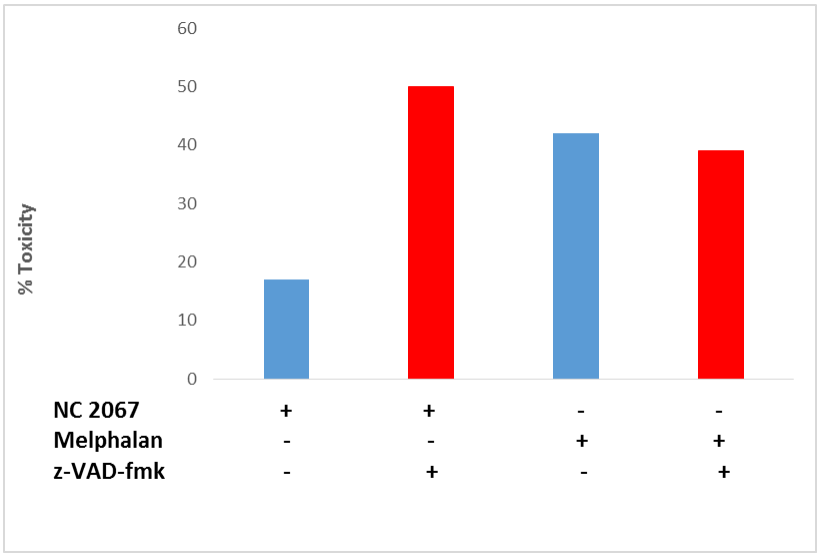

Figure 13.9- % toxicity of A375 melanoma cells treated with NC 2067 (1 μM) and Melphalan (36 μM) in presence and absence of z-VAD-fmk (50 μM).

14. REFERENCES

1. Weiss RB. Hypersensitivity reactions from taxol. Journal of Clinical Oncology 1990;8:1263-8.
2. Singh RSP, Das U, Dimmock JR, Alcorn J. A general HPLC-UV method for the quantitative determination of curcumin analogues containing the 1,5-diaryl-3-oxo-1,4-pentadienyl pharmacophore in rat biomatrices. Journal of Chromatography B: Analytical Technologies in the Biomedical and Life Sciences 2010;878:2796-802.
3. Michel D, Chitanda JM, Balogh R, et al. Design and evaluation of cyclodextrin-based delivery systems to incorporate poorly soluble curcumin analogs for the treatment of melanoma. European Journal of Pharmaceutics and Biopharmaceutics 2012;81:548-56.
4. Faraji AH, Wipf P. Nanoparticles in cellular drug delivery. Bioorganic and Medicinal Chemistry 2009;17:2950-62.
5. Lipinski CA, Lombardo F, Dominy BW, Feeney PJ. Experimental and computational approaches to estimate solubility and permeability in drug discovery and development settings. Advanced Drug Delivery Reviews 2000;46:3-26.
6. Choy YB, Prausnitz MR. The rule of five for non-oral routes of drug delivery: Ophthalmic, inhalation and transdermal. Pharmaceutical Research 2011;28:943-8.
7. Gelderblom H, Verweij J, Nooter K, Sparreboom A. Cremophor EL: The drawbacks and advantages of vehicle selection for drug formulation. European Journal of Cancer 2001;37:1590-8.
8. Steele RH, Limaye S, Cleland B, Chow J, Suranyi MG. Hypersensitivity reactions to the polysorbate contained in recombinant erythropoietin and darbepoietin. Nephrology 2005;10:317-20.
9. Karve S, Werner ME, Sukumar R, et al. Revival of the abandoned therapeutic wortmannin by nanoparticle drug delivery. Proceedings of the National Academy of Sciences of the United States of America 2012;109:8230-5.
10. Peer D, Karp JM, Hong S, Farokhzad OC, Margalit R, Langer R. Nanocarriers as an emerging platform for cancer therapy. Nature Nanotechnology 2007;2:751-60.
11. Venturoli D, Rippe B. Ficoll and dextran vs. globular proteins as probes for testing glomerular permselectivity: Effects of molecular size, shape, charge, and deformability. American Journal of Physiology - Renal Physiology 2005;288:F605-F13.
12. Moghimi SM, Hunter AC, Murray JC. Long-circulating and target-specific nanoparticles: Theory to practice. Pharmacological Reviews 2001;53:283-318.
13. Li SD, Huang L. Nanoparticles evading the reticuloendothelial system: Role of the supported bilayer. Biochimica et Biophysica Acta - Biomembranes 2009;1788:2259-66.
14. Hobbs SK, Monsky WL, Yuan F, et al. Regulation of transport pathways in tumor vessels: Role of tumor type and microenvironment. Proceedings of the National Academy of Sciences of the United States of America 1998;95:4607-12.
15. Maeda H, Wu J, Sawa T, Matsumura Y, Hori K. Tumor vascular permeability and the EPR effect in macromolecular therapeutics: A review. Journal of Controlled Release 2000;65:271-84.
16. Torchilin VP. Polymer-coated long-circulating microparticulate pharmaceuticals. Journal of Microencapsulation 1998;15:1-19.
17. Tan SJ, Jana NR, Gao S, Patra PK, Ying JY. Surface-ligand-dependent cellular interaction, subcellular localization, and cytotoxicity of polymer-coated quantum dots. Chemistry of Materials 2010;22:2239-47.
18. Gratton SEA, Ropp PA, Pohlhaus PD, et al. The effect of particle design on cellular internalization pathways. Proceedings of the National Academy of Sciences of the United States of America 2008;105:11613-8.

19. Rejman J, Oberle V, Zuhorn IS, Hoekstra D. Size-dependent internalization of particles via the pathways of clathrin-and caveolae-mediated endocytosis. Biochemical Journal 2004;377:159-69.
20. Desai MP, Labhasetwar V, Walter E, Levy RJ, Amidon GL. The mechanism of uptake of biodegradable microparticles in Caco-2 cells is size dependent. Pharmaceutical Research 1997;14:1568-73.
21. Chithrani BD, Ghazani AA, Chan WCW. Determining the size and shape dependence of gold nanoparticle uptake into mammalian cells. Nano Letters 2006;6:662-8.
22. Li Y, Wang J, Wientjes MG, Au JLS. Delivery of nanomedicines to extracellular and intracellular compartments of a solid tumor. Advanced Drug Delivery Reviews 2012;64:29-39.
23. Perumal OP, Inapagolla R, Kannan S, Kannan RM. The effect of surface functionality on cellular trafficking of dendrimers. Biomaterials 2008;29:3469-76.
24. Hu CMJ, Zhang L. Nanoparticle-based combination therapy toward overcoming drug resistance in cancer. Biochemical Pharmacology 2012;83:1104-11.
25. Batrakova EV, Li S, Elmquist WF, Miller DW, Alakhov VY, Kabanov AV. Mechanism of sensitization of MDR cancer cells by Pluronic block copolymers: Selective energy depletion. British Journal of Cancer 2001;85:1987-97.
26. Yamashiro DJ, Maxfield FR. Regulation of endocytic processes by pH. Trends in Pharmacological Sciences 1988;9:190-3.
27. Drummond DC, Zignani M, Leroux JC. Current status of pH-sensitive liposomes in drug delivery. Progress in Lipid Research 2000;39:409-60.
28. Marrache S, Dhar S. Engineering of blended nanoparticle platform for delivery of mitochondria-acting therapeutics. Proceedings of the National Academy of Sciences of the United States of America 2012;109:16288-93.
29. Tkachenko AG, Xie H, Coleman D, et al. Multifunctional gold nanoparticle-peptide complexes for nuclear targeting. Journal of the American Chemical Society 2003;125:4700-1.
30. Vasir JK, Labhasetwar V. Biodegradable nanoparticles for cytosolic delivery of therapeutics. Advanced Drug Delivery Reviews 2007;59:718-28.
31. Boddapati SV, D'Souza GGM, Erdogan S, Torchilin VP, Weissig V. Organelle-targeted nanocarriers: Specific delivery of liposomal ceramide to mitochondria enhances its cytotoxicity in vitro and in vivo. Nano Letters 2008;8:2559-63.
32. Patel NR, Hatziantoniou S, Georgopoulos A, et al. Mitochondria-targeted liposomes improve the apoptotic and cytotoxic action of sclareol. Journal of Liposome Research 2010;20:244-9.
33. Bangham AD, Standish MM, Watkins JC. Diffusion of univalent ions across the lamellae of swollen phospholipids. Journal of Molecular Biology 1965;13:238-52.
34. Radomska-Soukharev A. Stability of lipid excipients in solid lipid nanoparticles. Advanced Drug Delivery Reviews 2007;59:411-8.
35. Gin DL, Pecinovsky CS, Bara JE, Kerr RL. Functional lyotropic liquid crystal materials. Liquid Crystalline Functional Assemblies and Their Supramolecular Structures: Springer; 2008:181-222.
36. Lancelot A, Sierra T, Serrano JL. Nanostructured liquid-crystalline particles for drug delivery. Expert Opinion on Drug Delivery 2014;11:547-64.
37. Larsson K. Cubic lipid-water phases: Structures and biomembrane aspects. Journal of Physical Chemistry 1989;93:7304-14.
38. Shearman GC, Ces O, Templer RH, Seddon JM. Inverse lyotropic phases of lipids and membrane curvature. Journal of Physics Condensed Matter 2006;18:S1105-S24.
39. Fong C, Le T, Drummond CJ. Lyotropic liquid crystal engineering-ordered nanostructured small molecule amphiphile self-assembly materials by design. Chemical Society Reviews 2012;41:1297-322.

40. Boyd BJ, Whittaker DV, Khoo SM, Davey G. Hexosomes formed from glycerate surfactants-Formulation as a colloidal carrier for irinotecan. International Journal of Pharmaceutics 2006;318:154-62.
41. Zeng N, Gao X, Hu Q, et al. Lipid-based liquid crystalline nanoparticles as oral drug delivery vehicles for poorly water-soluble drugs: Cellular interaction and in vivo absorption. International Journal of Nanomedicine 2012;7:3703-18.
42. Géral C, Angelova A, Lesieur S. From molecular to nanotechnology strategies for delivery of neurotrophins: Emphasis on brain-derived neurotrophic factor (BDNF). Pharmaceutics 2013;5:127-67.
43. Houghton AN, Polsky D. Focus on melanoma. Cancer Cell 2002;2:275-8.
44. Bradish JR, Montironi R, Lopez-Beltran A, Post KM, MacLennan GT, Cheng L. Towards personalized therapy for patients with malignant melanoma: Molecular insights into the biology of BRAF mutations. Future Oncology 2013;9:245-53.
45. Huang S, DeGuzman A, Bucana CD, Fidler IJ. Nuclear factor-κB activity correlates with growth, angiogenesis, and metastasis of human melanoma cells in nude mice. Clinical Cancer Research 2000;6:2573-81.
46. Bradish JR, Cheng L. Molecular pathology of malignant melanoma: changing the clinical practice paradigm toward a personalized approach. Human Pathology 2014; 45(7): 1315-1326.
47. Su DM, Zhang Q, Wang X, et al. Two types of human malignant melanoma cell lines revealed by expression patterns of mitochondrial and survival-apoptosis genes: Implications for malignant melanoma therapy. Molecular Cancer Therapeutics 2009;8:1292-304.
48. La Porta CAM. Mechanism of drug sensitivity and resistance in melanoma. Current Cancer Drug Targets 2009;9:391-7.
49. Soengas MS, Lowe SW. Apoptosis and melanoma chemoresistance. Oncogene 2003;22:3138-51.
50. Tas F. Metastatic behavior in melanoma: Timing, pattern, survival, and influencing factors. Journal of Oncology 2012.
51. Balch CM, Gershenwald JE, Soong SJ, et al. Final version of 2009 AJCC melanoma staging and classification. Journal of Clinical Oncology 2009;27:6199-206.
52. Cohen LM. Lentigo maligna and lentigo maligna melanoma. Journal of the American Academy of Dermatology 1995;33:923-39.
53. Swetter SM, Boldrick JC, Jung SY, Egbert BM, Harvell JD. Increasing incidence of lentigo maligna melanoma subtypes: Northern California and national trends 1990-2000. Journal of Investigative Dermatology 2005;125:685-91.
54. Weinstock MA, Sober AJ. The risk of progression of lentigo maligna to lentigo maligna melanoma. British Journal of Dermatology 1987;116:303-10.
55. Rhodes AR. Melanocytic precursors of cutaneous melanoma. Estimated risks and guidelines for management. Medical Clinics of North America 1986;70:3-37.
56. Erickson C, Miller SJ. Treatment options in melanoma in situ: Topical and radiation therapy, excision and Mohs surgery. International Journal of Dermatology 2010;49:482-91.
57. Swetter SM, Chen FW, Kim DD, Egbert BM. Imiquimod 5% cream as primary or adjuvant therapy for melanoma in situ, lentigo maligna type. Journal of the American Academy of Dermatology 2015; 72(6): 1047-1053.
58. Wildemore Iv JK, Schuchter L, Mick R, et al. Locally recurrent malignant melanoma characteristics and outcomes: A single-institution study. Annals of Plastic Surgery 2001;46:488-94.
59. Lui P, Cashin R, Machado M, Hemels M, Corey-Lisle PK, Einarson TR. Treatments for metastatic melanoma: Synthesis of evidence from randomized trials. Cancer Treatment Reviews 2007;33:665-80.
60. Jacquillat C, Khayat D, Banzet P, et al. Final report of the French multicenter phase II study of the nitrosourea fotemustine in 153 evaluable patients with disseminated malignant melanoma including patients with cerebral metastases. Cancer 1990;66:1873-8.

61. Evans LM, Casper ES, Rosenbluth R. Phase II trial of carboplatin in advanced malignant melanoma. Cancer Treatment Reports 1987;71:171-2.
62. Eggermont AMM, Schadendorf D. Melanoma and Immunotherapy. Hematology/Oncology Clinics of North America 2009;23:547-64.
63. Doss LL, Memula N. The radioresponsiveness of melanoma. International Journal of Radiation Oncology Biology Physics 1982;8:1131-4.
64. Testori A, Rutkowski P, Marsden J, et al. Surgery and radiotherapy in the treatment of cutaneous melanoma. Annals of Oncology 2009;20:v22-v9.
65. Grimaldi AM, Cassidy PB, Leachmann S, Ascierto PA. Novel approaches in melanoma prevention and therapy. Cancer treatment and research 2014;159:443-55.
66. Flaherty KT, Puzanov I, Kim KB, et al. Inhibition of mutated, activated BRAF in metastatic melanoma. New England Journal of Medicine 2010;363:809-19.
67. Carvajal RD, Antonescu CR, Wolchok JD, et al. KIT as a therapeutic target in metastatic melanoma. JAMA - Journal of the American Medical Association 2011;305:2327-34.
68. McDermott D, Haanen J, Chen TT, Lorigan P, O'Day S. Efficacy and safety of ipilimumab in metastatic melanoma patients surviving more than 2 years following treatment in a phase III trial (MDX010-20). Annals of Oncology 2013;24:2694-8.
69. Ma C, Armstrong AW. Severe adverse events from the treatment of advanced melanoma: A systematic review of severe side effects associated with ipilimumab, vemurafenib, interferon alfa-2b, dacarbazine and interleukin-2. Journal of Dermatological Treatment 2014;25:401-8.
70. Nikolaou VA, Stratigos AJ, Flaherty KT, Tsao H. Melanoma: New insights and new therapies. Journal of Investigative Dermatology 2012;132:854-63.
71. Li L, Hou J, Liu X, et al. Nucleolin-targeting liposomes guided by aptamer AS1411 for the delivery of siRNA for the treatment of malignant melanomas. Biomaterials 2014;35:3840-50.
72. Paolino D, Cosco D, Muzzalupo R, Trapasso E, Picci N, Fresta M. Innovative bola-surfactant niosomes as topical delivery systems of 5-fluorouracil for the treatment of skin cancer. International Journal of Pharmaceutics 2008;353:233-42.
73. Chaudhuri P, Soni S, Sengupta S. Single-walled carbon nanotube-conjugated chemotherapy exhibits increased therapeutic index in melanoma. Nanotechnology 2010;21.
74. Schilrreff P, Mundiña-Weilenmann C, Romero EL, Morilla MJ. Selective cytotoxicity of PAMAM G5 core-PAMAM G2.5 shell tecto-dendrimers on melanoma cells. International Journal of Nanomedicine 2012;7:4121-33.
75. Pegoraro C, Cecchin D, Gracia LS, et al. Enhanced drug delivery to melanoma cells using PMPC-PDPA polymersomes. Cancer Letters 2013;334:328-37.
76. Müller RH, Radtke M, Wissing SA. Solid lipid nanoparticles (SLN) and nanostructured lipid carriers (NLC) in cosmetic and dermatological preparations. Advanced Drug Delivery Reviews 2002;54:S131-S55.
77. Souto EB, Almeida AJ, Müller RH. Lipid nanoparticles (SLN®, NLC®) for cutaneous drug delivery: Structure, protection and skin effects. Journal of Biomedical Nanotechnology 2007;3:317-31.
78. Hwang TL, Lee WR, Hua SC, Fang JY. Cisplatin encapsulated in phosphatidylethanolamine liposomes enhances the in vitro cytotoxicity and in vivo intratumor drug accumulation against melanomas. Journal of Dermatological Science 2007;46:11-20.
79. Mitrus I, Sochanik A, Cichoń T, Szala S. Combination of combretastatin A4 phosphate and doxorubicin-containing liposomes affects growth of B16-F10 tumors. Acta Biochimica Polonica 2009;56:161-5.
80. Shiraga E, Barichello JM, Ishida T, Kiwada H. A metronomic schedule of cyclophosphamide combined with PEGylated liposomal doxorubicin has a highly antitumor effect in an experimental pulmonary metastatic mouse model. International Journal of Pharmaceutics 2008;353:65-73.

81. Bedikian AY, Vardeleon A, Smith T, Campbell S, Namdari R. Pharmacokinetics and urinary excretion of vincristine sulfate liposomes injection in metastatic melanoma patients. Journal of Clinical Pharmacology 2006;46:727-37.
82. Ryuke Y, Mizuno M, Natsume A, et al. Growth inhibition of subcutaneous mouse melanoma and induction of natural killer cells by liposome-mediated interferon-β gene therapy. Melanoma Research 2003;13:349-56.
83. Villares GJ, Zigler M, Wang H, et al. Targeting melanoma growth and metastasis with systemic delivery of liposome-incorporated protease-activated receptor-1 small interfering RNA. Cancer Research 2008;68:9078-86.
84. Okumura K, Nakase M, Inui M, Nakamura S, Watanabe Y, Tagawa T. Bax mRNA therapy using cationic liposomes for human malignant melanoma. The journal of gene medicine 2008;10:910-7.
85. Mazzaglia A, Bondì ML, Scala A, et al. Supramolecular assemblies based on complexes of nonionic amphiphilic cyclodextrins and a meso-tetra(4-sulfonatophenyl)porphine tributyltin(IV) derivative: Potential nanotherapeutics against melanoma. Biomacromolecules 2013;14:3820-9.
86. Pizzimenti S, Ciamporcero E, Pettazzoni P, et al. The inclusion complex of 4-hydroxynonenal with a polymeric derivative of β-cyclodextrin enhances the antitumoral efficacy of the aldehyde in several tumor cell lines and in a three-dimensional human melanoma model. Free Radical Biology and Medicine 2013;65:765-77.
87. Yao H, Ng SS, Huo LF, et al. Effective melanoma immunotherapy with interleukin-2 delivered by a novel polymeric nanoparticle. Molecular Cancer Therapeutics 2011;10:1082-92.
88. Tuttle S, Hertan L, Katz JS. Indian gold treating cancer in the age of nano. Cancer Biology and Therapy 2011;11:474-6.
89. Ramachandran C, Rodriguez S, Ramachandran R, et al. Expression profiles of apoptotic genes induced by curcumin in human breast cancer and mammary epithelial cell lines. Anticancer Research 2005;25:3293-302.
90. Collett GP, Campbell FC. Curcumin induces c-jun N-terminal kinase-dependent apoptosis in HCT116 human colon cancer cells. Carcinogenesis 2004;25:2183-9.
91. Nagaraju GP, Zhu S, Wen J, et al. Novel synthetic curcumin analogues EF31 and UBS109 are potent DNA hypomethylating agents in pancreatic cancer. Cancer Letters 2013;341:195-203.
92. Duvoix A, Morceau F, Delhalle S, et al. Induction of apoptosis by curcumin: Mediation by glutathione S-transferase P1-1 inhibition. Biochemical Pharmacology 2003;66:1475-83.
93. Mangalathillam S, Rejinold NS, Nair A, Lakshmanan VK, Nair SV, Jayakumar R. Curcumin loaded chitin nanogels for skin cancer treatment via the transdermal route. Nanoscale 2012;4:239-50.
94. Yang K-Y, Lin L-C, Tseng T-Y, Wang S-C, Tsai T-H. Oral bioavailability of curcumin in rat and the herbal analysis from< i> Curcuma longa</i> by LC–MS/MS. Journal of Chromatography B 2007;853:183-9.
95. Lin YL, Liu YK, Tsai NM, et al. A Lipo-PEG-PEI complex for encapsulating curcumin that enhances its antitumor effects on curcumin-sensitive and curcumin-resistance cells. Nanomedicine: Nanotechnology, Biology, and Medicine 2012;8:318-27.
96. Kunwar A, Barik A, Pandey R, Priyadarsini KI. Transport of liposomal and albumin loaded curcumin to living cells: An absorption and fluorescence spectroscopic study. Biochimica et Biophysica Acta - General Subjects 2006;1760:1513-20.
97. Mulik RS, Mönkkönen J, Juvonen RO, Mahadik KR, Paradkar AR. Transferrin mediated solid lipid nanoparticles containing curcumin: Enhanced in vitro anticancer activity by induction of apoptosis. International Journal of Pharmaceutics 2010;398:190-203.
98. Chirio D, Gallarate M, Peira E, Battaglia L, Serpe L, Trotta M. Formulation of curcumin-loaded solid lipid nanoparticles produced by fatty acids coacervation technique. Journal of Microencapsulation 2011;28:537-48.

99. Ma Z, Haddadi A, Molavi O, Lavasanifar A, Lai R, Samuel J. Micelles of poly(ethylene oxide)-b-poly(ε-caprolactone) as vehicles for the solubilization, stabilization, and controlled delivery of curcumin. Journal of Biomedical Materials Research - Part A 2008;86:300-10.
100. Sun Y, Du L, Liu Y, et al. Transdermal delivery of the in situ hydrogels of curcumin and its inclusion complexes of hydroxypropyl-β-cyclodextrin for melanoma treatment. International Journal of Pharmaceutics 2014;469:31-9.
101. Yadav VR, Prasad S, Kannappan R, et al. Cyclodextrin-complexed curcumin exhibits anti-inflammatory and antiproliferative activities superior to those of curcumin through higher cellular uptake. Biochemical Pharmacology 2010;80:1021-32.
102. Yadav VR, Suresh S, Devi K, Yadav S. Effect of cyclodextrin complexation of curcumin on its solubility and antiangiogenic and anti-inflammatory activity in rat colitis model. AAPS PharmSciTech 2009;10:752-62.
103. Yallapu MM, Jaggi M, Chauhan SC. β-Cyclodextrin-curcumin self-assembly enhances curcumin delivery in prostate cancer cells. Colloids and Surfaces B: Biointerfaces 2010;79:113-25.
104. Yallapu MM, Jaggi M, Chauhan SC. Poly(β-cyclodextrin)/Curcumin Self-Assembly: A Novel Approach to Improve Curcumin Delivery and its Therapeutic Efficacy in Prostate Cancer Cells. Macromolecular Bioscience 2010;10:1141-51.
105. De Souza FF, Dos Santos MC, Dos Passos DCS, De Lima ECO, Guillo LA. Curcumin associated magnetite nanoparticles inhibit in vitro melanoma cell growth. Journal of Nanoscience and Nanotechnology 2011;11:7603-10.
106. Arezki A, Chabot GG, Quentin L, Scherman D, Jaouen G, Brulé E. Synthesis and biological evaluation of novel ferrocenyl curcuminoid derivatives. MedChemComm 2011;2:190-5.
107. Bill MA, Fuchs JR, Li C, et al. The small molecule curcumin analog FLLL32 induces apoptosis in melanoma cells via STAT3 inhibition and retains the cellular response to cytokines with anti-tumor activity. Molecular Cancer 2010;9:165.
108. Kudo C, Yamakoshi H, Sato A, et al. Synthesis of 86 species of 1,5-diaryl-3-oxo-1,4-pentadienes analogs of curcumin can yield a good lead in vivo. BMC Pharmacology 2011;11:4.
109. Pisano M, Pagnan G, Dettori MA, et al. Enhanced anti-tumor activity of a new curcumin-related compound against melanoma and neuroblastoma cells. Molecular Cancer 2010;9:137.
110. Faião-Flores F, Pardi PC, Santos RPd, Rando DG, Suárez JAPQ, Maria DA. Antiproliferative and antimetastatic activity of DM-1, sodium 4-[5-(4-hydroxy-3-methoxyphenyl)-3-oxo-penta-1, 4-dienyl]-2-methoxy-phenolate, in B16F10 melanoma. Appl cancer res 2008;28:72-9.
111. Das U, Alcorn J, Shrivastav A, et al. Design, synthesis and cytotoxic properties of novel 1-[4-(2-alkylaminoethoxy)phenylcarbonyl]-3,5-bis(arylidene)-4-piperidones and related compounds. European Journal of Medicinal Chemistry 2007;42:71-80.
112. Das U, Sharma RK, Dimmock JR. 1,5-Diaryl-3-oxo-1,4-pentadienes: A case for antineoplastics with multiple targets. Current Medicinal Chemistry 2009;16:2001-20.
113. Dimmock JR, Shyam K, Hamon NW. Evaluation of some Mannich bases derived from substituted acetophenones against P-388 lymphocytic leukemia and on respiration in isolated rat liver mitochondria. Journal of Pharmaceutical Sciences 1983;72:887-94.
114. Mutus B, Wagner JD, Talpas CJ, Dimmock JR, Phillips OA, Reid RS. 1-p-Chlorophenyl-4,4-dimethyl-5-diethylamino-1-penten-3-one hydrobromide, a sulfhydryl-specific compound which reacts irreversibly with protein thiols but reversibly with small molecular weight thiols. Analytical Biochemistry 1989;177:237-43.
115. Benvenuto JA, Connor TH, Monteith DK, et al. Degradation and inactivation of antitumor drugs. Journal of Pharmaceutical Sciences 1993;82:988-91.

116. Dimmock JR, Kandepu NM, Nazarali AJ, et al. Sequential cytotoxicity: A theory evaluated using novel 2-[4-(3-aryl-2-propenoyloxy)phenylmethylene]cyclohexanones and related compounds. Journal of Medicinal Chemistry 2000;43:3933-40.
117. Dimmock JR, Shyam K, Hamon NW. Bis-Mannich bases of styryl ketones as antileukemic agents. Neoplasma 1985;32:85-91.
118. Das U, Das S, Bandy B, Stables JP, Dimmock JR. N-Aroyl-3,5-bis(benzylidene)-4-piperidones: A novel class of antimycobacterial agents. Bioorganic and Medicinal Chemistry 2008;16:3602-7.
119. Das U, Sakagami H, Chu Q, Wang Q, kawase M, Selvakumar P, Sharma RK, Dimmock JR. 3,5-Bis(benzylidene)-1-[4-2-(morpholin-4-yl)ethoxyphenylcarbonyl]-4-piperidone hydrochloride: A lead tumor-specific cytotoxin which induces apoptosis and autophagy. Bioorganic and Medicinal Chemistry Letters 2010;20(3): 912-917.
120. U. D, J.R. D. In: Institute SR, ed. private communication ed2006.
121. Hashimoto H. Present status of industrial application of cyclodextrins in Japan. Journal of Inclusion Phenomena 2002;44:57-62.
122. Loftsson T, Duchêne D. Cyclodextrins and their pharmaceutical applications. International Journal of Pharmaceutics 2007;329:1-11.
123. Loftsson T, Brewster ME. Pharmaceutical applications of cyclodextrins. 1. Drug solubilization and stabilization. Journal of Pharmaceutical Sciences 1996;85:1017-25.
124. Saenger W, Jacob J, Gessler K, et al. Structures of the common cyclodextrins and their larger analogues - beyond the doughnut. Chemical Reviews 1998;98:1787-802.
125. Frömming KH, Szejtli J. Cyclodextrins in pharmacy: Kluwer Academic Pub; 1994.
126. Loftsson T, Brewster ME, Másson M. Role of cyclodextrins in improving oral drug delivery. American Journal of Drug Delivery 2004;2:261-75.
127. Szejtli J. Introduction and general overview of cyclodextrin chemistry. Chemical Reviews 1998;98:1743-53.
128. Ohtani Y, Irie T, Uekama K, Fukunaga K, Pitha J. Differential effects of α-, β- and γ-cyclodextrins on human erythrocytes. European Journal of Biochemistry 1989;186:17-22.
129. Irie T, Uekama K. Pharmaceutical applications of cyclodextrins. III. Toxicological issues and safety evaluation. Journal of Pharmaceutical Sciences 1997;86:147-62.
130. Kiss T, Fenyvesi F, Bácskay I, et al. Evaluation of the cytotoxicity of β-cyclodextrin derivatives: Evidence for the role of cholesterol extraction. European Journal of Pharmaceutical Sciences 2010;40:376-80.
131. Montassier P, Duchêne D, Poelman MC. Inclusion complexes of tretinoin with cyclodextrins. International Journal of Pharmaceutics 1997;153:199-209.
132. Ouyang HZ, Fang L, Zhu L, et al. Effect of external factors on the curcumin/2-hydroxypropyl-β-cyclodextrin: in vitro and in vivo study. Journal of Inclusion Phenomena and Macrocyclic Chemistry 2011:1-11.
133. Dandawate PR, Vyas A, Ahmad A, et al. Inclusion Complex of Novel Curcumin Analogue CDF and β-Cyclodextrin (1:2) and Its Enhanced In Vivo Anticancer Activity Against Pancreatic Cancer. Pharmaceutical Research 2012:1-12.
134. Motoyama K, Onodera R, Okamatsu A, et al. Potential use of the complex of doxorubicin with folate-conjugated methyl-β-cyclodextrin for tumor-selective cancer chemotherapy. Journal of drug targeting 2013:1-9.
135. Namgung R, Lee YM, Kim J, et al. Poly-cyclodextrin and poly-paclitaxel nano-assembly for anticancer therapy. Nature communications 2014;5.
136. Zhao M-X, Zhao M, Zeng E-Z, et al. Enhanced anti-cancer efficacy to cancer cells by doxorubicin loaded water-soluble amino acid-modified β-cyclodextrin platinum complexes. Journal of inorganic biochemistry 2014;137:31-9.

137. Chen J, Lu WL, Gu W, et al. Drug-in-cyclodextrin-in-liposomes: A promising delivery system for hydrophobic drugs. Expert Opinion on Drug Delivery 2014;11:565-77.
138. Jain SK, Gupta Y, Jain A, Amin S. Elastic liposomes bearing meloxicam-β-cyclodextrin for transdermal delivery. Current Drug Delivery 2008;5:207-14.
139. Piel G, Piette M, Barillaro V, Castagne D, Evrard B, Delattre L. Betamethasone-in-cyclodextrin-in-liposome: the effect of cyclodextrins on encapsulation efficiency and release kinetics. International journal of pharmaceutics 2006;312:75-82.
140. van de Manakker F, Vermonden T, van Nostrum CF, Hennink WE. Cyclodextrin-based polymeric materials: synthesis, properties, and pharmaceutical/biomedical applications. Biomacromolecules 2009;10:3157-75.
141. Cheng J, Khin KT, Jensen GS, Liu A, Davis ME. Synthesis of linear, β-cyclodextrin-based polymers and their camptothecin conjugates. Bioconjugate Chemistry 2003;14:1007-17.
142. Zhang J, Ellsworth K, Ma PX. Synthesis of β-cyclodextrin containing copolymer via "click" chemistry and its self-assembly in the presence of guest compounds. Macromolecular Rapid Communications 2012;33:664-71.
143. Sallas F, Darcy R. Amphiphilic cyclodextrins - Advances in synthesis and supramolecular chemistry. European Journal of Organic Chemistry 2008:957-69.
144. Memişoğlu E, Bochot A, Özalp M, Şen M, Duchêne D, Hincal AA. Direct formation of nanospheres from amphiphilic β-cyclodextrin inclusion complexes. Pharmaceutical Research 2003;20:117-25.
145. Choisnard L, Gèze A, Putaux JL, Wong YS, Wouessidjewe D. Nanoparticles of β-cyclodextrin esters obtained by self-assembling of biotransesterified β-cyclodextrins. Biomacromolecules 2006;7:515-20.
146. Yaméogo JBG, Gze A, Choisnard L, et al. Self-assembled biotransesterified cyclodextrins as Artemisinin nanocarriers - I: Formulation, lyoavailability and in vitro antimalarial activity assessment. European Journal of Pharmaceutics and Biopharmaceutics 2012;80:508-17.
147. Donohue R, Mazzaglia A, Ravoo BJ, Darcy R. Cationic β-cyclodextrin bilayer vesicles. Chemical Communications 2002:2864-5.
148. Srinivasachari S, Fichter KM, Reineke TM. Polycationic β-cyclodextrin "click clusters": Monodisperse and versatile scaffolds for nucleic acid delivery. Journal of the American Chemical Society 2008;130:4618-27.
149. Srinivasachari S, Reineke TM. Versatile supramolecular pDNA vehicles via "click polymerization" of β-cyclodextrin with oligoethyleneamines. Biomaterials 2009;30:928-38.
150. Saad M, Garbuzenko OB, Minko T. Co-delivery of siRNA and an anticancer drug for treatment of multidrug-resistant cancer. Nanomedicine 2008;3:761-76.
151. Wang Y, Gao S, Ye WH, Yoon HS, Yang YY. Co-delivery of drugs and DNA from cationic core-shell nanoparticles self-assembled from a biodegradable copolymer. Nature Materials 2006;5:791-6.
152. Zhang J, Sun H, Ma PX. Host-guest interaction mediated polymeric assemblies: Multifunctional nanoparticles for drug and gene delivery. ACS Nano 2010;4:1049-59.
153. Wettig SD, Verrall RE, Foldvari M. Gemini surfactants: A new family of building blocks for non-viral gene delivery systems. Current Gene Therapy 2008;8:9-23.
154. Yu D, Huang X, Deng M, et al. Effects of inorganic and organic salts on aggregation behavior of cationic gemini surfactants. Journal of Physical Chemistry B 2010;114:14955-64.
155. Rosenzweig HS, Rakhmanova VA, MacDonald RC. Diquaternary ammonium compounds as transfection agents. Bioconjugate Chemistry 2001;12:258-63.
156. Han Y, Wang Y. Aggregation behavior of gemini surfactants and their interaction with macromolecules in aqueous solution. Physical Chemistry Chemical Physics 2011;13:1939-56.

157. Wei XL, Wang XH, Sun DZ, et al. Phase and rheological behavior of a gemini cationic surfactant aqueous system. Soft Matter 2012;8:10115-22.
158. Hatakeyama ES, Wiesenauer BR, Gabriel CJ, Noble RD, Gin DL. Nanoporous, bicontinuous cubic lyotropic liquid crystal networks via polymerizable gemini ammonium surfactants. Chemistry of Materials 2010;22:4525-7.
159. Blackmore ES, Tiddy GJ. Phase behaviour and lyotropic liquid crystals in cationic surfactant–water systems. Journal of the Chemical Society, Faraday Transactions 2: Molecular and Chemical Physics 1988;84:1115-27.
160. Perez L, Torres JL, Manresa A, Solans C, Infante MR. Synthesis, aggregation, and biological properties of a new class of gemini cationic amphiphilic compounds from arginine, bis (Args). Langmuir 1996;12:5296-301.
161. Dreja M, Gramberg S, Tieke B. Cationic amphitropic gemini surfactants with hydrophilic oligo(oxyethylene) spacer chains. Chemical Communications 1998:1371-2.
162. Fuller S, Shinde NN, Tiddy GJT, Attard GS, Howell O. Thermotropic and lyotropic mesophase behavior of amphitropic diammonium surfactants. Langmuir 1996;12:1117-23.
163. Alami E, Levy H, Zana R, Skoulios A. Alkanediyl-. alpha.,. omega.-bis (dimethylalkylammonium bromide) surfactants. 2. Structure of the lyotropic mesophases in the presence of water. Langmuir 1993;9:940-4.
164. Bijma K, Rank E, Engberts JB. Effect of counterion structure on micellar growth of alkylpyridinium surfactants in aqueous solution. Journal of colloid and interface science 1998;205:245-56.
165. Singh J, Yang P, Michel D, Verrall RE, Foldvari M, Badea I. Amino acid-substituted gemini surfactant-based nanoparticles as safe and versatile gene delivery agents. Current Drug Delivery 2011;8:299-306.
166. Wettig SD, Badea I, Donkuru M, Verrall RE, Foldvari M. Structural and transfection properties of amine-substituted gemini surfactant-based nanoparticles. J Gene Med 2007;9:649-58.
167. Yang P, Singh J, Wettig S, Foldvari M, Verrall RE, Badea I. Enhanced gene expression in epithelial cells transfected with amino acid-substituted gemini nanoparticles. European Journal of Pharmaceutics and Biopharmaceutics 2010;75:311-20.
168. Donkuru M, Wettig SD, Verrall RE, Badea I, Foldvari M. Designing pH-sensitive gemini nanoparticles for non-viral gene delivery into keratinocytes. Journal of Materials Chemistry 2012;22:6232-44.
169. Badea I, Wettig S, Verrall R, Foldvari M. Topical non-invasive gene delivery using gemini nanoparticles in interferon-γ-deficient mice. European Journal of Pharmaceutics and Biopharmaceutics 2007;65:414-22.
170. Badea I, Virtanen C, Verrall RE, Rosenberg A, Foldvari M. Effect of topical interferon-γ gene therapy using gemini nanoparticles on pathophysiological markers of cutaneous scleroderma in Tsk/+ mice. Gene Therapy 2012; 19: 978-987.
171. Guerrero-Martínez A, Domínguez-Gutiérrez D, Palafox MA, Tardajos G. Studying the transfer process of a gemini surfactant from water to β-cyclodextrin at a molecular level. Chemical Physics Letters 2007;446:92-7.
172. Guerrero-Martínez A, Palafox MA, Tardajos G. Unexpected binding mode of gemini surfactants and γ-cyclodextrin: DOSY as a tool for the study of complexation. Chemical Physics Letters 2006;432:486-90.
173. Guerrero-Martínez A, González-Gaitano G, Viñas MH, Tardajos G. Inclusion complexes between β-cyclodextrin and a gemini surfactant in aqueous solution: An NMR study. Journal of Physical Chemistry B 2006;110:13819-28.

174. Nilsson M, Cabaleiro-Lago C, Valente AJM, Söderman O. Interactions between gemini surfactants, 12-s-12, and β-cyclodextrin as investigated by NMR diffusometry and electric conductometry. Langmuir 2006;22:8663-9.
175. Valente AJM, Söderman O. The formation of host-guest complexes between surfactants and cyclodextrins. Advances in Colloid and Interface Science 2013; 205: 156-176.
176. Leclercq L, Nardello-Rataj V, Rauwel G, Aubry JM. Structure-activity relationship of cyclodextrin/biocidal double-tailed ammonium surfactant host-guest complexes: Towards a delivery molecular mechanism? European Journal of Pharmaceutical Sciences 2010;41:265-75.
177. Carvalho RA, Correia HA, Valente AJM, Söderman O, Nilsson M. The effect of the head-group spacer length of 12-s-12 gemini surfactants in the host-guest association with β-cyclodextrin. Journal of Colloid and Interface Science 2011;354:725-32.
178. Faustino CMC, Calado ART, Garcia-Rio L. Interactions between β-cyclodextrin and an amino acid-based anionic gemini surfactant derived from cysteine. Journal of Colloid and Interface Science 2012;367:286-92.
179. Gao Y, Zhao X, Dong B, Zheng L, Li N, Zhang S. Inclusion complexes of β-cyclodextrin with ionic liquid surfactants. Journal of Physical Chemistry B 2006;110:8576-81.
180. Li S, Xing P, Hou Y, et al. Formation of a sheet-like hydrogel from vesicles via precipitates based on an ionic liquid-based surfactant and β-cyclodextrin. Journal of Molecular Liquids 2013;188:74-80.
181. Fernando Silva O, Fernández MA, Pennies SL, Gil RR, De Rossi RH. Synthesis and characterization of an amphiphilic cyclodextrin, a micelle with two recognition sites. Langmuir 2008;24:3718-26.
182. Rao L, Perez D, White E. Lamin proteolysis facilitates nuclear events during apoptosis. Journal of Cell Biology 1996;135:1441-55.
183. Kothakota S, Azuma T, Reinhard C, et al. Caspase-3-generated fragment of gelsolin: Effector of morphological change in apoptosis. Science 1997;278:294-8.
184. Zamzami N, Kroemer G. Condensed matter in cell death. Nature 1999;401:127-8.
185. Enari M, Sakahira H, Yokoyama H, Okawa K, Iwamatsu A, Nagata S. A caspase-activated DNase that degrades DNA during apoptosis, and its inhibitor ICAD. Nature 1998;391:43-50.
186. Fadok VA, Bratton DL, Frasch SC, Warner ML, Henson PM. The role of phosphatidylserine in recognition of apoptotic cells by phagocytes. Cell Death and Differentiation 1998;5:551-62.
187. Verhoven B, Schlegel RA, Williamson P. Mechanisms of phosphatidylserine exposure, a phagocyte recognition signal, on apoptotic T lymphocytes. Journal of Experimental Medicine 1995;182:1597-601.
188. Denecker G, Dooms H, Van Loo G, et al. Phosphatidyl serine exposure during apoptosis precedes release of cytochrome c and decrease in mitochondrial transmembrane potential. FEBS Letters 2000;465:47-52.
189. Vermes I, Haanen C, Steffens-Nakken H, Reutelingsperger C. A novel assay for apoptosis. Flow cytometric detection of phosphatidylserine expression on early apoptotic cells using fluorescein labelled Annexin V. Journal of Immunological Methods 1995;184:39-51.
190. Denecker G, Vercammen D, Declercq W, Vandenabeele P. Apoptotic and necrotic cell death induced by death domain receptors. Cellular and Molecular Life Sciences 2001;58:356-70.
191. Earnshaw WC, Martins LM, Kaufmann SH. Mammalian caspases: Structure, activation, substrates, and functions during apoptosis. 1999:383-424.
192. Kaufmann SH, Earnshaw WC. Induction of apoptosis by cancer chemotherapy. Experimental Cell Research 2000;256:42-9.
193. Klein S, McCormick F, Levitzki A. Killing time for cancer cells. Nature Reviews Cancer 2005;5:573-80.
194. Danial NN. BCL-2 family proteins: Critical checkpoints of apoptotic cell death. Clinical Cancer Research 2007;13:7254-63.

195. Debatin KM. Apoptosis pathways in cancer and cancer therapy. Cancer Immunology, Immunotherapy 2004;53:153-9.
196. Adrain C, Martin SJ. The mitochondrial apoptosome: A killer unleashed by the cytochrome seas. Trends in Biochemical Sciences 2001;26:390-7.
197. Weinberg F, Chandel NS. Mitochondrial metabolism and cancer. 2009:66-73.
198. Grek CL, Tew KD. Redox metabolism and malignancy. Current Opinion in Pharmacology 2010;10:362-8.
199. Ferri KF, Kroemer G. Mitochondria - The suicide organelles. BioEssays 2001;23:111-5.
200. Warburg O. On the origin of cancer cells. Science 1956;123:309-14.
201. Rigoulet M, Yoboue ED, Devin A. Mitochondrial ROS generation and its regulation: Mechanisms involved in H2O2 signaling. Antioxidants and Redox Signaling 2011;14:459-68.
202. Circu ML, Aw TY. Reactive oxygen species, cellular redox systems, and apoptosis. Free Radical Biology and Medicine 2010;48:749-62.
203. Slee EA, O'Connor DJ, Lu X. To die or not to die: How does p53 decide? Oncogene 2004;23:2809-18.
204. Teitz T, Lahti JM, Kidd VJ. Aggressive childhood neuroblastomas do not express caspase-8: An important component of programmed cell death. Journal of Molecular Medicine 2001;79:428-36.
205. Yang L, Cao Z, Yan H, Wood WC. Coexistence of High Levels of Apoptotic Signaling and Inhibitor of Apoptosis Proteins in Human Tumor Cells: Implication for Cancer Specific Therapy. Cancer Research 2003;63:6815-24.
206. Kroemer G, Galluzzi L, Brenner C. Mitochondrial membrane permeabilization in cell death. Physiological Reviews 2007;87:99-163.
207. Lim MLR, Lum MG, Hansen TM, Roucou X, Nagley P. On the release of cytochrome c from mitochondria during cell death signaling. Journal of Biomedical Science 2002;9:488-506.
208. Zorov DB, Filburn CR, Klotz LO, Zweier JL, Sollott SJ. Reactive oxygen species (ROS)-induced ROS release: A new phenomenon accompanying induction of the mitochondrial permeability transition in cardiac myocytes. Journal of Experimental Medicine 2000;192:1001-14.
209. Shen HM, Dong SY, Ong CN. Critical role of calcium overloading in cadmium-induced apoptosis in mouse thymocytes. Toxicology and Applied Pharmacology 2001;171:12-9.
210. Deniaud A, Sharaf El Dein O, Maillier E, et al. Endoplasmic reticulum stress induces calcium-dependent permeability transition, mitochondrial outer membrane permeabilization and apoptosis. Oncogene 2008;27:285-99.
211. Jiang MC, Yang-Yen HF, Yen JJY, Lin JK. Curcumin induces apoptosis in immortalized NIH 3T3 and malignant cancer cell lines. Nutrition and Cancer 1996;26:111-20.
212. Singh M, Singh N. Molecular mechanism of curcumin induced cytotoxicity in human cervical carcinoma cells. Molecular and Cellular Biochemistry 2009;325:107-19.
213. Guo LD, Chen XJ, Hu YH, Yu ZJ, Wang D, Liu JZ. Curcumin inhibits proliferation and induces apoptosis of human colorectal cancer cells by activating the mitochondria apoptotic pathway. Phytotherapy Research 2013;27:422-30.
214. Su CC, Lin JG, Li TM, et al. Curcumin-induced apoptosis of human colon cancer colo 205 cells through the production of ROS, Ca2+ and the activation of caspase-3. Anticancer Research 2006;26:4379-89.
215. Cao A, Li Q, Yin P, et al. Curcumin induces apoptosis in human gastric carcinoma AGS cells and colon carcinoma HT-29 cells through mitochondrial dysfunction and endoplasmic reticulum stress. Apoptosis 2013;18:1391-402.
216. Wang WH, Chiang IT, Ding K, et al. Curcumin-induced apoptosis in human hepatocellular carcinoma J5 cells: Critical role of Ca +2-dependent pathway. Evidence-based Complementary and Alternative Medicine 2012;2012.

217. Lin SS, Huang HP, Yang JS, et al. DNA damage and endoplasmic reticulum stress mediated curcumin-induced cell cycle arrest and apoptosis in human lung carcinoma A-549 cells through the activation caspases cascade- and mitochondrial-dependent pathway. Cancer Letters 2008;272:77-90.
218. Tan TW, Tsai HR, Lu HF, et al. Curcumin-induced cell cycle arrest and apoptosis in human acute promyelocytic leukemia HL-60 cells via MMP changes and caspase-3 activation. Anticancer Research 2006;26:4361-71.
219. Numsen Jr H. Mitochondrial reactive oxygen species affect sensitivity to curcumin-induced apoptosis. Free Radical Biology and Medicine 2008;44:1382-93.
220. Shankar S, Chen Q, Sarva K, Siddiqui I, Srivastava RK. Curcumin enhances the apoptosis-inducing potential of TRAIL in prostate cancer cells: Molecular mechanisms of apoptosis, migration and angiogenesis. Journal of Molecular Signaling 2007;2:10.
221. Basile V, Belluti S, Ferrari E, et al. bis-Dehydroxy-Curcumin Triggers Mitochondrial-Associated Cell Death in Human Colon Cancer Cells through ER-Stress Induced Autophagy. PLoS ONE 2013;8.
222. Li YB, Gao JL, Zhong ZF, Hoi PM, Lee SMY, Wang YT. Bisdemethoxycurcumin suppresses MCF-7 cells proliferation by inducing ROS accumulation and modulating senescence-related pathways. Pharmacological Reports 2013;65:700-9.
223. Peng YM, Zheng JB, Zhou YB, Li J. Characterization of a novel curcumin analog P1 as potent inhibitor of the NF-κB signaling pathway with distinct mechanisms. Acta Pharmacologica Sinica 2013;34:939-50.
224. Kasinski AL, Du Y, Thomas SL, et al. Inhibition of IκB kinase-nuclear factor-κB signaling pathway by 3,5-bis(2-flurobenzylidene)piperidin-4-one (EF24), a novel monoketone analog of curcumin? Molecular Pharmacology 2008;74:654-61.
225. Sato A, Kudo C, Yamakoshi H, et al. Curcumin analog GO-Y030 is a novel inhibitor of IKKβ that suppresses NF-κB signaling and induces apoptosis. Cancer Science 2011;102:1045-51.
226. Helal M, Das U, Bandy B, Islam A, Nazarali AJ, Dimmock JR. Mitochondrial dysfunction contributes to the cytotoxicity of some 3,5-bis(benzylidene)-4-piperidone derivatives in colon HCT-116 cells. Bioorganic and Medicinal Chemistry Letters 2013;23:1075-8.
227. Tan Q, Wu J, Li Y, Mei H, Zhao C, Zhang J. A supermolecular curcumin for enhanced antiproliferative and proapoptotic activities: Molecular characteristics, computer modeling and in vivo pharmacokinetics. Nanotechnology 2013;24.
228. Vandita K, Shashi B, Santosh KG, Pal KI. Enhanced apoptotic effect of curcumin loaded solid lipid nanoparticles. Molecular Pharmaceutics 2012;9:3411-21.
229. Qui S, Tan SS, Zhang JA, Liu A, Yuan JY, Rao GZ, Wang WY. Apoptosis induced by curcumin and its effect on c-myc and caspase-3 expressions in human melanoma A375 cell line. Academic journal of the first medical college of PLA 2005; 25(12): 1517-1521.
230. Bill MA, Bakan C, Benson Jr DM, Fuchs J, Young G, Lesinski GB. Curcumin induces proapoptotic effects against human melanoma cells and modulates the cellular response to immunotherapeutic cytokines. Molecular Cancer Therapeutics 2009;8:2726-35.
231. Bush JA, Cheung Jr KJJ, Li G. Curcumin induces apoptosis in human melanoma cells through a Fas receptor/caspase-8 pathway independent of p53. Experimental Cell Research 2001;271:305-14.
232. Carneiro MLB, Porfírio EP, Otake AH, Chammas R, Báo SN, Guillo LA. Morphological alterations and G0/G1 cell cycle arrest induced by curcumin in human SK-MEL-37 melanoma cells. Brazilian Archives of Biology and Technology 2010;53:343-52.
233. Karin M, Cao Y, Greten FR, Li ZW. NF-κB in cancer: From innocent bystander to major culprit. Nature Reviews Cancer 2002;2:301-10.
234. Marín YE, Wall BA, Wang S, et al. Curcumin downregulates the constitutive activity of NF-κB and induces apoptosis in novel mouse melanoma cells. Melanoma Research 2007;17:274-83.

235. Siwak DR, Shishodia S, Aggarwal BB, Kurzrock R. Curcumin-induced antiproliferative and proapoptotic effects in melanoma cells are associated with suppression of IκB kinase and nuclear factor κB activity and are independent of the B-Raf/mitogen-activated/ extracellular signal-regulated protein kinase pathway and the Akt pathway. Cancer 2005;104:879-90.
236. Zheng M, Ekmekcioglu S, Walch ET, Tang CH, Grimm EA. Inhibition of nuclear factor-κB and nitric oxide by curcumin induces G2/M cell cycle arrest and apoptosis in human melanoma cells. Melanoma Research 2004;14:165-71.
237. Bakhshi J, Weinstein L, Poksay KS, Nishinaga B, Bredesen DE, Rao RV. Coupling endoplasmic reticulum stress to the cell death program in mouse melanoma cells: Effect of curcumin. Apoptosis 2008;13:904-14.
238. Faião-Flores F, Suarez JAQ, Soto-Cerrato V, Espona-Fiedler M, Pérez-Tomás R, Maria DA. Bcl-2 family proteins and cytoskeleton changes involved in DM-1 cytotoxic effect on melanoma cells. Tumor Biology 2013;34:1235-43.
239. Yang CH, Yue J, Sims M, Pfeffer LM. The Curcumin Analog EF24 Targets NF-κB and miRNA-21, and Has Potent Anticancer Activity In Vitro and In Vivo. PLoS ONE 2013;8.
240. Morin D, Barthélémy S, Zini R, Labidalle S, Tillement JP. Curcumin induces the mitochondrial permeability transition pore mediated by membrane protein thiol oxidation. FEBS Letters 2001;495:131-6.
241. Ligeret H, Barthelemy S, Zini R, Tillement JP, Labidalle S, Morin D. Effects of curcumin and curcumin derivatives on mitochondrial permeability transition pore. Free Radical Biology and Medicine 2004;36:919-29.
242. Liu HS, Ke CS, Cheng HC, Huang CYF, Su CL. Curcumin-induced mitotic spindle defect and cell cycle arrest in human bladder cancer cells occurs partly through inhibition of aurora A. Molecular Pharmacology 2011;80:638-46.
243. Kang N, Wang MM, Wang YH, et al. Tetrahydrocurcumin induces G2/M cell cycle arrest and apoptosis involving p38 MAPK activation in human breast cancer cells. Food and Chemical Toxicology 2014;67:193-200.
244. Tima S, Ichikawa H, Ampasavate C, Okonogi S, Anuchapreeda S. Inhibitory effect of turmeric curcuminoids on FLT3 expression and cell cycle arrest in the FLT3-overexpressing EoL-1 leukemic cell line. Journal of Natural Products 2014;77:948-54.
245. Rozzo C, Fanciulli M, Fraumene C, et al. Molecular changes induced by the curcumin analogue D6 in human melanoma cells. Molecular Cancer 2013;12.
246. Liu L, Guo QX. The driving forces in the inclusion complexation of cyclodextrins. Journal of Inclusion Phenomena 2002;42:1-14.
247. Stella VJ, Rao VM, Zannou EA, Zia V. Mechanisms of drug release from cyclodextrin complexes. Advanced Drug Delivery Reviews 1999;36:3-16.
248. Corti G, Capasso G, Maestrelli F, Cirri M, Mura P. Physical-chemical characterization of binary systems of metformin hydrochloride with triacetyl-β-cyclodextrin. Journal of Pharmaceutical and Biomedical Analysis 2007;45:480-6.
249. Hirlekar R, Kadam V. Preformulation study of the inclusion complex irbesartan-β-cyclodextrin. AAPS PharmSciTech 2009;10:276-81.
250. Wang Jh, Cai Z. Investigation of inclusion complex of miconazole nitrate with β-cyclodextrin. Carbohydrate Polymers 2008;72:255-60.
251. Beijnen JH, Van Der Schoot SC, Nuijen B, et al. Complexation study of the anticancer agent EO-9 with 2-hydroxypropyl- β-cyclodextrin. Drug Development and Industrial Pharmacy 2008;34:1130-9.
252. Mangolim CS, Moriwaki C, Nogueira AC, et al. Curcumin-β-cyclodextrin inclusion complex: Stability, solubility, characterisation by FT-IR, FT-Raman, X-ray diffraction and photoacoustic spectroscopy, and food application. Food Chemistry 2014;153:361-70.

253. Giordano F, Novak C, Moyano JR. Thermal analysis of cyclodextrins and their inclusion compounds. Thermochimica Acta 2001;380:123-51.
254. Garnero C, Aiassa V, Longhi M. Sulfamethoxazole: Hydroxypropyl-β-cyclodextrin complex: Preparation and characterization. Journal of Pharmaceutical and Biomedical Analysis 2012;63:74-9.
255. Berbicz F, Nogueira AC, Neto AM, Natali MRM, Baesso ML, Matioli G. Use of photoacoustic spectroscopy in the characterization of inclusion complexes of benzophenone-3-hydroxypropyl-β-cyclodextrin and ex vivo evaluation of the percutaneous penetration of sunscreen. European Journal of Pharmaceutics and Biopharmaceutics 2011;79:449-57.
256. Takahashi AI, Veiga FJB, Ferraz HG. A literature review of cyclodextrin inclusion complexes characterization - Part III: Differential scanning calorimetry and thermogravimetry. International Journal of Pharmaceutical Sciences Review and Research 2012;12:16-20.
257. Li N, Zhang YH, Wu YN, Xiong XL. Inclusion complex of trimethoprim with β-cyclodextrin. Journal of Pharmaceutical and Biomedical Analysis 2005;39:824-9.
258. Trotta F, Zanetti M, Camino G. Thermal degradation of cyclodextrins. Polymer Degradation and Stability 2000;69:373-9.
259. de Araújo MVG, Vieira EKB, Lázaro GS, et al. Inclusion complexes of pyrimethamine in 2-hydroxypropyl-β-cyclodextrin: Characterization, phase solubility and molecular modelling. Bioorganic and Medicinal Chemistry 2007;15:5752-9.
260. Ammar HO, Salama HA, Ghorab M, Mahmoud AA. Formulation and biological evaluation of glimepiride-cyclodextrin-polymer systems. International Journal of Pharmaceutics 2006;309:129-38.
261. Xiang TX, Anderson BD. Inclusion complexes of purine nucleosides with cyclodextrins. II. Investigation of inclusion complex geometry and cavity microenvironment. International Journal of Pharmaceutics 1990;59:45-55.
262. Chow DD, Karara AH. Characterization, dissolution and bioavailability in rats of ibuprofen-β-cyclodextrin complex system. International Journal of Pharmaceutics 1986;28:95-101.
263. Uekama K, Narisawa S, Hirayama F, Otagiri M. Improvement of dissolution and absorption characteristics of benzodiazepines by cyclodextrin complexation. International Journal of Pharmaceutics 1983;16:327-38.
264. Higuchi T, Connors KA. Phase-solubility techniques. Adv Anal Chem Instrum 1965;4:117-212.
265. Takahashi AI, Veiga FJB, Ferraz HG. Literature review of cyclodextrins inclusion complexes characterization - Part I: Phase solubility diagram, dissolution and scanning electron microscopy. International Journal of Pharmaceutical Sciences Review and Research 2012;12:1-6.
266. Sathigari S, Chadha G, Lee YHP, et al. Physicochemical characterization of efavirenz-cyclodextrin inclusion complexes. AAPS PharmSciTech 2009;10:81-7.
267. Omar L, El-Barghouthi MI, Masoud NA, et al. Inclusion complexation of loratadine with natural and modified cyclodextrins: Phase solubility and thermodynamic studies. Journal of Solution Chemistry 2007;36:605-16.
268. Eid EEM, Abdul AB, Suliman FEO, Sukari MA, Rasedee A, Fatah SS. Characterization of the inclusion complex of zerumbone with hydroxypropyl-β-cyclodextrin. Carbohydrate Polymers 2011;83:1707-14.
269. Carrier RL, Miller LA, Ahmed I. The utility of cyclodextrins for enhancing oral bioavailability. Journal of Controlled Release 2007;123:78-99.
270. Ficarra R, Ficarra P, Di Bella MR, et al. Study of β-blockers/β-cyclodextrins inclusion complex by NMR, DSC, X-ray and SEM investigation. Journal of Pharmaceutical and Biomedical Analysis 2000;23:33-40.
271. Sinha VR, Anitha R, Ghosh S, Nanda A, Kumria R. Complexation of celecoxib with β-cyclodextrin: Characterization of the interaction in solution and in solid state. Journal of Pharmaceutical Sciences 2005;94:676-87.

272. Upadhyay SK, Ali SM. Solution structure of loperamide and β-cyclodextrin inclusion complexes using NMR spectroscopy. Journal of Chemical Sciences 2009;121:521-7.
273. Upadhyay SK, Kumar G. NMR and molecular modelling studies on the interaction of fluconazole with β-cyclodextrin. Chemistry Central Journal 2009;3.
274. Floare CG, Pirnau A, Bogdan M. 1H NMR spectroscopic characterization of inclusion complexes of tolfenamic and flufenamic acids with β-cyclodextrin. Journal of Molecular Structure 2013;1044:72-8.
275. Marques HMC, Hadgraft J, Kellaway IW, Pugh WJ. Studies of cyclodextrin inclusion complexes. II. Molecular modelling and 1H-NMR evidence for the salbutamol-β-cyclodextrin complex. International Journal of Pharmaceutics 1990;63:267-74.
276. Sambasevam KP, Mohamad S, Sarih NM, Ismail NA. Synthesis and characterization of the inclusion complex of β-cyclodextrin and azomethine. International Journal of Molecular Sciences 2013;14:3671-82.
277. Connors KA. The stability of cyclodextrin complexes in solution. Chemical Reviews 1997;97:1325-57.
278. Franco C, Schwingel L, Lula I, Sinisterra RD, Koester LS, Bassani VL. Studies on coumestrol/β-cyclodextrin association: Inclusion complex characterization. International Journal of Pharmaceutics 2009;369:5-11.
279. Qiu N, Cheng X, Wang G, et al. Inclusion complex of barbigerone with hydroxypropyl-β-cyclodextrin: Preparation and in vitro evaluation. Carbohydrate Polymers 2013;101:623-30.
280. Figueiras A, Sarraguça JMG, Carvalho RA, Pais AACC, Veiga FJB. Interaction of omeprazole with a methylated derivative of β-cyclodextrin: Phase solubility, NMR spectroscopy and molecular simulation. Pharmaceutical Research 2007;24:377-89.
281. Uekama K, Fujinaga T, Hirayama F. Improvement of the oral bioavailability of digitalis glycosides by cyclodextrin complexation. Journal of Pharmaceutical Sciences 1983;72:1338-41.
282. Job P. Spectrographic study of the formation of complexes in solution and their stability. Compt rend 1925;180:928-30.
283. Hirose K. A practical guide for the determination of binding constants. Journal of Inclusion Phenomena 2001;39:193-209.
284. Schneider H-J, Yatsimirsky AK. Principles and methods in supramolecular chemistry. 2000.
285. Calderini A, Pessine FBT. Synthesis and characterization of inclusion complex of the vasodilator drug minoxidil with β-cyclodextrin. Journal of Inclusion Phenomena and Macrocyclic Chemistry 2008;60:369-77.
286. Mieusset JL, Thiel B, Abraham M, Pačar M, Brinker UH. Decomposition of an oxodiazirine: Free versus incarcerated within the cavities of two α-cyclodextrins. Tetrahedron Letters 2013;54:681-3.
287. Benesi HA, Hildebrand JH. A spectrophotometric investigation of the interaction of iodine with aromatic hydrocarbons. Journal of the American Chemical Society 1949;71:2703-7.
288. Scott RL. Some comments on the Benesi-Hildebrand equation. Recueil des Travaux Chimiques des Pays-Bas 1956;75:787-9.
289. Neuhaus D. Nuclear overhauser effect. Encyclopedia of Magnetic Resonance 2000.
290. Bax A, Davis DG. MLEV-17-based two-dimensional homonuclear magnetization transfer spectroscopy. Journal of Magnetic Resonance (1969) 1985;65:355-60.
291. Yang LJ, Yang B, Chen W, Huang R, Yan SJ, Lin J. Host-guest system of nimbin and β-cyclodextrin or its derivatives: Preparation, characterization, inclusion mode, and solubilization. Journal of Agricultural and Food Chemistry 2010;58:8545-52.
292. Akita T, Matsui Y, Yamamoto T. A 1H NMR titration study on the binding constants for D- and l-tryptophan inclusion complexes with 6-O-α-D-glucosyl-β- cyclodextrin. Formation of 1:1 and 2:1 (host:guest) complexes. Journal of Molecular Structure 2014;1060:138-41.

293. Jug M, Mennini N, Kövér KE, Mura P. Comparative analysis of binary and ternary cyclodextrin complexes with econazole nitrate in solution and in solid state. Journal of Pharmaceutical and Biomedical Analysis 2014;91:81-91.
294. Snell G. X-Ray Sources and High-Throughput Data Collection Methods. Methods in molecular biology (Clifton, NJ) 2012;841:93.
295. Schwinger J. On the classical radiation of accelerated electrons. Physical Review 1949;75:1912-25.
296. Grochulski P, Fodje MN, George G. Status and vision for Structural Biology at the Canadian Light Source. Acta Physica Polonica A 2012;121:866-70.
297. Zubavichus YV, Slovokhotov YL. X-ray synchrotron radiation in physicochemical studies. Russian Chemical Reviews 2001;70:373-403.
298. Dong YD, Boyd BJ. Applications of X-ray scattering in pharmaceutical science. International Journal of Pharmaceutics 2011;417:101-11.
299. Lewis R. Medical applications of synchrotron radiation x-rays. Physics in Medicine and Biology 1997;42:1213-43.
300. Dauter Z, Jaskolski M, Wlodawer A. Impact of synchrotron radiation on macromolecular crystallography: A personal view. Journal of Synchrotron Radiation 2010;17:433-44.
301. Blundell TL, Patel S. High-throughput X-ray crystallography for drug discovery. Current Opinion in Pharmacology 2004;4(5):490-496.
302. Bragg WL. The diffraction of short electromagnetic waves by a crystal. 1913. p. 43-57.
303. Toma AC, Pfohl T. Small-Angle X-ray Scattering (SAXS) and Wide-Angle X-ray Scattering (WAXS) of Supramolecular Assemblies. Supramolecular Chemistry: From Molecules to Nanomaterials 2012.
304. Ezquerra TA, Nogales A, Gomez M. Applications of synchrotron light to scattering and diffraction in materials and life sciences: Springer Science & Business Media; 2009.
305. Rhodes G, Cooper JB. Crystallography Made Crystal Clear. Trends in Biotechnology 1994;12:142-.
306. Helliwell JR. Macromolecular crystallography with synchrotron radiation: Cambridge Univ Pr; 2005.
307. Saenger W, Steiner T. Cyclodextrin Inclusion Complexes: Host-Guest Interactions and Hydrogen-Bonding Networks. Acta Crystallographica Section A: Foundations of Crystallography 1998;54:798-805.
308. Zabel V, Saenger W, Mason SA. Neutron diffraction study of the hydrogen bonding in β-cyclodextrin undecahydrate at 120 K: From dynamic flip-flops to static homodromic chains. Journal of the American Chemical Society 1986;108:3664-73.
309. Ceborska M, Asztemborska M, Lipkowski J. Rare 'head-to-tail' arrangement of guest molecules in the inclusion complexes of (+)- and (-)-menthol with β-cyclodextrin. Chemical Physics Letters 2012;553:64-7.
310. Rietveld HM. Rietveld method - a historical perspective. Australian Journal of Physics 1988;41:113-6.
311. Cirri M, Righi MF, Maestrelli F, Mura P, Valleri M. Development of glyburide fast-dissolving tablets based on the combined use of cyclodextrins and polymers. Drug Development and Industrial Pharmacy 2009;35:73-82.
312. Zoppi A, Garnero C, Linck YG, Chattah AK, Monti GA, Longhi MR. Enalapril:β-CD complex: Stability enhancement in solid state. Carbohydrate Polymers 2011;86:716-21.
313. Zhu XL, Wang HB, Chen Q, Yang WC, Yang GF. Preparation and characterization of inclusion complex of iprodione and β-cyclodextrin to improve fungicidal activity. Journal of Agricultural and Food Chemistry 2007;55:3535-9.
314. Hussein K, Türk M, Wahl MA. Comparative evaluation of ibuprofen/β-cyclodextrin complexes obtained by supercritical carbon dioxide and other conventional methods. Pharmaceutical Research 2007;24:585-92.

315. Rietveld H. Line profiles of neutron powder-diffraction peaks for structure refinement. Acta Crystallographica 1967;22:151-2.
316. Rietveld HM. A profile refinement method for nuclear and magnetic structures. Journal of Applied Crystallography 1969;2:65-71.
317. Pecharsky VK, Zavalij PY. Fundamentals of powder diffraction and structural characterization of materials: Springer Verlag; 2009.
318. Rácz CP, Borodi G, Pop MM, Kacso I, Sánta S, Tomoaia-Cotisel M. Structure of the inclusion complex of B-cyclodextrin with lipoic acid from laboratory powder diffraction data. Acta Crystallographica Section B: Structural Science 2012;68:164-70.
319. Borodi G, Bratu I, Dragan F, Peschar R, Helmholdt RB, Hernanz A. Spectroscopic investigations and crystal structure from synchrotron powder data of the inclusion complex of β-cyclodextrin with atenolol. Spectrochimica Acta - Part A: Molecular and Biomolecular Spectroscopy 2008;70:1041-8.
320. Pop MM, Goubitz K, Borodi G, et al. Crystal structure of the inclusion complex of β-cyclodextrin with mefenamic acid from high-resolution synchrotron powder-diffraction data in combination with molecular-mechanics calculations. Acta Crystallographica Section B: Structural Science 2002;58:1036-43.
321. Svergun DI, Shtykova EV, Volkov VV, Feigin LA. Small-angle X-ray scattering, synchrotron radiation, and the structure of bio- and nanosystems. Crystallography Reports 2011;56:725-50.
322. Koch M. SAXS Instrumentation for Synchrotron Radiation then and now. 2010: IOP Publishing. p. 012001.
323. Stuhrmann HB. Anomalous small angle scattering. Quarterly Reviews of Biophysics 1981;14:433-60.
324. Guinier A. Heterogeneities in solid solutions. Solid State Physics 1959;9:293-398.
325. Porod G. Die Röntgenkleinwinkelstreuung von dichtgepackten kolloiden Systemen. Colloid & Polymer Science 1951;124:83-114.
326. Hyde ST. Identification of lyotropic liquid crystalline mesophases. Handbook of applied surface and colloid chemistry 2001:299-332.
327. Berni MG, Lawrence CJ, Machin D. A review of the rheology of the lamellar phase in surfactant systems. Advances in Colloid and Interface Science 2002;98:217-43.
328. Koltover I, Salditt T, Rädler JO, Safinya CR. An inverted hexagonal phase of cationic liposome-DNA complexes related to DNA release and delivery. Science 1998;281:78-81.
329. Bender J, Ericson MB, Merclin N, et al. Lipid cubic phases for improved topical drug delivery in photodynamic therapy. Journal of Controlled Release 2005;106:350-60.
330. Lopes LB, Ferreira DA, De Paula D, et al. Reverse hexagonal phase nanodispersion of monoolein and oleic acid for topical delivery of peptides: in vitro and in vivo skin penetration of cyclosporin A. Pharmaceutical Research 2006;23:1332-42.
331. Hirlekar R, Jain S, Patel M, Garse H, Kadam V. Hexosomes: A novel drug delivery system. Current Drug Delivery 2010;7:28-35.
332. Cohen-Avrahami M, Libster D, Aserin A, Garti N. Penetratin-induced transdermal delivery from H II mesophases of sodium diclofenac. Journal of Controlled Release 2012;159:419-28.
333. Costa-Balogh FO, Sparr E, Sousa JJS, Pais AC. Drug release from lipid liquid crystalline phases: Relation with phase behavior. Drug Development and Industrial Pharmacy 2010;36:470-81.
334. Le TC, Mulet X, Burden FR, Winkler DA. Predicting the complex phase behavior of self-assembling drug delivery nanoparticles. Molecular Pharmaceutics 2013;10:1368-77.
335. Tilley AJ, Dong YD, Chong JYT, et al. Transfer of lipid between triglyceride dispersions and lyotropic liquid crystal nanostructured particles using time-resolved SAXS. Soft Matter 2012;8:5696-708.
336. Angelov B, Angelova A, Vainio U, et al. Long-living intermediates during a lamellar to a diamond-cubic lipid phase transition: A small-angle X-ray scattering investigation. Langmuir 2009;25:3734-42.

337. Lukowski G, Kasbohm J, Pflegel P, Illing A, Wulff H. Crystallographic investigation of cetylpalmitate solid lipid nanoparticles. International Journal of Pharmaceutics 2000;196:201-5.
338. Schütze W, Müller-Goymann CC. Phase transformation of a liposomal dispersion into a micellar solution induced by drug-loading. Pharmaceutical Research 1998;15:538-43.
339. Guo X, Huang L. Recent advances in nonviral vectors for gene delivery. Accounts of Chemical Research 2012;45:971-9.
340. Ewert KK, Evans HM, Zidovska A, Bouxsein NF, Ahmad A, Safinya CR. A columnar phase of dendritic lipid-based cationic liposome-DNA complexes for gene delivery: Hexagonally ordered cylindrical micelles embedded in a DNA honeycomb lattice. Journal of the American Chemical Society 2006;128:3998-4006.
341. Bouxsein NF, McAllister CS, Ewert KK, Samuel CE, Safinya CR. Structure and gene silencing activities of monovalent and pentavalent cationic lipid vectors complexed with siRNA. Biochemistry 2007;46:4785-92.
342. Bell PC, Bergsma M, Dolbnya IP, et al. Transfection mediated by gemini surfactants: Engineered escape from the endosomal compartment. Journal of the American Chemical Society 2003;125:1551-8.
343. Pullmannová P, Bastos M, Bai G, et al. The ionic strength effect on the DNA complexation by DOPC-gemini surfactants liposomes. Biophysical Chemistry 2012;160:35-45.
344. Falsini S, Ristori S, Ciani L, et al. Time resolved SAXS to study the complexation of siRNA with cationic micelles of divalent surfactants. Soft Matter 2014;10:2226-33.
345. Wang H, Kaur T, Tavakoli N, Joseph J, Wettig S. Transfection and structural properties of phytanyl substituted gemini surfactant-based vectors for gene delivery. Physical Chemistry Chemical Physics 2013;15:20510-6.
346. Wei X, Fu S, Yin B, et al. Phase behaviors of Gemini cationic surfactants/n-butanol/water systems. Fluid Phase Equilibria 2010;287:146-50.
347. Perroni DV, Mahanthappa MK. Inverse Pm3n cubic micellar lyotropic phases from zwitterionic triazolium gemini surfactants. Soft Matter 2013;9:7919-22.
348. Parkin J, Shea C, Sant GR. Intravesical dimethyl sulfoxide (DMSO) for interstitial cystitis - A practical approach. Urology 1997;49:105-7.
349. Bisht S, Feldmann G, Soni S, Ravi R, Karikar C, Maitra A. Polymeric nanoparticle-encapsulated curcumin ("nanocurcumin"): A novel strategy for human cancer therapy. Journal of Nanobiotechnology 2007;5.
350. Nagaraju GP, Aliya S, Zafar SF, Basha R, Diaz R, El-Rayes BF. The impact of curcumin on breast cancer. Integrative Biology (United Kingdom) 2012;4:996-1007.
351. Kakkar V, Singh S, Singla D, Kaur IP. Exploring solid lipid nanoparticles to enhance the oral bioavailability of curcumin. Molecular Nutrition and Food Research 2011;55:495-503.
352. Tsai YM, Chien CF, Lin LC, Tsai TH. Curcumin and its nano-formulation: The kinetics of tissue distribution and blood-brain barrier penetration. International Journal of Pharmaceutics 2011;416:331-8.
353. Seeta Rama Raju G, Pavitra E, Purnachandra Nagaraju G, Ramesh K, El-Rayes BF, Yu JS. Imaging and curcumin delivery in pancreatic cancer cell lines using PEGylated α-Gd2(MoO4)3 mesoporous particles. Dalton Transactions 2014;43:3330-8.
354. Kazemi-Lomedasht F, Rami A, Zarghami N. Comparison of inhibitory effect of curcumin nanoparticles and free curcumin in human telomerase reverse transcriptase gene expression in breast cancer. Advanced Pharmaceutical Bulletin 2013;3:127-30.
355. Baglole KN, Boland PG, Wagner BD. Fluorescence enhancement of curcumin upon inclusion into parent and modified cyclodextrins. Journal of Photochemistry and Photobiology A: Chemistry 2005;173:230-7.

356. Tang B, Ma L, Wang HY, Zhang GY. Study on the supramolecular interaction of curcumin and α-cyclodextrin by spectrophotometry and its analytical application. Journal of Agricultural and Food Chemistry 2002;50:1355-61.
357. Rachmawati H, Edityaningrum CA, Mauludin R. Molecular Inclusion Complex of Curcumin-β-Cyclodextrin Nanoparticle to Enhance Curcumin Skin Permeability from Hydrophilic Matrix Gel. AAPS PharmSciTech 2013:1-10.
358. Fodje M, Grochulski P, Janzen K, Labiuk S, Gorin J, Berg R. 08B1-1: An automated beamline for macromolecular crystallography experiments at the Canadian Light Source. Journal of Synchrotron Radiation 2014;21:633-7.
359. Hammersley A. FIT2D: An introduction and overview. European Synchrotron Radiation Facility Internal Report ESRF97HA02T 1997.
360. Song LX, Guo XQ, Du FY, Bai L. Thermal degradation comparison of polypropylene glycol and its complex with β-cyclodextrin. Polymer Degradation and Stability 2010;95:508-15.
361. Benk M, Király Z. Thermodynamics of inclusion complex formation of β-cyclodextrin with a variety of surfactants differing in the nature of headgroup. Journal of Chemical Thermodynamics 2012;54:211-6.
362. Qiu XM, Sun DZ, Wei XL, Yin BL. Thermodynamic study of the inclusion interaction between Gemini surfactants and cyclodextrins by isothermal titration microcalorimetry. Journal of Solution Chemistry 2007;36:303-12.
363. Constantinides PP, Wasan KM. Lipid formulation strategies for enhancing intestinal transport and absorption of P-glycoprotein (P-gp) substrate drugs: In vitro/in vivo case studies. Journal of Pharmaceutical Sciences 2007;96:235-48.
364. Alami E, Abrahmsén-Alami S, Eastoe J, Grillo I, Heenan RK. Interactions between a nonionic gemini surfactant and cyclodextrins investigated by small-angle neutron scattering. Journal of Colloid and Interface Science 2002;255:403-9.
365. Zhang HX, Liu Y. Protein-binding properties of a designed steroidal lactam compound. Steroids 2014;80:30-6.
366. Das S, Das U, Michel D, Gorecki DKJ, Dimmock JR. Novel 3,5-bis(arylidene)-4-piperidone dimers: Potent cytotoxins against colon cancer cells. European Journal of Medicinal Chemistry 2013;64:321-8.
367. Silva SMC, Sousa JJS, Marques EF, Pais AACC, Michniak-Kohn BB. Structure Activity Relationships in Alkylammonium C12-Gemini Surfactants Used as Dermal Permeation Enhancers. BMC Biology 2013:1-9.
368. Bender ML, Komiyama M. Cyclodextrin chemistry: Springer-Verlag Berlin; 1978.
369. Crini G. Review: A history of cyclodextrins. Chemical Reviews 2014;114:10940-75.
370. Agashe H, Lagisetty P, Sahoo K, Bourne D, Grady B, Awasthi V. Liposome-encapsulated EF24-HPβCD inclusion complex: A preformulation study and biodistribution in a rat model. Journal of Nanoparticle Research 2011;13:2609-23.
371. Patro NM, Sultana A, Terao K, et al. Comparison and correlation of in vitro, in vivo and in silico evaluations of alpha, beta and gamma cyclodextrin complexes of curcumin. Journal of Inclusion Phenomena and Macrocyclic Chemistry 2014;78:471-83.
372. Jahed V, Zarrabi A, Bordbar AK, Hafezi MS. NMR (1H, ROESY) spectroscopic and molecular modelling investigations of supramolecular complex of β-cyclodextrin and curcumin. Food Chemistry 2014;165:241-6.
373. Ma M, Sun T, Xing P, et al. A supramolecular curcumin vesicle and its application in controlling curcumin release. Colloids and Surfaces A: Physicochemical and Engineering Aspects 2014;459:157-65.
374. Poorghorban M, Das U, Alaidi O, et al. Characterization of the host–guest complex of a curcumin analog with β-cyclodextrin and β-cyclodextrin–gemini surfactant and evaluation of its anticancer activity. International Journal of Nanomedicine 2015;10:503-15.

375. Bax A, Davis DG. Practical aspects of two-dimensional transverse NOE spectroscopy. Journal of Magnetic Resonance (1969) 1985;63:207-13.
376. Yang LJ, Ma SX, Zhou SY, et al. Preparation and characterization of inclusion complexes of naringenin with β-cyclodextrin or its derivative. Carbohydrate Polymers 2013;98:861-9.
377. Gil VMS, Oliveira NC. On the use of the method of continuous variations. Journal of Chemical Education 1990;67:473-8.
378. Inc. CCG. Molecular Operating Environment. 2012 ed. Montreal, Quebec, Canada2012.
379. Schneider HJ, Hacket F, Rüdiger V, Ikeda H. NMR studies of cyclodextrins and cyclodextrin complexes. Chemical Reviews 1998;98:1755-85.
380. Valente AJM, Söderman O. The formation of host-guest complexes between surfactants and cyclodextrins. Advances in Colloid and Interface Science 2014;205:156-76.
381. Wilson LD, Verrall RE. A 1H NMR study of cyclodextrin - Hydrocarbon surfactant inclusion complexes in aqueous solutions. Canadian Journal of Chemistry 1998;76:25-34.
382. Foldvari M, Badea I, Wettig S, Verrall R, Bagonluri M. Structural characterization of novel micro- and nano-scale non-viral DNA delivery systems for cutaneous gene therapy. 2005. p. 128-31.
383. Wood DJ, Hrùska FE, Saenger W. Proton NMR study of the inclusion of aromatic molecules in. alpha.-cyclodextrin. Journal of the American Chemical Society 1977;99:1735-40.
384. Wilson LD, Guo R. Preparation and sorption studies of polyester microsphere copolymers containing β-Cyclodextrin. Journal of Colloid and Interface Science 2012;387:250-61.
385. Blokzijl W, Engberts JBFN. Hydrophobic effects. Opinions and facts. Angewandte Chemie (International Edition in English) 1993;32:1545-79.
386. Maheshwari A, Sharma M, Sharma D. Investigation of the binding of roxatidine acetate hydrochloride with cyclomaltoheptaose (β-cyclodextrin) using IR and NMR spectroscopy. Carbohydrate Research 2011;346:1809-13.
387. Muñoz De La Peña A, Ndou TT, Zung JB, Greene KL, Live DH, Warner IM. Alcohol size as a factor in the ternary complexes formed with pyrene and β-cyclodextrin. Journal of the American Chemical Society 1991;113:1572-7.
388. Udachin KA, Ripmeester JA. A novel mode of inclusion for pyrene in β-cyclodextrin compounds: The crystal structures of β-cyclodextrin with cyclohexanol and pyrene, and with n-octanol and pyrene [6]. Journal of the American Chemical Society 1998;120:1080-1.
389. Wilson LD, Verrall RE. A Volumetric and NMR Study of Cyclodextrin-Inhalation Anesthetic Complexes in Aqueous Solutions. Canadian Journal of Chemistry 2015:1-7.
390. Guo Y, Aweda T, Black KCL, Liu Y. Chemistry and Theranostic applications of radiolabeled nanoparticles for cardiovascular, oncological, and pulmonary research. Current Topics in Medicinal Chemistry 2013;13:470-8.
391. Matsumura Y, Maeda H. A new concept for macromolecular therapeutics in cancer chemotherapy: Mechanism of tumoritropic accumulation of proteins and the antitumor agent smancs. Cancer Research 1986;46:6387-92.
392. Loo Y, Grigsby CL, Yamanaka YJ, et al. Comparative study of nanoparticle-mediated transfection in different GI epithelium co-culture models. Journal of Controlled Release 2012;160:48-56.
393. Toby BH, Von Dreele RB. GSAS-II: The genesis of a modern open-source all purpose crystallography software package. Journal of Applied Crystallography 2013;46:544-9.
394. Smiley ST, Reers M, Mottola-Hartshorn C, et al. Intracellular heterogeneity in mitochondrial membrane potentials revealed by a J-aggregate-forming lipophilic cation JC-1. Proceedings of the National Academy of Sciences of the United States of America 1991;88:3671-5.
395. Scaduto Jr RC, Grotyohann LW. Measurement of mitochondrial membrane potential using fluorescent rhodamine derivatives. Biophysical Journal 1999;76:469-77.
396. Conner SD, Schmid SL. Regulated portals of entry into the cell. Nature 2003;422:37-44.

397. Niemelä PS, Hyvönen MT, Vattulainen I. Influence of chain length and unsaturation on sphingomyelin bilayers. Biophysical Journal 2006;90:851-63.
398. Klionsky DJ, Emr SD. Autophagy as a regulated pathway of cellular degradation. Science 2000;290:1717-21.
399. Lee CY, Clough EA, Yellon P, Teslovich TM, Stephan DA, Baehrecke EH. Genome-wide analyses of steroid- and radiation-triggered programmed cell death in Drosophila. Current Biology 2003;13:350-7.
400. Chatterjee SJ, Pandey S. Chemo-resistant melanoma sensitized by tamoxifen to low dose curcumin treatment through induction of apoptosis and autophagy. Cancer Biology and Therapy 2011;11:216-28.
401. Aoki H, Takada Y, Kondo S, Sawaya R, Aggarwal BB, Kondo Y. Evidence that curcumin suppresses the growth of malignant gliomas in vitro and in vivo through induction of autophagy: Role of akt and extracellular signal-regulated kinase signaling pathways. Molecular Pharmacology 2007;72:29-39.
402. Lee YJ, Kim NY, Suh YA, Lee C. Involvement of ROS in curcumin-induced autophagic cell death. Korean Journal of Physiology and Pharmacology 2011;15:1-7.
403. Kim JY, Cho TJ, Woo BH, et al. Curcumin-induced autophagy contributes to the decreased survival of oral cancer cells. Archives of Oral Biology 2012;57:1018-25.
404. Qu W, Xiao J, Zhang H, et al. B19, a novel monocarbonyl analogue of curcumin, induces human ovarian cancer cell apoptosis via activation of endoplasmic reticulum stress and the autophagy signaling pathway. International Journal of Biological Sciences 2013;9:766-77.
405. Lin HY, Lin JN, Ma JW, et al. Demethoxycurcumin induces autophagic and apoptotic responses on breast cancer cells in photodynamic therapy. Journal of Functional Foods 2015;12:439-49.
406. Zhou T, Ye L, Bai Y, et al. Autophagy and apoptosis in hepatocellular carcinoma induced by EF25-(GSH)2: A novel curcumin analog. PLoS ONE 2014;9.
407. Guilbaud NF, Gas N, Dupont MA, Valette A. Effects of differentiation-inducing agents on maturation of human MCF-7 breast cancer cells. Journal of Cellular Physiology 1990;145:162-72.
408. Bernhard D, Tinhofer I, Tonko M, et al. Resveratrol causes arrest in the S-phase prior to Fas-independent apoptosis in CEM-C7H2 acute leukemia cells. Cell Death and Differentiation 2000;7:834-42.
409. Srinivas S, Anitha Sironmani T, Snanmugam G. Dimethyl sulfoxide inhibits the expression of early growth-response genes and arrests fibroblasts at quiescence. Experimental Cell Research 1991;196:279-86.
410. Benckhuijsen C, Osman AMMA, Hillebrand MJX, Smets LA. Glucocorticoid effect on melphalan cytotoxicity, cell-cycle position, cell size, and [3H]uridine incorporation in one of three human melanoma cell lines. Cancer Research 1987;47:4814-20.
411. Saengkrit N, Saesoo S, Srinuanchai W, Phunpee S, Ruktanonchai UR. Influence of curcumin-loaded cationic liposome on anticancer activity for cervical cancer therapy. Colloids and Surfaces B: Biointerfaces 2014;114:349-56.
412. Wang C, Li X, Wettig SD, Badea I, Foldvari M, Verrall RE. Investigation of complexes formed by interaction of cationic gemini surfactants with deoxyribonucleic acid. Physical Chemistry Chemical Physics 2007;9:1616-28.
413. Badea I, Verrall R, Baca-Estrada M, et al. In vivo cutaneous interferon-γ gene delivery using novel dicationic (gemini) surfactant-plasmid complexes. Journal of Gene Medicine 2005;7:1200-14.
414. Mochizuki S, Kanegae N, Nishina K, et al. The role of the helper lipid dioleoylphosphatidylethanolamine (DOPE) for DNA transfection cooperating with a cationic lipid bearing ethylenediamine. Biochimica et Biophysica Acta - Biomembranes 2013;1828:412-8.
415. Farhood H, Serbina N, Huang L. The role of dioleoyl phosphatidylethanolamine in cationic liposome mediated gene transfer. Biochimica et Biophysica Acta - Biomembranes 1995;1235:289-95.
416. Felgner JH, Kumar R, Sridhar CN, et al. Enhanced gene delivery and mechanism studies with a novel series of cationic lipid formulations. Journal of Biological Chemistry 1994;269:2550-61.

417. Litzinger DC, Huang L. Phosphatodylethanolamine liposomes: drug delivery, gene transfer and immunodiagnostic applications. BBA - Reviews on Biomembranes 1992;1113:201-27.
418. Ewert K, Slack NL, Ahmad A, et al. Cationic lipid-DNA complexes for gene therapy: Understanding the relationship between complex structure and gene delivery pathways at the molecular level. Current Medicinal Chemistry 2004;11:133-49.
419. Foldvari M, Wettig S, Badea I, Verrall R, Bagonluri M. Dicationic gemini surfactant gene delivery complexes contain cubic-lamellar mixed polymorphic phase. 2006. p. 400-3.
420. Shalaev EY, Steponkus PL. Phase diagram of 1,2-dioleoylphosphatidylethanolamine (DOPE): Water system at subzero temperatures and at low water contents. Biochimica et Biophysica Acta - Biomembranes 1999;1419:229-47.
421. Mulet X, Boyd BJ, Drummond CJ. Advances in drug delivery and medical imaging using colloidal lyotropic liquid crystalline dispersions. Journal of Colloid and Interface Science 2013;393:1-20.
422. Fodje M, Janzen K, Berg R, et al. MxDC and MxLIVE: Software for data acquisition, information management and remote access to macromolecular crystallography beamlines. Journal of Synchrotron Radiation 2012;19:274-80.
423. SMART S. XPREP. Area detector control and data integration and reduction software. Bruker Analytical X-ray Instruments Inc.: Madison, WI 1995.
424. Sheldrick GM. A short history of SHELX. Acta Crystallographica Section A: Foundations of Crystallography 2007;64:112-22.
425. Sheldrick GM. Experimental phasing with SHELXC/D/E: combining chain tracing with density modification. Acta Crystallographica Section D: Biological Crystallography 2010;66:479-85.
426. Sheldrick G. SHELXTL, Structure Determination Software Programs. Bruker AXS Inc, Madison, Wisconsin 1997.
427. Sayle RA, Milner-White EJ. RASMOL: biomolecular graphics for all. Trends in biochemical sciences 1995;20:374.
428. Armstrong D. Advanced Protocols in Oxidative Stress II: Springer; 2010.